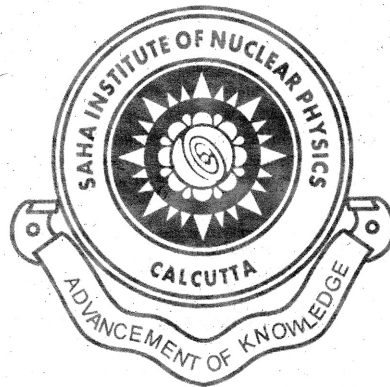


Saha Institute of Nuclear Physics
Annual Report
2011–2012



Saha Institute of Nuclear Physics
1/AF Bidhan Nagar, Kolkata 700 064
India

Tel: (33) 2337-5345-49 (5 lines)
Fax: (33)-2337-4637
<http://www.saha.ac.in>

Editorial Team

Prof Milan Kumar Sanyal
Prof Palash Baran Pal
Prof R Ranganathan
Prof Alokmay Datta
Prof Nitai P Bhattacharyya
Prof Abhijit Chakrabarti
Prof Satyajit Saha
Prof ANS Iyengar
Shri Swapan Kumar Banerjee
Smt Seema Bhattacharya
Shri Amalesh Chandra Saha

Creation

Prof Abhijit Chakrabarti
Shri Amit Kumar Saha

Photographs

Shri Pradip Das

Cover Design & Printed at

Sailee Press Pvt Ltd

Published by

Shri VV Mallikarjuna Rao, Registrar, SINP
on behalf of
Centre for Advanced Research & Education
Saha Institute of Nuclear Physics

January 11, 2013

Contents

Foreword	7
1 Biophysical Sciences including Chemistry	9
1.1 Summary of Research Activities of Divisions	9
1.1.1 Biophysics	9
1.1.2 C&MB	9
1.1.3 Chemical Sciences	10
1.1.4 Structural Genomics	10
1.2 Research Activities	11
1.2.1 Biophysics	11
1.2.2 C&MB	14
1.2.3 Chemical Sciences	19
1.2.4 Structural Genomics	29
1.3 Developmental Work	31
1.4 Publications	32
1.4.1 Publications in Books/Monographs & Volumes Edited	32
1.4.2 Journal Publication	32
1.5 Ph D Awarded	37
1.6 Seminars/Lectures given in Conference/Symposium/Schools	37
1.7 Teaching elsewhere	40
1.8 Miscellany	41
2 Condensed Matter Physics including Surface Physics and NanoScience	43
2.1 Summary of Research Activities of Divisions	43
2.1.1 Applied Material Science	43
2.1.2 Experimental Condensed Matter Physics	44
2.1.3 Surface Physics	46
2.1.4 Theoretical Condensed Matter Physics	47
2.2 Research Activities	49
2.2.1 Applied Material Science	49
2.2.2 Experimental Condensed Matter Physics	52
2.2.3 Surface Physics	58
2.2.4 Theoretical Condensed Matter Physics	69
2.3 Developmental Work	76
2.4 Publications	76
2.4.1 Publications in Books/Monographs & Volumes Edited	76
2.4.2 Papers in Journals	76

2.5	Ph D Awarded	83
2.6	Seminars/Lectures given in Conference/Symposium/Schools	83
2.7	Miscellany	86
3	Experimental Nuclear and Particle Physics	87
3.1	Summary of Research Activities of Divisions	87
3.1.1	Applied Nuclear Physics	87
3.1.2	High Energy Nuclear and Particle Physics	88
3.1.3	Nuclear Physics	89
3.2	Research Activities	89
3.2.1	Applied Nuclear Physics	89
3.2.2	High Energy Nuclear and Particle Physics	93
3.2.3	Nuclear Physics	100
3.3	Developmental Work	104
3.4	Publications	105
3.4.1	Papers in Journals	105
3.5	Seminars/Lectures given in Conference/Symposium/Schools	111
3.6	Teaching elsewhere	113
3.7	Miscellany	113
4	Plasma Physics & Computational Science	115
4.1	Summary of Research Activities of Divisions	115
4.1.1	Plasma Physics	115
4.2	Research Activities	116
4.3	Developmental Work	120
4.3.1	Plasma Physics	120
4.3.2	Computational Science	122
4.4	Publications	122
4.4.1	Papers in Journals	122
4.5	Seminars/Lectures given in Conference/Symposium/Schools	124
4.6	Teaching elsewhere	124
4.7	Miscellany	124
5	Theoretical Physics	125
5.1	Summary of Research Activities of Divisions	125
5.1.1	Astroparticle Physics and Cosmology	125
5.1.2	Theory	126
5.2	Research Activities	129
5.2.1	Astroparticle Physics and Cosmology	129
5.2.2	Theory	132
5.3	Developmental Work	145
5.3.1	Astroparticle Physics and Cosmology	145
5.4	Publications	145
5.4.1	Publications in Books/Monographs & Volumes Edited	145
5.4.2	Papers in Journals	145
5.5	Seminars/Lectures given in Conference/Symposium/Schools	149
5.6	Honours and Distinctions	152
5.7	Teaching elsewhere	152

5.8	Miscellany	152
6	Teaching	155
6.1	The Post-M Sc Associateship Course	155
6.1.1	Physics	155
6.1.2	Biophysical Sciences	157
6.2	Undergraduate Associateship Course	159
6.3	Summer Students' Programme	159
7	Research Fellows/Visiting Fellows/Research Associates	161
7.1	Research Fellows [as on March 31, 2012]	161
7.2	CSIR/UGC/DST/DBT/CAMCS Fellows, etc	162
7.3	Research Associate & Post Doctoral Fellow	163
8	Facilities	165
8.1	Centre for Advanced Research & Education	165
8.2	Electron Microscope Facility	166
8.3	Library	166
8.4	Radiological Safety	168
8.5	Central Workshop	168
8.6	Medical Unit	168
8.7	Building Maintenance (Civil)	169
8.8	Building Maintenance (Electrical)	169
8.9	Telephone Section	169
8.10	Auditorium Complex	169
8.11	Guest House	169
8.12	Departmental Canteen	169
9	Administration	171
9.1	Governing Council	171
9.2	Members of the Institute [as on March 31, 2012]	172
9.3	List of Retirement: 2011-2012	177
9.4	Voluntary Retirement: 2011-2012	177
9.5	List of Demise: 2011-2012	177
9.6	Audited Accounts	178
9.7	Purchase Section	180
10	External Collaborators	181
11	Index	185

Foreword

Research in basic sciences, performed at institutes like the Saha Institute of Nuclear Physics, epitomises the country's international stature in the global quest for scientific truth at the most fundamental level. Technological spinoffs from such research, while not immediate, is likely around the corner. The large number of doctoral students and postdoctoral fellows, who have been trained in research at SINP over the years, continues to add significantly to the national pool of scientifically trained human resource. This is Professor Meghnad Saha's legacy, celebrated and practised at the SINP through decades since its inception in 1950.

Major achievements have been accomplished in various fields of sciences like magnetic properties at Low temperature, semiconductor based quantum structures the study of nuclear and high energy physics through work done in the campus. SINP has developed an Indian beamlines for x-ray scattering research in Photon Factory synchrotron, KEK, Japan and this facility is being used by several institutes. In the field of biophysical sciences, SINP scientists have taken active initiative in disease biology particularly in hematological and neurodegenerative diseases.

Scientists from SINP have been a part of the International collaboration at Large Hadron Collider (LHC) in CERN, Geneva in three experimental areas ALICE, CMS and ISOLDE. SINP members have made significant contributions in the development of CMS experiment at CERN that has led to the observation of the new particle at 125.3 GeV, consistent with a Higgs Boson as predicted by the Standard Model of Particle Physics.

We have used about 250 Crore Rupees on 27 projects for the entire five-year plan period to develop several facilities which are equivalent to any state-of-the-art laboratories available internationally. These equipments are being used to carry out front-ranking research in various fields of Physics and Biology and the results are attracting attention worldwide. This annual report shows that research publications per year is consistently improving particularly in journals having higher impact factors. We are receiving large number of very strong applications from India and abroad for consideration of faculty position. In last two years we have received over 300 applications and recruited around 20 of them.

I am proud to write this foreword for our annual report and I am quite sure next year our performance will be even better.

Prof Milan K Sanyal
Director

January 11, 2013

Chapter 1

Biophysical Sciences including Chemistry

1.1 Summary of Research Activities of Divisions

1.1.1 Biophysics

The major emphasis of the research work in Biophysics Division is twofold: experimental approaches to understand the biomolecular recognition process in different intracellular phenomena and bioinformatics based theoretical approaches employing quantum mechanical calculations to understand the structure-function correlation in nucleic acids (DNA and different types of RNA). The biomolecular recognition studies include mode of actions of flavones and flavonoids, chemical biology of the aureolic acid group of antibiotics, modulation of chromatin structure by small DNA binding molecules and self association of wild type and mutant lamins involved in laminopathy. In addition we have also studied the biophysical properties of lamins to understand their roles as intermediary filaments.

1.1.2 C&MB

Over expression, purification, crystallization and preliminary X-ray diffraction analyses of CheY4, VcHsp 31 and recombinant thermo-stable variant of pro-papain have been carried out. Inhibitory role of C-terminus of ervatamin-C in proteolytic activity of the enzyme has been established. The topology of hydrophobic clusters, sustaining the native protein fold has been classified and prevalence of some commonly occurring structural motifs have been established which aggregate to form larger hydrophobic contact networks. Substrate of S-phase cell cycle kinase LdCyc1/CRK3 from *Leishmania* have identified and characterized. Several micro RNAs (miRNA), the negative regulator of protein coding gene expression, have been shown to target the Huntingtin (HTT) gene, whose mutation causes Huntingtons disease (HD). The expression of these miRNAs has been shown to decrease in cell and animal models of HD. Besides, it has been shown that miR-150 target TP53 gene, explaining the over expression of TP53 in HD. HIPPI, a molecular partner of HTT interacting protein HIP1, has been shown to regulate many genes involved in HD pathogenesis.

1.1.3 Chemical Sciences

It has been attempted to unravel the mechanistic pathways of various photoinduced charge-transfer processes using steady-state and time-resolved absorption and fluorescence, magnetic field effect and theoretical modeling. The effects of some NSAIDs and similar molecules on different biochemical processes and external agents and factors on protein folding and misfolding have been investigated. A new method for label free and rapid impedimetric sensing of *Escherichia coli* using antibody antigen bound on conducting polyaniline film has been reported. Environmental radioactivity present in eastern part of Kolkata, India has been assessed from the air and soil samples using gamma spectrometer.

1.1.4 Structural Genomics

Structural Genomics Division is carrying out research in the area of Disease Biology with a focus on two major disorders the hematological and neurological. The widely prevalent disease of Eastern India, HbE-thalassemia, along with sickle cell anemia, hereditary spherocytosis and leukemia are being studied as model for hematological disorders while Alzheimers, Huntingtons, and the Prion diseases are being studied for the neurodegenerative diseases. Differential proteomics studies are being done in these diseases using clinical samples of cerebrospinal fluid, plasma, urine, red cells, cell extracts and platelets. Hundreds of proteins from these different tissue types are annotated and 10-15 proteins are identified to be differentially expressed in diseases. Classes of redox regulators and chaperone proteins have been found to be up-regulated in hemoglobinopathy. Studies in cell proliferation and differentiation have implicated the roles of self renewal pathways and cross talk between signaling pathways in chronic to blast transformation of CD34+ CML stem cells isolated from patients. Moreover, we have established that cytoplasmic sequestration of the cell cycle inhibitor, p27 led to its interaction with polycomb group of genes (Bmi1, EZH2) and activation of the Rho/Rac GTPase pathway resulting in actin depolymerization which, in turn, caused cellular egression/mobilization from the bone marrow. Currently this pathway is also being investigated to understand the process of metastasis in epithelial cancer. Among the various diseases that affect the nervous system, some of the most debilitating neurodegenerative disorders are Alzheimers, Huntingtons and Prion Diseases. These late onset but eventually fatal diseases are all caused by altered metabolism of individual proteins that interfere with normal cellular homeostasis. The normal life cycle of a protein, characterized by its biogenesis, trafficking and degradation, are compromised in these disorders resulting in misfolding, misprocessing or mislocalization of the proteins. Most likely, the aberrant protein can then engage in atypical interactions and ultimately lead to a series of unknown events culminating in cell death. The major focus of our research in Alzheimers disease (AD) is to study the downstream pathogenesis of the disease, mediated through AICD and its adaptor network. AICD possesses conserved motifs that are now known to interact with cytosolic adaptor proteins and these interactions in turn affect different signaling pathways. We have shown that Grb2, one such adaptor, interacted with AICD in late endosomal compartments. The excess protein, thus entrapped, could be degraded by autophagy. The structure of AICD-YENPTY motif takes a different conformation in presence of its binding partner Grb2-SH2 vis-a-vis that of other AICD structures. Currently, we are also trying to provide a comprehensive understanding of the disruption of the intracellular protein trafficking pathways in late-onset neurodegenerative disorders. With Prion disease as a model system, we plan to simultaneously pursue two broad facets: first, understanding the significance of the ESCRT machinery and the endo-lysosomal pathway in PrP-mediated (Prion protein) neurodegenerative diseases. This will aim to provide a molecular explanation for how the loss of function mutation of Mahogunin results in Prion disease like pheno-

type of spongiform neurodegeneration. Secondly, we also aim to explore how the various essential molecular components that are regulated during endoplasmic reticular stress (ER stress) and aging, both of which manifest in late onset neurodegenerative diseases.

1.2 Research Activities

1.2.1 Biophysics

1.2.1.1 Interaction of nucleobases with wrinkled graphene surface: Dispersion Corrected DFT and AFM Studies

Graphene-nucleobase interaction is gaining importance due to its possible therapeutic applications. The dispersion interaction plays a major role in stacked aromatic compounds, such as graphene with amino acids or nucleobases. We have carried out detailed quantum chemical calculations of complexes of nanographene sheets and the nucleobases of DNA and RNA using dispersion corrected density functional theory. Binding energies show a trend as observed earlier by different theoretical and experimental measurements. However, in our present investigation, the optimized structures of the complex as well as isolated graphene show significant curvature, similar features are also observed by our Atomic Force Microscopic studies. Analysis of Natural Bond Orbital charges indicates the possibility of weak hydrogen bond-like interactions involving pyramidal amino groups of the nucleobases and pi-center of the nanographene.

Swati Panigrahi, Anuradha Bhattacharya, Sangam Banerjee, Dhananjay Bhattacharyya

1.2.1.2 Unzipping and binding of small interfering RNA with single walled carbon nanotube: A platform for small interfering RNA delivery

In an effort to design efficient platform for siRNA delivery, we combine all atom classical and quantum simulations to study the binding of small interfering RNA (siRNA) by pristine single wall carbon nanotube (SWCNT). Our results show that siRNA strongly binds to SWCNT surface via unzipping its base-pairs and the propensity of unzipping increases with the increase in the diameter of the SWCNTs. The unzipping and subsequent wrapping events are initiated and driven by van der Waals interactions between the aromatic rings of siRNA nucleobases and the SWCNT surface. However, molecular dynamics (MD) simulations of double strand DNA (dsDNA) of the same sequence show that the dsDNA undergoes much less unzipping and wrapping on the SWCNT in the simulation time scale of 70 ns. This interesting difference is due to smaller interaction energy of thymidine of dsDNA with the SWCNT compared to that of uridine of siRNA, as calculated by dispersion corrected density functional theory (DFT) methods. After the optimal binding of siRNA to SWCNT, the complex is very stable which serves as one of the major mechanisms of siRNA delivery for biomedical applications. Since siRNA has to undergo unwinding process with the effect of RNA-induced silencing complex, our proposed delivery mechanism by SWCNT possesses potential advantages in achieving RNA interference.

Mogurampelly Santosh†, Swati Panigrahi, Dhananjay Bhattacharyya, et al

1.2.1.3 Encapsulation of 3-hydroxyflavone in gamma-cyclodextrin nanocavities: Excited state proton transfer fluorescence and molecular docking studies

steady state and time resolved fluorescence spectroscopy have been used to explore the confinement of 3-hydroxyflavone (3HF), (a bioactive flavonol) in gamma-cyclodextrin (gamma-CDx) nanocavities in aqueous medium. With increasing concentrations of gamma-CDx, dramatic enhancements occur in the intensity and anisotropy of the excited state intramolecular proton transfer (ESIPT) tautomer fluorescence of 3HF. These observations indicate that 3HF readily enters the relatively hydrophobic cavity of gamma-cDx, where the chromone ring is well shielded from external H-bonding perturbation effects, thus facilitates the ESIPT process. Additionally, appearance of induced circular dichroism (ICD) bands is noted in the absorption region of 3HF, which further confirms the inclusion process. Docking calculations suggest that hydrogen bonding interactions are involved in the formation of the inclusion complex.

Biswapathik Pahari, Sandipan Chakraborty, Pradeep K Sengupta

1.2.1.4 Structure and Energy of Non-Canonical Basepairs: Comparison of Various Computational Chemistry Methods with Crystallographic Ensembles

Different types of non-canonical basepairs, in addition to the Watson-Crick ones, are observed quite frequently in RNA. Their importance in the three dimensional structure is not fully understood, but their various roles have been proposed by different groups. We have analyzed the energetics and geometry of 32 most frequently observed basepairs in the functional RNA crystal structures using different popular empirical, semi-empirical and ab initio quantum chemical methods and compared their optimized geometry with the crystal data. These basepairs are classified into three categories: polar, non-polar and sugar-mediated, depending on the types of atoms involved in hydrogen bonding. In case of polar basepairs, most of the methods give rise to optimized structures close to their initial geometry. The interaction energies also follow similar trends, with the polar ones having more attractive interaction energies. Some of the C-H center dot center dot center dot O/N hydrogen bond mediated non-polar basepairs are also found to be significantly stable in terms of their interaction energy values. Few polar basepairs, having amino or carboxyl groups not hydrogen bonded to anything, such as G:G H:W C, show large flexibility. Most of the non-polar basepairs, except A:G s:s T and A:G w:s C, are found to be stable; indicating C-H center dot center dot center dot O/N interaction also plays a prominent role in stabilizing the basepairs. The sugar mediated basepairs show variability in their structures, due to the involvement of flexible ribose sugar. These presumably indicate that the most of the polar basepairs along with few non-polar ones act as seed for RNA folding while few may act as some conformational switch in the RNA.

Swati Panigrahi, Rahul Pal, Dhananjay Bhattacharyya

1.2.1.5 Effect of DNA Groove Binder Distamycin A upon Chromatin Structure

Background:

Distamycin A is a prototype minor groove binder, which binds to B-form DNA, preferentially at A/T rich sites. Extensive work in the past few decades has characterized the binding at the level of double stranded DNA. However, effect of the same on physiological DNA, i.e. DNA complexed in chromatin, has not been well studied. Here we elucidate from a structural perspective, the interaction of distamycin with soluble chromatin, isolated from Sprague-Dawley rat.

Methodology/Principal Findings:

Chromatin is a hierarchical assemblage of DNA and protein. Therefore, in order to characterize the interaction of the same with distamycin, we have classified the system into various levels, according to the requirements of the method adopted, and the information to be obtained. Isothermal titration calorimetry has been employed to characterize the binding at the levels of chromatin, chromatosome and chromosomal DNA. Thermodynamic parameters obtained thereof, identify enthalpy as the driving force for the association, with comparable binding affinity and free energy for chromatin and chromosomal DNA. Reaction enthalpies at different temperatures were utilized to evaluate the change in specific heat capacity (C_p), which, in turn, indicated a possible binding associated structural change. Ligand induced structural alterations have been monitored by two complementary methods - dynamic light scattering, and transmission electron microscopy. They indicate compaction of chromatin. Using transmission electron microscopy, we have visualized the effect of distamycin upon chromatin architecture at di- and trinucleosome levels. Our results elucidate the simultaneous involvement of linker bending and internucleosomal angle contraction in compaction process induced by distamycin.

Conclusions/Significance:

We summarize here, for the first time, the thermodynamic parameters for the interaction of distamycin with soluble chromatin, and elucidate its effect on chromatin architecture. The study provides insight into a ligand induced compaction phenomenon, and suggests new mechanisms of chromatin architectural alteration.

Parijat Majumder, Dipak Dasgupta

1.2.1.6 Correlation of testicular toxicity and oxidative stress induced by chlorpyrifos in rats

Effect of chlorpyrifos pesticide on testicular oxidative damage was studied in Sprague-Dawley rats at varying doses. At lower doses (5 and 10 mg/kg body weight/30 days), reduction in plasma levels of testosterone and follicular stimulating hormone (FSH) and luteinizing hormone (LH) along with significant shrinkage of seminiferous tubules and drastic changes in germ cells were seen. But these adverse changes of testes were restored with the revival of serum testosterone and FSH and LH at higher doses (20 and 30 mg/kg body weight/30 days). Similarly, levels of testicular lipid peroxidation and diene conjugates were elevated whereas activities of antioxidant enzymes (superoxide dismutase, catalase and glutathione peroxidase), steroidogenic (Δ^5 , 3 β -HSD and Δ^5 , 17 β -HSD) enzymes and angiotensinogen-converting enzyme and glutathione content including lipid protein content of testes were decreased at low doses. But at higher doses, reductions in level of lipid peroxidation (as revealed by malondialdehyde [MDA] value) and conjugated dienes were found and on the contrary, revivals of testicular antiperoxidative/antioxidant enzymes defense systems, angiotensinogen-converting enzyme (ACE), steroidogenic enzymes, lipid protein and antioxidant glutathione content were observed. Therefore, the present study indicated from the results that chlorpyrifos had a dual effect at both doses on oxidative stress changes, but at higher doses, the cells were triggering its natural defense mechanism to combat the insult of lower doses of chlorpyrifos and became operative possibly through corrective measure of antioxidant enzymes defense system and pituitary gonadotropins hormones feedback mechanisms on testes.

Tapas Kumar Mandal, Niladri Sekhar Das

1.2.1.7 Wetting Property of the Edges of Monoatomic Step on Graphite: Frictional-Force Microscopy and ab Initio Quantum Chemical Studies

In this work, we present the wetting property of the edges of a monoatomic step on graphite. We have used frictional force microscope to experimentally investigate the wetting property of these edges. We have carried out quantum chemical calculations on a model system of nanographene to characterize hydrogen-bonding interactions between water and two different edges of the graphene, namely, the zigzag and arm-chair edges, to explain our experimental results. We have clearly observed two distinct frictional properties along the monoatomic steps on graphite surface under varying conditions of humidity. The distinct frictional properties of the different wetting properties of the edges have been attributed to the different wetting properties associated with two different edges. Our subsequent quantum experimental findings with edge-specific graphene-water interaction.

Swati Panigrahi, Anuradha Bhattacharya...Dhananjay Bhattacharyya, Sangam Banerjee

1.2.1.8 Biphasic Association of T7 RNA Polymerase and a Nucleotide Analogue, Cibacron Blue as a Model to Understand the Role of Initiating Nucleotide in the Mechanism of Enzyme Action

T7 RNA polymerase (T7 RNAP) is an enzyme that utilizes ribonucleotides to synthesize the nascent RNA chain in a template - dependent manner. Here we have studied the interaction of T7 RNAP with cibacron blue, an anthraquinone monochlorotriazine dye, its effect on the function of the enzyme and the probable mode of binding of the dye. We have used difference absorption spectroscopy and isothermal titration calorimetry to show that the dye binds T7 RNAP in a biphasic manner. The first phase of the binding is characterized by inactivation of the enzyme. The second binding site overlaps with the common substrate-binding site of the enzyme. We have carried out docking experiment to map the binding site of the dye in the promoter bound protein. Competitive displacement of the dye from the high affinity site by labeled GTP and isothermal titration calorimetry of high affinity GTP bound enzyme with the dye suggests a strong correlation between the high affinity dye binding and the high affinity GTP binding in T7 RNAP reported earlier from our laboratory.

Sudipta Pal...Rahul Banerjee, Dipak Dasgupta

1.2.2 C&MB

1.2.2.1 Overexpression, purification, crystallization and preliminary X-ray analysis of CheY4 from *Vibrio cholerae* O395

Chemotaxis and motility greatly influence the infectivity of *Vibrio cholerae*, although the role of chemotaxis genes in *V. cholerae* pathogenesis is poorly understood. In contrast to the single copy of CheY found in *Escherichia coli* and *Salmonella typhimurium*, four CheYs (CheY1-CheY4) are present in *V. cholerae*. While insertional disruption of the *cheY4* gene results in decreased motility, insertional duplication of this gene increases motility and causes enhanced expression of the two major virulence genes. Additionally, *cheY3/cheY4* influences the activation of the transcription factor NF- κ B, which triggers the generation of acute inflammatory responses. *V. cholerae* CheY4

was cloned, overexpressed and purified by Ni-NTA affinity chromatography followed by gel filtration. Crystals of CheY4 grown in space group $C2$ diffracted to 1.67 Å resolution, with unit-cell parameters $a = 94.4$, $b = 31.9$, $c = 32.6$ Å, $\beta = 96.5^\circ$, whereas crystals grown in space group $P3_221$ diffracted to 1.9 Å resolution, with unit-cell parameters $a = b = 56.104$, $c = 72.283$ Å, $\gamma = 120^\circ$.

Maitree Biswas†, Susmita Khamrui, Udayaditya Sen, et al

1.2.2.2 Micro RNA-214,-150,-146a and-125b target Huntingtin gene

We observed earlier that expressions of several micro RNAs (miRNAs) are altered in a cell model of Huntington's disease (HD). As genes involved in different neurodegenerative diseases are targeted by miRNAs, we searched databases to find out whether Huntingtin gene (HTT), mutation to which causes HD, is a target of any miRNA. Among many miRNAs that are predicted to target HTT, we showed using various experimental approaches that miR-214, miR-150, miR-146a and miR-125b could target both human HTT and mouse Htt. Luciferase reporter vectors containing 3'-UTRs of mouse and human HTT showed reduction in relative luciferase activities on exogenous expression of cloned miRNAs. Loss of function studies with miRNA inhibitors led to the revival of luciferase activities of cloned 3'-UTR of HTT. Exogenous expression of these miRNAs reduced the expression of endogenous Htt in mouse cells. Expression of miRNAs with mutations at seed sequences neither reduced the reporter luciferase activities nor the endogenous expression of Htt. Taking together, we showed that miR-214, miR-150, miR-146a and miR-125b targeted HTT. Besides, the exogenous expression of wild type miRNAs reduced HTT aggregates formed by the recombinant exon1 of HTT gene that codes for 83Q tagged with 3'-UTR of Htt, as observed by filter retardation assay and confocal microscopy. In summary, regulation of HTT by miRNAs might provide a new mechanism for the modulation of HD.

Mithun Sinha, Jayeeta Ghose, Nitai P Bhattacharyya

1.2.2.3 Cloning, expression, purification, crystallization and preliminary X-ray analysis of the 31 kDa *Vibrio cholera* heat-shock protein VcHsp31

The Gram-negative bacterium *Vibrio cholerae*, which is responsible for the diarrhoeal disease cholera in humans, induces the expression of numerous heat-shock genes. VcHsp31 is a 31 kDa putative heat-shock protein that belongs to the DJ-1/PfpI superfamily, functioning as both a chaperone and a protease. VcHsp31 has been cloned, overexpressed and purified by Ni²⁺-NTA affinity chromatography followed by gel filtration. Crystals of VcHsp31 were grown in the presence of PEG 6000 and MPD; they belonged to space group $P2_1$ and diffracted to 1.9 Å resolution. Assuming the presence of six molecules in the asymmetric unit, the Matthews coefficient was estimated to be 1.97 Å³ Da⁻¹, corresponding to a solvent content of 37.4%.

Samir Das...Udayaditya Sen

1.2.2.4 Wnt/Ca2+ signaling pathway: a brief overview

The non-canonical Wnt/Ca2+ signaling cascade is less characterized than their canonical counterpart, the Wnt/beta-catenin pathway. The non-canonical Wnt signaling pathways are diverse,

defined as planer cell polarity pathway, Wnt-RAP1 signaling pathway, Wnt-Ror2 signaling pathway, Wnt-PKA pathway, Wnt-GSK3MT pathway, Wnt-aPKC pathway, Wnt-RYK pathway, Wnt-mTOR pathway, and Wnt/calcium signaling pathway. All these pathways exhibit a considerable degree of overlap between them. The Wnt/Ca²⁺ signaling pathway was deciphered as a crucial mediator in development. However, now there is substantial evidence that the signaling cascade is involved in many other molecular phenomena. Many aspects of Wnt/Ca²⁺ pathway are yet enigmatic. This review will give a brief overview of the fundamental and evolving concepts of the Wnt/Ca²⁺ signaling pathway.

Antara De

1.2.2.5 Regulation of RE1 Protein Silencing Transcription Factor (REST) Expression by HIP1 Protein Interactor (HIPPI)

Earlier we have shown that the proapoptotic protein HIPPI (huntingtin interacting protein 1 (HIP1) protein interactor) along with its molecular partner HIP1 could regulate transcription of the caspase-1 gene. Here we report that RE1-silencing transcription factor/neuron-restrictive silencer factor (REST/NRSF) is a new transcriptional target of HIPPI. HIPPI could bind to the promoter of REST and increased its expression in neuronal as well as non-neuronal cells. Such activation of REST down-regulated expression of REST target genes, such as brain-derived neurotrophic factor (BDNF) or proenkephalin (PENK). The ability of HIPPI to activate REST gene transcription was dependent on HIP1, the nuclear transporter of HIPPI. Using a Huntington disease cell model, we have demonstrated that feeble interaction of HIP1 with mutant huntingtin protein resulted in increased nuclear accumulation of HIPPI and HIP1, leading to higher occupancy of HIPPI at the REST promoter, triggering its transcriptional activation and consequent repression of REST target genes. This novel transcription regulatory mechanism of REST by HIPPI may contribute to the deregulation of transcription observed in the cell model of Huntington disease.

Moumita Datta, Nitai P Bhattacharyya

1.2.2.6 Genome wide gene expression regulation by HIP1 Protein Interactor, HIPPI: Prediction and validation

Background: HIP1 Protein Interactor (HIPPI) is a pro-apoptotic protein that induces Caspase8 mediated apoptosis in cell. We have shown earlier that HIPPI could interact with a specific 9 bp sequence motif, defined as the HIPPI binding site (HBS), present in the upstream promoter of Caspase1 gene and regulate its expression. We also have shown that HIPPI, without any known nuclear localization signal, could be transported to the nucleus by HIP1, a NLS containing nucleocytoplasmic shuttling protein. Thus our present work aims at the investigation of the role of HIPPI as a global transcription regulator.

Results: We carried out genome wide search for the presence of HBS in the upstream sequences of genes. Our result suggests that HBS was predominantly located within 2 Kb upstream from transcription start site. Transcription factors like CREBP1, TBP, OCT1, EVI1 and P53 half site were significantly enriched in the 100 bp vicinity of HBS indicating that they might co-operate with HIPPI for transcription regulation. To illustrate the role of HIPPI on transcriptome, we performed gene expression profiling by microarray. Exogenous expression of HIPPI in HeLa cells resulted in up-regulation of 580 genes ($p < 0.05$) while 457 genes were down-regulated. Several

transcription factors including CBP, REST, C/EBP beta were altered by HIPPI in this study. HIPPI also interacted with P53 in the protein level. This interaction occurred exclusively in the nuclear compartment and was absent in cells where HIP1 was knocked down. HIPPI-P53 interaction was necessary for HIPPI mediated up-regulation of Caspase1 gene. Finally, we analyzed published microarray data obtained with post mortem brains of Huntington's disease (HD) patients to investigate the possible involvement of HIPPI in HD pathogenesis. We observed that along with the transcription factors like CREB, P300, SREBP1, Sp1 etc. which are already known to be involved in HD, HIPPI binding site was also significantly over-represented in the upstream sequences of genes altered in HD.

Conclusions: Taken together, the results suggest that HIPPI could act as an important transcription regulator in cell regulating a vast array of genes, particularly transcription factors and at least, in part, play a role in transcription deregulation observed in HD.

Moumita Datta, Ananyo Choudhury†, Ansuman Lahiri†, Nitai P Bhattacharyya

1.2.2.7 Identification of substrates of an S-phase cell cycle kinase from *Leishmania donovani*

Despite the importance of cyclin-Cdk related kinases (CRK) in regulation of cell and life cycle of kinetoplastida parasites, only limited knowledge about their substrates are presently available. Here, the potential substrates were searched for an S-phase LdCyc1-CRK3 complex from *Leishmania donovani* based on the presence of Cdk target phosphorylation site together with the cyclin interacting Cy-motif in genome-derived putative protein sequences. Three substrates could be identified with one of them being a unique protein with no known homologues. Another identified substrate is similar to MYST family of histone acetyl transferase and the third one contains Ku-70 related conserved domains. All the substrates interact directly with LdCyc1 and are phosphorylated in a Cy-motif dependent manner suggesting the importance of Cy-motif for their functions.

Anup Kumar Maity, Alakananda Goswami, Partha Saha

1.2.2.8 C-Terminal extension of a plant cysteine protease modulates proteolytic activity through a partial inhibitory mechanism

The amino acid sequence of ervatamin-C, a thermostable cysteine protease from a tropical plant, revealed an additional 24-amino-acid extension at its C-terminus (CT). The role of this extension peptide in zymogen activation, catalytic activity, folding and stability of the protease is reported. For this study, we expressed two recombinant forms of the protease in *Escherichia coli*, one retaining the CT-extension and the other with it truncated. The enzyme with the extension shows autocatalytic zymogen activation at a higher pH of 8.0, whereas deletion of the extension results in a more active form of the enzyme. This CT-extension was not found to be cleaved during autocatalysis or by limited proteolysis by different external proteases. Molecular modeling and simulation studies revealed that the CT-extension blocks some of the substrate-binding unprimed subsites including the specificity-determining subsite (S2) of the enzyme and thereby partially occludes accessibility of the substrates to the active site, which also corroborates the experimental observations. The CT-extension in the model structure shows tight packing with the catalytic domain of the enzyme, mediated by strong hydrophobic and H-bond interactions, thus restricting accessibility of its cleavage sites to the protease itself or to the external proteases. Kinetic stability analyses (T(50) and

t(1/2)) and refolding experiments show similar thermal stability and refolding efficiency for both forms. These data suggest that the CT-extension has an inhibitory role in the proteolytic activity of ervatamin-C but does not have a major role either in stabilizing the enzyme or in its folding mechanism.

Sruti Dutta, Debi Choudhury, Jiban K Dattagupta, Sampa Biswas

1.2.2.9 Regulation of miR-146a by RelA/NFkB and p53 in *STHdh*^(Q111)/*Hdh*^(Q111) Cells, a Cell Model of Huntington's Disease

Huntington's disease (HD) is caused by the expansion of N-terminal polymorphic poly Q stretch of the protein huntingtin (HTT). Deregulated microRNAs and loss of function of transcription factors recruited to mutant HTT aggregates could cause characteristic transcriptional deregulation associated with HD. We observed earlier that expressions of miR-125b, miR-146a and miR-150 are decreased in *STHdh*^{Q111}/*Hdh*^{Q111} cells, a model for HD in comparison to those of wild type *STHdh*^{Q7}/*Hdh*^{Q7} cells. In the present manuscript, we show by luciferase reporter assays and real time PCR that decreased miR-146a expression in *STHdh*^{Q111}/*Hdh*^{Q111} cells is due to decreased expression and activity of p65 subunit of NFkB (RelA/NFkB). By reporter luciferase assay, RT-PCR and western blot analysis, we also show that both miR-150 and miR-125b target p53. This partially explains the up regulation of p53 observed in HD. Elevated p53 interacts with RelA/NFkB, reduces its expression and activity and decreases the expression of miR-146a, while knocking down p53 increases RelA/NFkB and miR-146a expressions. We also demonstrate that expression of p53 is increased and levels of RelA/NFkB, miR-146a, miR-150 and miR-125b are decreased in striatum of R6/2 mice, a mouse model of HD and in cell models of HD. In a cell model, this effect could be reversed by exogenous expression of chaperone like proteins HYPK and Hsp70. We conclude that (i) miR-125b and miR-150 target p53, which in turn regulates RelA/NFkB and miR-146a expressions; (ii) reduced miR-125b and miR-150 expressions, increased p53 level and decreased RelA/NFkB and miR-146a expressions originate from mutant HTT (iii) p53 directly or indirectly regulates the expression of miR-146a. Our observation of interplay between transcription factors and miRNAs using HD cell model provides an important platform upon which further work is to be done to establish if such regulation plays any role in HD pathogenesis.

Jayeeta Ghose, Mithun Sinha, Eashita Das, Nihar R Jana†, NP Bhattacharyya

1.2.2.10 Mapping the distribution of packing topologies within protein interiors shows predominant preference for specific packing motifs

Background: Mapping protein primary sequences to their three dimensional folds referred to as the 'second genetic code' remains an unsolved scientific problem. A crucial part of the problem concerns the geometrical specificity in side chain association leading to densely packed protein cores, a hallmark of correctly folded native structures. Thus, any model of packing within proteins should constitute an indispensable component of protein folding and design. Results: In this study an attempt has been made to find, characterize and classify recurring patterns in the packing of side chain atoms within a protein which sustains its native fold. The interaction of side chain atoms within the protein core has been represented as a contact network based on the surface complementarity and overlap between associating side chain surfaces. Some network topologies definitely appear to be preferred and they have been termed 'packing motifs', analogous to super secondary

structures in proteins. Study of the distribution of these motifs reveals the ubiquitous presence of typical smaller graphs, which appear to get linked or coalesce to give larger graphs, reminiscent of the nucleation-condensation model in protein folding. One such frequently occurring motif, also envisaged as the unit of clustering, the three residue clique was invariably found in regions of dense packing. Finally, topological measures based on surface contact networks appeared to be effective in discriminating sequences native to a specific fold amongst a set of decoys. Conclusions: Out of innumerable topological possibilities, only a finite number of specific packing motifs are actually realized in proteins. This small number of motifs could serve as a basis set in the construction of larger networks. Of these, the triplet clique exhibits distinct preference both in terms of composition and geometry.

Sankar Basu, Dhananjay Bhattacharyya, Rahul Banerjee

1.2.2.11 Crystallization and preliminary X-ray diffraction studies of the precursor protein of a thermostable variant of papain

The crystallization of a recombinant thermostable variant of pro-papain has been carried out. The mutant pro-enzyme was expressed in *Escherichia coli* as inclusion bodies, refolded, purified and crystallized. The crystals belonged to space group $P2_1$, with unit-cell parameters $a=42.9$, $b=74.8$, $c=116.5$ Å, $\beta=93.0^\circ$, and diffracted to 2.6 Å resolution using synchrotron radiation. Assuming the presence of two molecules in the asymmetric unit, the calculated Matthews coefficient is 2.28 Å³ Da⁻¹, corresponding to a solvent content of 46%. Initial attempts to solve the structure using molecular-replacement techniques were successful.

Sumana Roy, Debi Choudhury, Chandana Chakrabarti, Sampa Biswas, JK Dattagupta

1.2.3 Chemical Sciences

1.2.3.1 Probable nuclear reactions to produce proton rich rhenium radionuclides

The crux of the present work is to explore the various channels leading to the production of proton rich rhenium radionuclides, (181-186)Re, for different applications. The possible production routes encompass both light and heavy ion induced reactions up to a maximum 100 MeV projectile energy starting from threshold. The nuclear reaction model codes ALICE91 and PACE-II were employed in this endeavour. Excitation functions of the rhenium radionuclides have been calculated using the aforesaid nuclear reaction model codes and compared with the measured data wherever available. The contributions of preequilibrium and equilibrium reaction mechanisms to the total reaction cross section were analysed. For the first time, this study talks about the possibility of light-heavy ion ((6,7)Li and (9)Be) induced production of proton rich rhenium radionuclides.

Moumita Maiti

1.2.3.2 Binding of Cu(II) complexes of oxicam NSAIDs to alternating AT and homopolymeric AT sequences: differential response to variation in backbone structure

Besides their principal functions as painkillers and anti-inflammatory agents, drugs belonging to the nonsteroidal anti-inflammatory drug (NSAID) group also have anticancer properties. Cu(II) complexes of these drugs enhance the anticancer effect. How they exert this effect is not clear. As a possible molecular mechanism, our group has already shown that the Cu(II) complexes of two oxicam NSAIDs with anticancer properties, viz. piroxicam and meloxicam, can directly bind to the DNA backbone. AT stretches are abundant in the eukaryotic genome. These stretches are more accessible to binding of different ligands, resulting in expression of different functions. AT stretches containing both alternating base pairs and homopolymeric bases in individual strands show subtle differences in backbone structures. It is therefore of interest to see how the Cu(II)-NSAID complexes respond to such differences in backbone structure. Binding studies of these complexes with alternating polydA-dT and homopolymeric polydA-polydT have been conducted using UV-vis absorption titration studies, UV melting studies and circular dichroism spectroscopy. Competitive binding with the standard intercalator ethidium bromide and the minor groove binder 4',6-diamidino-2-phenylindole was monitored using fluorescence to identify the possible binding mode. Our results show that Cu(II)-NSAID complexes are highly sensitive to the subtle differences in backbone structures of polydA-dT and polydA-polydT and respond to them by exhibiting different binding properties, such as binding constants, effect on duplex stability and binding modes. Both complexes have a similar binding mode with polydA-dT, the results point to a mixed mode of binding.

Sreeja Chakraborty, Esha Sehanobish†, Munna Sarkar

1.2.3.3 Interaction of Merocyanine 540 with serum albumins: Photophysical and binding studies

Photophysical studies on binding interactions of a negatively charged anti-tumor photosensitizer, Merocyanine 540 (MC 540), with serum proteins, bovine serum albumin (BSA) and human serum albumin (HSA), have been performed using absorption and steady-state as well as time-resolved fluorescence techniques. Formation of ground state complex has been confirmed from the detailed studies of absorption spectra of MC 540 in presence of SAs producing isosbestic points. Binding between the proteins and MC 540, which perturbs the existing equilibrium between the fluorescent monomer and its non-fluorescent dimer, induces a remarkable enhancement in fluorescence anisotropy and intensity of MC 540 along with a red shift of its maximum. The binding stoichiometry of MC 540 and SAs are more than 1.0 which depicts that two types of complexes, i.e., 1:1 and 2:1 are formed with addition of varied concentration of protein. Both the steady-state and time-resolved fluorescence results show that in 2:1 complex one of the MC 540 molecules is exposed towards aqueous environment with a greater extent when bound with HSA compared to BSA due to the structural flexibility of that protein. Thermodynamic analyses using van Hoff plot indicate that the binding between MC 540 and individual SA is an entropy-driven phenomenon. The probable hydrophobic binding site has been located by denaturation of proteins, micropolarity measurement and Förster resonance energy transfer and that is further supported by molecular docking studies. Changes in circular dichroism spectra of BSA in presence of MC 540 depict secondary structural changes of the protein. The induced-CD shows that BSA due to its rigid structure generates chirality in MC

540 much more efficiently compared to HSA.

Mousumi Banerjee, Uttam Pal, Arijita Subudhhi, Abhijit Chakrabarti, Samita Basu

1.2.3.4 First experiment at tasca towards x-ray fingerprinting of element 115 decay chains

To identify the atomic number of superheavy nuclei produced in Ca-48-induced fusion-evaporation reactions, an experiment aiming at measuring characteristic X-rays is being prepared at GSI, Darmstadt, Germany. The gas-filled separator TASCAs will be employed, sending the residues towards the multi-coincidence detector setup TASI Spec. Two ion-optical modes relying on differing magnetic polarities of the quadrupole magnets can be used at TASCAs. New simulations and experimental tests of transmission and background suppression for these two focusing modes into TASI Spec are presented.

U Forsberg†...S Lahiri, M Maiti

1.2.3.5 Influence of 2'-Deoxy Sugar Moiety on Excited-State Protonation Equilibrium of Adenine and Adenosine with Acridine inside SDS Micelles: A Time-Resolved Study with Quantum Chemical Calculations

The protonation dynamics of the DNA base adenine (Ade) and its nucleoside 2'-deoxyadenosine (d-Ade) are investigated by monitoring the deprotonation kinetics of an N-heterocyclic DNA intercalator, acridine (Acr), in the confined environment of sodium dodecyl sulfate (SDS) micelles. Protonation of acridine (AcrH^+) occurs at the hydrophilic interface and this species remains in dynamic equilibrium with its deprotonated counterpart (Acr) inside the hydrophobic core of SDS micelles. Quenching of the fluorescence of AcrH^{+*} at 478 nm is observed after addition of Ade and d-Ade with Stern-Volmer constant (k_{SV}) 298 and 75M^{-1} , respectively, with a concomitant increment in Acr^* at 425 nm. Time-resolved fluorescence studies reveal quenching in the lifetime of AcrH^{+*} . The relative amplitude of AcrH^{+*} decreases from 0.97 to 0.51 and 0.97 to 0.89 with equimolar addition of Ade and d-Ade, respectively. These observations are explained by excited-state proton transfer (ESPT) from AcrH^{+*} to the bases. The reduced KSV value and negligible change in the relative amplitudes of AcrH^{+*} with d-Ade infer that ESPT is hindered substantially by the presence of a 2'-deoxy sugar unit. Transient time-resolved absorption spectra of Acr reflect that Ade reduces the absorbance of ${}^3\text{AcrH}^{+*}$; however, d-Ade keeps it unaltered for more than a time delay of 2 microsec. The optimized geometries calculated by quantum chemical methods reflect deprotonation of AcrH^{+*} with protonation at the N1 position of Ade, while it remains protonated with d-Ade. The hindered ESPT between AcrH^{+*} and d-Ade singles out the significance of the 2'-deoxy sugar moiety in controlling the deprotonation kinetics.

Manas Kumar Sarangi, Dhananjay Bhattacharyya, Samita Basu

1.2.3.6 Magnetic Field Effect on Photoinduced Electron Transfer Reaction Associated with Hydrogen Bond Formation in Homogeneous Medium

The effect of low magnetic field (MF) of the order of 0.01-0.08 T on the reactions involving spin-correlated radical ion pairs generated through electron transfer as intermediates is an interplay

between diffusion dynamics and spin dynamics of the individual radical ions in the solvent cage. In this paper, we have made an attempt to study photoinduced electron transfer reactions between three aromatic amines and acridone in ethanol medium using a weak external MF. Although the MF effect is conventionally observed appreciably in heterogeneous organized medium, in the present case a considerable MF effect is obtained in homogeneous medium, i.e., ethanol. The occurrence of this rare phenomenon has been attributed to the presence of water molecules as impurities in ethanol.

Brotati Chakraborty, Samita Basu

1.2.3.7 Separation of no-carrier-added Gd-149 from C-12 activated natural praseodymium matrix

Gd-149 was produced from the C-12 induced reaction on natural praseodymium target. No-carrier-added (nca) Gd-149 was separated from the bulk target matrix by liquid-liquid extraction (LLX) using cation exchanger di-(2-ethylhexyl)phosphoric acid (HDEHP) dissolved in cyclohexane. High separation factor of 2,450 was achieved at the optimal experimental condition when 1% HDEHP and 0.1 M HCl were used as organic and aqueous phases respectively. The result was also compared with the previous reports.

Moumita Maiti, Susanta Lahiri, BS Tomar†

1.2.3.8 A comparative study on the interaction with calf thymus DNA of a Ni(II) complex of the anticancer drug adriamycin and a Ni(II) complex of sodium 1,4-dihydroxy-9,10-anthraquinone-2-sulphonate

The anthracycline drug adriamycin and its metal complexes are efficient in treating several forms of human cancers with recognized antineoplastic activity attributed to strong interactions with DNA within the target cells. The hydroxy-9,10-anthraquinone unit present in the molecule controls and regulates drug action. Metal ions when linked to adriamycin help to reduce the generation of radicals responsible for toxic side effects. A complex of adriamycin with Ni(II) was prepared and its physicochemical characteristics and DNA-binding ability were compared to a Ni(II) complex of sodium-1,4-dihydroxy-9,10-anthraquinone-2-sulphonate (NaLH₂), an analog of adriamycin. Interactions with calf thymus DNA of both complexes were studied by UV-Vis and fluorescence spectroscopy. Binding parameters determined for both complexes agree with each other. Binding of the Ni(II)-adriamycin complex to DNA was five to eight times stronger than for the Ni(II) complex of the hydroxy-9,10-anthraquinone analog, Na-2[Ni(NaLH)(2)Cl-2]center dot 2H(2)O, i.e., Ni(NaLH)(2). The difference in binding was attributed to the presence of sugar units in adriamycin and to its absence in NaLH₂. Although the Ni(II) complex of the hydroxy-9,10-anthraquinone analog of adriamycin [Ni(NaLH)(2)] was slightly weaker in binding DNA than the drug and its Ni(II) complex, a much lower cost of the former justifies its consideration as a substitute for the anthracycline drugs that are now in use.

Partha Sarathi Guin†, PC Mandal, Saurabh Das†

1.2.3.9 Recent developments in nuclear data measurements and chemical separation methods in accelerator production of astatine and technetium radionuclides

The cyclotron produced neutron deficient technetium radionuclides (Tc-93, Tc94(m+g), Tc-95, Tc-96) have gained renewed interest in various fields, including nuclear imaging, provided they can be obtained in a pure form. Similarly, At-211 due to its moderate half-life and high intensity α -particle energy (both from At-211 as well as its transient decay product Po-211) is of prime interest in targeted therapy. Another interest is to study the astatine chemistry, which is least studied compared to other halogens due to its non-occurrence in natural systems. For maximum production of these radionuclides various parameters need to be standardized. A chemical separation is required to achieve high radiochemical purity before in-vivo application. This review describes various production routes of neutron deficient astatine and technetium radionuclides that have been reported after the year 2000. The analytical chemistry developed for separation of no-carrier-added (nca) Tc and At radionuclides in the same period is also discussed in detail.

S Lahiri, M Maiti

1.2.3.10 Effect of Lipid Molecule Headgroup Mismatch on Non Steroidal Anti-Inflammatory Drugs Induced Membrane Fusion

Membrane fusion is an essential process guiding many important biological events, which most commonly requires the aid of proteins and peptides as fusogenic agents. Small drug induced fusion at low drug concentration is a rare event. Only three drugs, namely, meloxicam (Mx), piroxicam (Px), and tenoxicam (Tx), belonging to the oxicam group of non steroidal anti-inflammatory drugs (NSAIDs) have been shown by us to induce membrane fusion successfully at low drug concentration. A better elucidation of the mechanism and the effect of different parameters in modulating the fusion process will allow the use of these common drugs to induce and control membrane fusion in various biochemical processes. In this study, we monitor the effect of lipid headgroup size mismatch in the bilayer on oxicam NSAIDs induced membrane fusion, by introducing dimyristoylphosphatidylethanolamine (DMPE) in dimyristoylphosphatidylcholine (DMPC) small unilamellar vesicles (SUVs). Such headgroup mismatch affects various lipid parameters which includes inhibition of trans-bilayer motion, domain formation, decrease in curvature, etc. Changes in various lipidic parameters introduce defects in the membrane bilayer and thereby modulate membrane fusion. SUVs formed by DMPC with increasing DMPE content (10, 20, and 30 mol%) were used as simple model membranes. Transmission electron microscopy (TEM) and differential scanning calorimetry (DSC) were used to characterize the DMPC-DMPE mixed vesicles. Fluorescence assays were used to probe the time dependence of lipid mixing, content mixing, and leakage and also used to determine the partitioning of the drugs in the membrane bilayer. How the inhibition of trans-bilayer motion, heterogeneous distribution of lipids, decrease in vesicle curvature, etc., arising due to headgroup mismatch affect the fusion process has been isolated and identified here. Mx amplifies these effects maximally followed by Px and Tx. This has been correlated to the enhanced partitioning of the hydrophobic Mx compared to the more hydrophilic Px and Tx in the mixed bilayer.

Sutapa Mondal, Munna Sarkar

1.2.3.11 Production cross section of At radionuclides from ${}^7\text{Li} + {}^{\text{nat}}\text{Pb}$ and ${}^9\text{Be} + {}^{\text{nat}}\text{Tl}$ reactions

Earlier we reported theoretical studies on the probable production of astatine radionuclides from ${}^6,7\text{Li}$ - and ${}^9\text{Be}$ -induced reactions on natural lead and thallium targets, respectively. The production of astatine radionuclides were investigated experimentally with two heavy-ion-induced reactions: ${}^9\text{Be} + {}^{\text{nat}}\text{Tl}$ and ${}^7\text{Li} + {}^{\text{nat}}\text{Pb}$. Formation cross sections of the evaporation residues, ${}^{207,208,209,210}\text{At}$, produced in the (HI,xn) channel, were measured by the stacked-foil technique followed by off-line spectrometry at low incident energies (<50 MeV). Measured excitation functions were interpreted in terms of a compound nuclear reaction mechanism using Weisskopf-Ewing and Hauser-Feshbach models. Measured cross-section values are lower than the respective theoretical predictions.

Moumita Maiti, Lahiri Susanta

1.2.3.12 Binding interaction of photoactive drug Merocyanine 540 with fiber like protein spectrin: A spectroscopic approach

Merocyanine 540 (MC 540) belongs to the family of benzoxazolmerocyanine dyes with heterocyclic aromatic groups linked by a polymethine chain. Optical characteristics of such compounds are very sensitive to the changes in environmental factors, which make it a useful tool in biophysical research. We have studied the binding interaction of MC 540 with a fiber like network forming protein, spectrin, which was reported to interact with a large number of other proteins, e.g. actin, adducin, ankyrin and band 4.1, and also with a variety of hydrophobic ligands, tertiary amine local anesthetics and antitumor antibiotics chromomycin and mithramycin. Spectrin binds with MC 540 with a moderate affinity that has been studied using absorption and fluorescence spectroscopy. Thermodynamic basis of such a binding of MC 540 to erythroid spectrin is also understood from fluorescence quenching data. In addition to the evaluation of the binding affinities and associated thermodynamic parameters, the circular dichroism (CD) spectroscopy also throws light on the structural basis of recognition and conformational changes of the membrane skeletal protein, spectrin bound with the drug MC 540. Theoretical docking studies help to predict probable binding site of MC 540 in spectrin.

Mousumi Banerjee, Abhijit Chakrabarti, Samita Basu

1.2.3.13 Photochemical E(trans)-Z(cis)-E Isomerization of an Amphiphilic Cholest-5-en-3 beta-yl(E)-9-anthracenprop-2-enoate on Solid Substrate

Surface morphology and photochemical isomerization properties; of monolayers of anthracene acrylic acid derivative with cholesterol (a new class of bistable compound), cholest-5-en-3 beta-yl(E)-9-anthracenprop-2-enoate (CAE), transferred onto quartz substrates were studied. The spectroscopic and photochromic behavior of CAE on solid substrates and in solution are compared keeping in mind the possible application of CAE in constructing molecular electronic devices. Monolayers of the trans(E)-isomer of CAE transferred from the air water interface onto quartz plates show regular distribution of "holes" in the film, whereas similar monolayers of the cis(Z)-isomer of CAE (similar to 96%) show very smooth surfaces, free from any definite structures. The surface pressure-area (pi-A) isotherms of both.. monolayers at the air water interface are found to be irreversible, indicating formation of 2D/3D aggregates for both isomers. The surface potential area

(Delta V-A) isotherms of the two isomers predict the orientation of their molecular dipoles to be different. The fluorescence peak intensity of the E-isomer of CAE in transferred monolayers shows a sharp decrease upon irradiation with 405 nm light, indicating the successful E-to-Z isomerization in the monolayer. Fluorescence excitation and emission polarization studies on the solid substrate also confirm the change of molecular orientation resulting from the E-to-Z isomerization. The isomerization rate is found to be faster in solid substrates than that in the solution phase. Six alternate monolayers of E-CAE and triplet sensitizer (lipophilic porphyrin) film shows 5% efficiency of Z-to-E isomerization upon exciting on 550 nm, where porphyrin has substantial absorbance where as film of 24 monolayers of mixture solution of the E-isomer of CAE (1 mM) and lipophilic porphyrin (1 mM) in chloroform increases 5-fold efficiency of Z-to-E conversion. These results suggest that the E-CAE has the potential to be used in making optical data storage devices employing the trans-cis isomerization process.

Suthari Prashanthi†...Soumen Basak, et al

1.2.3.14 New measurement of cross sections of evaporation residues from the $^{nat}\text{Pr}+^{12}\text{C}$ reaction: A comparative study on the production of ^{149}Tb

Production cross sections of evaporation residues, ^{149}Tb , ^{150}Tb , ^{151}Tb , and ^{149}Gd , are measured using the stacked foil technique followed by off-line γ -spectrometry in ^{12}C -induced reactions on naturally abundant mononuclidic praseodymium target in the 44- to 79-MeV incident energy range. Measured data are interpreted by comparison with previous measurements and theoretical predictions of the nuclear reaction model code PACE4. About 5% and 14% of the theoretical cross sections have been measured for ^{149}Tb and ^{150}Tb , respectively. The new cross sections of ^{149}Tb complement those measured earlier by α spectrometry. Cross sections of ^{151}Tb are comparable to the theory. Cumulative cross sections of ^{149}Gd shed light on the nuclear reaction mechanism. In addition, the discussion shows the feasibility of producing ^{149}Tb in ρ - and α -induced reactions on gadolinium isotopes.

Moumita Maiti

1.2.3.15 Production and separation of no-carrier-added thallium isotopes from proton irradiated $^{nat}\text{Hg}_2\text{Cl}_2$ matrix

For the first time, $^{nat}\text{Hg}_2\text{Cl}_2$ target has been used to produce no-carrier-added-NCA $^{197,198,199,200,201}\text{Tl}$ radionuclides using $^{nat}\text{Hg}(p, xn)$ reaction. Liquid-liquid extraction technique was employed in order to separate radiothallium from the bulk mercury matrix using liquid anion exchanger trioctylamine (TOA) dissolved in cyclohexane. In order to verify the presence of stable Hg in Tl fraction, the entire process was repeated with stable salts of Hg and Tl and the extent of separation was examined by Inductively Coupled Plasma Optical Emission Spectroscopy (ICP-OES). High separation factors were observed both by radiometric and ICP-OES technique when 0.1 M HNO_3 and 0.1 M TOA were used as aqueous and organic phase, respectively. The Hg contamination was less than 0.3 ppm in the aqueous phase containing Tl after three times of extraction at the optimal condition.

Binita Dutta, Moumita Maiti, Susanta Lahiri

1.2.3.16 Separation of ^{134}Cs and ^{133}Ba radionuclides by calcium alginate beads

The uptake behavior of long-lived radionuclides such as ^{134}Cs (2.06 years), ^{137}Cs (30 years) or ^{133}Ba (10.54 years) on calcium alginate (CA) beads have been investigated. The CA beads are able to remove ^{133}Ba (92%) at pH 7 after 90 min of exposure from the binary mixture of two. The separation method of short-lived daughter ^{137}Ba (2.55 min) from its long-lived parent ^{137}Cs (30 years) using this CA beads have also been developed.

Ajoy Mandal, Susanta Lahiri

1.2.3.17 First superheavy element experiments at the GSI recoil separator TASCA: The production and decay of element 114 in the $^{244}\text{Pu}(^{48}\text{Ca},3-4n)$ reaction

Experiments with the new recoil separator, Transactinide Separator and Chemistry Apparatus (TASCA), at the GSI were performed by using beams of ^{48}Ca to irradiate targets of $^{206-208}\text{Pb}$, which led to the production of $^{252-254}\text{No}$ isotopes. These studies allowed for evaluation of the performance of TASCA when coupled to a new detector and electronics system. By following these studies, the isotopes of element 114 ($^{288-291}114$) were produced in irradiations of ^{244}Pu targets with ^{48}Ca beams at compound nucleus excitation energies around 41.7 and 37.5 MeV, demonstrating TASCA's ability to perform experiments with picobarn-level cross sections. A total of 15 decay chains were observed and were assigned to the decay of $^{288-291}114$. A new α -decay branch in ^{281}Ds was observed, leading to the new nucleus ^{277}Hs .

JM Gates†, S Lahiri, M Maiti, et al

1.2.3.18 The recoil transfer chamberAn interface to connect the physical preseparator TASCA with chemistry and counting setups

Performing experiments with transactinide elements demands highly sensitive detection methods due to the extremely low production rates (one-atom-at-a-time conditions). Preseparation with a physical recoil separator is a powerful method to significantly reduce the background in experiments with sufficiently long-lived isotopes ($t_{1/2} \geq 0.5$ s). In the last years, the new gas-filled TransActinide Separator and Chemistry Apparatus (TASCA) was installed and successfully commissioned at GSI. Here, we report on the design and performance of a Recoil Transfer Chamber (RTC) for TASCAan interface to connect various chemistry and counting setups with the separator. Nuclear reaction products recoiling out of the target are separated according to their magnetic rigidity within TASCA, and the wanted products are guided to the focal plane of TASCA. In the focal plane, they pass a thin Mylar window that separates the ~ 1 mbar atmosphere in TASCA from the RTC kept at ~ 1 bar. The ions are stopped in the RTC and transported by a continuous gas flow from the RTC to the ancillary setup. In this paper, we report on measurements of the transportation yields under various conditions and on the first chemistry experiments at TASCAan electrochemistry experiment with osmium and an ion exchange experiment with the transactinide element rutherfordium.

J Evena†, J Ballofa†, W Bröchle†...D Nayak, et al

1.2.3.19 Deciphering the host-guest chemistry of Acridine Yellow and Cucurbit[7]uril: An integrated spectroscopic and calorimetric study

The study of binding of small molecules with supramolecular architecture comprises of one of the thriving areas of research today. In the present study, spectroscopic techniques have been used to decipher the interaction of Acridine Yellow with Cucurbit[7]uril and explore the consequence of host-guest interaction on the photophysical properties of the dye. Moreover, isothermal titration calorimetry has been used to unravel the thermodynamics of interaction. The probable causes of incongruity of the results obtained from spectroscopy and calorimetry have been rationalized. ^1H NMR study and geometry optimization of the guest molecule confirm the actual mode of host-guest interaction.

Brotati Chakraborty, Samita Basu

1.2.3.20 Associated electron and proton transfer between Acridine and Triethylamine in AOT reverse micelles probed by laser flash photolysis with magnetic field

Laser flash photolysis with magnetic field (MF ~ 0.08 T) has been used to study interaction between Acridine (Acr) and Triethylamine (TEA) in reverse micelles with $w_o=2.5-40$. Dynamic protonation equilibrium exists between ^3Acr and $^3\text{AcrH}^+$. The intermediates indicate excited-state proton transfer (PT) between $^3\text{AcrH}^+$ and TEA. However, application of MF highlights the formation of geminate radical ion pairs (RIPs) with triplet spin-correlation, a signature of latent photoinduced electron transfer between $^3\text{AcrH}^+$ and TEA co-exists with PT. Magnetic field effect (MFE) is prominent for smaller w_o showing importance of optimum separation between RIP to maximize MFE, whereas PT remains unaltered.

Manas Kumar Sarangi, Samita Basu

1.2.3.21 Synthesis and photo physical properties of Au @ Ag (core @ shell) nanoparticles disperse in poly vinyl alcohol matrix

Synthesis of core @ shell (Au @ Ag) nanoparticle with varying silver composition has been carried out in aqueous poly vinyl alcohol (PVA) matrix. Core gold nanoparticle (~ 15 nm) has been synthesized through seed-mediated growth process. Synthesis of silver shell with increasing thickness ($\sim 1-5$ nm) has been done by reducing Ag^+ over the gold sol in the presence of mild reducing ascorbic acid. Characterization of Au @ Ag nanoparticles has been done by UV-Vis, High resolution transmission electron microscope (HRTEM) and energy dispersive X-ray (EDX) spectroscopic study. The blue shift of surface plasmon resonance (SPR) band with increasing mole fraction of silver has been interpreted due to dampening of core, i.e. Au SPR by Ag. The dependence of nonlinear optical response of spherical core @ shell nanoparticles has been investigated as a function of relative composition of each metal. Simulation of SPR extinction spectra based on quasi-static theory is done. A comparison of our experimental and the simulated extinction spectra using quasi-static theory of nanoshell suggests that our synthesized bimetallic particles have core @ shell structure rather than bimetallic alloy particles.

Santanu Pyne†, Priyanka Sarkar†, Samita Basu, et al

1.2.3.22 Direct observation of radical intermediates during electron transfer between DNA and a ternary copper complex

The photoinduced electron transfer (PET) reaction within a ternary copper complex $[\text{Cu}(\text{phen})(\text{Htrp})]^+$ (Htrp: L-tryptophanato; phen: 1,10-phenanthroline) (**1**) and in presence of DNA has been studied in homogeneous buffer medium and in reverse micelles. An intramolecular electron transfer occurs within the photoexcited complex (**1**) from tryptophan to phen. The copper complex can displace ethidium bromide from DNA backbone and on photoexcitation can oxidize DNA in a deoxygenated environment due to intermolecular electron transfer, although the intramolecular electron transfer is thermodynamically favorable. A prominent magnetic field effect (MFE) has been found even in homogeneous aqueous medium for the triplet born radicals both in case of intra and intermolecular electron transfer reactions. In case of intramolecular electron transfer the observation of MFE is similar to that of linked donor-acceptor system. However the observation of MFE for the intermolecular electron transfer between non-covalently bound complex-DNA systems is rather rare. Some non-covalent weak interaction, e.g. hydrophobic interaction between the phen ligand and DNA base pairs and electrostatic force of attraction between $[\text{Cu}(\text{phen})(\text{Htrp})]^+$ complex and DNA may lead to partial intercalation of the copper complex within DNA that is responsible for such a rare observation.

Debarati Dey, Samita Basu

1.2.3.23 Separation of no-carrier-added $^{107,109}\text{Cd}$ from proton induced silver target: classical chemistry still relevant

The classical chemistry like precipitation technique is relevant even in modern days trans-disciplinary research from the view point of green chemistry. A definite demand of no-carrier-added (nca) cadmium tracers, namely $^{107,109}\text{Cd}$, has been realized for diverse applications. Development of efficient separation technique is therefore important to address the purity of the tracers for various applications. No-carrier-added $^{107,109}\text{Cd}$ radionuclides were produced by bombarding natural silver target matrix with 13 MeV protons, which gave ~ 15 MBq/ $\mu\text{A h}$ yield for nca ^{107}Cd . The nca cadmium radionuclides were separated from the natural silver target matrix by precipitating Ag as AgCl. The developed method is an example wherein green chemistry is used in trans-disciplinary research. The method is also simple, fast, cost effective and environmentally benign.

Moumita Maiti, Susanta Lahiri, BS Tomar†

1.2.3.24 Photophysical behavior of acridine with amines within the micellar microenvironment of SDS: a time-resolved fluorescence and laser flash photolysis study

The photophysical behavior of acridine (Acr) shows a facilitated water assisted protonation equilibrium between its deprotonated ($\text{Acr}^* \sim 3.4$ ns) and protonated forms ($\text{AcrH}^{+*} \sim 33$ ns) within a confined environment of sodium dodecyl sulphate (SDS) micelles above the critical micellar concentration of 8 mM. The acidic interface of the micelles is capable of protonating Acr whereas deprotonated Acr is partitioned into the hydrophobic core. The time-resolved-area-normalized-emission spectra confirm the presence of both Acr^* and AcrH^{+*} , while time-resolved-emission spectra depict time evolution between them. Quenching of AcrH^{+*} with triethylamine (TEA) results in a

linear SternVolmer (SV) plot, whereas non-linearity arises with N,N-dimethylaniline (DMA). Both steady-state and time-resolved quenching results with TEA are explained on the basis of excited state proton transfer (ESPT), however the reasons behind the quenching of excited Acr with DMA are proposed as ESPT followed by a photoinduced electron transfer. Partitioning of DMA at the interface makes it accessible for both Acr* and AcrH⁺* in hydrophobic and hydrophilic regions of micelles respectively. The rate of electron transfer at the interface is found to be slower compared to that in the hydrophobic core. Characterization of transient intermediates formed during ESPT and PET between Acr and amines by laser-flash photolysis also supports the observation obtained during fluorescence studies. The mode of interactions between Acr and amines inside micelles is controlled by the localization of the proton/electron donors and acceptors in different hydrophobic or hydrophilic regions of such nano-confined environments.

Manas Kumar Sarangi, Samita Basu

1.2.4 Structural Genomics

1.2.4.1 Faster heme loss from hemoglobin E than HbS, in acidic pH: Effect of aminophospholipids

We report studies on loss of heme at or below pH 3.0 from two clinically important hemoglobin variants, HbE and HbS, in the presence and absence of phospholipid membranes. The kinetics of heme loss has been studied at pH 3.0 to simulate the same at a faster rate than at physiological pH, for spectroscopic investigation. Results obtained from the study clearly establish the probable fate of the lost heme to partition into the phospholipid bilayer independent of the pH range. This is also of particular importance to membranes containing the aminophospholipid and cholesterol which are predominantly localized in the inner leaflet of erythrocytes. Absorption measurements indicated such loss of heme when the Soret peak at 415 nm blue-shifted to 380 nm at pH 3.0. The extent of this blue shift decreased from 35 nm to 15 nm in the presence of small unilamellar vesicles of both dimyristoyl- and dioleoyl-based phosphatidylcholine and phosphatidylethanolamine, indicating partitioning of the released heme in the membrane bilayer. The kinetics of heme loss was faster from HbE than HbA and HbS, obeying first-order reaction kinetics. Released heme could be involved in the premature destruction of erythrocytes in hemoglobin disorders.

Mousumi Banerjee, Malini Pramanik, Dipankar Bhattacharya, Mohin Lahiry, Samita Basu, Abhijit Chakrabarti

1.2.4.2 Functional Implications of the Conformational Switch in AICD Peptide upon Binding to Grb2-SH2 Domain

It has been hypothesized previously that synergistic effect of both amyloid precursor protein intracellular C-terminal domain (AICD) and A β aggregation could contribute to Alzheimer's disease pathogenesis. Structural studies of AICD have found no stable globular fold over a broad range of pH. Present work is based on the premises that a conformational switch involving the flipping of C-terminal helix of AICD would be essential for effective binding with the Src homology 2 (SH2) domain of growth factor receptor binding protein-2 (Grb2) and subsequent initiation of Grb2-mediated endo-lysosomal pathway. High-resolution crystal structures of Grb2-SH2 domain bound to AICD peptides reveal a unique mode of binding where the peptides assume a noncanonical conformation that is unlike other structures of AICD peptides bound to protein-tyrosine-binding domains or that

of its free state; rather, a flipping of the C-terminal helix of AICD is evident. The involvement of different AICD residues in Grb2-SH2 interaction is further elucidated through fluorescence-based assays. Our results reveal the significance of a specific interaction of the two molecules to optimize the rapid transport of AICD inside endosomal vesicles presumably to reduce the cytotoxic load.

Samir Das, Mithu Raychaudhuri, Udayaditya Sen, Debashis Mukhopadhyay

1.2.4.3 F-cell levels are altered with erythrocyte density in sickle cell disease

Lighter cells from density fractionated erythrocytes of sickle cell disease (SCD) patients carry higher amount of externalized phosphatidylserine (PS) and cell surface glycoporphins compared to the denser counterparts. Further analysis also revealed that the denser cells contained higher levels of fetal hemoglobin (HbF) compared to the lighter cells, supported by the presence of larger number of F-cells in these populations. In this report, we have found direct evidence on the higher survival of the HbF rich erythrocytes in SCD.

Sumanta Basu... Abhijit Chakrabarti

1.2.4.4 Intrinsically Unstructured Proteins and Neurodegenerative Diseases: Conformational Promiscuity at its Best

Neurodegenerative diseases are complex, multifactorial disorders where misfolding of proteins cause aberrant protein protein interactions. They are not usually characterized by specific mutations especially for nonfamilial disease types. Most of the causative proteins, however, are intrinsically unstructured (IUP), loss of whose fine balance could play pivotal role in these processes. Very fast conformational switch of these IUPs between different functional forms, so as to choose different interaction partners and different functional niches within the cell, is the basic premise on which these proteins maintain their interaction network. We are working on the hypothesis that even small perturbations in conformation leads to disruption of the network and to the disease phenotype. Based on a comprehensive data search, the evidence was obtained for the role of IUPs in neurodegenerative disorders, and their mode of action through conformational promiscuity is elaborated through three case studies.

Samir Das, Debashis Mukhopadhyay

1.2.4.5 Cytosolic aggregates perturb the degradation of nontranslocated secretory and membrane proteins

A wide range of diseases are associated with the accumulation of cytosolic protein aggregates. The effects of these aggregates on various aspects of normal cellular protein homeostasis remain to be determined. Here we find that cytosolic aggregates, without necessarily disrupting proteasome function, can markedly delay the normally rapid degradation of nontranslocated secretory and membrane protein precursors. In the case of mammalian prion protein (PrP), the nontranslocated fraction is recruited into preexisting aggregates before its triage for degradation. This recruitment permits the growth and persistence of cytosolic PrP aggregates, explaining their apparent "self-conversion" seen in earlier studies of transient proteasome inhibition. For other proteins, the

aggregate-mediated delay in precursor degradation led to aggregation and/or soluble residence in the cytosol, often causing aberrant cellular morphology. Remarkably, improving signal sequence efficiency mitigated these effects of aggregates. These observations identify a previously unappreciated consequence of cytosolic aggregates for nontranslocated secretory and membrane proteins, a minor but potentially disruptive population the rapid disposal of which is critical to maintaining cellular homeostasis.

Oishee Chakrabarti, Neena S Rane†, Ramanujan S Hegde†

1.2.4.6 Elevated levels of redox regulators, membrane-bound globin chains, and cytoskeletal protein fragments in hereditary spherocytosis erythrocyte proteome

Objective: Hereditary spherocytosis (HS), a common inherited hemolytic anemia characterized by decreased deformability, reduced surface to volume ratio, and increased osmotic fragility of the spheroidal erythrocytes, is associated with several mutations of alpha-and beta-spectrin, ankyrin, band 3, band 4.2. HS manifests itself with high degrees of clinical heterogeneity and the molecular events leading to premature hemolysis of the spherocytes are unclear. We have employed proteomic techniques to identify differentially regulated proteins in the membrane and hemoglobin-depleted cytosol of HS erythrocytes. **Methods:** We have employed 2-D gel electrophoresis and tandem matrix assisted laser desorption ionization-time of flight/time of flight mass spectrometry to investigate the differential proteome profiling of membrane and hemoglobin-depleted cytosol of erythrocytes isolated from the peripheral blood samples of HS patients and normal volunteers. **Results:** Our study showed that redox regulators are up-regulated; while a co-chaperone and a nucleotide kinase are down-regulated in HS erythrocyte cytosol. We observed elevated levels of membrane-associated globin chains and low-molecular weight fragments of several major cytoskeletal proteins. **Conclusion:** The observed changes in the erythrocyte proteomes indicate altered redox regulation, nucleotide metabolism, protein aggregation and/or degradation, cytoskeletal disorganization, and severe oxidative stress in HS. Taken together, this study could enlighten upon disease progression and pathophysiology of HS.

Sutapa Saha, Rajeswari Ramanathan, Avik Basu, Debasis Banerjee†, Abhijit Chakrabarti

1.3 Developmental Work

1.3.0.7 Environmental Activity Assessment

To search for a possible distribution of the radioactivity from Fukushima reactor accident (on March 11, 2011) in the eastern region of the Indian continent we have analysed air and soil samples for presence of potential radioisotopes like ^{137}Cs , ^{131}I , ^{133}Xe and others. Qualitative assessment of the radioactivity distribution in the environment around the area was carried out. Presence of potential candidates like ^{137}Cs , ^{131}I , ^{133}Xe or others from the Fukushima fallout could not be conclusively ascertained till date. This work was carried out with the logistic support from CBAUNP project.

Maitreyee Nandy, M Saha Sarkar, A Bisoi, S Ray, D Pramanik†, B Chatterjee†, A Priyant†

1.4 Publications

1.4.1 Publications in Books/Monographs & Volumes Edited

Brotati Chakraborty, Adity Bose and Samita Basu, Electron transfer and hydrogen abstraction in biologically relevant systems in Selectivity, Control, and Fine Tuning in High-Energy Chemistry, Eds: Dmitri V Stass and Vladimir I Feldman (Research Signpost, India, 2011, 93p)

Sayantani Ghosh, Arunabha Chakrabarti, Debashis Mukhopadhyay, 'Patch'-ing Up the Neurons: Revival or Enervation? in Hedgehog Signalling, Ed Gerald Litwack, Vitamins and Hormones, V 88 (Academic Press, Burlington, 2012, 439p)

1.4.2 Journal Publication

1.4.2.1 Biophysics

AK Pal, D Pal†, A new concept of photon having coexistent wave-particle duality, Physics Essays **25** (2012) 34

Biswapathik Pahari, Sandipan Chakraborty, Pradeep K Sengupta, Encapsulation of 3-hydroxyflavone in gamma-cyclodextrin nanocavities: Excited state proton transfer fluorescence and molecular docking studies, Journal of Molecular Structure **1006** (2011) 483

Manjit K Bhattacharyya†, P Grihanjali Devi, Dipak Dasgupta, Sanchay J Bora†, Birinchi K Das†, Solid and solution structures and DNA binding properties of [M-II(4-CNpy)(2)(SO4)(H2O)(3)]center dot H2O for M = Cu, Co, Ni, Polyhedron **35** (2012) 62

Mita Ghosh, Arun K Pal, Radio-protective activity of gallic acid in a bacterial system, Journal of Natural Pharmaceuticals **2** (2011) 210

Mita Ghosh, Arun K Pal, Radioprotection imparted by four spices in a bacterial system, Pharmacognosy Communications **2** (2012) 42

Mogurampelly Santosh†, Swati Panigrahi, Dhananjay Bhattacharyya, AK Sood†, Prabal K Maiti†, Unzipping and binding of small interfering RNA with single walled carbon nanotube: A platform for small interfering RNA delivery, Journal of Chemical Physics **136** (2012) Art No: 065106

Parijat Majumder, Dipak Dasgupta, Effect of DNA Groove Binder Distamycin A upon Chromatin Structure, PLOS ONE **6** (2011) Art No: e26486

Sudipta Pal, Mili Das†, Rahul Banerjee, Dipak Dasgupta, Biphasic Association of T7 RNA Polymerase and a Nucleotide Analogue, Cibacron Blue as a Model to Understand the Role of Initiating Nucleotide in the Mechanism of Enzyme Action, Journal of Biomolecular Structure & Dynamics **29** (2011) 153

Swati Panigrahi, Anuradha Bhattacharya, Sangam Banerjee, Dhananjay Bhattacharyya, Interaction of nucleobases with wrinkled graphene surface: Dispersion Corrected DFT and AFM Studies,

Journal of Physical Chemistry **C116** (2012) 4374

Swati Panigrahi, Rahul Pal, Dhananjay Bhattacharyya, Structure and Energy of Non-Canonical Basepairs: Comparison of Various Computational Chemistry Methods with Crystallographic Ensembles, *Journal of Biomolecular Structure & Dynamics* **29** (2011) 541

Swati Panigrahi, Anuradha Bhattacharya, Debashree Bandyopadhyay†, Slawomir J Grabowski†, Dhananjay Bhattacharyya, Sangam Banerjee, Wetting Property of the Edges of Monoatomic Step on Graphite: Frictional-Force Microscopy and ab Initio Quantum Chemical Studies, *Journal of Physical Chemistry* **C115** (2011) 14819

Tapas Kumart Mandal, Niladri Sekhar Das, Correlation of testicular toxicity and oxidative stress induced by chlorpyrifos in rats, *Human & Experimental Toxicology* **30** (2011) 1529

1.4.2.2 Chemical Sciences

Ajoy Mandal, Susanta Lahiri, Separation of Cs-134 and Ba-133 radionuclides by calcium alginate beads, *Journal of Radioanalytical and Nuclear Chemistry* **290** (2011) 115

Binita Dutta, Moumita Maiti, Susanta Lahiri, Production and separation of no-carrier-added thallium isotopes from proton irradiated (Hg₂Cl₂)-Hg-nat matrix, *Applied Radiation and Isotopes* **69** (2011) 1337

Brotati Chakraborty, Samita Basu, Deciphering the host-guest chemistry of Acridine Yellow and Cucurbit[7]uril: An integrated spectroscopic and calorimetric study, *Chemical Physics Letters* **507** (2011) 74

Brotati Chakraborty, Samita Basu, Magnetic Field Effect on Photoinduced Electron Transfer Reaction Associated with Hydrogen Bond Formation in Homogeneous Medium, *Applied Magnetic Resonance* **42** (2012) 5

Debarati Dey, Samita Basu, Direct observation of radical intermediates during electron transfer between DNA and a ternary copper complex, *Journal of Luminescence* **131** (2011) 732

J Evena†, J Ballofa†, W Bröchle†...D Nayak, et al, The recoil transfer chamberAn interface to connect the physical preseparator TASCA with chemistry and counting setups, *Nuclear Instruments and Methods in Physics Research Section A* **638** (2011) 157

JM Gates†, S Lahiri, M Maiti, et al, First superheavy element experiments at the GSI recoil separator TASCA: The production and decay of element 114 in the ²⁴⁴Pu(⁴⁸Ca,3-4n) reaction, *Physical Review* **C83** (2011) Art No: 054618

Manas Kumar Sarangi, Dhananjay Bhattacharyya, Samita Basu, Influence of 2'-Deoxy Sugar Moiety on Excited-State Protonation Equilibrium of Adenine and Adenosine with Acridine inside SDS Micelles: A Time-Resolved Study with Quantum Chemical Calculations, *Chem Phys Chem* **13** (2012) 525

Manas Kumar Sarangi, Samita Basu, Associated electron and proton transfer between Acridine

and Triethylamine in AOT reverse micelles probed by laser flash photolysis with magnetic field, *Chemical Physics Letters* **506** (2011) 205

Manas Kumar Sarangi, Samita Basu, Photophysical behavior of acridine with amines within the micellar microenvironment of SDS: a time-resolved fluorescence and laser flash photolysis study, *Physical Chemistry Chemical Physics* **13** (2011) 16821

Moumita Maiti, Susanta Lahiri, BS Tomar†, Separation of no-carrier-added Gd-149 from C-12 activated natural praseodymium matrix, *Journal of Radioanalytical and Nuclear Chemistry* **291** (2012) 427

Moumita Maiti, New measurement of cross sections of evaporation residues from the Pr-nat+C-12 reaction: A comparative study on the production of Tb-149, *Physical Review* **C84** (2011) Art No: 044615

Moumita Maiti, Probable nuclear reactions to produce proton rich rhenium radionuclides, *Journal of Radioanalytical and Nuclear Chemistry* **290** (2011) 11

Moumita Maiti, Susanta Lahiri, Production cross section of At radionuclides from ${}^7\text{Li}+{}^{\text{nat}}\text{Pb}$ and ${}^9\text{Be}+{}^{\text{nat}}\text{Tl}$ reactions, *Physical Review* **C84** (2011) Art No: 067601

Moumita Maiti, Susanta Lahiri, BS Tomar† Separation of no-carrier-added Cd-107, Cd-109 from proton induced silver target: classical chemistry still relevant, *Journal of Radioanalytical and Nuclear Chemistry* **288** (2011) 115

Mousumi Banerjee, Abhijit Chakrabarti, Samita Basu, Binding interaction of photoactive drug Merocyanine 540 with fiber like protein spectrin: A spectroscopic approach, *Journal of the Indian Chemical Society* **88** (2011) 1895

Mousumi Banerjee, Uttam Pal, Arijita Subudhhi, Abhijit Chakrabarti, Samita Basu, Interaction of Merocyanine 540 with serum albumins: Photophysical and binding studies, *Journal of Photochemistry and Photobiology* **B108** (2012) 23

Partha Sarathi Guin†, PC Mandal, Saurabh Das†, A comparative study on the interaction with calf thymus DNA of a Ni(II) complex of the anticancer drug adriamycin and a Ni(II) complex of sodium 1,4-dihydroxy-9,10-anthraquinone-2-sulphonate, *Journal of Coordination Chemistry* **65** (2012) 705

Piyal Das†, Partha Sarathi Guin†, Parikshit C Mandal, et al, Cyclic voltammetric studies of 1,2,4-trihydroxy-9,10-anthraquinone, its interaction with calf thymus DNA and anti-leukemic activity on MOLT-4 cell lines: a comparison with anthracycline anticancer drugs, *Journal of Physical Organic Chemistry* **24** (2011) 774

S Lahiri, M Maiti, Recent developments in nuclear data measurements and chemical separation methods in accelerator production of astatine and technetium radionuclides, *Radiochimica Acta* **100** (2012) 85

Santanu Pyne†, Priyanka Sarkar†, Samita Basu, et al, Synthesis and photo physical properties of Au @ Ag (core @ shell) nanoparticles disperse in poly vinyl alcohol matrix, *Journal of Nanopar-*

title Research **13** (2011) 1759

Sreeja Chakraborty, Esha Sehanobish†, Munna Sarkar, Binding of Cu(II) complexes of oxicam NSAIDs to alternating AT and homopolymeric AT sequences: differential response to variation in backbone structure, *Journal of Biological Inorganic Chemistry* **17** (2012) 475

Susanta Lahiri, SK Das†, ARCEBS in brief, *Journal of Radioanalytical and Nuclear Chemistry* **290** (2011) 1

Sutapa Mondal, Munna Sarkar, Effect of Lipid Molecule Headgroup Mismatch on Non Steroidal Anti-Inflammatory Drugs Induced Membrane Fusion, *Langmuir* **27** (2011) 15054

Suthari Prashanthi†, P Hemant Kumar†, D Siva†, Srinivasa Rao Lanke†, V Jayathirtha Rao†, Soumen Basak, Prakriti Ranjan Bangal†, Photochemical E(trans)-Z(cis)-E Isomerization of an Amphiphilic Cholest-5-en-3 beta-yl(E)-9-anthraceneprop-2-enoate on Solid Substrate, *Journal of Physical Chemistry* **C115** (2011) 20682

U Forsberg†, P Golubev†, LG Sarmiento, S Lahiri, M Maiti, First experiment at tasca towards x-ray fingerprinting of element 115 decay chains, *Acta Physica Polonica* **B43** (2012) 305

1.4.2.3 C&MB

Antara De, Wnt/Ca²⁺ signaling pathway: a brief overview, *Acta Biochimica Et Biophysica Sinica* **43** (2011) 745

Anup Kumar Maity, Alakananda Goswami, Partha Saha, Identification of substrates of an S-phase cell cycle kinase from *Leishmania donovani*, *FEBS Letters* **585** (2011) 2635

Jayeeta Ghose, Mithun Sinha, Eashita Das, Nihar R Jana†, NP Bhattacharyya, Regulation of miR-146a by RelA/NFkB and p53 in STHdh(Q111)/Hdh(Q111) Cells, a Cell Model of Huntington's Disease, *PLOS One* **6** (2011) Art No: e23837

Maitree Biswas†, Susmita Khamrui, Udayaditya Sen, Jhimli Dasgupta†, Overexpression, purification, crystallization and preliminary X-ray analysis of CheY4 from *Vibrio cholerae* O395, *Acta Crystallographica* **F67** (2011) 1645

Mithun Sinha, Jayeeta Ghose, Nitai P Bhattacharyya, Micro RNA-214,-150,-146a and-125b target Huntingtin gene, *RNA Biology* **8** (2011) 1005

Moumita Datta, Ananyo Choudhury†, Ansuman Lahiri†, Nitai P Bhattacharyya, Genome wide gene expression regulation by HIP1 Protein Interactor, HIPPI: Prediction and validation, *BMC Genomics* **12** (2011) Art No: 463

Moumita Datta, Nitai P Bhattacharyya, Regulation of RE1 Protein Silencing Transcription Factor (REST) Expression by HIP1 Protein Interactor (HIPPI), *Journal of Biological Chemistry* **286** (2011) 33759

Samir Das, Sanjay Dey†, Trina Roy†, Udayaditya Sen, Cloning, expression, purification, crystal-

lization and preliminary X-ray analysis of the 31 kDa *Vibrio cholera* heat-shock protein VcHsp31, *Acta Crystallographica* **F67** (2011) 1382

Sankar Basu, Dhananjay Bhattacharyya, Rahul Banerjee, Mapping the distribution of packing topologies within protein interiors shows predominant preference for specific packing motifs, *BMC Bioinformatics* **12** (2011) Art No: 195

Sruti Dutta, Debi Choudhury, Jiban K Dattagupta, Sampa Biswas, C-Terminal extension of a plant cysteine protease modulates proteolytic activity through a partial inhibitory mechanism, *FEBS Journal* **278** (2011) 3012

Sumana Roy, Debi Choudhury, Chandana Chakrabarti, Sampa Biswas, JK Dattagupta, Crystallization and preliminary X-ray diffraction studies of the precursor protein of a thermostable variant of papain, *Acta Crystallographica* **F67** (2011) 634

1.4.2.4 Structural Geneomics

Debashree Das, Kamalika Sen†, Species dependent aqueous biphasic extraction of some heavy metals, *Journal of Industrial and Engineering Chemistry* **18** (2012) 855

Mousumi Banerjee, Malini Pramanik, Dipankar Bhattacharya, Mohin Lahiry, Samita Basu, Abhijit Chakrabarti, Faster heme loss from hemoglobin E than HbS, in acidic pH: Effect of aminophospholipids, *Journal of Biosciences* **36** (2011) 809

Oishee Chakrabarti, Neena S Ranee†, Ramanujan S Hegde†, Cytosolic aggregates perturb the degradation of nontranslocated secretory and membrane proteins, *Molecular Biology of the Cell* **22** (2011) 1625

Samir Das, Debashis Mukhopadhyay, Intrinsically Unstructured Proteins and Neurodegenerative Diseases: Conformational Promiscuity at its Best, *IUBMB Life* **63** Special Issue (2011) 478

Samir Das, Mithu Raychaudhuri, Udayaditya Sen, Debashis Mukhopadhyay, Functional Implications of the Conformational Switch in AICD Peptide upon Binding to Grb2-SH2 Domain, *Journal of Molecular Biology* **414** (2011) 217

Sumanta Basu... Abhijit Chakrabarti, F-cell levels are altered with erythrocyte density in sickle cell disease, *Blood Cells Molecules and Diseases* **47** (2011) 117

Sutapa Saha, Rajeswari Ramanathan, Avik Basu, Debasis Banerjee†, Abhijit Chakrabarti, Elevated levels of redox regulators, membrane-bound globin chains, and cytoskeletal protein fragments in hereditary spherocytosis erythrocyte proteome, *European Journal of Haematology* **87** (2011) 259

Swasti Raychaudhuri†, Kamalika Roy Choudhury†, Shreoshi Palchoudhuri†, Shradha Chopra†, Nitai P Bhattacharyya, Debashis Mukhopadhyay, Spectroscopic studies reveal conformational flexibility of intrinsically unstructured protein HYPK, *J Biophysical Chemistry* **2** (2011) 434

1.5 Ph D Awarded

Madhumita Chakrabarti [Abhijit Chakrabarti] , Fluorescence & NMR Spectroscopic Studies on Structure & Conformation of Transcription Activator Proteins: RFXANK and DNA Binding Domain of RFX5, Jadavpur University, May 10, 2011

1.6 Seminars/Lectures given in Conference/Symposium/Schools

Abhijit Chakrabarti

Plasma proteomics in acute Leukemia, The Indian Proteomics Conference, Annual Meeting of the Proteomics Society (India), Trends in Translational Proteomics, Parkland Retreat, JNU, New Delh, Apr 3-5, 2011

Differential expression of red cell proteins in hemoglobinopathy, International Symposium on Mass Spectrometry in Life Sciences, National Centre for Biological Sciences (NCBS), Bangalore, Aug 23-26, 2011

Differential Proteomic Studies of Platelets in Hematological Disorders, 14th ISMAS (Indian Society for Mass Spectrometry) Symposium cum Workshop on Mass Spectrometry in Tea County, Munnar, Nov 7-11, 2011

Eryptosis in Hemoglobinopathy, National seminar on living systems in post genomic era, Fakir Mohan University, Balasore, Orissa, Dec 21, 2011

Clinical Proteomics : case studies in hematological disorders, Seminar cum workshop on Proteomics - Principles, Methods and Applications, Aravind Medical Research Foundation, Madurai, Apr 16, 2011

Debashis Mukhopadhyay

Degeneration and Regeneration: Molecules, Pathways and the Role of AICD, the National Science Day seminar organized by Department of Biophysics, Molecular Biology and Bioinformatics, University of Calcutta, Feb 28,2011

When Growth is Stalled Alzheimers Disease in Perspective, IICB, Kolkata, Aug 13-14, 2011

Comparative Proteomics and Genomics of the CSF from Patients of Spinal Cord Injury: A Perspective of Molecular Biology in Regenerative Medicine, the International Conference on Spinal Injuries, spinal pathologies and their management (ISSICON 2011), Kolkata, Nov 46, 2011

Fishing-out Novel Adaptors of Amyloid Precursor Protein Intracellular Domain and Its Effects on Cellular Proteomic Expression, Department of Biochemistry, Delhi University (South Campus), Mar 29, 2011

Dhananjay Bhattacharyya

HD-RNAS: An automated hierarchical database of RNA structures, Sixth RNA Group Meet 2012, organized by MCBL Department, IISc, Bangalore, Mar 30-31, 2012

Role of Non-Canonical Base Pairs in RNA Structures, International Conference on 'Computational Biology and Functional Genomics, organised by SASTRA University, Tanjavur, Jan 5-6, 2012

Effect of Temperature on DNA Double Helix: An Insight from Molecular Dynamics Simulation, Nucleic Acids in Disease and Disorders, organized by The Kusuma School of Biological Sciences, IIT-Delhi, Dec 5-7, 2011

Structural and Functional Classification of RNA Structures: Efforts and Applications, Interface between Computer Science and Biology, organized by Jamia Milia Islamia University, Delhi, Nov 15-17, 2011

Recent advances on RNA Structure, Workshop on Bioinformatics in Genomics, Proteomics and Metabolomics, organized by Biotechnology Department, IIT-Kharagpur, Sept 22, 2011

Structural Studies of Double Helical DNA: Effect of Terminal Base pair, Conference on Biomolecular Simulations: Algorithms and Applications, organized by School of Computational and Integrative Sciences, Jawaharlal Nehru University, New Delhi, Mar 15-16, 2011

Sequence Directed DNA Flexibility, Indian Institute of Technology, Kanpur, Mar 9, 2012

Nucleic Acid Base Pairs and their Stacking: Geometry and Energetics, SN Bose Center for Basic Science, May 2, 2011

Maitreyee Nandy

Radiation in Space Biological Effects, 14 Day National Workshop on Foundations of Space Science & Technology, organised by Kalpana Chawla Centre for Space and Nano Sciences, Kolkata & Ramakrishna Mission Vivekananda University, W.Bengal, India, June 2012

Radioactivity Generation in Pb and Pb-Bi alloys by Protons A Comparative Study from MeV to GeV, Conference on Accelerator Radiation Safety (CARS2011) Organised by Indian Society for Particle Accelerators, Bhabha Atomic Research Centre, Mumbai, November 16-18, 2011

Moumita Maiti

Nuclear and chemical data for life sciences (Young Scientist Award Lecture), The 10th International Conference on Nuclear Analytical Methods in the Life Sciences (NAMLS-10), Swissotel Nai Lert Park, Bangkok, Thailand, Jan 15-20, 2012

Separation of no-carrier-added ruthenium from ^{12}C irradiated natural yttrium target by aqueous biphasic extraction, 3rd International Nuclear Chemistry Congress, Palermo, Italy, Sept 18-23, 2011

New production routes of Ho-163 for neutrino mass detection, Kirchhoff Institute for Physics, Heidelberg University, Germany

Oishee Chakrabarti

Alternate functions of genes involved in late-onset neurodegeneration, XXXV All India Cell Biology conference and Symposium on Membrane Dynamics and Disease, Bhubaneswar, Dec 2011

Parijat Majumder

Effect of Distamycin A on Chromatin Dynamics, Recent Advances in Chemical and Physical Biology, organized by SINP, Kolkata and MBI, Singapore, Mar 5-7, 2012

Partha Saha

Ubiquitination mediated inter-domain interaction modulates the ribonuclease activity of a RNA binding protein (LdCSBP) from *Leishmania*, 6th RNA Group (India) Meeting, organized by Department of Microbiology and Cell Biology, Indian Institute of Science, Bangalore, Mar 30-31, 2012

Samita Basu

Electronic spectroscopy: an elegant tool for elucidation of pathways of photoinduced chemical and biological reactions (Key Note Address and Chairperson), Current Trend in Chemistry, organized by the Department of Chemistry, Deshabandhu Mahavidyalaya (DBM) in collaboration with the Department of Chemistry, Banwarilal Bhalotia College, Nov 25, 2011

Importance of structure of reactants and medium on spin chemistry probed by magnetic field effect, The Spin Chemistry Meeting 2011 (SCM 2011), Noordwijk, the Netherlands, May 15-20, 2011

Photoinduced phenomena and importance of magnetic field effect, Academic Staff College, University of Calcutta, Kolkata, Jul 8, 2011

Magnetic field effect on photoinduced electron transfer between calf thymus DNA and ternary copper complex, ESF Conference in Partnership with LFUI on Charge Transfer in Biosystems, Obergurgl, Austria, Jul 17-22, 2011

Magnetic field effect corroborated with docking study to explore photoinduced electron transfer in drug-protein interaction, ESF Conference in Partnership with LFUI on Charge Transfer in Biosystems, Obergurgl, Austria, Jul 17-22, 2011

Saptaparni Ghosh

Structural Transition in the Human Telomeric DNA Sequence $d[(TTAGGG)_4]$ upon interaction With Putative Anticancer Agents, Sanguinarine And Ellipticine, The 17th Conversation, organized by State University of New York, Albany, Jun 14-18, 2011

Susanta Lahiri

In situ γ -radiation: an unique and environmentally benign tool for nano particle synthesis (Plenary talk), International conference on Frontiers in Nanoscience, Nanotechnology and their Applications (NanoSciTech-2012), Panjab University, Chandigarh, India, Feb 15-18, 2012

Search of new elements after Madam Curie, National Seminar on Modern Trends of Chemistry in 21st Century, St. Pauls College, Kolkata, India, Feb 6-7, 2012

Production and separation of ^{111}In : an important radionuclide in life sciences, Tenth International Conference on Nuclear Analytical Methods in the Life Sciences (NAMLS-10), Bangkok, Thailand, Jan 15-20, 2012

Artificial radioactivity in the beneficial use of mankind and its production by accelerators, International Seminar On Radioactivity, Curies and Social Commitments Of the Scientists The Asiatic Society, Kolkata, India, Dec 20-21, 2011

A tale of three cities, IYC-2011 seminar on Journey of An Atom through 100 years, Bethune College, Kolkata, Dec 15-16, 2011

A tale of three cities(An IYC Seminar lecture), Bharatiya Vidya Bhaban, Bidhannagar, Kolkata, Dec 07, 2011

A tribute to Madam Curie, International Year of Chemistry: A tribute to Madam Curie Eastern Zonal Cultural Centre, Bidhannagar, Kolkata, Sept 26, 2011

Synthesis of molybdenum nanoparticles by in situ γ -radioation, 3rd International Nuclear Chemistry Congress (3rd INCC), Sicily, Ital, Sept 18-23, 2011

Production and separation of radioisotopes of clinical importance, Acharya Prafulla Chandra Ray Memorial Symposium on Chemistry Today, University of Calcutta, Kolkata, Aug 2-3, 2011

1.7 Teaching elsewhere

Debashis Mukhopadhyay

Course on Proteomics in the UGC-DSA sponsored school on Research Methodologies, Department of Biophysics, Molecular Biology and Bioinformatics, Univ of Calcutta, Oct 14, 2011

Proteomics, M Sc, Department of Biophysics, Molecular Biology and Genetics, Univ of Calcutta

Proteomics/ Crystallography, M Sc 3rd Semester of Biotechnology (GCGEB), Univ of Calcutta

Proteomics/ Crystallography, M Sc 3rd Semester of the Dept of Genetics, Univ of Calcutta

Proteomics/ Crystallography, M Sc 3rd Semester of the Dept of Microbiology, Univ of Calcutta

Proteomics/ Crystallography, M Sc 3rd Semester of Neurosciences (SNPCN), Univ of Calcutta

Structural Biology/Proteomics, Integrated M Sc, Dept of Biotechnology, St Xaviers College, Kolkata

Molecular Modeling, M Sc (Pharma), NIPER, Kolkata

Dhananjay Bhattacharyya

Quantum and Classical Simulations for Bio-molecular Structure and Interaction, The Physics behind electronics and its application, Sammillani Mahavidyalaya Baghajatin, Dec 1, 2011

Partha Saha

DNA Replication, M Sc (Biotechnology, Microbiology, Genetics, Neurobiology) 1st Semester, Univ. of Calcutta

Recombination and Transposition, M Sc (Biotechnology, Microbiology, Genetics, Neurobiology) 2nd Semester, Univ. of Calcutta

Samita Basu

Spectroscopy, M Sc (Inorganic Chemistry special), Univ. of Calcutta

Photochemistry, M Sc (Physical Chemistry special), Midnapore College, Vidyasagar University, West Bengal

Applications of UV-Visible Spectroscopy, DST-Inspire Internship Science Camp 2011, Jagadis Bose National Science Talent Search, Kolkata, Aug 25, 2011

Electronic Spectroscopy: an elegant tool for elucidation of pathways of photoinduced chemical and biological reactions, National Seminar on Current Trend in Chemistry organized by the Department of Chemistry, De shabandhu Mahavidyalaya (DBM) in collaboration with the Department of Chemistry, Banwarilal Bhalotia College, Nov 25, 2011

Chemical Bonding, DST Science Camp, Jagadis Bose National Science Talent Search, Kolkata, Nov 23, 2011

Electronic Configuration, Periodic Table & Ionic and Covalent bonding - a correlation, Science Camp, Jagadis Bose National Science Talent Search, Kolkata, Feb 7-10, 2012

1.8 Miscellany

Binita Dutta

Best oral presentation award, Tenth International Conference on Nuclear Analytical Methods in the Life Sciences (NAMLS-10), Jan 15-20, 2012, Bangkok, Thailand

Moumita Maiti

Recipient of International Young Scientist Award (YSA) 2012 for achievements in nuclear and analytical methodology and its applications to the life sciences bestowed by International Committee on Nuclear Analytical Methods in the Life Sciences (NAMLS-IC) and International Atomic Energy Agency (IAEA). The award presented during January 15-20, 2012

Celebration of International Year of Chemistry (IYC-2011)

The year 2011 was declared as International Year of Chemistry (IYC) by the UNESCO. IYC was also dedicated to the 100 years of the second Nobel Prize of Madam Curie, the starting point of radiochemistry, a very important and vibrant branch of sciences.

The Saha Institute of Nuclear Physics, a premier research institute of India, celebrated the IYC in a befitting way by the lectures of eminent scientists during 15-16 November, 2011. The institute has connection with Curie family from its very first day. The Institute of Nuclear Physics (Later named as the Saha Institute of Nuclear Physics after the demise of its founder, Professor Meghnad Saha) was inaugurated by the Nobel laureate Madame Irene Curie on 11 January 1950. Therefore in the celebration of IYC we invited Professor Pierre Joliot, a renowned biophysicist and son of Madame Irene Curie and grandson of Madame Marie Curie. Professor Heino Nitsche from Lawrence Berkley National Laboratory, USA, Professor Milan K Sanyal and Professor Susanta Lahiri from SINP, and Professor Kankan Bhattacharyya from IACS were the other speakers in the celebration. As a part of our commitment to the young talents, we also involved undergraduate students and their teachers in this program. We organized quiz and poster competitions related to IYC amongst the students of selected colleges and Universities.

International Conference on Omics Meets Disease

International Conference on Omics Meets Disease and IIIrd Annual Meeting of Proteomics Society (India) was organized by Saha Institute of Nuclear Physics (SINP), Indian Institute of Chemical Biology (CSIR-IICB) & University of Calcutta and was held in SINP during December 15-18, 2011.



About 200 delegates including eminent scientists of national and international repute participated in the conference.

Chapter 2

Condensed Matter Physics including Surface Physics and NanoScience

2.1 Summary of Research Activities of Divisions

2.1.1 Applied Material Science

Soft Materials Studies: Experiment and Simulation

Calf-thymus DNA, spin-coated from pristine and 500mM NaCl solutions in water, show formation of well defined thin films. The X-ray reflectivity studies reveal pristine film consists of three layers i.e. lateral stacks of three layers of DNA molecules whereas the salted film has lesser thickness ~ 1.5 times of DNA chain width, indicating enhanced lateral entanglement.

Pressure area isotherm of a stearic acid monolayer is recorded and the corresponding image viewed using a Brewster Angle Microscope. Au nanoparticles have been introduced into the monolayer at two different concentrations. The changes in the pressure area isotherm of the system as it progressively changes from a complex to a simpler two dimensional liquid have been studied.

The relationship between the change in viscosity of a solution of 50 g asphaltene in 100 ml toluene and the methyl to methylene (CH_3/CH_2) ratio of the asphaltene, when exposed to ultrasonic irradiation, has been studied. The asphaltene used was extracted from refinery sedimentation. Adopting Fourier transform infrared spectroscopy (FTIR) and viscosity measurement as the probing tools, it is found that the viscosity initially decreases but eventually it starts to increase with prolonged duration of ultrasound irradiation. Viscosity decrease is accompanied by an increase in CH_3/CH_2 ratio, which, however, is reversed as the viscosity starts rising in the latter period of irradiation. Thus a clear correspondence exists between the two, viz. when asphaltene is exposed to ultrasonic irradiation its viscosity is inversely proportional to its CH_3/CH_2 ratio. The accuracy of the photo-acoustic (PA) technique to assess blood oxygen saturation (SO_2) using two laser beams was examined theoretically. A Monte Carlo technique was used to simulate 2D tissue configurations, and the PA signals from many red blood cells (RBCs) were constructed by summing the signals emitted by the individual cells. The level of oxygenation of each cell was assumed to be identical in a configuration. The cellular oxygenation state defined the blood oxygen saturation (SO_2) and

also controlled the PA signal amplitude. The PA amplitude was observed to vary linearly with blood SO_2 . It was nearly 4.6 times less and 8.2 times greater at $\text{SO}_2=100\%$ than that of 0% for the 600 and 1064 nm incident optical radiations, respectively. The blood SO_2 was estimated using the PA amplitudes generated at these wavelengths. The estimated values matched perfectly with that of the actual SO_2 confirming the suitability of the PA technique to determine blood SO_2 noninvasively.

2.1.2 Experimental Condensed Matter Physics

Dielectric constant and Thermal expansion: A facility for the study of Dielectric properties and electrical polarization using Wayne Kerr high frequency LCR bridge at high frequencies 20Hz-10MHz at temperatures 2-310K (can be extended up to 600K) has been installed. Also, a facility for thermal expansion down to 4.2K with magnetic field up to 9T has been installed. The thermal expansion of single crystal of Sb_2Te_3 topological insulator has been investigated. The temperature dependence of the linear thermal expansion along the hexagonal c axis (ΔL), exhibits a clear anomaly in the temperature region 204-236 K.

Microwave spectroscopy: Studies on broadband microwave absorption and dielectric properties of low dimensional materials: A new facility, under the XI th plan programme, has been developed to study the broadband microwave absorption, dielectric properties and different S-parameters of lower dimensional materials e.g. conducting polymers and their composites, carbon nanotubes, fibres and nanowires etc. in the X-band (8.0–12.0 GHz). For this purpose, a Vector Network Analyzer (VNA) operating in the frequency range 10.0 MHz–26.0 GHz has been procured from Agilent Technologies Inc. and was successfully installed. Interpenetrating polymer networks (IPNs) of polyacrylics and polyurethanes were synthesized to be used as solid polymer electrolytes. Varying the composition of polymethylmethacrylate (PMMA), polyacrylonitrile (PAN) and polyurethanes (PU), series of interpenetrating polymer networks were synthesized. Microwave dielectric absorption and S-parameter measurements have been completed on these samples.

NMR technique has been used to study the effect of interfacial hydrogen bonding on the behavior of the freezing/melting processes in two organic liquids, namely, ethylene glycol $[(\text{CH}_2\text{OH})_2]$ and isopropanol $[\text{CH}_3\text{CH}(\text{OH})\text{CH}_3]$, confined in nanopores of ZSM-5 zeolite. The organic molecules adjacent to the pore wall and those at the center of the pores show different mobilities and freezing/melting behaviour as revealed by the measurement of ^1H spin-spin relaxation time. NMR studies also indicate that freezing of organic molecules in the confinement of nanosize pores is not accompanied with a long range structural ordering. ^{31}P nuclear-magnetic-resonance NMR studies have been performed in trimer spin chain compound $\text{Ca}_3\text{CuNi}_2(\text{PO}_4)_4$, in the temperature range 4–300 K. The temperature dependence of the spin-lattice relaxation rate $1/T_1$ shows a clear signature of long-range magnetic order in $\text{Ca}_3\text{CuNi}_2(\text{PO}_4)_4$ below 16 K. T_N agrees quite satisfactorily with that obtained from the derivative of the molar susceptibility versus T plot. A comparison of the behavior of the $1/T_1$ data in $\text{Ca}_3\text{CuNi}_2(\text{PO}_4)_4$ with those in $\text{Sr}_3\text{Cu}_3(\text{PO}_4)_4$ clearly suggests that the mechanism of the relaxation changes from a two magnon-mediated Raman process in the former to a three magnon-mediated process in the latter.

High pressure at High magnetic field: Large variations in the magnetic ordering behavior of EuCu_2As_2 with the application of external pressure and magnetic field: The influence of external pressure on the electrical transport and magnetic properties of EuCu_2As_2 , crystallizing in ThCr_2Si_2 -type structure is reported. The system has been known to be an antiferromagnet below

$T_N \approx 15$ K, in the absence of external magnetic fields. We find that there is a gradual reduction of T_N with the application of magnetic field with an extrapolated value of the critical field of around 20 kOe which can drive T_N to zero. But above 20 kOe and at low temperatures, the system appears to be transformed into a ferromagnetic state, interestingly avoiding quantum critical point. Electrical resistivity under pressure (< 11 GPa) reveals that magnetic ordering temperature is pushed up dramatically to higher temperature which is quite interesting while comparing with the behavior in isostructural FeAs based systems containing Eu. Above 7 GPa, pressure-induced state appears to be ferromagnetic. The results thus reveal interesting changes in the magnetic ordering behavior of this compound with increasing pressure and magnetic fields.

Evidence of interfacial magnetoelectricity in oxide heterostructure: Multiple state Memory Effect Magnetoelectricity or the coupling of electric and magnetic order parameters in a single system has been observed in complex oxide ferromagnetic metal / dielectric bilayer system. The heterostructures were prepared by Pulsed Laser Deposition. The bilayer structure used for this study consists of two layers of conventional half metallic $\text{La}_{0.67}\text{Sr}_{0.33}\text{MnO}_3$ and 1% Nb doped SrTiO_3 on Si/SiO₂ substrate. Detailed Magnetotransport measurements in the range 10K-300K show the presence of distinct resistance states: Multiple states as well as hysteretic IV behavior between 60K-140K. The observed results have been interpreted in the light of Magnetoelectricity at the interface of the ferromagnet-ferroelectric bilayer.

Giant Enhancement of Magnetoresistance of Nanocrystalline $\text{La}_{0.45}\text{Ca}_{0.55}\text{MnO}_3$: The enhancement of magnetoresistance (MR) has been observed in case of nanocrystalline $\text{La}_{0.45}\text{Ca}_{0.55}\text{MnO}_3$ in comparison with its polycrystalline bulk form. It appears that the robust charge ordered state (COS) formed in bulk sample becomes unstable, when the sample is prepared in nanocrystalline form and can be destabilized in the presence of magnetic field giving rise to enormous MR.

Experimental and Theoretical Investigation of Magnetocaloric Behavior in HoRu_2Si_2 : The magnetic and magnetocaloric properties of intermetallic compound HoRu_2Si_2 have been investigated from experimental as well as theoretical point of view. Experiments on polycrystalline sample indicate an antiferromagnetic phase transition at 18 K. The theoretical investigation has been done using a microscopic model and analyzed as a function of model parameters. The theoretical investigation giving better understanding of the magnetic and magnetocaloric behavior of the system. These results suggest strong ferromagnetic interaction in the layer structure.

Effect of substitution on transition metal sites in rare earth ternary silicides: The RCo_2Si_2 (R = rare earth) compounds crystallize in tetragonal body centered ThCr_2Si_2 type structure with the space group I4/mmm where R, Co and Si atoms occupy the 2a, 4d and 4e positions respectively. The structure can be described as a stacking of atomic layers in the direction of c-axis in a sequence R-Si-Co-Si-R. Magnetic properties of these compounds are already well known. We are studying the effect of partial substitution of Co by V on the magnetic properties of CeCo_2Si_2 , PrCo_2Si_2 , and NdCo_2Si_2 . Magnetization measurements were carried out under field cooled conditions during the cooling cycle in between 300-5 K at a field of 5 kOe. The data show that in case of CeCo_2Si_2 , PrCo_2Si_2 and NdCo_2Si_2 , substitution of cobalt by vanadium results in significant changes in their magnetic properties. In the parent compound cerium is in a valence fluctuating state and the parent compound CeCo_2Si_2 is known to be a weak paramagnet. Upon substitution of Co by V, the samples exhibit significant temperature dependence of magnetism below about 20 K. Both PrCo_2Si_2 and NdCo_2Si_2 are antiferromagnetic with $T_N = 32$ and 34 K respectively. substitu-

tion by V results in slight decrease of T_N . However, with increase in V content, the susceptibilities deviate from Curie-Weiss behaviour showing a rapid increase in magnetization below about 50 K. The samples $\text{PrCo}_{2-x}\text{V}_x\text{Si}_2$ and $\text{NdCo}_{2-x}\text{V}_x\text{Si}_2$ at $x \leq 0.3$ seem to exhibit ferrimagnetic transitions at about 70 and 60 K respectively. Further studies are in progress.

Study of magnetic properties of CoCu nanoparticles: Nano structured CoCu granular alloys (Co: 1%-20%) have been prepared by borohydride (NaBH_4) reduction of CuCl_2 , $2\text{H}_2\text{O}$ and CoCl_2 , $6\text{H}_2\text{O}$ salt solutions with CTAB as the capping reagent, and characterized by inductively coupled plasma optical emission (ICPOE) spectroscopy, x-ray diffraction (XRD) and transmission electron microscopy (TEM). The studies show broadening of x-ray diffraction peaks of fcc Cu lattice as a result of small particle size and a reduction of lattice parameter due to alloying. TEM studies show a lognormal distribution of particle size with nearly 75% of particles having diameter of 5-10 nm. Magnetic measurements were performed under ZFC-FC condition with a probing field of 100 Oe at temperatures of 5300 K. The sample with $\sim 1\%$ Co are paramagnetic, but samples with Co concentration of $\sim 3\%$ and above are characterizes by some blocking temperature (T_B) distributions.

Unusual pressure response of electronic transport properties of a Kondo insulator CeRu_4Sn_6 : The effect of hydrostatic pressure (up to 20.6 kbar) on the electrical resistivity (1.8 K to 300 K) of a Kondo insulator CeRu_4Sn_6 , crystallizing in a tetragonal structure with space group $I-42m$ has been studied. The absolute value of resistivity is found to increase monotonically with pressure in the entire temperature range. The hybridization gap, contrary to common observation on other Ce systems, is also found to increase up to 15.1 kbar. Magnetoresistance under pressure appears interesting. For instance, at 1.8 K and at 15.1 kbar, MR is negative till about 100 kOe, showing a minimum around 60 kOe, subsequently showing a sign change; magnetoresistance becomes positive at and above 10 K and at same pressure. These results indicate subtle changes induced by magnetic field on the hybridization gap.

2.1.3 Surface Physics

Research activities of the Surface Physics Division mainly encompass the physical and chemical methods of growing low-dimensional structures with tunable morphology and mechanical/electrical/magnetic/optical properties, epitaxial growth of semiconductor quantum structures and their applications in micro-nano technology. Modifications of materials using medium and low-energy ion beams, such as fabrication of decorated and modified surfaces as growth templates, synthesis of quantum dot-composites for photonic/plasmonic applications, etc. are also active areas of our ongoing research. The division has also been involved in the growth of magnetic and photonic structures through nano-manipulation and self-assembly, development of polymer-based photovoltaics and other molecular electronic systems and study of their morphology-transport correlations. Glimpses of some important activities are given in the following.

Morphological and structural characterizations of Molecular Beam epitaxy (MBE) - grown Si/Ge superlattice structures have been extensively done using simultaneous analysis of x-ray reflectivity and x-ray diffraction data. Consistent analysis of the data collected in the Indian Beamline at Photon Factory Synchrotron (KEK, Japan) has allowed for the determination of electron density and strain profiles as a function of depth in the multilayer stacks. A procedure for accurate compositional analysis of such Si/Ge superlattice structures and MBE-grown $\text{Si}_{1-x}\text{Ge}_x$ ($0 < x < 0.72$) alloys has been proposed based on MCsn+-SIMS approach. The new methodology has proved to be an efficient approach for Matrix effect minimization in SIMS quantification. Formation mechanisms

of multiply-charged secondary ions in sputtering process have been explained in the framework of symmetric and asymmetric collisions. Appreciable nonlinear optical responses ((3)) in ion-beam induced silver nanoclusters in sapphire with temporal responses in picosecond to femtosecond time domain have shown great relevance to futuristic switching materials in nanophotonics. Cathodoluminescence (CL) in high-resolution scanning electron microscopy (HRSEM) has demonstrated to be an important study on ion-induced ripple patterns on Si. A blue shift of the red peak to a yellow peak (at ~ 575 nm) in CL has been observed for recrystallized patterned sample under high temperature annealing. Localized surface plasmon resonances associated with photon emission in a truncated tetrahedral gold nanoparticle on a silicon substrate are specially mapped showing stronger photon emission in the visible range near the tips of the particle in contact with the substrate compared to the edges of the particle. FDTD simulations of the spectra and cathodoluminescence images are reported to be for the first time. Variable polarization synchrotron radiation has been utilized to map the valence band electronic structure of graphite by angle-resolved photoemission spectroscopy (ARPES). The measured ARPES has shown asymmetry in intensity around M point of the Brillouin zone mimicking different partial wave character of s1 and s3 bands.

Study on micron-sized pit formation on Ge surfaces due to 26 keV Si- ion bombardment is another area of research on materials modifications using medium and low-energy ion beams. A two-field continuum model developed for small slope approximations has described the pit formation and growth at the very beginning stage of ion bombardment. The growth of the pits at later times (high fluence) has been explained by the gradient-dependent erosion mechanisms due to primary ion beam as well by secondary flux of particles originating from steep slopes. Periodic ripple formation on GaAs under 60 keV Ar ion bombardment has been observed. Parameters like rms roughness, ripple wavelength, amplitude, etc. have been measured through AFM image analysis.

Study on magnetism in ZnO nanoparticle samples with intrinsic Fe impurities (~ 50 ppm) has shown super-paramagnetic behavior. Under annealing a magnetic hysteresis along with coercive field below the blocking temperature has been found to be almost independent of the cooling field. A simple model has been proposed to explain the reduction of magnetization as being due to a vortex-state-like flux closure formation. Study on structural and magnetic properties of NiO particles through x-ray diffraction, extended x-ray absorption fine structure (EXAFS) and magnetization measurements has demonstrated an unusual finite magnetic moment in antiferromagnetic materials.

Incorporation of gold in polypyrrole nanotubes using a cost-effective template based single-step chemical synthesis technique have exhibited switching transition that reduces the resistance of the wires by several orders of magnitude under certain bias around and below 30 K. A deviation from a perfect 2D-hexagonal (p6m) structure for CTAB-silica mesostructured films has been observed through X-ray reflectivity and grazing incidence small angle X-ray scattering. The deviation has been understood in terms of the shape and ordering of the micelles inside the film with or without the silica coating-layer's contribution. Swelling dynamics of spin-coated ultrathin polyacrylamide films, annealed at the onset of thermal degradation temperature (220 C) of polyacrylamide, have been studied using in-situ X-ray reflectivity to understand the effects of thermal modification of the polymer to their swelling dynamics.

2.1.4 Theoretical Condensed Matter Physics

Thermoelectric effects in strongly correlated systems and effect of strong correlations in band insulators are being studied. In high T_c superconductors a wide ranging connection between the doping dependence of the transition temperature T_c and the room temperature thermopower has been observed. A universal correlation between these two quantities exists with the thermopower

vanishing at optimum doping. An interpretation of this universality has been provided in terms of a possible underlying quantum critical point (QCP) at T_c . Central to the viewpoint is the recently noted Kelvin formula relating the thermopower to the density derivative of the entropy. The effect of strong correlations in a band insulator has also been studied and interesting antiferromagnetic (AFM) and ferrimagnetic Half metallic phases seen to arise as an effect of strong correlations in a band insulator. A simple tight-binding band insulator with two bands in the presence of an on-site Coulomb repulsion, the Hubbard U is studied. At half filling, with increasing U , there occurs a first order transition between the paramagnetic band insulator and an AFM phase at some threshold U_1 . Inside the AFM phase, a half metal phase appears at U_2 greater than U_1 beyond which the system becomes an AFM Mott insulator. In the doped case, turning on U results in a continuous transition from paramagnetic metal to ferri-magnetic half metal followed by a first order transition, at a higher value of U , to the para-magnetic metal again.

Many of the transition metal oxides have both strong electron-phonon (e-ph) and strong electron-electron (e-e) interaction and can be studied using the Hubbard-Holstein model. An effective Hamiltonian for the one-dimensional Hubbard-Holstein model has been derived and the phase diagram at various fillings obtained. As e-e interaction is increased, the system transits from an antiferromagnetic cluster to a correlated nearest-neighbor singlet phase. It has been explicitly demonstrated that superfluidity and charge-density-wave (CDW) occur mutually exclusively with CDW manifesting itself only at one-third filling.

In the area of mesoscopic systems, it has been shown analytically that the conductance of a mesoscopic ring comes across an absolute minimum when the strengths of Rashba and Dresselhaus spin-orbit interactions are equal. The way of estimating the strength of Dresselhaus spin-orbit interaction has been also been suggested. Generation of a pure spin current is a major challenge to the physicists even today. A quantum device has been recently suggested which behaves like a spin filter. Scientists have shown that the transport properties of a single benzene molecule changes drastically under the influence of dephasing mechanism. The development of a second quantized formalism for finding the distribution of persistent current in a quantum network is made.

Investigation on bipolaron formation in the Holstein-Hubbard and Frohlich-Hubbard model on a 1-d lattice is done exactly. The role of extended electron-electron interaction on the effective mass and stability of bipolarons were also studied. The properties of fermions and bosons in a 3-d optical lattice under anisotropic harmonic trap have been investigated. The Drude weight shows very interesting behavior under anisotropic trap. Possible experiments to verify the theoretical predictions have been investigated.

Scientists are actively involved in understanding possible universality classes of absorbing phase transition (APT). There has been a long debate on whether APT can be discontinuous. Recent provision of an example and explanation with exact results indicated that APT can occur discontinuously. In models with additional conserved fields, where APT is known to have unusual critical behaviour, it has been shown that the flow to generic universality class (namely directed percolation or DP) is observed, once conservation is broken. In a very recent work it has been also shown that the fixed energy sandpile models (claimed in the literature to form an independent universality class) actually belong to DP class.

A coarse-grained effective two-dimensional hydrodynamic theory as a theoretical model for a coupled system of a fluid membrane and a thin layer of a polar active fluid in its ordered state that is anchored to the membrane has been constructed. It is shown that such a system is prone to generic instabilities through the interplay of nonequilibrium drive, polar order and membrane fluctuation. In a related problem, they elucidated the visco-elastic properties of an active gel by studying the dynamics of a small tracer particle inside it. They showed that the diffusion coefficient can depend

on system size (L) and diverges as L approaches an instability threshold. Direct Numerical Simulations and shell model studies on binary fluid mixture that velocity and concentration gradient structure functions exhibit multiscaling and extended self-similarity. In contrast to the well-known passive scalar turbulence problem, concentration structure functions show simple scaling. The XY model out of equilibrium by introducing a non-zero noise cross-correlation of amplitude Dx in a stochastic Langevin description has been derived.

The quantum annealing algorithms for more general classes of multi-variable optimisation problems further developed. The two-fractal overlap model of earthquake dynamics has been extended further to the cases of dry friction and discussed them extensively in a recent review appeared in Reviews in Modern Physics 2012. The kinetic exchange models for income and wealth distributions in societies have been further developed and extended for the cases collective opinion formations in the societies.

2.2 Research Activities

2.2.1 Applied Material Science

2.2.1.1 Microstructural and magnetic characterization of fly ash from Kolaghat Thermal Power Plant in West Bengal, India

This paper reports on the physical nature of the fly ash sample of the Kolaghat Thermal Power Plant, India with an emphasis on its ultrafine nature. This paper also deals with the measurement of the magnetic properties of the fine particles of the fly ash sample. Particle sizes of this fly ash sample estimated from the SEM images lie within 0.165.50 μm , and the EDX spectral analysis indicates the presence of O, Al, Si, C, Fe, Mg, Na, K and Ti in this sample. From the XRD study, it is found that physical nature of conglomeration in the fly ash is crystalline and the major components are mullite ($\text{Al}_6\text{Si}_2\text{O}_{13}$) and quartz (SiO_2). Additionally, the presence of hematite, microcline, magnetite, maghemite and free iron in smaller fractions cannot be ruled out. A large magnetization observed at 5 K indicates the presence of magnetic components possibly due to superparamagnetism owing to very fine magnetic particles present. The hyperfine parameters obtained from the ^{57}Fe Mössbauer spectroscopy, in general, support the observations made from the XRD analysis and in particular, provides the quantitative estimation of the different iron ions present in the sample. Precisely, this report presents experimental data on physical aspects of the fly ash sample of a thermal power plant which consists of coarse, fine and ultrafine magnetic particulate materials (PMs) and deals with an in-depth analysis of it.

A Bhattacharjee[†], H Mandal, M Roy, et al

2.2.1.2 Solidlike and liquidlike behavior in monolayers and multilayers of metal-bearing amphiphiles

Atomic force microscopy (AFM) of cadmium stearate (CdSt) and cobalt stearate (CoSt) Langmuir-Blodgett films show differences in their in-plane morphologies. CdSt films, with a huge number of in-plane "pinhole" defects, follow self-affine behavior, whereas CoSt films, which are almost void of such in-plane defects, show deviation from self-affinity especially at small length scales, suggesting liquidlike behavior, imparting flexibility to the system, in plane. Phase images of CoSt obtained from tapping mode AFM show gentle undulations or hemispherelike features in contrast to its smooth topography, unlike the CdSt system where both height and phase images show self-affine

domains. Near edge x-ray absorption fine structure spectroscopy indicates no preferred in-plane orientation of the head group in CoSt films. The undulating features in CoSt is explained by invoking a radially symmetric orientational distribution in the tilt of adjacent hydrocarbon tails, causing a small in-plane density variation which shows up in the phase image. These orientational disorders in adjacent tails probably allow "filling up" of in-plane defects thereby giving rise to its excellent in-plane coverage and hence a "liquidlike" behavior in CoSt. Brewster angle microscopy shows that parent Langmuir monolayers of stearic acid in the presence of Cd and Co ions in the aqueous subphase behave as two-dimensional "solids" and "liquids," respectively, suggesting the phenomena to be inherent in the amphiphiles and probably independent of their organization as monolayers and multilayers.

Smita Mukherjee, Alokmay Datta, et al

2.2.1.3 Nonuniversal behavior of the helicity modulus in a dense defect system

An extensive Monte Carlo simulation has been performed on a two-dimensional modified XY model that behaves like a dense defect system. Topological defects are shown to introduce disorder in the system, which makes the helicity modulus jump nonuniversal. The results corroborate the experimental observation of a nonuniversal jump of the superconducting density in high- T_c superconducting films.

Suman Sinha

2.2.1.4 Studies on Al/ZrO₂/GaAs metal-oxide-semiconductor capacitors and determination of its electrical parameters in the frequency range of 10 kHz-1 MHz

Aluminum (Al)/zirconium oxide (ZrO₂)/GaAs metal-oxide-semiconductor (MOS) capacitors were fabricated on p -GaAs. The carrier concentration of n -GaAs was varied by metal organic chemical vapor deposition. The ZrO₂ gate dielectrics were prepared by the sol-gel process and then spin-coated onto GaAs substrates. Three different thicknesses of the ZrO₂ layer, viz., 25, 40 and 50 nm, were used to study the effect of oxide thickness on different MOS parameters. Sulfur (S) passivation of the GaAs surface was done to control the interface state densities before ZrO₂ deposition. It was found that S passivation resulted in both low hysteresis and high accumulation capacitance of the device. Frequency dependent studies on the dielectric characterizations were made in the frequency range of 10 kHz-1 MHz. It was found that within this frequency range dispersion of the oxide capacitance was 2%/decade. It was observed that interface trap densities (D_{it}) increased with an increase in the carrier concentration of n -GaAs from a value of $1.5 \times 10^{12} \text{ cm}^{-2} \text{ eV}^{-1}$ at $1 \times 10^{14} \text{ cm}^{-3}$ to a value of $3.8 \times 10^{12} \text{ cm}^{-2} \text{ eV}^{-1}$ at $3 \times 10^{16} \text{ cm}^{-3}$ doping concentration of the semiconductor. It was also found that D_{it} increased with an increase in the oxide thickness from a value of $0.75 \times 10^{12} \text{ cm}^{-2} \text{ eV}^{-1}$ at 25 nm to a value of $2.4 \times 10^{12} \text{ cm}^{-2} \text{ eV}^{-1}$ at 50 nm thickness of the oxide layer. Studies on temperature dependent current densities indicated that the leakage current decreased by three orders of magnitude with the change in temperature from 290 to 80 K. Leakage current was also found to decrease with an increase in the thickness of the dielectric layer due to a decrease in the transmission probability. Loss tangent was found to decrease with frequency, whereas the ac conductivity showed an opposite trend. Considering different MOS parameters investigated in the present study, it was observed that ZrO₂ could be a potential candidate

for GaAs based MOS devices.

Souvik Kundu†...Supratic Chakraborty, et al

2.2.1.5 A preliminary study on the nature of particulate matters in vehicle fuel wastes

Powder X-ray diffraction (XRD), scanning electron microscopy (SEM), and tunneling electron microscopy (TEM) studies of two solid vehicle wastes (pollutants) from petrol- and diesel-fueled engines of Kolkata (India) have detected a significant amount of ultrafine particles in the nanometer scale in these wastes. Both powder XRD and selected area electron diffraction from TEM have confirmed the existence of inhomogeneous distribution of nanocrystallites in these pollutants. Energy dispersive X-ray spectrometry shows that these wastes contain mainly carbon and oxygen as the constituent components. These pollutants are magnetic in nature as seen with SQUID magnetometry, and the presence of a high amount of carbon presumably is likely the origin of the magnetic property.

Ashis Bhattacharjee†...Madhusudan Roy, Tapas Kumar Chini

2.2.1.6 Langmuir-Blodgett deposition selects carboxylate headgroup coordination

Infrared reflection-absorption spectroscopy results on stearic acid Langmuir monolayers containing Mn, Co, and Cd ions show that on the water surface, the ions induce unidentate and bidentate (both chelate and bridged) coordination in the carboxylate headgroup with some trace of undissociated acid. Moreover, with Cd and Mn ions in subphase, the preferred coordination is found to be unidentate, whereas for Co, bidentate chelate is most preferred. After transfer onto amorphous substrate, not all coordinations are found to exist in the same ratio for the deposited metal stearate monolayers. More specifically, after transfer, Mn is found to coordinate with the carboxylate group as bidentate chelate, Cd as unidentate and bidentate bridged (with unidentate as the preferred coordination), and Co as preferably bidentate bridged (although all coordinations are present). Results suggest a specific interaction in each case, as the metal-carboxylate pair at the water surface is transferred to the substrate surface during Langmuir-Blodgett deposition.

Mukherjee Smita, Alokmay Datta

2.2.1.7 Crossover from layering to island formation in Langmuir-Blodgett growth: Role of long-range intermolecular forces

Combined studies by atomic force microscopy, x-ray reflectivity, and Fourier transform infrared spectroscopy on transition-metal stearate (M-St, M = Mn, Co, Zn, and Cd) Langmuir-Blodgett films clearly indicate association of bidentate coordination of the metal-carboxylate head group to layer-by-layer growth as observed in MnSt and CoSt and partially in ZnSt. Crossover to islandlike growth, as observed in CdSt and ZnSt, is associated with the presence of unidentate coordination in the head group. Morphological evolutions as obtained from one, three, and nine monolayers (MLs) of M-St films are consistent with Frank van der Merwe, Stranski-Krastanov, and Volmer Weber growth modes for M = Mn/Co, Zn, and Cd, respectively, as previously assigned, and are found to vary with number (n) of metal atoms per head group, viz. $n = 1$ (Mn/Co), $n = 0.75$ (Zn),

and $n = 0.5$ (Cd). The parameter n is found to decide head-group coordination such that $n = 1.0$ corresponds to bidentate and $n = 0.5$ corresponds to unidentate coordination; the intermediate value in Zn corresponds to a mixture of both. The dependence of the growth mode on head-group structure is explained by the fact that in bidentate head groups, with the in-plane dipole moment being zero, intermolecular forces between adjacent molecules are absent and hence growth proceeds via layering. On the other hand, in unidentate head groups, the existence of a nonzero in-plane dipole moment results in the development of weak in-plane intermolecular forces between adjacent molecules causing in-plane clustering leading to islandlike growth.

Smita Mukherjee, Alokmay Datta

2.2.2 Experimental Condensed Matter Physics

2.2.2.1 Large variations in the magnetic ordering behavior of EuCu_2As_2 with the application of external pressure and magnetic field

The influence of external pressure on the electrical transport and magnetic properties of EuCu_2As_2 , crystallizing in a ThCr_2Si_2 -type structure, is reported. The system is known to be an antiferromagnet below $T_N \approx 15$ K in the absence of external magnetic fields. We find that there is a gradual reduction of T_N with the application of a magnetic field with an extrapolated value of the critical field of around 18 kOe which can drive T_N to zero. Electrical resistivity under pressure (<11 GPa) reveals that the magnetic ordering temperature is pushed up dramatically to higher temperatures which is quite interesting if compared with the behavior in isostructural FeAs-based systems containing Eu. Above 7 GPa, the pressure-induced state appears to be ferromagnetic. The results thus reveal interesting changes in the magnetic ordering behavior of this compound with increasing pressure and magnetic fields.

K Sengupta...R Ranganathan, et al

2.2.2.2 Glassy behavior in the layered perovskites $\text{La}_{2-x}\text{Sr}_x\text{CoO}_4$ ($1.1 \leq x \leq 1.3$)

The glassy behavior of the phase segregated state in the layered cobaltite $\text{La}_{2x}\text{Sr}_x\text{CoO}_4$ has been studied. The role of the inter-cluster interactions as well as the disordered spins at the paramagnetic/ferromagnetic interface, behind the observed glassy behavior have been investigated. The disordered spins at the interface appear to be strongly pinned, and they contribute little to the observed glassy behavior. On the other hand, the inter-cluster interactions play the key role. Both the Co^{4+} and Co^{3+} ions are in the intermediate spin state.

S Mukherjee†, Rajarshi Mukherjee†, S Banerjee, R Ranganathan, Uday Kumar†

2.2.2.3 Anisotropic magnetic properties and giant magnetocaloric effect in antiferromagnetic RMnO_3 crystals ($\text{R} = \text{Dy, Tb, Ho, and Yb}$)

We have systematically investigated the magnetic properties and magnetocaloric effect (MCE) in RMnO_3 ($\text{R} = \text{Dy, Tb, Ho, and Yb}$) single crystals. Above a critical value of applied field (H_c), RMnO_3 undergo a first-order antiferromagnetic (AFM) to ferromagnetic (FM) transition below the ordering temperature (T_N^R) of R^{3+} moment and a second-order FM to paramagnetic (PM)

transition above T_N^R . Both H and T dependence of M shows that the system is highly anisotropic in the FM as well as PM states and, as a result, the magnetic entropy change (ΔS_M) is extremely sensitive to the direction of applied field and can be negative (normal MCE) or positive (inverse MCE). For hexagonal HoMnO_3 and YbMnO_3 systems, a very small inverse MCE is observed only for H parallel to c axis and it decreases with increasing H and crosses over to normal one above H_c . On the other hand, for orthorhombic DyMnO_3 and TbMnO_3 , though the inverse MCE disappears above H_c along easy axis of magnetization, it increases rapidly with H along hard axis of magnetization for $T \ll T_N^R$. Except for YbMnO_3 , the values of ΔS_M , relative cooling power and adiabatic temperature change along easy axis of magnetization are quite large in the field-induced FM state for a moderate field strength. The large values of these parameters, together with negligible hysteresis, suggest that the multiferroic manganites could be potential materials for magnetic refrigeration in the low-temperature region.

A Midya, SN Das, P Mandal, et al

2.2.2.4 Fe-spin reorientation in PrFeAsO : Evidences from resistivity and specific heat studies

We report the magnetic field dependence of resistivity (ρ) and specific heat (C) for the non-superconducting PrFeAsO compound. Our study shows a hitherto unobserved anomaly at T_{SR} in the resistivity and specific heat data, which arises as a result of the interplay of antiferromagnetic (AFM) Pr and Fe sublattices. Below the AFM transition temperature (T_N^{Pr}), Pr moment orders along the crystallographic c axis and its effect on the iron subsystem causes a reorientation of the ordered in-plane Fe moments in a direction out of the ab plane. Application of magnetic field introduces disorder in the AFM Pr sublattice, which, in turn, reduces the out-of-plane Pr-Fe exchange interaction responsible for Fe spin reorientation. Both in $\rho(T)$ and $d(C/T)/dT$ curves, the peak at T_{SR} broadens with the increase of H due to the introduction of the disorder in the AFM Pr sublattice by magnetic field. In the $\rho(T)$ curve, the peak shifts toward lower temperature with H and disappears above 6T, while in the $d(C/T)/dT$ curve, the peak remains visible up to 14T. The broadening of the anomaly at T_N^{Pr} in $C(T)$ with increasing H further confirms that magnetic field induces disorder in the AFM Pr sublattice.

D Bhoi, P Mandal, P Choudhury†, et al

2.2.2.5 Effect of magnetic field and pressure on charge-orbital ordering in $\text{Pr}(\text{Sr}_{1-x}\text{Ca}_x)_2\text{Mn}_2\text{O}_7$ ($x=0.4$ and 0.9) single crystals

The magnetic properties of half-doped $\text{Pr}(\text{Sr}_{1-x}\text{Ca}_x)_2\text{Mn}_2\text{O}_7$ ($x=0.4$ and 0.9) single crystals have been investigated under magnetic field (H) and hydrostatic pressure (P). Analysis of magnetization data reveals that, for $x=0.4$ sample, only one charge-orbital ordering (CO-OO) transition occurs which decreases very slowly with P , while the antiferromagnetic ordering transition shifts towards higher temperature with the increase of P . For $x=0.9$ sample, with the increase of P , the low-temperature CO-OO transition temperature decreases and the high-temperature CO-OO transition remains unaffected while antiferromagnetic and structural transition temperatures increase.

R Thiyagarajan†...P Mandal, et al

2.2.2.6 Critical behavior in single-crystalline $\text{La}_{0.67}\text{Sr}_{0.33}\text{CoO}_3$

The critical behavior of $\text{La}_{0.67}\text{Sr}_{0.33}\text{CoO}_3$ single crystal has been investigated from the bulk magnetization measurements around the Curie temperature (T_C). The detailed analysis of the magnetization indicates the occurrence of a continuous ferromagnetic to paramagnetic phase transition at 223.0 K. The critical exponents $\beta=0.361\pm0.007$, $\gamma=1.31\pm0.001$, and $\delta=4.64\pm0.01$ characterizing this second order phase transition, have been estimated using different techniques such as the Kouvel-Fisher plot, the Arrott-Noaksplot, and critical isotherm analysis. With these values of T_C , β , and γ , one can scale the magnetization below and above T_C following a single equation of state. The consistency in the values of the critical exponents obtained from different methods and the well-obeyed scaling behavior confirm that the calculated exponents are unambiguous and purely intrinsic to the system. These values of the exponents match well with those theoretically predicted for the three-dimensional Heisenberg model with nearest-neighbor interaction.

N Khan, A Midya, K Mydeen†, P Mandal, A Loidl†, D Prabhakaran†

2.2.2.7 Valence behavior of Eu-ions in intermetallic compound $\text{Ce}_{0.5}\text{Eu}_{0.5}\text{Pd}_3\text{B}_{0.5}$

We have studied the valence behavior of rare-earth ions, in particular Eu-ions, in a cubic intermetallic compound $\text{Ce}_{0.5}\text{Eu}_{0.5}\text{Pd}_3\text{B}_{0.5}$ which is a homogeneous solid solution of two mixed-valent compounds CePd_3 and EuPd_3B . Results of ^{151}Eu Mossbauer spectroscopic measurements show that two different valence states, i.e., divalent- and trivalent-like states of Eu-ions exist in the compound. The possible reason for the observed heterogeneous valency vis--vis the variation in the chemical environment and the number of nearest-neighbor B atoms surrounding the Eu-ions has been discussed. Our results demonstrate that B incorporation in such Eu-based cubic intermetallic compounds leads to a situation where heterogeneous-valence state of Eu-ions is an energetically favorable ground state.

Abhishek Pandey†, Chandan Mazumdar, R Ranganathan, et al

2.2.2.8 Surface spin glass and exchange bias effect in $\text{Sm}_{0.5}\text{Ca}_{0.5}\text{MnO}_3$ manganites nano particles

In this letter, we report that the charge/orbital order state of bulk antiferromagnetic $\text{Sm}_{0.5}\text{Ca}_{0.5}\text{MnO}_3$ is suppressed and confirms the appearance of weak ferromagnetism below 65 K followed by a low temperature spin glass like transition at 41 K in its nano metric counterpart. Exchange anisotropy effect has been observed in the nano manganites and can be tuned by the strength of the cooling magnetic field (H-cool). The values of exchange fields (H-E), coercivity (H-C), remanence asymmetry (M-E) and magnetic coercivity (M-C) are found to strongly depend on cooling magnetic field and temperature. H-E increases with increasing H-cool but for larger H-cool, H-E tends to decrease due to the growth of ferromagnetic cluster size. Magnetic training effect has also been observed and it has been analyzed thoroughly using spin relaxation model. A proposed phenomenological core-shell type model is attributed to an exchange coupling between the spin-glass like shell (surrounding) and antiferromagnetic core of $\text{Sm}_{0.5}\text{Ca}_{0.5}\text{MnO}_3$ nano manganites mainly on the basis of uncompensated surface spins. Results suggest that the intrinsic phase inhomogeneity due to the surface effects of the nanostructured manganites may cause exchange

anisotropy, which is of special interests for potential application in multifunctional spintronic devices.

SK Giri†, A Poddar, TK Nath†

2.2.2.9 Influence of annealing temperature on the structural, topographical and optical properties of sol-gel derived ZnO thin films

This investigation deals with the effect of annealing temperature on the structural, topographical and optical properties of Zinc Oxide thin films prepared by sol-gel method. The structural properties were studied using X-ray diffraction and the recorded patterns indicated that all the films had a preferred orientation along (002) plane and the crystallinity along with the grain size were augmented with annealing temperature. The topographical modification of the films due to heat treatment was probed by atomic force microscopy which revealed that annealing roughened the surface of the film. The optical properties were examined by a UV-visible spectrophotometer which exhibited that maximum transmittance reached nearly 90% and it diminished with increasing annealing temperature.

Sengupta Joydip, RK Sahoo†, KK Bardhan, CD Mukherjee

2.2.2.10 Nonlinearity exponents in lightly doped conducting polymers

The I-V characteristics of four conducting polymer systems such as doped polypyrrole, poly(3,4-ethylenedioxythiophene), polydiacetylene, and polyaniline in as many physical forms have been investigated at different temperatures, quenched disorder, and magnetic fields. Transport data clearly show the existence of a single electric-field scale in each system. Based upon this observation, a phenomenological scaling analysis is performed, leading to the extraction of a numerical value for a nonlinearity exponent called $x(M)$ which serves to characterize a set of I-V curves. The conductivity starts deviating from an Ohmic value $\sigma(0)$ above an onset electric field F_0 which scales according to F_0 similar to $\sigma(xM)(0)$. The electric-field-dependent data are shown to be described by the multistep tunneling model of Glazman-Matveev [JETP 67, 1276 (1988)] in a near-perfect manner over nine orders of magnitude in conductivity and five orders of magnitude in electric field. Furthermore, xM is found to possess both positive and negative values lying between $-1/2$ and $3/4$. There is no theory at present for this exponent. Some issues concerning applicability of the Glazman-Matveev model are discussed.

D Talukdar, UN Nandi†, KK Bardhan A De, CD Mukherjee

2.2.2.11 Current-driven orbital order-disorder transition in LaMnO₃

We report a significant influence of electric current on the orbital order-disorder transition in LaMnO₃. The transition temperature T_{OO} , thermal hysteresis in the resistivity (ρ) versus temperature (T) plot around T_{OO} , and latent heat L associated with the transition decrease with an increase in current density. Eventually, at a critical current density, L reaches zero. The transition zone, on the other hand, broadens with an increase in current density. The states at ordered, disordered, and transition zones are all found to be stable within the time window from similar to

10^{-3} to similar to 10^4 s.

Parthasarathi Mondal†, Dipten Bhattacharya†, P Mandal

2.2.2.12 Magnetic and electrical transport properties of $\text{La}_{0.5}\text{A}_{0.5}\text{CoO}_3$ nanoparticles (A=Sr, Ca, and Ba)

We have investigated the effect of particle size on the electrical transport and magnetic properties of $\text{La}_{0.5}\text{A}_{0.5}\text{CoO}_3$ (A = Sr, Ca, and Ba) nanoparticles synthesized by sol-gel technique. A size-induced metal to insulator transition is observed in the resistivity behaviour of Sr- and Ba-doped samples as the dimension changes from higher to lower ones. The magnetoresistance exhibits almost linear behaviour throughout the studied field range. The zero-field-cooled (ZFC) and field-cooled (FC) magnetizations display a broad paramagnetic to ferromagnetic transition at T-C with a large magnetic irreversibility. The magnetization results indicate that Co^{3+} ions are in the intermediate spin state but Co^{4+} ions stay in a mixture of intermediate and high spin states. The observed frequency dependent shoulder in the in-phase and the peak in the out of phase component of the ac susceptibility indicate the glassy nature of the samples. The analysis of the ac magnetization results suggests that the magnetic behaviour is consistent with the cluster glass model.

B Roy, S Das

2.2.2.13 Cluster glass behaviour in Co-substituted double perovskite $\text{Ca}_2\text{FeMoO}_6$

The transport and magnetic properties of the double perovskite compounds $\text{Ca}_2\text{Fe}_{1-x}\text{Co}_x\text{MoO}_6$ ($0.1 \leq x \leq 0.4$) have been explored through resistivity [$\rho(T)$], dc magnetisation [$M(H, T)$] and ac susceptibility [$\chi(T, f)$] measurements. Introduction of Co increases the lattice volume implying the divalent nature of cobalt in this system. For all the samples, $\rho(T)$ behaviour over the temperature range (25-273 K) can be adequately described by considering possible disorder-enhanced electron-electron interaction effect as well as spin-wave contribution. Our results reveal that with the increase of Co concentration, the ferromagnetic Curie temperatures (T_c) gradually reduced due to the incorporation of antiferromagnetic Co^{2+} - Mo^{6+} pairs replacing ferromagnetic Fe^{3+} - Mo^{5+} pairs. A cluster-glass like behaviour is also observed in the system due to the presence of highly spin-disordered regions.

Asok Poddar, Chandan Mazumdar

2.2.2.14 Quantum magnetoresistance of the PrFeAsO oxypnictide

We report the observation of an unusual H dependence of transverse magnetoresistance (MR) in the PrFeAsO , one of the parent compound of pnictide superconductors. Below the spin density wave transition, MR is large, positive and increases with decreasing temperature. At low temperatures, MR increases linearly with H up to 14 T. For $T \geq 40$ K, MR versus H curve develops a weak curvature in the low-field region which indicates a crossover from H linear to H^2 dependence as $H \rightarrow 0$. The H linear MR originates from the Dirac cone states and has been explained by the

quantum mechanical model proposed by Abrikosov.

D Bhoi, P Mandal, P Choudhury†

2.2.2.15 The magnetization of $\text{PrFeAsO}_{0.60}\text{F}_{0.12}$ superconductor

The magnetization of the $\text{PrFeAsO}_{0.60}\text{F}_{0.12}$ polycrystalline sample has been measured as functions of temperature and magnetic field (H). The observed total magnetization is the sum of a superconducting irreversible magnetization and a paramagnetic magnetization. Analysis of dc susceptibility $\chi(T)$ in the normal state shows that the paramagnetic component of magnetization comes from the Pr^{3+} magnetic moments. The intragrain critical current density (J_L) derived from the magnetization data is large. The $J_L(H)$ curve displays a second peak which shifts towards the high-field region with decreasing temperature. In the low-field region, a plateau up to a field H^* followed by a power law $H^{5/8}$ behavior of $J_L(H)$ is the characteristic of the strong pinning. A vortex phase diagram for the present superconductor has been obtained from the magnetization and resistivity data.

D Bhoi, P Mandal, P Choudhury† et al

2.2.2.16 Electrical Transport and Magnetic Properties of PEDOT-Ferrite Nanocomposites

We have studied the temperature-dependent transport and magnetic properties of the nanocomposites, containing varied amounts of CoFe_2O_4 , NiFe_2O_4 , and Fe_3O_4 nanoparticles embedded in the conducting poly(3,4-ethylenedioxythiophene) or PEDOT matrix, in the temperature range 77-300 K. Resistivities of all the composites, including pure PEDOT follows the Mott VRH relation $\rho - \rho_0 T^{-1/4}$ over the studied temperature range. This suggests that hopping is the mechanism of transport in these systems. Plots of $(\ln\rho - \ln\rho_0)/A$ as a function of temperature for all the studied samples are found to collapse on a single curve. Although, the conduction mechanism does not change with nanoparticle inclusions in the polymer matrix, the hopping parameters change in the nanocomposites. Magnetic studies of ferrite nanoparticles and nanocomposites show signature of superparamagnetic blocking, with a distribution of particle size. The spin structure on the surface of any particle is different from that of the core.

Asok Poddar...Amitabha De...Sangam Banerjee

2.2.2.17 Effect of Si/Ge ratio on resistivity and thermopower in $\text{Gd}_5\text{Si}_x\text{Ge}_{4-x}$ magnetocaloric compounds

The effect of Si/Ge ratio on resistivity and thermopower behavior has been investigated in the magnetocaloric ferromagnetic $\text{Gd}_5\text{Si}_x\text{Ge}_{4-x}$ compounds with $x=1.7-2.3$. Microstructural studies reveal the presence of $\text{Gd}-5(\text{Si}, \text{Ge})_4$ -matrix phase (5:4-type) along with traces of secondary phases (5:5 or 5:3-type). The $x=1.7$ and 2.0 samples display the presence of a first order structural transition from orthorhombic to monoclinic phase followed by a magnetic transition of the monoclinic phase. The alloys with $x=2.2$ and 2.3 display only magnetic transitions of the orthorhombic phase. A low temperature feature apparent in the AC susceptibility and resistivity data below 100 K reflects

an antiferromagnetic transition of secondary phase(s) present in these compounds. The resistivity behavior study correlates with microstructural studies. A large change in thermopower of $-8 \mu\text{V}/\text{K}$ was obtained at the magneto-structural transition for the $x=2$ compound.

DM Raj Kumar†, Asok Poddar, R Ranganathan, et al

2.2.3 Surface Physics

2.2.3.1 Hydroxyapatite-supported Cu(I)-catalysed cyanation of styrenyl bromides with $\text{K-4}[\text{Fe}(\text{CN})_6]$: an easy access to cinnamitriles

An efficient cyanation of styrenyl bromides by $\text{K-4}[\text{Fe}(\text{CN})_6]$ has been achieved under the catalysis of hydroxyapatite-supported copper(I) producing a variety of functionalized cinnamitriles in high yields. The stereochemistry of the styrenyl double bond is preserved during the process providing the same stereoisomer of product.

Debasree Saha†, Laksmikanta Adak†, M Mukherjee, et al

2.2.3.2 Pit formation on the $\text{Ge}(1\ 0\ 0)$ surfaces by normal incident Si^- ion implantation

We have observed micron size pit formation on Ge surface due to bombardment of 26 keV Si^- ion at normal incidence in the fluence range 1×10^{18} and 7×10^{18} ions/cm². Scanning electron microscopy (SEM) and atomic force microscopy (AFM) are used to follow the evolution of the surface morphology. The pits are of various shapes, e. g., crescent-shaped, kidney-like or circular structures. The two-field continuum model developed for small slope approximations can describe the pit formation and growth at the very beginning of ion bombardment. The growth of the pits at late times (high fluence) can be explained by the gradient dependent erosion mechanisms due to primary ion beam as well by secondary flux of particles originating from steep slopes. Energy dispersive X-ray analysis attached to SEM is employed to obtain the chemical information of the pitted surface. The depletion of Si at the bottom of the pits is explained due to lower diffusivity of Si in Ge.

SA Mollick, S Karmakar, A Metya, D Ghose

2.2.3.3 Nanostructures on GaAs surfaces due to 60 keV Ar^+ -ion beam sputtering

The effect of 60 keV Ar^+ -ion beam sputtering on the surface topography of p-type GaAs(1 0 0) was investigated by varying angle of incidence of the ion ($0\text{-}60^\circ$) with respect to substrate normal and the ion fluence (2×10^{17} - 3×10^{18} ions/cm²) at an ion flux of 3.75×10^{13} ions/cm²-s. For normal incidence and at a fluence of 2×10^{17} ions/cm², holes and islands are observed with the former having an average size and density of 31 nm and 4.9×10^9 holes/cm², respectively. For 30° and 45° off-normal incidence, in general, a smooth surface appears which is unaffected by increase of fluence. At 60° off-normal incidence dots are observed while for the highest fluence of 3×10^{18} ions/cm² early stage of ripple formation along with dots is observed with amplitude of 4 nm. The applicability and limitations of the existing theories of ion induced pattern formation to account

for the observed surface topographies are discussed.

V Venugopal†...SR Bhattacharyya...

2.2.3.4 Growth process of GaAs ripples as a function of incident Ar-ion dose

We report periodic ripple formation on GaAs sputtered by 60 keV Ar ions at an angle of 60° over a large range of ion doses from 1×10^{17} to 1×10^{19} ions/cm² under Atomic Force Microscopy (AFM) study. Initially in the dose range between 1×10^{17} and 4×10^{17} ions/cm², only very small roughness is formed on the surface and from the dose of 5×10^{17} ions/cm², the ripples start to form and attain a well-defined structure at a dose around 9×10^{17} ions/cm², remain stable and then from a dose of 4×10^{18} ions/cm², the ripple structures become very rough, periodicity breaks down and step-like features become prominent all over the surface. Parameters like rms roughness, ripple wavelength, amplitude etc. are measured from the AFM image analysis. The results are discussed with the help existing formalism with the understanding of preferential sputtering of one of the components of GaAs.

D Datta, Shyamal Mondal, SR Bhattacharyya

2.2.3.5 Effect of thermal annealing and neutron irradiation in 6H-SiC implanted with silver at 350°C and 600°C

The effect of thermal annealing and neutron irradiation in 6H-SiC implanted with silver at 350°C and 600°C have been investigated using Rutherford backscattering spectrometry (RBS), Rutherford backscattering spectrometry in channeling mode (RBS-C) and scanning electron spectroscopy (SEM). Implantation at 600°C and 350°C caused the 6H-SiC to retain crystallinity. The 600°C samples had less distortions compared to 350°C implanted samples. Annealing of the radiation damage created during implantation is also reported. No diffusion of silver was detected after thermal annealing but a shift of the silver peak toward the surface due to thermal etching was observed. The amount of etched SiC has also been estimated by comparing the peak position before and after annealing. Similarly no diffusion was observed after low dose neutron irradiation of the samples.

TT Hlatshwayo†...P Chakraborty

2.2.3.6 Behavior of iodine implanted in highly oriented pyrolytic graphite (HOPG) after heat treatment

The behavior of iodine implanted in highly oriented pyrolytic graphite (HOPG) has been investigated using Rutherford backscattering spectrometry (RBS), scanning electron microscopy (SEM) and X-ray diffraction (XRD). Iodine ions were implanted into HOPG using an energy of 360 keV and a dose of 1×10^{15} atoms cm² at room temperature. The implanted samples were annealed in vacuum at 900°C, 1000°C, 1100°C and 1200°C, all for 9 h. The results revealed that iodine was released from the HOPG at the above annealing temperatures. RBS evaluation of the full width at half maximum (FWHM) and the number of iodine atoms before and after annealing did not reveal Fickian diffusion as the mechanism by which the iodine atoms were released from the HOPG. Evaluation of (0 0 2) peak intensities using XRD revealed an increase in preferred orientation of

the graphitic layers after heat treatment of 1200°C. The high resolution SEM micrographs of the HOPG samples before and after heat treatment showed no evidence of alterations on the polished surface.

Mxolisi B Mukhawana†...Purushottam Chakraborty

2.2.3.7 Ion-Beam-Synthesized Colloidal Silver Nanoclusters in Crystalline Sapphire as Third-Order Optical Material

Silver ion implantation in single-crystalline sapphire has given rise to the formation of silver nanoparticle-sapphire composites, which have been imaged using transmission electron microscopy, and confirmed using linear optical absorption and Rutherford backscattering spectrometry. Nonlinear refractive index and two-photon absorption of these nanocomposites have been observed using Z-scan and Anti-resonant Interferometric Nonlinear Spectroscopy (ARINS) in the close proximity of surface plasmon resonance (SPR) wavelength of silver nanoclusters (similar to 400 nm) and at similar to 807 nm, respectively. Both sign and value of the nonlinear parameters were determined, and the third-order optical susceptibility ($\chi^{(3)}$) of the composites has been found to be significant. Such metal nanocomposites in glasses and sapphires having appreciable $\chi^{(3)}$ with temporal responses in picosecond to femtosecond time domain have great relevance to futuristic switching materials in nanophotonics.

Anna Kozakiewicz‡, Binita Ghosh, Purushottam Chakraborty, et al

2.2.3.8 Morphology induced magnetic instabilities on oxide antiferromagnetic surfaces

The role of interfacial disorder and roughness has been pointed out several times in ferromagnetic-antiferromagnetic exchange coupled systems. However, effect of surface morphology on magnetic properties of bare antiferromagnetic material has been mostly ignored. Here we report our experimental observations of magnetic instabilities on high temperature air annealed NiO(100) surfaces through treatment of successive vacuum and oxygen annealing above Nel temperature. Preferential spin-orientations are found to be governed by surface morphology with enhanced roughness and oxygen diffusion process. Stable domain distribution has been observed on smoother surfaces, which are found to be mostly inactive to these annealing treatments.

Suman Mandal, Krishnakumar SR Menon

2.2.3.9 Substrate and drying effect in shape and ordering of micelles inside CTAB-silica mesostructured films

Deviation from a perfect 2D-hexagonal ($p6m$) structure, for CTAB-silica mesostructured films prepared by adding different amounts of excess ethanol to a solution of CTAB and TEOS just before spin coating on OH- and H-terminated Si substrates, is observed from combined X-ray reflectivity and grazing incidence small angle X-ray scattering measurements. Such a deviation can be well understood in terms of the shape and ordering of the micelles, with or without the silica coating layer's contribution, inside the film. For example, cylindrical shaped micelles, which are initially

circular on a hydrophilic OH-terminated Si substrate in order to form a perfect 2D-hexagonal structure, become elliptical (extended along the in-plane) on a hydrophobic H-terminated Si substrate to form a slightly compressed 2D-hexagonal structure due to a different attachment of the film to the substrate. With time, due to the drying of the silica materials and its restricted movement along the in-plane direction, the films on both the substrates are compressed along the out-of-plane direction only, to form observed centered rectangular (c2mm) structures. Also, due to the asymmetric shrinkage, stress is developed, which deteriorates the ordering in the film. The final shape of the micelles, including the silica coating layer's contribution, shows maximum and minimum deviations from the circular shape inside the thick film on a OH-Si substrate and the thin film on a H-Si substrate, respectively. The deviation in the shape of the micelles itself, which is of actual importance, seems to be maximum and minimum inside the thick film on a H-Si substrate and the thin film on a OH-Si substrate, respectively, and is essentially determined by the substrate nature and initial silica wall thickness.

P Chatterjee, S Hazra, H Amenitsch†

2.2.3.10 High Ferromagnetic Transition Temperature in PbS and PbS: Mn Nanowires

Spontaneous magnetization measured in the temperature range 5-300 K with high ferromagnetic transition temperature (T_c) has been observed in both undoped and Mn doped (2-8 mol%) PbS nanowires (diameter 30 nm) in polymer. For undoped sample, we find T_c similar to 290 K while for doped samples T_c varies between 310-340 K depending on Mn concentrations. Both T_c and coercive fields are critically dependent on Mn concentrations. Coercive fields show a $T^{-0.5}$ dependence with temperature for a moderate concentration of Mn (4 mol%) in PbS while it deviates from $T^{-0.5}$ behavior for higher Mn concentrations. Anionic defects arising out of nonstoichiometric growth is solely responsible for the observed magnetism in undoped PbS nanowires. The role of intrinsic strain along with reduced dimensionality in determining such high T_c and overall magnetizations has been discussed.

Swapan K Mandal†, Arup Ratan Mandal, Sangam Banerjee

2.2.3.11 Finite size versus surface effects on magnetic properties of antiferromagnetic particles

The observation of finite magnetic moment in antiferromagnetic materials is quite unusual and has been immensely investigated in nanoparticle systems. Here, the structural and magnetic properties of NiO particles are explored by x-ray diffraction, extended x-ray absorption fine structure, and magnetization measurements. Using similar-sized particles with different surface defect structure, we show that the observed magnetic enhancement, which is present even beyond finite-size limit, is due to the surface effects. However, the well known spin glass freezing is found to occur only in nano-regime.

Suman Mandal, Krishnakumar SR Menon, SK Mahatha, S Banerjee

2.2.3.12 Reorganization of Au nanoparticle Langmuir-Blodgett films on wet chemically passivated Si (001) surfaces

Growth of dodecanethiol-encapsulated Au nanoparticles on differently terminated (OH-, H-, or Br-terminated) Si(001) substrates by Langmuir-Blodgett method at a constant monolayer surface pressure and their out-of-plane structural modification with time have been investigated. As the substrates have different gradations in the hydrophilic/hydrophobic nature, three different out-of-plane structures have been formed. On H-terminated Si (hydrophobic surface), a fluctuating monolayer of Au nanoparticles has been formed, whereas on Br- (coexistence of hydrophilic and hydrophobic surfaces) and OH-terminated Si (hydrophilic surfaces), trilayer of Au nanoparticles have been formed, but the top layer coverage is more for the OH-terminated Si. The growth of Au nanoparticles on H-terminated Si is similar to the Frank-van der Marwe mode, whereas on Br- and OH-terminated Si, the growth is similar to the Stranski-Krastanov mode. These three different structures modify with time and finally become a thicker monolayer of high density, and positions of nanoparticles within the monolayer become random. AFM images of the films also show that positions of the Au nanoparticles are random. Density of the final layer becomes maximum on OH-terminated Si and minimum on H-terminated Si, whereas it becomes intermediate on Br-terminated Si. Reorganization thus helps to obtain nanostructures of tunable nanoparticle density.

Sarathi Kundu†, JK Bal

2.2.3.13 Enhanced ultraviolet-visible cathodoluminescence from Ar⁺ beam-induced nano-patterned silicon

Cathodoluminescence (CL) of 60 keV Ar ion beam-induced ripple patterned Si in a high resolution scanning electron microscope (HRSEM) shows strong room temperature (RT) luminescence bands compared to a nonpatterned or patterned recrystallized Si. Site-specific CL spectroscopy and imaging data indicate while the top and front surface of ripples contribute predominantly to the red and near infra-red (IR) emission at similar to 650 and 750 nm respectively, the back surface contributes mostly to ultraviolet (UV) emission ~ 365 nm. When the patterned sample is recrystallized after high temperature annealing, one observes a blue shift of the red peak to a yellow peak ~ 575 nm. Nanostructured Si of varying sizes (~ 0.2 -5 nm) located around amorphous/crystalline (a/c)-interface and beyond it appears to be probable origin of luminescence observed in the present study.

Pabitra Das, Tapas Kumar Chini

2.2.3.14 Mean-field solutions of kinetic-exchange opinion models

We present here the exact solution of an infinite range, discrete, opinion formation model. The model shows an active-absorbing phase transition, similar to that numerically found in its recently proposed continuous version [Lallouache et al., Phys. Rev. E 82, 056112 (2010)]. Apart from the two-agent interactions here we also report the effect of having three-agent interactions. The phase diagram has a continuous transition line (two-agent interaction dominated) and a discontinuous

transition line (three-agent interaction dominated) separated by a tricritical point.

Soumyajyoti Biswas

2.2.3.15 Structural and morphological characterization of molecular beam epitaxy grown Si/Ge multilayer using X-ray scattering techniques

Si/Ge multilayers are of great technological importance as is evident from the research studies of the past two decades. Here, we have presented a method for the morphological and structural characterization of such MBE grown epitaxial Si/Ge superlattice structures using simultaneous analysis of x-ray reflectivity and x-ray diffraction data, respectively. The consistent analysis of the data collected in the Indian Beamline at Photon Factory Synchrotron have allowed for the determination of electron density and strain profile as a function of depth.

M Sharma, MK Sanyal, MK Mukhopadhyay, MK Bera, B Saha, P Chakraborty

2.2.3.16 Application of differential charging in XPS for structural study of Langmuir-Blodgett films

Differential charging in XPS was recently shown to be a novel technique for studying in-depth structural information of discrete cadmium layers in LangmuirBlodgett (LB) multilayer films. Here we report structural modification in multilayer LB films after sulfidation using differential charging in angle-dependent XPS that are not observable by the x-ray reflectivity technique. An AFM study suggests less modification in compact LB films in comparison to the non-compact ones. The differential charging in the LB multilayers changes after sulfidation due to the formation of cadmium sulfide nanostructures in the cadmium arachidate LB matrix, which was reflected prominently in the differential charging of Cd 3d_{5/2} XPS peaks. It was found that, even after sulfidation, the compact multilayer LB films were differentially charged in the out-of-plane (in-depth) direction, whereas this kind of differential charging was not apparent in rough and non-compact films. Our results clearly indicate that for LB films with compact structure a partial layered structure survives the impact of particle formation, whereas for non-compact films the modification is large and no specific conclusion could be drawn. While x-ray reflectivity cannot provide specific information about the internal structure of the post-sulfidation films it shows that the total thickness of the films reduces in all cases.

AKM Maidul Islam, M Mukherjee

2.2.3.17 Driven k-mers: Correlations in space and time

Steady-state properties of hard objects with exclusion interaction and a driven motion along a one-dimensional periodic lattice are investigated. The process is a generalization of the asymmetric simple exclusion process (ASEP) to particles of length k , and is called the k -ASEP. Here, we analyze both static and dynamic properties of the k -ASEP. Density correlations are found to display interesting features, such as pronounced oscillations in both space and time, as a consequence of the extended length of the particles. At long times, the density autocorrelation decays exponentially in time, except at a special k -dependent density when it decays as a power law. In the limit of large

k at a finite density of occupied sites, the appropriately scaled system reduces to a nonequilibrium generalization of the Tonks gas describing the motion of hard rods along a continuous line. This allows us to obtain in a simple way the known two-particle distribution for the Tonks gas. For large but finite k, we also obtain the leading-order correction to the Tonks result.

Shamik Gupta†, Mustansir Barma†, Urna Basu, PK Mohanty

2.2.3.18 Surface antiferromagnetic domain imaging using low-energy unpolarized electrons

We report on the surface antiferromagnetic (AFM) domain imaging of the prototype antiferromagnet NiO(100) using an electron-microscopy-based laboratory method. Coherently exchange-scattered electrons from the surface AFM lattice are utilized in a low-energy electron microscope to resolve the surface domain structure. Direct comparison with x-ray magnetic linear dichroism photoemission electron microscopy demonstrates a complimentary nature. High surface sensitivity combined with improved spatial resolution of this method enables studying of nanosized magnetic domains in NiO(100) thin films and their thickness-dependent evolution.

Krishnakumar SR Menon, Suman Mandal, Jayanta Das, et al

2.2.3.19 Unoccupied electronic structure of graphite probed by angle-resolved photoemission spectroscopy

We report the observation of anomalous bands in graphite valence band structure in angle-resolved photoemission spectroscopy (ARPES) experiments. The photon energy dependence of these bands shows a constant kinetic energy nature. Our results are supported by the very low energy electron diffraction data reported on graphite surfaces which essentially map the unoccupied states representing the photoemission final states. This suggests that the ARPES technique is capable of probing the unoccupied electronic states governed by the secondary electron emission process, along with the occupied bands of solids.

SK Mahatha, Krishnakumar SR Menon, T Balasubramanian†

2.2.3.20 Modifications of local structures of Gd₂O₃ on incorporation of SiO₂

In the present work we have reported the results of investigations on local structures of e-beam evaporated (Gd₂O₃-SiO₂) composite thin films by synchrotron based EXAFS measurements. The evolution of local structure in the case of the Gd₂O₃-SiO₂ system is found to be different from the HfO₂-SiO₂ system reported by us earlier. The EXAFS analysis has shown that the Gd-O bond length decreases monotonically as SiO₂ content in the films increases. Also the amplitudes of the peaks in the FT-EXAFS spectra of the samples, which depend jointly on the coordination numbers as well as the Debye-Waller factors (measure of disorder) are found to decrease monotonically with increase in SiO₂ contents in the Gd₂O₃ matrix. Atomic force microscopy (AFM) measurements of the samples also show continuous evolution of amorphous-like denser microstructure with increase in SiO₂ content in the films. Hence incorporation of SiO₂ in the Gd₂O₃ matrix, results in a continuous change in oxygen coordination yielding a change in the Gd-O bond length and also results

in a continuous increase in amorphousness and a smoother morphology of the samples and, unlike the $\text{HfO}_2\text{-SiO}_2$ system, does not show any maximum for a particular SiO_2 concentration.

NC Das†, S Hazra, JK Bal, et al

2.2.3.21 Role of Interfacial Interaction in Orientation of Poly(N-isopropylacrylamide) Chains on Silicon Substrate

Studies of self-assembled PNIPAM films on hydrophilic and hydrophobic substrates that are grown below and above lower critical solution temperature (LCST) have been performed to understand the role of intramolecular and polymer substrate interactions in self-assembly using near edge X-ray absorption fine structure (NEXAFS) spectroscopy, atomic-force microscopic (AFM) and density functional theory (DFT). The NEXAFS spectra suggest that the polymer chains are oriented similarly on hydrophilic as well as hydrophobic substrate although the chains were having different morphologies in the solution, whereas, AFM studies shows that the morphology of the polymer chains on the two substrates are widely different. NEXAFS absorption spectra for free molecule and that with effects of substrate were calculated using DFT. The results show that on hydrophobic substrate polymer substrate interaction is stronger as compared to that with hydrophilic one, however, for both cases this interaction plays dominant role over the intramolecular interaction for the orientation of the chains on the substrate. Matching of the calculated and experimental NEXAFS spectra shows on both types of substrates only a fraction of the attached molecules are oriented. Effect of external force on polymer substrate attachment was studied with the spin-coated films on hydrophilic substrate. Our results show that in this case substrate attachment plays an important role unlike the case of self-assembly on hydrophilic substrate, where the polymer substrate interaction is weak.

C -H Wang†, S Mukherjee, AKM Maidul Islam...M Mukherjee

2.2.3.22 Role of initial morphology in H₂S treated cadmium arachidate Langmuir - Blodgett films

To examine the issues like the shape of the CdS clusters, time and thickness dependence of chemical conversion and to study the correlation between the pre and post sulfidation structure of the LB films on CdS formation, a set of multilayer cadmium arachidate LB films grown with different morphology and thickness have been studied using AFM, TEM, X-ray reflectivity and XPS. Microscopic evidence of formation of nearly uniform CdS nanoparticles of around 4.5 nm in the LB matrix was observed. In relatively compact films, mount like structures were found to develop due to out-of-plane molecular motion, whereas, for non compact films, expansion and molecular rearrangement appears to reduce the height non-uniformity and smooth out the surface as a result of sulfidation. Full conversion of cadmium arachidate to CdS was not achieved in the LB matrix even after a long exposure and the time required for conversion was found to be independent of film thickness, both contrary to the earlier observation. A partial conversion of a maximum of around 60% could be achieved in the films of various thickness and compactness indicating that partial survival of the layered structure after sulfidation may be possible in initially compact films.

AKM Maidul Islam, M Mukherjee

2.2.3.23 Surface spin orientation of NiO(100) and interfacial coupling of Fe/NiO(100) revisited with soft X-ray spectromicroscopy

Accurate retrieval of spin-axis orientation at the antiferromagnetic (AFM) surface requires involved consideration of the crystal field effect in X-ray magnetic linear dichroism (XMLD), which was neglected until recently. Here, we present a unique determination of surface spin-axes of the prototype antiferromagnet NiO(100) from detailed angular-dependent measurements using different polarizations of incident light by considering the recently developed angular dependence of the XMLD effect. The bulk twin domains terminating on the (100) surface have also been determined from the angular dependence of the experimental contrast at the oxygen K edge. The effect of Fe deposition on the AFM domain pattern was followed in situ and the interfacial exchange coupling of as-deposited Fe/NiO(100) has been explored using the recent formalism of XMLD. Unlike Co/NiO(100), we realize only the rough perpendicular coupling between Fe moments and compensated Ni spin-axes. The uncompensated spins (UCS) at the interface were also characterized and a mechanism of interfacial coupling is suggested.

Suman Mandal, Krishnakumar SR Menon, et al

2.2.3.24 Microscopic investigation of surface and interfacial magnetic domain structure of Fe-NiO(100) system

We report our experimental observation of microscopic modification, reconstruction and evolution of the antiferromagnetic domain structure of the NiO(1 0 0) surface in view of the exchange bias effect. Some domain patterns (called non-equilibrium domains) as observed on the as-cleaved surface do not follow the well-known bulk symmetry traces on the (1 0 0) surface. But, bulk-terminated domains (called equilibrium domains) are found to be renucleated up on cooling the sample from above the Neel temperature, unless domains are strongly pinned by crystalline defects. We also observe certain domain evolution after annealing the crystal at various temperatures above the Neel temperature. Influence of growth condition on the ferromagnetic domain structure of the Fe film deposited on NiO(1 0 0) has been followed in situ. While for thin film case (7 ML), no influence of growth has been observed, for thicker film (21 ML) the Fe domain structure is found to be determined by both growth-induced and exchange anisotropy. Thus, our observations depict a thickness-dependent interplay between growth-induced and exchange anisotropy in ferromagnetic film grown on the antiferromagnetic substrate.

Suman Mandal, Krishnakumar SR Menon, Francesco Maccherozzi†, et al

2.2.3.25 Iron oxide nanoparticles coated with gold: Enhanced magnetic moment due to interfacial effects

In this paper, we show that when nanoparticles of Fe₃O₄ are coated with gold there is a distinct enhancement of magnetization by a factor of six. This increase of magnetization has been attributed to large orbital magnetic moment formation at the magnetic particle/Au (core/shell) interface. Our theoretical analysis indicates that the enhanced magnetism observed in Fe₃O₄-Au (core-shell) nanoparticles is an interfacial effect. The origin of magnetism in Au as an interfacial phenomenon is supported by the observation of positive magnetization in citrate coated gold nanoparticles. In citrate coated gold nanoparticles, we observe a crossover from positive magnetization value to

negative magnetization value upon increasing magnetic field indicating cancellation of interfacial magnetization by the diamagnetic contribution from the bulk. We propose a theoretical formalism which semi-quantitatively explains our experimental results and supports the origin of magnetization in Au as an interfacial effect.

S Banerjee, SO Raja†, M Sardar†, et al

2.2.3.26 Large third-order optical nonlinearity of silver colloids in silica glasses synthesized by ion implantation

Silver ion implantations in fused silica glasses have been made to synthesize silver nanocluster-glass composites and a combination of 'Anti-Resonant Interferometric Nonlinear Spectroscopy (ARINS)' and 'Z-scan' techniques has been employed for the measurement of the third-order optical susceptibility of these nanocomposites. The ARINS technique utilizes the dressing of two unequal-intensity counter-propagating pulsed optical beams with differential nonlinear phases, which occurs upon traversing the sample. This difference in phase manifests itself in the intensity-dependent transmission, measurement of which enables us to extract the values of nonlinear refractive index (η_2) and nonlinear absorption coefficient (β), finally yielding the real and imaginary parts of the third-order dielectric susceptibility $\chi^{(3)}$. The real and imaginary parts of $\chi^{(3)}$ are obtained in the orders of 10^{-10} e.s.u for silver nanocluster-glass composites. The present value of $\chi^{(3)}$, to our knowledge, is extremely accurate and much more reliable compared to the values previously obtained by other workers for similar silver-glass nanocomposites using only Z-scan technique. Optical nonlinearity has been explained to be due to two-photon absorption in the present nanocomposite glasses and is essentially of electronic origin.

Binita Ghosh, Purushottam Chakraborty

2.2.3.27 Swelling Dynamics of Ultrathin Films of Strong Polyelectrolytes

Solvent mass uptake and the swelling of ultrathin polyelectrolyte films (within thickness range 157-375 angstrom) in the presence of water vapor have been performed to study the effect of long-range Coulombic interaction between charged segments of a polyelectrolyte chain on its swelling dynamics. Films were prepared from aqueous solution of poly(sodium 4-styrenesulfonate) (NaPSS) on hydrophilic silicon substrate using the spin-coating method. Diffusion coefficient of water has been obtained from the solvent mass uptake study using gravimetric measurement and was found to increase with the increase of film thickness. Swelling dynamics of the polymer films in the presence of water vapor, on the other hand, have been studied in situ using the X-ray reflectivity technique. The diffusion coefficient of the NaPSS chains has been found to be of the order of 10^{-18} cm²/s and was independent of the film thickness, whereas the fraction of charged monomer which determines the strength of the repulsive interaction between the polymer segments shows the confinement effect and increases linearly with the film thickness.

Tanusree Samanta, M Mukherjee

2.2.3.28 Structural reordering in monolayers of gold nanoparticles during transfer from water surface to solid substrate

Structural reordering in monolayers of gold nanoparticles during transfer from water surface to solid substrate has been studied by synchrotron x-ray scattering techniques. Grazing incidence diffraction (GID) and grazing incidence x-ray off-specular scattering (GIXOS) measurements were performed as a function of time to track the in-plane and out-of-plane structural reordering in the transferred monolayers. GID measurements show shift in the in-plane particle-particle correlation peak toward the lower in-plane momentum transfer value, signifying possible expansion of triangular lattice formed on the water surface. However, GIXOS data and supportive microscopy measurements clearly show compactification in the in-plane structure and associated out-of-plane movements. A model that assumes the possibility of a two-dimensional short-range structural reordering from triangular to square-like lattice as a function of time could explain all the data. The observed change in the electron densities of the nanoparticles before and after the structural reordering matches well with the expected change in the calculated electron densities of the nanoparticles arranged in triangular (pretransition) and square-like (post-transition) symmetry.

R Banerjee, MK Sanyal, MK Bera, et al

2.2.3.29 Study of surface magnetism, exchange bias effect, and enhanced ferromagnetism in $\alpha\text{-Fe}_{1.4}\text{Ti}_{0.6}\text{O}_3$ alloy

Magnetic properties of mechanical alloyed $\alpha\text{-Fe}_{1.4}\text{Ti}_{0.6}\text{O}_3$ were studied at broad scale of temperatures, starting from room temperature down to 5 K. Morin transition of the base compound $\alpha\text{-Fe}_2\text{O}_3$ was not observed after Ti doping. Enhanced ferromagnetism and exchange bias effect were exhibited in the alloyed compound $\alpha\text{-Fe}_{1.4}\text{Ti}_{0.6}\text{O}_3$. The observations were examined from different aspects of the alloying process, e. g., magnetic solution (spin ordering) at the interfaces of rhombohedral planes and core-shell structure of the nano-grains. Interfacial magnetic modifications were seen to be affected by the factors associated with grain size variation during alloy formation and thermal annealing of the alloy. Detailed analyses were made to understand the surface magnetism and exchange bias effect in the samples. Magnetic features of the present samples in many cases were found to be unconventional in comparison with the simple grain size effect of magnetic particles.

N Naresh†...B Ghosh, S Banerjee

2.2.3.30 Template Synthesis and Characterizations of Nickel Nanorods

Currently there is a considerable interest in the fabrication of nanoscale magnets, motivated by the technological interest involving the miniaturization of sensors and the continuous increase in the magnetic storage density. Ni nanorods (NRs) could serve as nanoscale magnets in such magnetic memories. They can also be used as magneto-optical switches in the field called photonics. Template assisted electrodeposition process proved to be an elegant chemical approach because it is simple and inexpensive and one can fabricate arrays of similar shaped, sized nanorods with large quantity. Here we have grown Ni nanorods using electro-deposition process and investigated using an Analytical Transmission Electron Microscope. Transmission Electron Microscopy (TEM) images and diffraction patterns reveal the polycrystalline nature of grown Ni nanorods and the

composition of these nanorods were verified using energy dispersive X-ray (EDX) spectroscopy. Further study is in progress to grow the full length NRs with improved crystalline quality.

Tanmay Ghosh, Biswarup Satpati

2.2.4 Theoretical Condensed Matter Physics

2.2.4.1 Integer quantum Hall effect in a square lattice revisited

We investigate the phenomenon of integer quantum Hall effect in a square lattice, subjected to a perpendicular magnetic field, through Landauer-Buttiker formalism within the tight-binding framework. The oscillating nature of longitudinal resistance and near complete suppression of momentum relaxation processes are examined by studying the flow of charge current using Landauer-Keldysh prescription. Our analysis for the lattice model corroborates the finding obtained in the continuum model and provides a simple physical understanding

Santanu K Maiti, Moumita Dey, SN Karmakar

2.2.4.2 Continuous transition of social efficiencies in the stochastic-strategy minority game

We show that in a variant of the minority game problem, the agents can reach a state of maximum social efficiency, where the fluctuation between the two choices is minimum, by following a simple stochastic strategy. By imagining a social scenario where the agents can only guess about the number of excess people in the majority, we show that as long as the guessed value is sufficiently close to the reality, the system can reach a state of full efficiency or minimum fluctuation. A continuous transition to less efficient condition is observed when the guessed value becomes worse. Hence, people can optimize their guess for excess population to optimize the period of being in the majority state. We also consider the situation where a finite fraction of agents always decide completely randomly (random trader) as opposed to the rest of the population who follow a certain strategy (chartist). For a single random trader the system becomes fully efficient with majority-minority crossover occurring every 2 days on average. For just two random traders, all the agents have equal gain with arbitrarily small fluctuations.

Soumyajyoti Biswas, Asim Ghosh...Tapan Naskar, Bikas K Chakrabarti

2.2.4.3 Percolation in a kinetic opinion exchange model

We study the percolation transition of the geometrical clusters in the square-lattice LCCC model [a kinetic opinion exchange model introduced by Lallouache, Chakrabarti, Chakraborti, and Chakrabarti, Phys. Rev. E 82, 056112 (2010)] with the change in conviction and influencing parameter. The cluster is comprised of the adjacent sites having an opinion value greater than or equal to a prefixed threshold value of opinion (Ω). The transition point is different from that obtained for the transition of the order parameter (average opinion value) found by Lallouache et al. Although the transition point varies with the change in the threshold value of the opinion, the critical exponents for the percolation transition obtained from the data collapses of the maximum cluster size, the cluster size distribution, and the Binder cumulant remain the same. The exponents

are also independent of the values of convection and influencing parameters, indicating the robustness of this transition. The exponents do not match any other known percolation exponents (e. g., the static Ising, dynamic Ising, and standard percolation). This means that the LCCC model belongs to a separate universality class.

Anjan Kumar Chandra

2.2.4.4 Fluctuating hydrodynamics and turbulence in a rotating fluid: Universal properties

We analyze the statistical properties of three-dimensional (3D) turbulence in a rotating fluid. To this end we introduce a generating functional to study the statistical properties of the velocity field \mathbf{v} . We obtain the master equation from the Navier-Stokes equation in a rotating frame and thence a set of exact hierarchical equations for the velocity structure functions for arbitrary angular velocity Ω . In particular we obtain the differential forms for the analogs of the well-known von Karman-Howarth relation for 3D fluid turbulence. We examine their behavior in the limit of large rotation. Our results clearly suggest dissimilar statistical behavior and scaling along directions parallel and perpendicular to Ω . The hierarchical relations yield strong evidence that the nature of the flows for large rotation is not identical to pure two-dimensional flows. To complement these results, by using an effective model in the small- Ω limit, within a one-loop approximation, we show that the equal-time correlation of the velocity components parallel to Ω displays Kolmogorov scaling $q^{-5/3}$ wherein as for all other components, the equal-time correlators scale as q^{-3} in the inertial range where q is a wave vector in 3D. Our results are generally testable in experiments and/or direct numerical simulations of the Navier-Stokes equation in a rotating frame.

Abhik Basu, Jayanta K Bhattacharjee†

2.2.4.5 Phase transitions in crowd dynamics of resource allocation

We define and study a class of resource allocation processes where gN agents, by repeatedly visiting N resources, try to converge to an optimal configuration where each resource is occupied by at most one agent. The process exhibits a phase transition, as the density g of agents grows, from an absorbing to an active phase. In the latter, even if the number of resources is in principle enough for all agents ($g < 1$), the system never settles to a frozen configuration. We recast these processes in terms of zero-range interacting particles, studying analytically the mean field dynamics and investigating numerically the phase transition in finite dimensions. We find a good agreement with the critical exponents of the stochastic fixed-energy sandpile. The lack of coordination in the active phase also leads to a nontrivial faster-is-slower effect.

Asim Ghosh...Bikas K Chakrabarti

2.2.4.6 Continuous universality in nonequilibrium relaxational dynamics of O(2) symmetric systems

We elucidate a nonconserved relaxational nonequilibrium dynamics of a O(2) symmetric model. We drive the system out of equilibrium by introducing a nonzero noise cross correlation of amplitude

$D-x$ in a stochastic Langevin description of the system, while maintaining the $O(2)$ symmetry of the order parameter space. By performing dynamic renormalization group calculations in a field-theoretic set up, we analyze the ensuing nonequilibrium steady states and evaluate the scaling exponents near the critical point, which now depend explicitly on $D-x$. Since the latter remains unrenormalized, we obtain universality classes varying continuously with $D-x$. More interestingly, by changing $D-x$ continuously from zero, we can make our system move away from its equilibrium behavior (i.e., when $D-x=0$) continuously and incrementally.

Niladri Sarkar, Abhik Basu

2.2.4.7 A brief study on coevolution of Ising dynamics

We consider coevolution of site state and network structures from different initial substrates: a one dimensional Ising chain, a scale free network and network with non-linear degree dependence. The dynamics is governed by a preassigned stability parameter S , and a rewiring factor α , that determines whether the Ising spin at the chosen site flips or whether the site gets rewired to another site in the system. We have observed the steady state average stability and magnetisation for both kinds of systems to have an idea about the effect of initial network topology. Although the average stability shows almost similar behaviour, the magnetisation depends on the initial condition we start from. Apart from the local dynamics, the global effect on the dynamics has also been studied. These studies show interesting variations in the steady state values of average stability and magnetisation for different values of S and α , which helps in indicating the gradual change of existing social networks.

KB Hajra, AK Chandra

2.2.4.8 Physics of a metal-correlated barrier-metal heterostructure

We consider a heterostructure of a metal and a barrier with onsite correlation at half filling using the unrestricted HartreeFock method. We find that, above a certain value of correlation strength in the barrier planes, the system is an antiferromagnetic insulator, while below this value the system is gapless with no spin density wave order but still with considerable charge inhomogeneity being present across the planes. The energy spectrum is found to have multiple gaps as the correlation strength is increased. The system is insulating for values of correlation above the critical value at which the gap at half filling opens up.

Sanjay Gupta, Tribikram Gupta†

2.2.4.9 Emergent cooperation amongst competing agents in minority games

We study a variation of the minority game. There are N agents. Each has to choose between one of two alternatives every day, and there is a reward to each member of the smaller group. The agents cannot communicate with each other, but try to guess the choice others will make, based only on the past history of the number of people choosing the two alternatives. We describe a simple probabilistic strategy using which the agents, acting independently, and trying to maximize their individual expected payoff, still achieve a very efficient overall utilization of resources, and

the average deviation of the number of happy agents per clay from the maximum possible can be made $O(N^{\epsilon})$, for any $\epsilon > 0$. We also show that a single agent does not expect to gain by not following the strategy.

Deepak Dhar†, V Sasidevan†, Bikas K Chakrabarti

2.2.4.10 Universality of scaling and multiscaling in turbulent symmetric binary fluids

We elucidate the universal scaling and multiscaling properties of the nonequilibrium steady states in a driven symmetric binary fluid (SBF) mixture in its homogeneous miscible phase in three dimensions. We show, via direct numerical simulations (DNSs) that structure functions of the velocity and the concentration gradient exhibit multiscaling in three dimensions (3D) and extended self-similarity. We also find that, in contrast to the well-known passive scalar turbulence problem, structure functions of the concentration show simple scaling. We propose a shell model for SBF turbulence that preserves all the invariances in the ideal limit of the SBF equations and reduces to a well-known shell model for fluid turbulence in the zero concentration field limit. We show that the shell model has the same scaling properties as the three-dimensional SBF equations. Our combined results from our DNSs of the SBF equations and shell-model studies consistently bring out the multiscaling of the velocity and concentration gradient fields and simple scaling of the concentration field.

Samriddhi Sankar Ray†, Abhik Basu

2.2.4.11 Determination of Rashba and Dresselhaus spin-orbit fields

Determination of Rashba and Dresselhaus spin-orbit interaction strengths in a particular sample remains a challenge even today. In this article, we investigate the possibilities of measuring the absolute values of these interaction strengths by calculating persistent charge and spin currents in a mesoscopic ring. Our numerical results can be verified experimentally.

Santanu K Maiti

2.2.4.12 Magneto-transport in a mesoscopic ring with Rashba and Dresselhaus spin-orbit interactions

Electronic transport in a one-dimensional mesoscopic ring threaded by a magnetic flux is studied in the presence of Rashba and Dresselhaus spin-orbit interactions. A completely analytical technique within a tight-binding formalism unveils the spin-split bands in the presence of the spin-orbit interactions and leads to a method of determining the strength of the Dresselhaus interaction. In addition to this, the persistent currents for ordered and disordered rings have been investigated numerically. It is observed that the presence of the spin-orbit interaction, in general, leads to an enhanced amplitude of the persistent current. Numerical results corroborate the respective analytical findings.

Santanu K Maiti, Moumita Dey...SN Karmakar

2.2.4.13 Phase diagram of the one-dimensional Hubbard-Holstein model at quarter filling

We derive an effective Hamiltonian for the one-dimensional Hubbard-Holstein model, valid in a regime of both strong electron-electron (e-e) and electron-phonon (e-ph) interactions and in the nonadiabatic limit ($t/\omega_0 \leq 1$), by using a nonperturbative approach. We obtain the phase diagram at quarter filling by employing a modified Lanczos method and studying various density-density correlations. The spin-spin AF (antiferromagnetic) interactions and nearest-neighbor repulsion, resulting from the e-e and the e-ph interactions, respectively, are the dominant terms (compared to hopping) and compete to determine the various correlated phases. As e-e interaction (U/t) is increased, the system transits from an AF cluster to a correlated singlet phase through a discontinuous transition at all strong e-ph couplings $2 \leq g \leq 3$ considered. At higher values of U/t and moderately strong e-ph interactions ($2 \leq g \leq 2.6$), the singlets break up to form an AF order and then to a paramagnetic order all in a single sublattice; whereas at larger values of g (>2.6), the system jumps directly to the spin disordered charge-density-wave (CDW) phase.

Sahinur Reja, Sudhakar Yarlagadda, Peter B Littlewood†

2.2.4.14 On the way to meet the experimental observation of persistent current in a mesoscopic cylinder: A mean field study

The behavior of persistent current in a mesoscopic cylinder threaded by an Aharonov-Bohm flux ϕ is carefully investigated within a Hartree-Fock mean field approach. We examine the combined effect of second-neighbor hopping integral and Hubbard correlation on the enhancement of persistent current in presence of disorder. A significant change in current amplitude is observed compared to the traditional nearest-neighbor hopping model and the current amplitude becomes quite comparable to experimental realizations. Our analysis is found to exhibit several interesting results which have so far remained unaddressed.

Santanu K Maiti

2.2.4.15 Threshold-induced phase transition in kinetic exchange models

We study an ideal-gas-like model where the particles exchange energy stochastically, through energy-conserving scattering processes, which take place if and only if at least one of the two particles has energy below a certain energy threshold (interactions are initiated by such low-energy particles). This model has an intriguing phase transition in the sense that there is a critical value of the energy threshold below which the number of particles in the steady state goes to zero, and above which the average number of particles in the steady state is nonzero. This phase transition is associated with standard features like "critical slowing down" and nontrivial values of some critical exponents characterizing the variation of thermodynamic quantities near the threshold energy. The features are exhibited not only in the mean-field version but also in the lattice versions.

Asim Ghosh, Urna Basu...Bikas K Chakrabarti

2.2.4.16 Effect of dephasing on electron transport in a molecular wire: Green's function approach

The effect of dephasing on electron transport through a benzene molecule is carefully examined using a phenomenological model introduced by Buttiker. Within a tight-binding framework all the calculations are performed based on the Green's function formalism. We investigate the influence of dephasing on transmission probability and current-voltage characteristics for three different configurations (ortho, meta and para) of the molecular system depending on the locations of two contacting leads. The presence of dephasing provides a significant change in the spectral properties of the molecule and exhibits several interesting patterns that have so far remain unexplored.

Moumita Dey, Santanu K Maiti, SN Karmakar

2.2.4.17 A novel approach to discontinuous bond percolation transition

We introduce a bond percolation procedure on a D-dimensional lattice where two neighbouring sites are connected by N channels, each operated by valves at both ends. Out of a total of N, randomly chosen n valves are open at every site. A bond is said to connect two sites if there is at least one channel between them, which has open valves at both ends. We show analytically that in all spatial dimensions, this system undergoes a discontinuous percolation transition in the $N \rightarrow \infty$ limit when $\gamma = \frac{\ln n}{\ln N}$ crosses a threshold. It must be emphasized that, in contrast to the ordinary percolation models, here the transition occurs even in one-dimensional systems, albeit discontinuously. We also show that a special kind of discontinuous percolation occurs only in one dimension when N depends on the system size.

Urna Basu, Mahashweta Basu, Anasuya Kundu ; PK Mohanty

2.2.4.18 Absorbing phase transition in a four-state predator-prey model in one dimension

The model of competition between densities of two different species, called predator and prey, is studied on a one-dimensional periodic lattice, where each site can be in one of the four states, say, empty, or occupied by a single predator, or occupied by a single prey, or by both. Along with the pairwise death of predators and growth of prey, we introduce an interaction where the predators can eat one of the neighboring prey and reproduce a new predator there instantly. The model shows a non-equilibrium phase transition into an unusual absorbing state where predators are absent and the lattice is fully occupied by prey. The critical exponents of the system are found to be different from those of the directed percolation universality class and they are robust against addition of explicit diffusion.

Rakesh Chatterjee, PK Mohanty, Abhik Basu

2.2.4.19 Phase separation transition in a driven diffusive system with anti-ferromagnetic interaction

One-dimensional non-equilibrium systems with short-range interaction can undergo phase transitions from homogeneous states to phase separated states as interaction (epsilon) among particles is increased. One of the model systems where such a transition has been observed is

the extended Katz-Lebowitz-Spohn (KLS) model with ferromagnetically interacting particles at $\epsilon = 4/5$. Here, the system remains homogeneous for small interaction strength ($\epsilon \ll 4/5$), and for anti-ferromagnetic interactions ($\epsilon < 0$). We show that the phase separation transitions can also occur in anti-ferromagnetic systems if interaction among particles depends explicitly on the size of the block (n) they belong to. We study this transition in detail for a specific case $\epsilon = \delta/n$, where phase separation occurs for $\delta < -1$.

Anasuya Kundu, PK Mohanty

2.2.4.20 Quantum transport through mesoscopic rings: a way of current modulation

We explore the possibilities of current modulation at nano-scale level using mesoscopic rings. A single mesoscopic ring or an array of such rings is used for current modulation where each ring is threaded by a time varying magnetic flux ϕ which plays the central role in the modulation action. Within a tight-binding framework, all the calculations are done based on the Green's function formalism. We present numerical results for the two-terminal conductance and current which support the essential features of current modulation. The analysis may be helpful in fabricating mesoscopic or nano-scale electronic.

Santanu K Maiti

2.2.4.21 Fluctuations and symmetries in two-dimensional active gels

Motivated by the unique physical properties of biological active matter, e. g., cytoskeletal dynamics in eukaryotic cells, we set up effective two-dimensional (2d) coarse-grained hydrodynamic equations for the dynamics of thin active gels with polar or nematic symmetries. We use the well-known three-dimensional (3d) descriptions (K. Kruse et al., *Eur. Phys. J. E* 16, 5 (2005); A. Basu et al., *Eur. Phys. J. E* 27, 149 (2008)) for thin active-gel samples confined between parallel plates with appropriate boundary conditions to derive the effective 2d constitutive relations between appropriate thermodynamic fluxes and generalised forces for small deviations from equilibrium. We consider three distinct cases, characterised by spatial symmetries and boundary conditions, and show how such considerations dictate the structure of the constitutive relations. We use these to study the linear instabilities, calculate the correlation functions and the diffusion constant of a small tagged particle, and elucidate their dependences on the activity or nonequilibrium drive.

N Sarkar, A Basu

2.2.4.22 Implementation of Classical Logic Gates at Nano-Scale Level Using Magnetic Quantum Rings: A Theoretical Study

We explore the possibilities of designing classical logic gates at nano-scale level using magnetic quantum rings. A single ring is used for designing OR, NOT, XOR, XNOR and NAND gates, while AND and NOR gate responses are achieved using two such rings and in all the cases each ring is threaded by a magnetic flux ϕ which plays the central role in the logic gate operation. We adopt a simple tight-binding Hamiltonian to describe the model where a magnetic quantum ring is attached to two semi-infinite one-dimensional non-magnetic electrodes. Based on single

particle Green's function formalism all the calculations which describe two-terminal conductance and current through the quantum ring are performed numerically. The analysis may be helpful in fabricating mesoscopic or nano-scale logic gates.

Santanu K Maiti

2.2.4.23 Phase transition in an exactly solvable extinction model

We introduce a model of biological evolution in which species evolve in response to biotic interactions and fluctuating environmental stress. The species may either become extinct or mutate to acquire a new fitness value when the effective stress level is greater than their individual fitness. The model exhibits a phase transition to a completely extinct phase as the environmental stress or the mutation rate is varied. We discuss the generic conditions for which this transition is continuous. The model is exactly solvable and the critical behavior is characterized by an unusual dynamic exponent $z = 1/3$. Apart from predicting large-scale evolution, the model can be applied to understand the trends in the available fossil data.

Debarshee Bagchi, PK Mohanty

2.3 Developmental Work

2.3.0.1 Completion of the Clean Room

A clean room laboratory of class 100 and 1000 grades, comprising of growth, lithography and etch facilities, has been constructed for fabrication of semiconductor devices. The total area of the room is about 700 sq. ft. with an ambience of 211°C and relative humidity of 45.2.5

Supratic Chakraborty, Madhusudan Roy, Alokmay Datta

2.4 Publications

2.4.1 Publications in Books/Monographs & Volumes Edited

Binita Ghosh, Purushottam Chakraborty, Optical nonlinearities of colloidal metal quantum dot - glass composites for nanophotonics, in Nanocomposites and Polymers with Analytical Methods, Ed: John Cuppoletti, (Intech Publishers, 2011, 201p)

2.4.2 Papers in Journals

2.4.2.1 Applied Material Science

A Bhattacharjee†, H Mandal†, M Roy, J Kusz†, W Hofmeister†, Microstructural and magnetic characterization of fly ash from Kolaghat Thermal Power Plant in West Bengal, India, Journal of Magnetism and Magnetic Materials **323** (2011) 3007

Ashis Bhattacharjee†; Haradhan Mandal†, Madhusudan Roy, Tapas Kumar Chini, A preliminary study on the nature of particulate matters in vehicle fuel wastes, *Environmental Monitoring and Assessment* **176** (2011) 473

Smita Mukherjee, Alokmay Datta, Crossover from layering to island formation in Langmuir-Blodgett growth: Role of long-range intermolecular forces, *Physical Review* **E83** (2011) Art No: 041604

Smita Mukherjee, Alokmay Datta, Langmuir-Blodgett deposition selects carboxylate headgroup coordination, *Physical Review* **E84** (2011) Art No: 041601

Smita Mukherjee, Alokmay Datta, Angelo Giglia†, Nicola Mahne†, Stefano Nannarone†, Solid-like and liquidlike behavior in monolayers and multilayers of metal-bearing amphiphiles, *Physical Review* **E84** (2011) Art No: 021606

Souvik Kundu†, Sandipta Roy†, P Banerji†, Supratic Chakraborty, T Shripathi†, Studies on Al/ZrO(2)/GaAs metal-oxide-semiconductor capacitors and determination of its electrical parameters in the frequency range of 10 kHz-1 MHz, *Journal of Vacuum Science & Technology* **B29** (2011) Art No: 031203

2.4.2.2 Experimental Condensed Matter Physics

A Midya, SN Das, P Mandal, Anisotropic magnetic properties and giant magnetocaloric effect in antiferromagnetic RMnO₃ crystals (R = Dy, Tb, Ho, and Yb), *Physical Review* **B84** (2011) Art No: 235127

Abhishek Pandey†, Chandan Mazumdar, R Ranganathan, et al, Valence behavior of Eu-ions in intermetallic compound Ce_{0.5}Eu_{0.5}Pd₃B_{0.5}, *Journal of Magnetism and Magnetic Materials* **323** (2011) 3281

Asok Poddar, Mazumdar Chandan, Cluster glass behaviour in Co-substituted double perovskite Ca₂FeMoO₆, *Materials Research Bulletin* **46** (2011) 682

Asok Poddar...Amitabha De...Sangam Banerjee, Electrical Transport and Magnetic Properties of PEDOT-Ferrite Nanocomposites, *Polymer Composites* **32** (2011) 629

B Roy, S Das, Magnetic and electrical transport properties of La_{0.5}A_{0.5}CoO₃ nanoparticles (A = Sr, Ca, and Ba), *Journal of Alloys and Compounds* **509** (2011) 5537

Barnana Pal, Ordering in Two Dimensional Lennard-Jones Clusters, *ISRN Condensed Matter Physics*, Article ID 342642 (2012)

D Bhoi, P Mandal, et al, Quantum magnetoresistance of the PrFeAsO oxypnictide, *Applied Physics Letters* **98** (2011) Art No: 172105

D Bhoi, P Mandal, et al, The magnetization of PrFeAsO_{0.6}F_{0.12} superconductor, *Physica* **C471** (2011) 258

D Bhoi, P Mandal, et al, Fe-spin reorientation in PrFeAsO: Evidences from resistivity and specific

heat studies, *Journal of Applied Physics* **110** (2011) Art No: 113722

DM Raj Kumar†, Asok Poddar, R Ranganathan, et al, Effect of Si/Ge ratio on resistivity and thermopower in $\text{Gd}_5\text{Si}_x\text{Ge}_{4-x}$ magnetocaloric compounds, *Journal of Magnetism and Magnetic Materials* **323** (2011) 1750

D Talukdar...KK Bardhan, A De, CD Mukherjee, Nonlinearity exponents in lightly doped conducting polymers, *Physical Review* **B84** (2011) Art No: 054205

Joydip Sengupta...KK Bardhan, CD Mukherjee, Influence of annealing temperature on the structural, topographical and optical properties of sol-gel derived ZnO thin films, *Materials Letters* **65** (2011) 2572

K Sengupta†...R Ranganathan, et al, Large variations in the magnetic ordering behavior of EuCu_2As_2 with the application of external pressure and magnetic field, *Journal of Physics-Condensed Matter* **24** (2012) Art No: 096004

N Khan, A Midya, K Mydeen†, P Mandal, Critical behavior in single crystalline $\text{La}_{0.67}\text{Sr}_{0.33}\text{CoO}_3$, *Phys Rev* **B82** (2010) 064422

Parthasarathi Mondal†...P Mandal, Current-driven orbital order-disorder transition in LaMnO_3 , *Physical Review* **B84** (2011) Art No: 075111

R Thiyagarajan†...P Mandal, et al, Effect of magnetic field and pressure on charge-orbital ordering in $\text{Pr}(\text{Sr}_{1-x}\text{Ca}_x)_2\text{Mn}_2\text{O}_7$ ($x=0.4$ and 0.9) single crystals, *Journal of Applied Physics* **110** (2011) Art No: 093905

Rangana Bhattacharya, Souvik Chatterjee, SS Bhattacharyya, Preparation and probing of coherent vibrational wave packets in the ground electronic state of HD^+ , *Physical Review* **A85** (2012) Art No: 033424

SK Giri†, A Poddar, et al, Surface spin glass and exchange bias effect in $\text{Sm}_{0.5}\text{Ca}_{0.5}\text{MnO}_3$ manganites nano particles, *AIP Advances* **1** (2011) Art No: 032110

S Mukherjee†...S Banerjee, R Ranganathan, et al, Glassy behavior in the layered perovskites $\text{La}_{2-x}\text{Sr}_x\text{CoO}_4$ ($1.1 \leq x \leq 1.3$), *Journal of Magnetism and Magnetic Materials* **324** (2012) 928

2.4.2.3 Surface Physics

AKM Maidul Islam, M Mukherjee, Application of differential charging in XPS for structural study of Langmuir-Blodgett films, *Journal of Physics-Condensed Matter* **23** (2011) Art No: 435005

AKM Maidul Islam, M Mukherjee, Role of initial morphology in H_2S treated cadmium arachidate Langmuir - Blodgett films, *Colloids and Surfaces* **A385** (2011) 104

Anna Kozakiewicz†, Binita Ghosh, Purushottam Chakraborty, Trevor Derry†, SR Naidoo†, Paul Franklyn†, Ion-Beam-Synthesized Colloidal Silver Nanoclusters in Crystalline Sapphire as Third-Order Optical Material, *IEEE Photonics Journal* **4** (2012) 205

Binita Ghosh, Purushottam Chakraborty, Large third-order optical nonlinearity of silver colloids in silica glasses synthesized by ion implantation, Nuclear Instruments & Methods in Physics Research **B269** Special Issue (2011) 1321

Brahmananda Chakraborty†, B Satpati, P Modak†, et al, Enhancement of field emission characteristics in aligned multiwalled carbon nanotubes due to 70 MeV Ni⁶⁺ ion irradiation, International Journal of Nanoscience **10** (2011) 1057

C -H Wang†, S Mukherjee, AKM Maidul Islam, Y-W Yang†, M Mukherjee, Role of Interfacial Interaction in Orientation of Poly(N-isopropylacrylamide) Chains on Silicon Substrate, Macromolecules **44** (2011) 5750

D Datta, Shyamal Mondal, SR Bhattacharyya, Growth process of GaAs ripples as a function of incident Ar-ion dose, Applied Surface Science **258** (2012) 4152

Debasree Saha†, Laksmikanta Adak†, M Mukherjee, Brindaban C Ranu†, Hydroxyapatite-supported Cu(I)-catalysed cyanation of styrenyl bromides with K-4[Fe(CN)(6)]: an easy access to cinnamionitriles, Organic & Biomolecular Chemistry **10** (2012) 952

Krishnakumar SR Menon, Suman Mandal, Jayanta Das, et al, Surface antiferromagnetic domain imaging using low-energy unpolarized electrons, Physical Review **B84** (2011) Art No: 132402

M Sharma, MK Sanyal, MK Mukhopadhyay, MK Bera, B Saha, P Chakraborty, Structural and morphological characterization of molecular beam epitaxy grown Si/Ge multilayer using X-ray scattering techniques, Journal of Applied Physics **110** (2011) Art No: 102204

Mxolisi B Mukhawana†, Christiaan C Theron†, Johan B Malherbe†, Nic G Van der Berg†, Andre J Botha†, Wiebke Grote†, Elke Wendler†, Werner Wescht†, Purushottam Chakraborty, Behavior of iodine implanted in highly oriented pyrolytic graphite (HOPG) after heat treatment, Nuclear Instruments & Methods in Physics Research **B273** (2012) 65

NC Das†, S Hazra, JK Bal, et al, Modifications of local structures of Gd₂O₃ on incorporation of SiO₂, Journal of Applied Physics **110** (2011) Art No: 063527

N Naresh†, RN Bhowmik†, B Ghosh, S Banerjee, Study of surface magnetism, exchange bias effect, and enhanced ferromagnetism in α -Fe_{1.4}Ti_{0.6}O₃ alloy, Journal of Applied Physics **109** (2011) Art No: 093913

P Chatterjee, S Hazra, H Amenitsch†, Substrate and drying effect in shape and ordering of micelles inside CTAB-silica mesostructured films, Soft Matter **8** (2012) 2956

P Das, TK Chini, Enhanced ultraviolet-visible cathodoluminescence from Ar⁺ beam-induced nanopatterned silicon, J Lumin **131** (2011) 2769

P Das, TK Chini, An advanced cathodoluminescence facility in a high-resolution scanning electron microscope for nanostructure characterization, Current Science **101** (2011) 849

Pabitra Das, Tapas Kumar Chini, Enhanced ultraviolet-visible cathodoluminescence from Ar⁺ beam-induced nano-patterned silicon, *Journal of Luminescence* **131** (2011) 2769

Pabitra Das, Tapas Kumar Chini, An advanced cathodoluminescence facility in a high-resolution scanning electron microscope for nanostructure characterization, *Current Science* **101** (2011) 849

Parthasarathi Mondal†, Dipten Bhattacharya†, Anwesha Maity†, AKM Maidul Islam, Manabendra Mukherjee, Evolution of orbital phases with particle size in nanoscale stoichiometric LaMnO₃, *Journal of Applied Physics*, **109** (2011) Art No: 084327

Purushottam Chakraborty, Quantitative MCsn⁺ - SIMS for direct compositional analysis of interfaces of low-dimensional structures, *AIP Conf Proc* **1451** (2012) 5

R Banerjee, MK Sanyal, MK Bera, et al, Structural reordering in monolayers of gold nanoparticles during transfer from water surface to solid substrate, *Physical Review* **E83** (2011) Art No: 051605

Rajkumar Kore†, Biswarup Satpati, Rajendra Srivastava†, Synthesis of Dicationic Ionic Liquids and their Application in the Preparation of Hierarchical Zeolite Beta, *Chemistry-A European Journal* **17** (2011) 14360

SA Mollick, S Karmakar, A Metya, D Ghose, Pit formation on the Ge(100) surfaces by normal incident Si- ion implantation, *Applied Surface Science* **258** (2012) 4129

S Banerjee, SO Raja†, M Sardar†, et al, Iron oxide nanoparticles coated with gold: Enhanced magnetic moment due to interfacial effects, *Journal of Applied Physics* **109** (2011) Art No: 123902

SK Mahatha, SR Krishnakumar Menon, T Balasubramanian†, Unoccupied electronic structure of graphite probed by angle-resolved photoemission spectroscopy, *Physical Review* **B84** (2011) Art No: 113106

Sarathi Kundu†, JK Bal, Reorganization of Au nanoparticle Langmuir-Blodgett films on wet chemically passivated Si (001) surfaces, *Journal of Applied Physics* **110** (2011) Art No: 114302

Suman Mandal, Krishnakumar SR Menon, Francesco Maccherozzi†, Rachid Belkhou†, Surface spin orientation of NiO(100) and interfacial coupling of Fe/NiO(100) revisited with soft X-ray spectroscopy, *EPL* **95** (2011) Art No: 27006

Suman Mandal, Krishnakumar SR Menon, Francesco Maccherozzi†, et al, Microscopic investigation of surface and interfacial magnetic domain structure of Fe-NiO(100) system, *Journal of Physics* **D44** (2011) Art No: 255003

Suman Mandal, Krishnakumar SR Menon, Morphology induced magnetic instabilities on oxide antiferromagnetic surfaces, *European Physical Journal* **B85** (2012) Art No: 2

Suman Mandal, Krishnakumar SR Menon, SK Mahatha, S Banerjee, Finite size versus surface effects on magnetic properties of antiferromagnetic particles, *Applied Physics Letters* **99** (2011) Art No: 232507

Swapan K Mandal†, Arup Ratan Mandal, Sangam Banerjee, High Ferromagnetic Transition Temperature in PbS and PbS: Mn Nanowires, *Acs Applied Materials & Interfaces* **4** (2012) 205

Tanmay Ghosh, Biswarup Satpati, Template synthesis and characterizations of nickel nanorods, *AIP Conf Proc* **1447** (2012) 405

Tanusree Samanta, M Mukherjee, Swelling Dynamics of Ultrathin Films of Strong Polyelectrolytes, *Macromolecules* **44** (2011) 3935

TT Hlatshwayo†, JB Malherbe†, NG van der Berg†, AJ Botha†, P Chakraborty, Effect of thermal annealing and neutron irradiation in 6H-SiC implanted with silver at 350°C and 600°C, *Nuclear Instruments & Methods in Physics Research* **B273** (2012) 61

V Venugopal†, Sandeep Kumar Garg†, Tanmoy Basu†, Om Prakash Sinha†, D Kanjilal†, SR Bhattacharyya, T Som†, Nanostructures on GaAs surfaces due to 60 keV Ar⁺-ion beam sputtering, *Applied Surface Science* **258** (2012) 4144

2.4.2.4 Theoretical Condensed Matter Physics

A Ayyer†, EA Carlen†, JL Lebowitz†, PK Mohanty, et al, Phase Diagram of the ABC Model on an Interval (vol 137, pg 1166, 2009), *Journal of Statistical Physics* **144** (2011) 920

Abhik Basu, Jayanta K Bhattacharjee†, Fluctuating hydrodynamics and turbulence in a rotating fluid: Universal properties, *Physical Review* **E85** (2012) Art No: 026311

Anasuya Kundu, PK Mohanty, Phase separation transition in a driven diffusive system with anti-ferromagnetic interaction, *Physica* **A390** (2011) 1585

Anjan Kumar Chandra, Percolation in a kinetic opinion exchange model, *Physical Review* **E85** (2012) Art No: 021149

Asim Ghosh, Daniele De Martino†, Arnab Chatterjee†, Matteo Marsili†, Bikas K Chakrabarti, Phase transitions in crowd dynamics of resource allocation, *Physical Review* **E85** (2012) Art No: 021116

Asim Ghosh, Urna Basu, Anirban Chakraborti†, Bikas K Chakrabarti, Threshold-induced phase transition in kinetic exchange models, *Physical Review* **E83** (2011) Art No: 061130

BK Chakrabarti, Comments by BK Chakrabarti on the Visioneer white papers by D. Helbing and S. Baliatti, *European Physical Journal-Special Topics* **195** (2011) 145

Debarshee Bagchi, PK Mohanty, Phase transition in an exactly solvable extinction model, *Physical Review* **E84** (2011) Art No: 061921

Deepak Dhar†, V Sasidevan†, Bikas K Chakrabarti, Emergent cooperation amongst competing agents in minority games, *Physica* **A390** (2011) 3477

KB Hajra, AK Chandra, A brief study on coevolution of Ising dynamics, *European Physical Journal* **B85** (2012) Art No: 27

Moumita Dey, Santanu K Maiti, SN Karmakar, Effect of dephasing on electron transport in a molecular wire: Green's function approach, *Organic Electronics* **12** (2011) 1017

Moumita Dey, Santanu K Maiti, SN Karmakar, Magnetic field induced metal-insulator transition in a kagome nanoribbon, *Journal of Applied Physics* **110** (2011) Art No: 094306

N Sarkar, A Basu, Fluctuations and symmetries in two-dimensional active gels, *European Physical Journal* **E34** (2011) Art No: 44

Niladri Sarkar, Abhik Basu, Continuous universality in nonequilibrium relaxational dynamics of $O(2)$ symmetric systems, *Physical Review* **E85** (2012) Art No: 021113

Rakesh Chatterjee, PK Mohanty, Abhik Basu, Absorbing phase transition in a four-state predator-prey model in one dimension, *Journal of Statistical Mechanics-Theory and Experiment* (2011) Art No: L05001

Sahinur Reja, Sudhakar Yarlagadda, Peter B Littlewood†, Phase diagram of the one-dimensional Hubbard-Holstein model at quarter filling, *Physical Review* **B84** (2011) Art No: 085127

Samriddhi Sankar Ray†, Abhik Basu, Universality of scaling and multiscaling in turbulent symmetric binary fluids, *Physical Review* **E84** (2011) Art No: 036316

Sanjay Gupta, Tribikram Gupta†, Physics of a metal-correlated barrier-metal heterostructure, *Solid State Communications* **152** (2012) 53

Santanu K Maiti, Determination of Rashba and Dresselhaus spin-orbit fields, *Journal of Applied Physics* **110** (2011) Art No: 064306

Santanu K Maiti, Implementation of Classical Logic Gates at Nano-Scale Level Using Magnetic Quantum Rings: A Theoretical Study, *Journal of Computational and Theoretical Nanoscience* **8** (2011) 676

Santanu K Maiti, On the way to meet the experimental observation of persistent current in a mesoscopic cylinder: A mean field study, *Physica Status Solidi* **B248** (2011) 1933

Santanu K Maiti, Quantum transport through mesoscopic rings: a way of current modulation, *Journal of Computational and Theoretical Nanoscience* **8** (2011) 1977

Santanu K Maiti, Moumita Dey, SN Karmakar, Integer quantum Hall effect in a square lattice revisited, *Physics Letters* **A376** (2012) 1366

Santanu K Maiti, Moumita Dey, Shreekantha Sil†, Arunava Chakrabarti†, SN Karmakar, Magneto-transport in a mesoscopic ring with Rashba and Dresselhaus spin-orbit interactions, *EPL* **95** (2011) Art No: 57008

Shamik Gupta†, *Mustansir Barma*†, *Urna Basu*, Driven k-mers: Correlations in space and time, Physical Review **E84** (2011) Art No: 041102

Soumyajyoti Biswas, Mean-field solutions of kinetic-exchange opinion models, Physical Review **E84** (2011) Art No: 056106

Soumyajyoti Biswas, *Asim Ghosh*, *Arnab Chatterjee*†, *Tapan Naskar*, *Bikas K Chakrabarti*, Continuous transition of social efficiencies in the stochastic-strategy minority game, Physical Review **E85** (2012) Art No: 031104

Suman Sinha, Nonuniversal behavior of the helicity modulus in a dense defect system, Physical Review **E84** (2011) Art No: 010102

Urna Basu, *Hinrichsen Hayer*†, Identifying universality classes of absorbing phase transitions by block renormalization, Journal of Statistical Mechanics-Theory and Experiment, Art No: P11023

Urna Basu, *Mahashweta Basu*, *Anasuya Kundu*, *PK Mohanty*, A novel approach to discontinuous bond percolation transition, EPL **94** (2011) Art No: 46002

2.5 Ph D Awarded

Binita Ghosh [Purushottam Chakraborty], Linear and nonlinear optical properties of metal nanocluster-glass composite, University of Calcutta, June 2011

2.6 Seminars/Lectures given in Conference/Symposium/Schools

Alokmay Datta

Solid and Liquid Amphiphilic Films and Their Wetting and De-wetting, Physics Department, Kyoto University, Japan, Jun 8, 2011

A Different Look at Wetting & Dewetting using Synchrotron X-rays, Trends in Surface Science and Related Areas (TSSRA), Jadavpur University, Nov 8, 2011

Arti Garg

Effect of Impurities on Superconducting State of Cuprates, CK Majumdar memorial workshop on Condensed Matter Physics, IACS, Kolkata, Nov 11, 2011

Correlation Induced Half-Metal Antiferromagnet in a band insulator, International Conference on Physics of Novel and Emerging Materials (ICPNEM), IACS, Kolkata, Nov 15-17, 2011

Biswarup Satpati

Growth of indium antimonide quantum dots: a case study, Internatioanl Conference on Electron Nanoscopy and XXXII Annual Meeting of EMSI, Ramoji Film City, Hyderabad, July 6-8, 2011

TEM Sample Preparation for Materials Science, Workshop on Electron Microscopy, jointly organized by IOP and IIT, Bhubaneswar, Nov 23-25, 2011

Transmission Electron Microscopy: Eye for the World of Nanoscience, National Seminar on Recent Trends on Novel Materials, organized by the Dept. of Physics & Technophysics, Vidyasagar University, Midnapore, Nov 29-30, 2011

Electron microscopy and its application in Material Sciences/Chemistry/Nanotechnology, Workshop on Electron Microscopy and its Application, organized by Advanced Instrumentation Research Facility, Jawaharlal Nehru University, New Delhi, Feb 28-29, 2012

Milan K Sanyal

Applications of Synchrotron X-rays Techniques in Materials Science, 2nd Professor S.P. Sengupta Memorial Lecture at C.V. Raman Hall, Indian Association for the Cultivation of Science, May 18, 2011

Nano-Science at the Interface of Chemistry and Physics, 150th Birth Anniversary of Acharya Prafulla Chandra Ray and 100th Anniversary of the Nobel Prize Award to Madam Curie, Indian Chemical Society, University of Calcutta, August 2, 2011.

Formation and ordering of nanomaterials at liquid-liquid interface, Materials Science Division Seminar, Argonne National Laboratory, August 31, 2011

Confinement-induced ordering in nano-structured materials, Condensed Matter Physics Seminar, John Hopkins University, September 2, 2011

Ordering of organic nano-layers on water surface, Condensed-Matter Physics & Materials Science Seminar, Brookhaven National Laboratory, September 6, 2011

X-ray scattering study of reversible crystallization on water surface, Department of Physics, University of California, San Diego, September 9, 2011

Metallic behaviour of polymer nanowires, Current Topics in Condensed Matter, IISER-Kolkata, October 7-9, 2011

X-ray scattering study of crystallization of nanostructures on water surface, Diamond Jubilee Research Career of Prof. C.N.R. Rao, Vedic Village, Kolkata, October 29, 2011

Archaeology Science: Scientific Tools for PROBING the Past, Sixteenth Foundation Day Oration, Centre for Archaeology Studies & Training, Eastern India, Kolkata, November 5, 2011

QUASICRYSTALS : Nobel Prize (2011) for Dan Shechtman, Saha Institute of Nuclear Physics, Kolkata, November 9, 2011

Low-dimensional Physics using Chemically-grown Nano-structured Materials, International Year of Chemistry, Saha Institute of Nuclear Physics, Kolkata, November 16, 2011

Low-dimensional Physics using Nano-structured Materials, Seminar at RAL-Diamond, Oxford, December 16, 2011

Quasi-one-dimensional electronic transport properties of composite nanowires synthesized in membrane-pores, ICONSAT-12, Hyderabad, January 21, 2012

Prabhat Mandal

Griffiths Phase in manganites, International Conference on Functional Materials, Harish Chandra Research Institute, Allahabad, Apr 2-3, 2011

Purushottam Chakraborty

Optical Nonlinearities of Colloidal Metal Quantum Dots in Silica Glasses for Photonic Applications, 3rd International Conference on Current Developments in Atomic, Molecular and Optical and Nanophysics, University of Delhi, Dec 14-16, 2011

Quantitative $MCsn^+$ -SIMS for Direct Composition Analysis of Surfaces/Interfaces of Low-Dimensional Structures, Indian Vacuum Society Symposium on Thin Films: Science & Technology (IVSTFST 2011), BARC, Mumbai, Nov 9-12, 2011

High-resolution $MCsn^+$ -SIMS for compositional analysis of self-assembled quantum structures, Workshop on Surface Engineering of Metals and Alloys (SEMA-2012), Indian Institute of Metals, Bengal Engineering and Science University (BESU), Kolkata, March 1-2, 2012

High-resolution $MCsn^+$ -SIMS for compositional analysis of self-assembled quantum structures, 20th International Conference on Ion Beam Analysis (IBA 2011), Itapema, Brazil, Apr 10-15, 2011

Ratan Saha

Blood tissue characterization using photo-acoustics, West Bengal State University, Barasat, West Bengal, Nov 14, 2011

Photo-acoustic Assessment of Blood Oxygen Saturation (Ratan K Saha, Subhajit Karmakar, and Madhusudan Roy), Second International Conference on Trends in Optics and Photonics, Kolkata, Dec 7-9, 2011

Sudhakar Yarlagadda

Phase diagram of the one-dimensional Hubbard-Holstein model, International Conference-cum-School on Strongly Correlated and Disordered Systems, IISc, Bangalore, Dec 9-22, 2011

Strong multiferroicity and giant magnetoelectric effect in (Insulator) $/(LaMnO_3)_n/(SrMnO_3)_n/$ (Insulator) heterostructure, International Conference on Correlated Oxides: novel quantum states, device physics and energy technologies, Cambridge Univ, Mar 19-24, 2012

Study of maximal bipartite entanglement and robustness in resonating-valence-bond states, IMSC, Dec 7, 2011

Tapas Kumar Chini

Intense cathodoluminescence from ion-induced ripple patterned porous silicon, Internatioanl Conference on Electron Nanoscopy and XXXII Annual Meeting of electron Microscopy Society of India (EMSI), Ramoji Film City, Hyderabad, Jul 6-8, 2011

Spectro-microscopy of nanostructured materials using cathodoluminescence in scanning electron microscope (CL-SEM), Workshop on Electron Microscopy (WEM11), Institute of Physics, Bhubaneswar, Nov 23-25, 2011

Optical properties of nanostructured materials using cathodoluminescence in scanning electron microscope (CL-SEM), National Seminar on Recent Trends on Novel Materials (RTNM-11), Vidyasagar University, Midnapore, Nov 29, 2011

2.7 Miscellany**Purushottam Chakraborty**

Adjunct Professor of Physics of the University of Pretoria, South Africa

Chapter 3

Experimental Nuclear and Particle Physics

3.1 Summary of Research Activities of Divisions

3.1.1 Applied Nuclear Physics

Basic and applied research using nuclear tools and techniques to explore structure and dynamics of nuclei, atoms, large biomolecules and nanomaterials are conducted by the divisional members. Detector development and related theoretical simulation, keeping specific physics experiments in mind, are also being pursued. A laser spectroscopy laboratory to address research problems in the emerging areas of atomic, molecular and optical physics is being set up within the division. As part of the cognitive science initiative, our members have ventured into the area of computerized simulation of vision. Collaboration with scientists from India and abroad, working on several important experiments in the research areas pursued by our members are continued.

Structural properties, defects and phase transitions in condensed matter systems, nanomaterials (like colloidal graphene oxide polyaniline nanocomposite), porous matter and bio-materials, metal oxides and intermetallic composites are investigated using positron / positronium life time spectroscopy, Doppler broadening spectroscopy, age-momentum correlation spectroscopy and time differential perturbed angular correlation. Optical absorption and positron annihilation studies on nickel oxide nanoparticles, showing the effects of quantum size effects manifesting as increase of band gaps and electron momentum redistribution was successfully completed. Important findings of TDPAC spectroscopy include identification of phase transition in crystalline metal halides and metal oxide thin films, pinning down the dehydration pathway in Hafnium halides via measurement of nuclear quadrupole interaction and search for ferromagnetism in metal oxides. As part of the in-house development, an experimental set-up for electron impact excitation in solid targets and gaseous materials was completed during this period. The set-up involves a 1-50 keV 100 A electron gun, a large volume UHV chamber with associated pumping system, and a Peltier-cooled PIN diode X-ray detector mounted inside the chamber with provision to mount an electron spectrometer for Auger spectroscopy and related experiments. L-shell X-rays production cross sections

are measured in heavy atoms (like Gold and other neighbouring elements). Empirical model-based calculations are attempted with a view to understand the experimental data. Collaboration with scientists working in experiments and also in atomic collision theories within India and abroad are formed along this direction. High spin states and associated nuclear structure of proton rich heavy nuclei at the extremes of stability have been investigated using the Indian National Gamma-ray Detector Array (INGA) and stable heavy ion beams from the national accelerator facilities at TIFR, Mumbai and IUAC, New Delhi. Obtained results will shed light on the stability of these nuclei against nuclear fission, and also on the use of these nuclei as testing ground for fundamental symmetry violation. Our divisional scientists are also involved in the research planning, simulation and development of radiation detectors for the RD-51 collaboration in CERN, and also in the proposed INDIA-BASED NEUTRINO OBSERVATORY (INO) as part of the national multi-institutional collaboration. Simulation of detector performance and design optimization of various grid based gaseous detectors, micropattern gaseous detectors (MPGD), RPC and TPC detectors are successfully done by the scientists involved. These detectors are employed in various high energy physics experiments, dark matter search experiments conducted at various national and international labs as collaboration initiative. Experimental studies on MPGD physics have also been initiated. Members of our division are concentrating on modeling various phenomena associated with visual perception where the models are inspired mainly by the biological vision. Currently temporal dynamics of brightness induction, stochastic resonance in vision and filling in of blind spot phenomena are the three areas where we are concentrating our studies. These studies will be further supplemented by suitable psychophysical experiments for which, we are setting up our laboratory.

3.1.2 High Energy Nuclear and Particle Physics

The High Energy Nuclear and Particle Physics division is involved in two major experiments at the Large Hadron Collider at CERN. SINP has been involved in the ALICE experiment since 1997. The experiment, focused for studies of minimum bias events in proton-proton and lead-lead collisions, has started taking data since late 2009. The Large Hadron Collider has provided large amount of data during the period between 2010 and 2012. The beam energy has gone up during 2012 to reveal new features in the data. The ALICE group in the institute constructed a part of the forward muon spectrometer which has been working satisfactorily during the entire period. Some collision data are collected with no magnetic field and these data are used to align different components of the spectrometer to the desired accuracy. The high level trigger for muons, also designed by the SINP group, has been performing with very high efficiency. The data show evidence of suppression of charged particle production, jet quenching and other features which are some of the signatures of formation of very dense medium in Pb-Pb collisions. The group is actively pursuing analysis of heavy quark and quarkonia production and also phenomenological studies of photon production in quark gluon plasma and heavy fermion in dense and warm plasma. A group is formed within the institute which applied for participation in the Compact Muon Solenoid (CMS) experiment and has been welcome within the CMS collaboration. The group has major responsibilities in two activities: detector performance studies of the hadron calorimeter and data quality monitoring. In addition, the group has the highest level expertise in detector simulation and some of the simulation coordination effort is coming to the group. The group has undertaken responsibilities in the upgrade program of the hadron calorimeter and there the main emphasis is on the back end electronics of the forward hadron calorimeter which needs to be replaced during the long shut down period between 2013-14. The large amount of data collected by the CMS experiment has led to a very important discovery in the area of high energy physics. A new particle

is observed at a mass around 125 GeV in a number of final states. This could be the first hint of the elusive Higgs boson. Members of the group are associated in the analysis of the data for this search mainly through the Higgs decays to τ leptons in association with a vector boson or Higgs decaying to 4 leptons two of which are τ 's. Members are also actively involved in the analysis of collision data for search of excited leptons, evidence of extra dimension through studies of mono-photon events, studies of strong interaction through multi-jet events and event shape analysis. During this year CMS published several important papers validating various aspects of the Standard Model and certainly the discovery of this new particle. Important results also came from studies of heavy ion collision where suppression of heavy quark final states including quarkonia and jet quenching are reported.

3.1.3 Nuclear Physics

The research activities of the Nuclear Physics Division are broadly aimed at studying nuclear structure and nuclear reaction mechanism from spectroscopic data obtained from experiments carried out at the different Accelerator Centres in India and abroad. In addition, the divisional members are participating in the setting up of the new facility FRENA for research in Nuclear Astrophysics. The members are also pursuing research activities in theoretical Nuclear Physics, X-ray fluorescence (XRF) spectrometry and various development activities.

The research highlights include (i) search for deformed structures in ^{134}Cs , (ii) observation of shears mechanism in ^{83}Kr and study of strongly deformed states in ^{113}Sb , (iii) identification of a slow E3 transition in ^{136}Cs , (iv) study of one- and two- proton transfer reactions for the system $^{28}\text{Si} + ^{90,94}\text{Zr}$, (v) measurement of the complete and incomplete fusion cross-sections for ^6Li with ^{159}Tb at energies near the Coulomb barrier, (vi) study of the alpha spectroscopic factor of O-16 from its breakup using Continuum Discretized Coupled Channel (CDCC) method and (vii) observation of heavy cluster structure of O-18 from inclusive measurement of the mass fragments emitted in $^{18}\text{O} + ^{12}\text{C}$ reaction at 80 MeV. The theoretical research activities include the study of neutron-rich He nuclei using the relativistic mean field approach and extraction of the ANC of the ^{16}O sub-threshold states from $^{12}\text{C}(^6\text{Li}, d)$ reaction at near barrier energies. Besides, large basis untruncated shell-model (SM) calculations have been done for nuclei with $50 \leq Z \leq 56$ and $82 \leq N \leq 88$ in the $\pi(gdsh) \otimes \nu(hfpi)$ valence space above the ^{132}Sn core using both realistic CWG and empirical SMPN (1+2)-body Hamiltonians. Similar large basis SM calculations for nuclei around the line of stability in the upper sd shell have indicated the need for change of the *sdfp* energy gap for reliable reproduction of the experimental data.

Energy dispersive X-ray fluorescence (EDXRF) and Electron probe X-ray microanalysis (EPMA) studies of soil samples contaminated by municipal solid waste showed highly elevated levels of Cu, Zn, and Pb in the top-soil far exceeding the ecological screening limits for soil. The study also revealed moderately elevated levels of Ti, Cr, Mn, Fe, Ni and Sr in the soil samples compared to natural countryside soil.

3.2 Research Activities

3.2.1 Applied Nuclear Physics

3.2.1.1 Even-odd effects in Z and N distributions of fragments emitted at intermediate energies

Even-odd effects in Z and N distributions of light fragments emitted at forward angles in nuclear collisions $^{40}\text{Ca} + ^{40}\text{Ca}$, $^{40}\text{Ca} + ^{48}\text{Ca}$, and $^{48}\text{Ca} + ^{48}\text{Ca}$ at 25 MeV/nucleon and identified in charge

and mass with the Chimera multidetector have been analyzed. The amplitude of even-odd staggering effects seems to be related to the neutron to proton ratio N/Z of the entrance channels. A qualitative explanation of this effect, taking into account the deexcitation phase of primary excited fragments, is discussed.

I Lombardo†, C Agodi†, R Alba†, MB Chatterjee et al

3.2.1.2 First observation of high spin states and isomeric decay in ^{210}Fr

The first observation of the prompt and the delayed gamma transitions involving the high spin states in ^{210}Fr is reported. The decay of the high spin states and the isomeric levels of ^{210}Fr , identified for the first time from the known sequence of low-lying transitions found earlier in the a decay of ^{214}Ac , were studied. High spin states of the doubly-odd ^{210}Fr , which were produced by the fusion evaporation reaction $^{197}\text{Au}(\text{O}^{-16}, \text{xn})^{213-x}\text{Fr}$, were populated and the subsequent emitted. rays were detected through the high-sensitivity germanium clover detector array INGA. The level scheme up to yrast levels of 5.3 MeV excitation energy and $\sim 20\hbar$ over bar angular momentum could be established for the first time through $\gamma\gamma, \gamma\gamma\Delta T$ coincidence, and DCO ratio measurements. A new low-lying isomeric transition at $E\gamma = 203(2)$ keV was observed. The half-life was measured to be $T_1/2 = 41(2)$ ns. The measured half-life was compared with the corresponding single-particle estimate, based on the level scheme obtained from the experiment.

D Kanjilal, S Saha, S Bhattacharya, A Goswami, R Kshetri, et al

3.2.1.3 Evidence for alpha-particle condensation in nuclei from the Hoyle state de-excitation

The fragmentation of quasi-projectiles from the nuclear reaction $^{40}\text{Ca} + ^{12}\text{C}$ at 25 MeV/nucleon was used to produce excited states candidates to α -particle condensation. Complete kinematic characterization of individual decay events, made possible by a high-granularity 4π charged particle multi-detector, reveals that $7.5 \pm 4.0\%$ of the particle decays of the Hoyle state correspond to direct decays in three equal-energy α -particles.

Ad R Raduta†, B Borderie†, E Geraci†... MB Chatterjee et al

3.2.1.4 Isospin Aspects in Nuclear Reactions Involving Ca Beams at 25 MeV/nucleon

Isospin dependence of dynamical and thermodynamical properties observed in reactions $(40)\text{Ca} + (40,48)\text{Ca}$ and $(40)\text{Ca} + (46)\text{Ti}$ at 25 MeV/nucleon has been studied. We used the CHIMERA multi-detector array. Strong isospin effects are seen in the isotopic distributions of light nuclei and in the competition between different reaction mechanisms in semi-central collisions. We will show also preliminary results obtained in nuclear collision $(48)\text{Ca} + (48)\text{Ca}$ at 25MeV/nucleon, having very high N/Z value in the entrance channel ($N/Z = 1.4$). The enhancement of evaporation residue production confirms the strong role played by the N/Z degree of freedom in nuclear dynamics.

I Lombardo†, C Agodi†, R Alba†, MB Chatterjee et al

3.2.1.5 Development of collective structures over noncollective excitations in ^{139}Nd

High-spin states in ^{139}Nd were investigated using the reaction $^{96}\text{Zr} (^{48}\text{Ca}, 5n)$ at a beam energy of 195 MeV and γ -ray coincidences were acquired with the Euroball spectrometer. Apart from several dipole bands at medium excitation energy, three quadrupole bands have been observed at high spin. Linking transitions connecting two of the high-spin bands to low-energy states have been observed. Calculations based on the cranked-Nilsson-Strutinsky formalism have been used to assign configurations for the high-spin quadrupole bands.

S Bhowal† S Bhattacharya, et al

3.2.1.6 Post irradiated microstructural characterization of Zr-1Nb alloy by X-ray diffraction technique and positron annihilation spectroscopy

Zr-1Nb samples were irradiated with 116 MeV O(5+) ions at different doses ranging from 5×10^{17} to 8×10^{18} O(5+)/m(2). X-ray diffraction line profile analysis was performed to characterize the microstructural parameters of these samples. Average domain size, microstrain and dislocation density were estimated as a function of dose. An anomaly was observed in the values of these parameters at a dose of 2×10^{18} O(5+)/m(2). Positron annihilation spectroscopy was used to determine the existence and nature of vacancy clusters in the samples. Isochronal annealing was carried out for a sample to study the evolution of defect clusters.

PS Chowdhury†...PMG Nambissan

3.2.1.7 Electron transparency of a Micromegas mesh

Measurements of the electron transparency of a Micromegas mesh are compared to simulations. The flux conservation argument is shown to lead to inaccurate estimates of the transparency, the importance of accurate geometric modelling of the mesh is discussed and the effect of the dipole moment of the mesh is demonstrated. This study provides a validation of the microscopic simulation methods specifically developed for micropattern devices where the characteristic dimensions are of the same order of magnitude as the electron mean free path in the gas.

K Nikolopoulos†, P Bhattacharya, et al

3.2.1.8 Hafnium oxide thin films studied by time differential perturbed angular correlations

We report on the study of hafnium oxide thin films grown by pulsed laser deposition at various partial oxygen pressures by Time Differential Perturbed Angular Correlations using the nuclear probe $^{181}\text{Hf}(\beta^-)6181\text{Ta}$ to determine the nuclear quadrupole interaction (NQI), and by x-ray diffraction. The samples were neutron activated and measured at room temperature as received as well as after annealing in air. All spectra exhibited two to three inequivalent probe sites, even after annealing. At 0.3 mbar oxygen partial pressure and annealing for 5 hs at 1073 K the majority (88%) of the sites exhibited NQI parameters as reported for the bulk monoclinic phase [$\omega_Q = 125.4(2)\text{Mrad/s}$, $\eta = 0.335(5)$]. We can exclude amorphous as well as cubic and tetragonal hafnium oxide phases in

the annealed samples. There was no indication of room-temperature ferromagnetism.

CC Dey, S Dey, SC Bedi, et al

3.2.1.9 Light clusters emission in nuclear reactions at 25 MeV/nucleon with different N/Z of entrance channels

We discuss results on the emission of light clusters in nuclear reactions $(40)\text{Ca} + (40,48)\text{Ca}, (46)\text{Ti}$ at 25 MeV/nucleon. They were detected and identified in mass and charge by means of the CHIMERA 4 pi array. Inclusive emission at forward angles shows that isotopic yields of Li and Be nuclei are related to the N/Z values of entrance channels. Moreover, structure effects and even-odd staggering in charge distributions of intermediate mass fragments emitted at forward angles will be shown. In agreement with previous experimental findings, odd-even effects are clearly visible in N approximate to Z systems, while are less pronounced in the neutron rich collision $(40)\text{Ca} + (48)\text{Ca}$. These experimental findings are compared to preliminary data obtained in $(48)\text{Ca} + (48)\text{Ca}$ collision at 25 MeV/nucleon.

I Lombardo†, C Agodi†, R Alba†, MB Chatterjee et al

3.2.1.10 Mn substitution effects and associated defects in zno nanoparticles studied by positron annihilation

Nanocrystalline ZnO particles substituted with different concentrations (0-30%) of Mn were synthesized by using a modified ceramic route and characterized by X-ray diffraction, transmission electron microscopy, selected area electron diffraction and energy dispersive X-ray analysis methods. Positron lifetime and coincidence Doppler broadening measurements were used as probes to identify the vacancy-type defects present in them and monitor the changes while doping. The predominant positron trapping center in the undoped ZnO is identified as the trivacancy-type cluster $V(\text{Zn}+\text{O}+\text{Zn})$, which is negatively charged, and it transformed to the neutral divacancy $V(\text{Zn}+\text{O})$ on doping with Mn(2+) ions. The intensity of the defect-specific positron lifetime component got reduced initially indicating partial occupancy of the vacancies by the doped cations but then recovered on further doping due to the additional Zn vacancies created as a result of the increasing strain introduced by the Mn ions of larger radius. The creation of a new phase $\text{ZnMn}(2)\text{O}(4)$ thereafter changed the course of variation of the annihilation parameters, as the positrons got increasingly trapped in the vacancies at the tetrahedral and octahedral sites of the spinel nanomanganite.

B Roy†, B Karmakar†, PMG Nambissan, M Pal†

3.2.1.11 Probing the defects in nano-semiconductors using positrons

Positron annihilation spectroscopy (PAS) is a very useful tool to study the defect properties of nanoscale materials. The ability of thermalized positrons to diffuse over to the surfaces of nanocrystallites prior to annihilation helps to explore the disordered atomic arrangement over there and is very useful in understanding the structure and properties of nanomaterials. As examples, the results of studies on FeS₂ nanorods and ZnS nanoparticles are presented. In semiconductor nanoparticles, there are positron trapping sites within the grains also and these are characterised by using appropriate models on the measured positron lifetimes. We have observed vivid changes in the measured

positron lifetimes and Doppler broadened gamma ray spectral lineshapes during structural transformations prompted by substitutional effects in Mn²⁺-doped ZnS nanorods. Interestingly, the nanoparticles did not exhibit the transformation, implying the morphologies of the nanosystems playing a decisive role. Quantum confinement effect in CdS nanoparticles was another phenomenon that could be seen through positron annihilation experiments. Coincidence Doppler broadening measurements have been useful to identify the elemental environment around the vacancy clusters that trap positrons. Recent studies on nanocrystalline oxide and sulphide semiconductors are also discussed.

PMG Nambissan

3.2.2 High Energy Nuclear and Particle Physics

3.2.2.1 Search for the Standard Model Higgs Boson in the Decay Channel $H \rightarrow ZZ \rightarrow 4\ell$ in pp Collisions at $\sqrt{s}=7$ TeV

A search for a Higgs boson in the four-lepton decay channel $H \rightarrow ZZ$, with each Z boson decaying to an electron or muon pair, is reported. The search covers Higgs boson mass hypotheses in the range of $110 < m_H < 600$ GeV. The analysis uses data corresponding to an integrated luminosity of 4.7 fb^{-1} recorded by the CMS detector in pp collisions at $\sqrt{s}=7$ TeV from the LHC. Seventy-two events are observed with four-lepton invariant mass $m_{4\ell} > 100$ GeV (with 13 below 160 GeV), while 67.1 ± 6.0 (9.5 ± 1.3) events are expected from background. The four-lepton mass distribution is consistent with the expectation of standard model background production of ZZ pairs. Upper limits at 95% confidence level exclude the standard model Higgs boson in the ranges of 134158 GeV, 180305 GeV, and 340465 GeV. Small excesses of events are observed around masses of 119, 126, and 320 GeV, making the observed limits weaker than expected in the absence of a signal.

CMS Collaboration

3.2.2.2 Search for the standard model Higgs boson in the $H \rightarrow ZZ \rightarrow \ell^+\ell^-\tau^+\tau^-$ decay channel in pp collisions at $\sqrt{s}=7$ TeV

A search is reported for the standard model Higgs boson in the $\rightarrow ZZ \rightarrow \ell^+\ell^-\tau^+\tau^-$ decay mode, where $\ell=\mu$ or e, in proton-proton collisions at $\sqrt{s}=7$ TeV, corresponding to an integrated luminosity of 4.7 fb^{-1} collected with the CMS detector at the LHC. No evidence is found for a significant deviation from the background expectation. An upper limit four to twelve times larger than the predicted value is set at 95% confidence level for the product of the standard model Higgs boson production cross section and decay branching fraction in the mass range $190 < m_H < 600$ GeV.

CMS Collaboration

3.2.2.3 Measurement of the rapidity and transverse momentum distributions of Z bosons in pp collisions at $\sqrt{s}=7$ TeV

Measurements of the normalized rapidity (y) and transverse-momentum ($q(T)$) distributions of Drell-Yan muon and electron pairs in the Z-boson mass region ($60 < M_{\ell\ell} < 120$ GeV) are reported. The results are obtained using a data sample of proton-proton collisions at a center-of-mass energy

of 7 TeV, collected by the CMS experiment at the Large Hadron Collider (LHC), corresponding to an integrated luminosity of 36 pb¹. The distributions are measured over the ranges $|y| < 3.5$ and $q(T) < 600$ GeV and compared with quantum chromodynamics (QCD) calculations using recent parton distribution functions to model the momenta of the quarks and gluons in the protons. Overall agreement is observed between the models and data for the rapidity distribution, while no single model describes the Z transverse-momentum distribution over the full range.

CMS Collaboration

3.2.2.4 Jet production rates in association with W and Z bosons in pp collisions at $\sqrt{s}=7$ TeV

Measurements of jet production rates in association with W and Z bosons for jet transverse momenta above 30 GeV are reported, using a sample of proton-proton collision events recorded by CMS $\sqrt{s}=7$ TeV, corresponding to an integrated luminosity of 36 pb⁻¹. The study includes the measurement of the normalized inclusive rates of jets $\sigma(V+geq = \eta \text{ jets})\sigma(V)$, where V represents either a W or a Z. In addition, the ratio of W to Z cross sections and the W charge asymmetry as a function of the number of associated jets are measured. A test of scaling $\sqrt{s}=7$ TeV is also presented. The measurements provide a stringent test of perturbative-QCD calculations and are sensitive to the possible presence of new physics. The results are in agreement with the predictions of a simulation that uses explicit matrix element calculations for final states with jets.

CMS Collaboration

3.2.2.5 Search for Supersymmetry at the LHC in Events with Jets and Missing Transverse Energy

search for events with jets and missing transverse energy is performed in a data sample of pp collisions collected at $\sqrt{s}=7$ TeV by the CMS experiment at the LHC. The analyzed data sample corresponds to an integrated luminosity of 1.14fb⁻¹. In this search, a kinematic variable $i\alpha_T$ is used as the main discriminator between events with genuine and misreconstructed missing transverse energy. No excess of events over the standard model expectation is found. Exclusion limits in the parameter space of the constrained minimal supersymmetric extension of the standard model are set. In this model, squark masses below 1.1 TeV are excluded at 95% C.L. Gluino masses below 1.1 TeV are also ruled out at 95% C.L. for values of the universal scalar mass parameter below 500 GeV.

CMS Collaboration

3.2.2.6 Search for physics beyond the standard model using multilepton signatures in pp collisions at $\sqrt{s}=7$ TeV

A search for physics beyond the standard model in events with at least three leptons and any number of jets is presented. The data sample corresponds to 35 pb⁻¹ of integrated luminosity in pp collisions at \sqrt{s} collected by the CMS experiment at the LHC. A number of exclusive multileptonic channels are investigated and standard model backgrounds are suppressed by requiring sufficient

missing transverse energy, invariant mass inconsistent with that of the Z boson, or high jet activity. Control samples in data are used to ascertain the robustness of background evaluation techniques and to minimise the reliance on simulation. The observations are consistent with background expectations. These results constrain previously unexplored regions of super symmetric parameter space.

CMS Collaboration

3.2.2.7 Measurement of the inclusive W and Z production cross sections in pp collisions at $\sqrt{s}=7$ TeV with the CMS experiment

A measurement of inclusive W and Z production cross sections in pp collisions at $\sqrt{s}=7$ TeV is presented. The electron and muon decay channels are analyzed in a data sample collected with the CMS detector at the LHC and corresponding to an integrated luminosity of 36 pb^{-1} . The measured inclusive cross sections are $\sigma(\text{pp} \rightarrow \text{WX}) \times \text{B}(\text{W} \rightarrow l\nu) = 10.31 \pm 0.02 \text{ (stat.)} \pm 0.09 \text{ (syst.)} \pm 0.10 \text{ (th.)} \pm 0.41 \text{ (lumi.) nb}$ and $\sigma(\text{pp} \rightarrow \text{ZX}) \times \text{B}(\text{Z} \rightarrow l^+l^-) = 0.974 \pm 0.007 \text{ (stat.)} \pm 0.007 \text{ (syst.)} \pm 0.018 \text{ (th.)} \pm 0.039 \text{ (lumi.) nb}$, limited to the dilepton invariant mass range 60 to 120 GeV. The luminosity-independent cross section ratios are $(\sigma(\text{pp} \rightarrow \text{WX}) \times \text{B}(\text{W} \rightarrow l\nu)) / (\sigma(\text{pp} \rightarrow \text{ZX}) \times \text{B}(\text{Z} \rightarrow l^+l^-)) = 10.54 \pm 0.07 \text{ (stat.)} \pm 0.08 \text{ (syst.)} \pm 0.16 \text{ (th.)}$ and $(\sigma(\text{pp} \rightarrow \text{W}^+X) \times \text{B}(\text{W}^+ \rightarrow l^+\nu)) / (\sigma(\text{pp} \rightarrow \text{W}^-X) \times \text{B}(\text{W}^- \rightarrow l^-\bar{\nu})) = 1.421 \pm 0.006 \text{ (stat.)} \pm 0.014 \text{ (syst.)} \pm 0.029 \text{ (th.)}$. The measured values agree with next-to-next-to-leading order QCD cross section calculations based on recent parton distribution functions.

CMS Collaboration

3.2.2.8 Search for new physics with jets and missing transverse momentum in pp collisions at $\sqrt{s}=7$ TeV

A search for new physics is presented based on an event signature of at least three jets accompanied by large missing transverse momentum, using a data sample corresponding to an integrated luminosity of 36 pb^{-1} collected in proton-proton collisions at $\sqrt{s}=7$ TeV with the CMS detector at the LHC. No excess of events is observed above the expected standard model backgrounds, which are all estimated from the data. Exclusion limits are presented for the constrained minimal super symmetric extension of the standard model. Cross section limits are also presented using simplified models with new particles decaying to an undetected particle and one or two jets.

CMS Collaboration

3.2.2.9 Heavy flavour decay muon production at forward rapidity in proton-proton collisions at $\sqrt{s}=7$ TeV

The production of muons from heavy flavour decays is measured at forward rapidity in proton-proton collisions at View the MathML source collected with the ALICE experiment at the LHC. The analysis is carried out on a data sample corresponding to an integrated luminosity $\text{Lint}=16.5 \text{ nb}^{-1}$. The transverse momentum and rapidity differential production cross sections of muons from heavy flavour decays are measured in the rapidity range $2.5 < y < 4$, over the transverse momentum range

$2 < p_T < 12$ GeV/c. The results are compared to predictions based on perturbative QCD calculations.

ALICE Collaboration

3.2.2.10 J/ ψ Polarization in pp Collisions at $\sqrt{s}=7$ TeV

The ALICE Collaboration has studied J/ ψ production in pp collisions at $\sqrt{s}=7$ TeV at the LHC through its muon pair decay. The polar and azimuthal angle distributions of the decay muons were measured, and results on the J/ ψ polarization parameters λ_θ and λ_ϕ were obtained. The study was performed in the kinematic region $2.5 < \gamma < 4$, $2 < p_T < 8$ GeV/c, in the helicity and Collins-Soper reference frames. In both frames, the polarization parameters are compatible with zero, within uncertainties.

ALICE Collaboration

3.2.2.11 Rapidity and transverse momentum dependence of inclusive J/ ψ production in pp collisions at $\sqrt{s}=7$ TeV

The ALICE experiment at the LHC has studied inclusive J/ ψ production at central and forward rapidities in pp collisions at $\sqrt{s}=7$ TeV. In this Letter, we report on the first results obtained detecting the J/ ψ through the dilepton decay into e^+e^- and $\mu^+\mu^-$ pairs in the rapidity ranges $|\eta| < 0.9$ and $2.5 < \gamma < 4$, respectively, and with acceptance down to zero pT. In the dielectron channel the analysis was carried out on a data sample corresponding to an integrated luminosity $\text{Lint}=5.6$ nb⁻¹ and the number of signal events is View the MathML source; the corresponding figures in the dimuon channel are $\text{Lint}=15.6$ nb⁻¹ and View the MathML source. The measured production cross sections are View the MathML source and View the MathML source. The differential cross sections, in transverse momentum and rapidity, of the J/ ψ were also measured.

ALICE Collaboration

3.2.2.12 Event Reconstruction Performance of the ALICE High Level Trigger p plus p for Collisions

The ALICE High Level Trigger comprises a large computing cluster, dedicated interfaces and software applications. It allows on-line event reconstruction of the full data stream of the ALICE experiment at up to 25 GByte/s. The commissioning campaign has passed an important phase since the startup of the Large Hadron Collider in November 2009. The system has been transferred into continuous operation with focus on the event reconstruction and first simple trigger applications. The paper reports for the first time on the achieved event reconstruction performance in the ALICE central barrel region.

ALICE Collaboration

3.2.2.13 ALICE HLT High Speed Tracking on GPU

The on-line event reconstruction in ALICE is performed by the High Level Trigger, which should process up to 2000 events per second in proton-proton collisions and up to 300 central events per second in heavy-ion collisions, corresponding to an input data stream of 30 GB/s. In order to fulfill the time requirements, a fast on-line tracker has been developed. The algorithm combines a Cellular Automaton method being used for a fast pattern recognition and the Kalman Filter method for fitting of found trajectories and for the final track selection. The tracker was adapted to run on Graphics Processing Units (GPU) using the NVIDIA Compute Unified Device Architecture (CUDA) framework. The implementation of the algorithm had to be adjusted at many points to allow for an efficient usage of the graphics cards. In particular, achieving a good overall workload for many processor cores, efficient transfer to and from the GPU, as well as optimized utilization of the different memories the GPU offers turned out to be critical. To cope with these problems a dynamic scheduler was introduced, which redistributes the workload among the processor cores. Additionally a pipeline was implemented so that the tracking on the GPU, the initialization and the output processed by the CPU, as well as the DMA transfer can overlap. The GPU tracking algorithm significantly outperforms the CPU version for large events while it entirely maintains its efficiency.

ALICE Collaboration

3.2.2.14 Performance and First Physics Results of the ALICE Muon Spectrometer

A precise measurement of the heavy-flavor production cross-sections in pp collisions is an essential baseline for the heavy-ion program. In addition it is a crucial test of pQCD models in the new energy regime at LHC. ALICE measures the muons from the decay of charmonium resonances and from the semileptonic decay of heavy-flavored hadrons in its forward ($-4.0 < \eta < -2.5$) Muon Spectrometer. We discuss the status of the detector and present results of data taken in pp collisions at $\sqrt{s}=7$ TeV.

ALICE Collaboration (Debasish Das)

3.2.2.15 Small quadrupole deformation for the dipole bands in ^{112}In

High spin states in ^{112}In were investigated using the $^{100}\text{Mo}(^{16}\text{O},p3n)$ reaction at 80 MeV. The excited level has been observed up to 5.6 MeV excitation energy and spin $\sim 20\hbar$ with the level scheme showing three dipole bands. Polarization and lifetime measurements were carried out for the dipole bands. Tilted axis cranking model calculations were performed for different quasiparticle configurations of this doubly odd nucleus. Comparison of the calculations of the model with the B(M1) transition strengths of the positive- and negative-parity bands firmly established their configurations.

T Trivedi†...S Roy, S Chattopadhyay

3.2.2.16 Non-Fermi liquid behavior of the drag and diffusion coefficients in QED plasma

We calculate the drag and diffusion coefficients in low temperature QED plasma and go beyond the leading order approximation. The non-Fermi-liquid behavior of these coefficients are clearly revealed. We observe that the subleading contributions due to the exchange of soft transverse photon in both cases are larger than the leading order terms coming from the longitudinal sector. The results are presented in closed form at zero and low temperature.

Sreemoyee Sarkar, Abhee K Dutt-Mazumder

3.2.2.17 Nuclear modification factor in an anisotropic quark-gluon plasma

We calculate the nuclear modification factor (RAA) of light hadrons by taking into account the initial state momentum anisotropy of the quark-gluon plasma (QGP) expected to be formed in relativistic heavy ion collisions. Such an anisotropy can result from the initial rapid longitudinal expansion of the matter. A phenomenological model for the space-time evolution of the anisotropic QGP is used to obtain the time dependence of the anisotropy parameter ξ and the hard momentum scale, p_{hard} . The result is then compared with the PHENIX experimental data to constrain the isotropization time scale, τ_{iso} for fixed initial conditions (FIC). It is shown that the extracted value of τ_{iso} lies in the range $0.5 \leq \tau_{iso} \leq 1.5$. However, using a fixed final multiplicity (FFM) condition does not lead to any firm conclusion about the extraction of the isotropization time. The present calculation is also extended to contrast with the recent measurement of nuclear modification factor by the ALICE collaboration at $\sqrt{s}=2.76$ TeV. It is argued that in the present approach, the extraction of τ_{iso} at this energy is uncertain and, therefore, refinement of the model is necessary. The sensitivity of the results on the initial conditions has been discussed. We also present the nuclear modification factor at Large Hadron Collider (LHC) energies with $\sqrt{s}=5.5$ TeV.

Mahatsab Mandal, Lusaka Bhattacharya, Roy Pradip

3.2.2.18 Non-Fermi liquid corrections to the neutrino mean free path in dense quark matter

We calculate the neutrino mean free path with non-Fermi liquid corrections in quark matter from scattering and absorption processes for both degenerate and nondegenerate neutrinos. We show that the mean free path decreases due to the non-Fermi liquid corrections, leading to $1/\text{mean}^{-l} \sim [\dots + \dots C_F^2 \alpha_s^2 \ln(m_D/T)^2]$. This reduction results in a higher rate of scattering.

Kausik Pal†, Abhee K Dutt-Mazumder

3.2.2.19 $\rho - \omega$ mixing and density dependent CSV potential

We construct the charge symmetry violating (CSV) nucleon-nucleon potential in nuclear matter induced by the $\rho - \omega$ mixing due to the neutron-proton mass difference driven by the NN loop. Analytical expression for the two-body CSV potential is presented.

S Biswas†, P Roy, AK Dutt-Mazumder

3.2.2.20 Fermi liquid description of relativistic high density matter

We calculate pionic contribution to the relativistic Fermi Liquid parameters (RFLPs) using Chiral Effective Lagrangian. The RFLPs so determined are then used to calculate chemical potential, exchange energy due to π N interaction. We also compare the results of exchange energy from two loop ring diagrams involving sigma, omega and pi meson with what one obtains from the relativistic Fermi Liquid theory (RFLT).

K Pal, AK Dutt-Mazumder

3.2.2.21 Radiative energy loss in an anisotropic quark-gluon plasma

We calculate radiative energy loss of heavy and light quarks in an anisotropic medium (static) in a first-order opacity expansion. Such an anisotropy can result from the initial rapid longitudinal expansion of the matter created in relativistic heavy-ion collisions. Significant dependency of the energy loss on the anisotropy parameter ξ and the direction of propagation of the partons with respect to the anisotropy axis is found. It is shown that the introduction of early-time momentum-space anisotropy can enhance the fractional energy loss in the direction of the anisotropy, whereas it decreases when the parton propagates perpendicular to the direction of the anisotropy.

Pradip Roy, Abhee K Dutt-Mazumder

3.2.2.22 Estimation of isotropization time ($\tau(\text{iso})$) of QGP from direct photons

We calculate transverse momentum distribution of direct photons from various sources by taking into account the initial state momentum anisotropy of quark gluon plasma (QGP). The total photon yield is then compared with the recent measurement of photon transverse momentum distribution by the PHENIX collaboration. It is also demonstrated that the presence of such an anisotropy can describe the PHENIX photon data better than the isotropic case in the present model. We show that the isotropization time thus extracted lies within the range for the initial condition used here.

Lusaka Bhattacharya

3.2.2.23 Effect of running coupling on photons from jetplasma interaction in relativistic heavy-ion collisions

We discuss the role of collisional energy loss on high p_T photon data measured by PHENIX collaboration by calculating photon yield in jetplasma interaction. The phase space distribution of the participating jet is dynamically evolved by solving the FokkerPlanck equation. We treat the strong coupling constant α_s as a function of momentum and temperature while calculating the drag and diffusion coefficients. It is observed that the quenching factor is substantially modified as compared to the case when s is taken as constant. It is shown that the data are reasonably well reproduced when contributions from all the relevant sources are taken into account. Predictions at higher beam energies relevant for LHC experiment have been made.

Lusaka Bhattacharya, Pradip Roy

3.2.3 Nuclear Physics

3.2.3.1 Helium nuclei around the neutron drip line

Neutron rich He nuclei have been investigated using the relativistic mean field approach in coordinate space. Elastic partial scattering cross sections for proton scattering in inverse kinematics have been calculated using the theoretically obtained density for ${}^6,8\text{He}$ and compared with the experiment. The energies of the low-lying resonance states in the neutron unstable nuclei ${}^5,7\text{He}$ have also been calculated and compared with experimental observations.

Madhubrata Bhattacharya†, G Gangopadhyay†, Subinit Roy

3.2.3.2 Measurements and coupled reaction channels analysis of one- and two-proton transfer reactions for the ${}^{28}\text{Si} + {}^{90,94}\text{Zr}$ systems

Measurements of angular distributions for one- and two-proton stripping reactions for ${}^{28}\text{Si} + {}^{90,94}\text{Zr}$ systems were performed at 120 MeV. The experiment was carried out with the ${}^{28}\text{Si}$ beam at Inter University Accelerator Center, New Delhi. The theoretical calculations were performed using the quantum mechanical coupled reaction channels code fresco. The distorted wave Born approximation calculations reproduced the experimental angular distributions for the one-proton transfer channel for both the systems reasonably well but failed for the two-proton transfer channel. Coupled channels calculations including various intermediate states (involving target and projectile inelastic excitations before and/or after transfer) along with the sequential transfer were able to reproduce the two-proton transfer angular distributions for both the systems reasonably well. It seems that at an energy above the Coulomb barrier, there is significant contribution of the indirect multistep and sequential transfer to the two-proton stripping reaction.

Sunil Kalkat†, S Mandal†, Santosh Chakraborty, et al

3.2.3.3 On the performance of the HVE high-current accelerator system light-ion 3 MV TandatronTM

High Voltage Engineering has successfully completed the factory tests of a 3 MV TandatronTM based accelerator system, fulfilling the rigorous requirements of the Facility for Research in Experimental Nuclear Astrophysics, part of the Saha Institute of Nuclear Physics, Kolkata, India. To satisfy requirements, High Voltage Engineering has developed a unique high-current light-ion injector. The injector includes two multicusp ion sources, one for H^- and one for He^+ , and a Na charge exchange canal. Extensive measurements yield routine production of about $70\ \mu\text{A}$ analyzed He^- and $1\ \text{mA}\ \text{H}^-$. The TandatronTM, designed and tested at 3 kW of beam power features low ripple (27 V-RMS at 3 MV), a particle transmission of at least 60% over the entire terminal voltage range, 200 kV up to 3 MV. In addition, the dual slit stabilization system ensures long term terminal voltage stability, $\pm 30\ \text{V}$ per hour at 3 MV.

FRENA Grp

3.2.3.4 Correlations of heavy quarks produced at the Large Hadron Collider

We study the correlations of heavy quarks produced in relativistic heavy-ion collisions and find them to be quite sensitive to the effects of the medium and the production mechanisms. In order to put this on a quantitative footing, as a first step, we analyze the azimuthal, transverse momentum, and rapidity correlations of heavy quark-antiquark ($Q\bar{Q}$) pairs in pp collisions at $\mathcal{O}(\alpha 3_s)$. This sets the stage for the identification and study of medium modification of similar correlations in the relativistic collision of heavy nuclei at the Large Hadron Collider. Next we study the additional production of charm quarks in heavy ion collisions due to multiple scatterings, namely jet-jet collisions, jet-thermal collisions, and thermal interactions. We find that these give rise to azimuthal correlations which are quite different from those arising from the prompt initial production at leading order and at next to leading order.

Mohammed Younus†, Umme Jamil, Dinesh K Srivastava†

3.2.3.5 Nondestructive Characterization of Municipal-Solid-Waste-Contaminated Surface Soil by Energy-Dispersive X-ray Fluorescence and Low-Z (Atomic Number) Particle Electron Probe X-ray Microanalysis

The long-term environmental impact of municipal solid waste (MSW) landfilling is still under investigation due to the lack of detailed characterization studies. A MSW landfill site, popularly known as Dhapa, in the eastern fringe of the metropolis of Kolkata, India, is the subject of present study. A vast area of Dhapa, adjoining the current core MSW dump site and evolving from the raw MSW dumping in the past, is presently used for the cultivation of vegetables. The inorganic chemical characteristics of the MSW-contaminated Dhapa surface soil (covering a 2-km stretch of the area) along with a natural composite (geogenic) soil sample (from a small countryside farm), for comparison, were investigated using two complementary nondestructive analytical techniques, energy-dispersive X-ray fluorescence (EDXRF) for bulk analysis and low-Z (atomic number) particle electron probe X-ray microanalysis (low-Z particle EPMA) for single-particle analysis. The bulk concentrations of K, Rb, and Zr remain almost unchanged in all the soil samples. The Dhapa soil is found to be polluted with heavy metals such as Cu, Zn, and Pb (highly elevated) and Ti, Cr, Mn, Fe, Ni, and Sr (moderately elevated), compared to the natural countryside soil. These high bulk concentration levels of heavy metals were compared with the Ecological Soil Screening Levels for these elements (U.S. Environment Protection Agency) to assess the potential risk on the immediate biotic environment. Low-Z particle EPMA results showed that the aluminosilicate-containing particles were the most abundant, followed by SiO(2), CaCO(3)-containing, and carbonaceous particles in the Dhapa samples, whereas in the countryside sample only aluminosilicate-containing and SiO(2) particles were observed. The mineral particles encountered in the countryside sample are solely of geogenic origin, whereas those from the Dhapa samples seem to have evolved from a mixture of raw dumped MSW, urban dust, and other contributing factors such as wind, precipitation, weather patterns, farming, and water logging, resulting in their diverse chemical compositions and the abundant observation of carbonaceous species. Particles containing C and P were more abundant in the Dhapa samples than in the countryside soil sample, suggesting that MSW-contaminated soils are more fertile. However, the levels of particles containing potentially toxic heavy metals such as Cr, Mn, Ni, Cu, Zn, and/or Pb in the Dhapa samples were significant, corroborated by their high bulk concentration levels (EDXRF), causing deep concern for the immediate environment and

contamination of the food chain through food crops.

Dhrubajyoti Gupta, Rita Ghosh, Ajoy K Mitra, Subinit Roy, Manoranjan Sarkar, et al

3.2.3.6 The ANC of ^{16}O subthreshold states from $^{12}\text{C}(^6\text{Li}, d)$ reaction at energies near the barrier

The ANC of the 2^+ (6.92 MeV) and 1^+ (7.12 MeV) subthreshold states of ^{16}O have been extracted from the normalization of $^{12}\text{C}(^6\text{Li}, d)$ angular distribution to a Finite Range Distorted Wave Born Approximation (FRDWBA) calculation. The theoretical analysis indicates a peripheral reaction and the extracted ANCs are not sensitive to the number of nodes in the bound state potential. The uncertainty from the entrance channel potential is minimized to 8% for the 6.92 and 11% for the 7.12 MeV state if the normalization is performed at the grazing angle. The uncertainty from the exit channel potential at the grazing angle is found to be 10% and 12% respectively for the 7.12 and 6.92 MeV states.

Sucheta Adhikari, Chinmay Basu

3.2.3.7 Structural change of the unique-parity $\pi h_{11/2} \otimes \nu h_{11/2}$ configuration in ^{134}Cs

A bandlike structure, based on the $\pi h_{11/2} \otimes \nu h_{11/2}$ configuration, has been identified for the first time in ^{134}Cs in a gamma-ray spectroscopic study using fusion evaporation reactions. The nature of this band in ^{134}Cs has been found to be distinctly different than the nearly degenerate doublet rotational band structures, observed in the lighter Cs isotopes for the same configuration. Both the total Routhian surface and the tilted axis cranking calculations were performed to understand the experimental observations. The present results suggest that the $N=77$ defines the border of the deformed structure in the $A \sim 130$ region while approaching $N=82$.

H Pai†...A Goswami

3.2.3.8 Study of Three-Quasiparticle Band in ^{83}Kr

Excited states of ^{83}Kr , populated in the $^{76}\text{Ge}(^{11}\text{B}, 3np \gamma)$ reaction at a beam energy of 50 MeV, have been studied. The $\Delta I = 1$ band, built upon the 2,510.0 keV state, has been observed up to 5,639.4 keV with spin $(27/2^-)$. Mean lifetimes have been measured up to spin $23/2^-$ in $\Delta I = 1$ band using the Doppler shift attenuation method. The $B(M1)$ rates derived from the measured lifetimes decrease smoothly with spin indicating that the angular momentum belonging to this band are generated by the shears mechanism.

Ganguly, Aparajita Dey, P Banerjee, S Bhattacharya, RP Singh, S Muralithar, R Kumar, RK Bhowmik

3.2.3.9 Experimental study of the $\pi h(11/2)$ band in Sb-113

In the present work, the excited states of Sb-113 were populated in the $\text{Mo-100}(\text{Ne-20}, p6n)$ reaction at a beam energy of 136 MeV. States only up to $59/2(-)$ were observed in the $\Delta J = 2$ band. Mean lifetimes for the five states (from 4460 to 7998 keV) were measured for the first time using

Doppler shift attenuation method. An upper limit of the lifetime (0.14 ps) was estimated for the 9061 keV, 47/2(-) state. The B(E2) values, derived from the present lifetime results, correspond to a large quadrupole deformation of $\beta(2) = 0.32$. The observed reduction in the experimental B(E2) values for the 918.4 keV (spin 39/2(-) \rightarrow aEuro parts per thousand 35/2 (-)) and 985 keV (spin 43/2(-) \rightarrow aEuro parts per thousand 39/2(-)) transitions may be interpreted as due to the proton alignment in the g (7/2) orbital. The dynamic moment of inertia was observed to be about half of the rigid body value at the highest observed frequency.

S Ganguly†, P Banerjee...S Bhattacharya

3.2.3.10 Identification of the slow E3 transition $^{136}\text{Cs}^m \rightarrow ^{136}\text{Cs}$ with conversion electrons

We performed at ISOLDE the spectroscopy of the decay of the 8(-) isomer in Cs-136 by γ and conversion-electron detection. For the first time the excitation energy of the isomer and the multipolarity of its decay have been measured. The half-life of the isomeric state was remeasured to $T_{1/2} = 17.5(2)$ s. This isomer decays via a very slow 518-keV E3 transition to the ground state. In addition to this, a much weaker decay branch via a 413-keV M4 and a subsequent 105-keV E2 transition has been found. Thus we have found a new level at 105 keV with spin 4(+) between the isomeric and the ground state. The results are discussed in comparison to shell-model calculations.

Wimmer K†, M Saha Sarkar et al

3.2.3.11 Fusion of ^6Li with ^{159}Tb at near-barrier energies

Complete and incomplete fusion cross sections for Li-6 + Tb-159 have been measured at energies around the Coulomb barrier by the gamma-ray method. The measurements show that the complete fusion cross sections at above-barrier energies are suppressed by similar to 34% compared to coupled-channel calculations. A comparison of the complete fusion cross sections at above-barrier energies with the existing data for B-11, B-10 + Tb-159 and Li-7 + Tb-159 shows that the extent of suppression is correlated with the alpha separation energies of the projectiles. It has been argued that the Dy isotopes produced in the reaction Li-6 + Tb-159 at below-barrier energies are primarily due to the d transfer to unbound states of Tb-159, while both transfer and incomplete fusion processes contribute at above-barrier energies.

MK Pradhan, A Mukherjee, P Basu, A Goswami, R Kshetri, Subinit Roy, P Roy Chowdhury, M Saha Sarkar, et al

3.2.3.12 Multinucleon transfer reactions for the $^{28}\text{Si}+^{90,94}\text{Zr}$ systems in the region below and near the Coulomb barrier

Measurements on multinucleon transfer reactions for $^{28}\text{Si}+^{90,94}\text{Zr}$ systems were performed at sub- and near-barrier energies. The fact that ^{90}Zr has a closed neutron shell ($N = 50$) and ^{94}Zr has four neutrons outside the closed shell, allows us to investigate the effects of shell closure and pairing correlation on multinucleon transfer mechanism. The experiment was performed with pulsed ^{28}Si beam using the Heavy Ion Reaction Analyzer (HIRA) at Inter University Accelerator Centre

(IUAC), New Delhi. Based on the Q-value considerations, it turned out that pickup channels were neutron transfer whereas stripping channels were proton transfer. For the $^{28}\text{Si}+^{90}\text{Zr}$ system, the values of the slope parameter for two-neutron pickup turned out to be less than that for one-neutron pickup. The values of the slope parameter were almost the same for two-, three-, and four-neutron pickup channels in the case of the $^{28}\text{Si}+^{94}\text{Zr}$ system. The transfer probabilities in the case of the $^{28}\text{Si}+^{94}\text{Zr}$ system were much larger than those for the $^{28}\text{Si}+^{90}\text{Zr}$ system, further supporting the fact that there is a correlation between the transfer channels and sub-barrier fusion cross-section enhancement. An odd-even staggering was observed in the extracted transfer probabilities at the barrier radius implying the role of pairing correlation in transfer reactions.

Sunil Kalkal†, UD Pramanik, et al

3.2.3.13 Alpha spectroscopic factor of O-16 from its breakup using continuum discretized coupled channel(CDCC) method

In this work we extract the alpha spectroscopic factor (S-alpha) of O-16 ground state from breakup reaction. The CDCC theory is used to extract S-alpha by comparison with O-16 breakup data from a light target (Al-27). Extracted values show a small dependence on the single particle binding potential of O-16 at forward angles. At incident energies between 72 to 125 MeV S-alpha varies from 2.29-2.83 (Wood Saxon binding potential) and between 2.42-3.72 (Gaussian potential).

Sucheta Adhikari, Chinmay Basu

3.2.3.14 Observation of heavy cluster structure of O-18 by inclusive measurement of intermediate mass fragment emitted in O-18+C-12 reaction at 80 MeV

An inclusive measurement of the Intermediate Mass Fragments(IMF) with Z=3,4,5 emitted from O-18+C-12 reaction at 80 MeV has been done. Reaction model analysis show that at such low energies IMF s are emitted primarily from projectile breakup. This indicates possible heavy cluster configurations of the O-18 nucleus.

C Basu, S Adhikari, AK Mitra, et al

3.3 Developmental Work

3.3.0.15 Simulation of Gaseous Detectors

Several MPGDs such as the Micromegas, MSGC, GEM, MHSP etc. have been analyzed numerically to estimate several measurable quantities such as gain, efficiency, transparency etc. The results have been compared successfully with numerical and experimental data reported by others. Detailed simulation of different aspects of the device like effect of surface roughness of the resistive electrodes on the detector signal and the role of SF6 in gas mixture has been carried out under INO Collaboration.

Purba Bhattacharya, Nayana Majumdar, Supratik Mukhopadhyay, Sudeb Bhattacharya, Satyajit Saha, Saikat Biswas†, Subhasis Chattopadhyay†, Md Salim†, Rashid Hasan†, B Satyanarayana†

3.3.0.16 Development and Upgrade of Detector Simulation Software

A much faster and accurate version of the solver has been developed which has been distributed to the users through the CERN web-site and the singular value decomposition (SVD) algorithm for handling singular systems has been implemented as an option. An improvement of existing CMS software by including the geometry of the Gaseous Electron Multiplier (GEM) as detection modules in high eta region has been initiated under GEMS for CMS Collaboration.

Supratik Mukhopadhyay, Nayana Majumdar, Purba Bhattacharya, Sudeb Bhattacharya, Sunanda Banerjee

3.4 Publications

3.4.1 Papers in Journals

3.4.1.1 Applied Nuclear Physics

Ad R Raduta†, B Borderie†, E Geraci†... MB Chatterjee et al, Evidence for alpha-particle condensation in nuclei from the Hoyle state deexcitation, *Physics Letters* **B705** (2011) 65

B Roy†...Nambissan PMG, et al, Mn substitution effects and associated defects in zno nanoparticles studied by positron annihilation, *NANO* **6** (2011) 173

CC Dey, S Dey, SC Bedi, et al, Hafnium oxide thin films studied by time differential perturbed angular correlations, *Journal of Applied Physics* **109** (2011) Art No: 113918

D Kanjilal†, S Saha, S Bhattacharya, A Goswami, R Kshetri, R Raut, S Muralithar†, RP Singh, G Mukherjee, B Mukherjee, First observation of high spin states and isomeric decay in ^{210}Fr , *Physical Review* **C84** (2011) Art No: 064321

I Lombardo†, C Agodi†, R Alba†, MB Chatterjee et al, Isospin Aspects in Nuclear Reactions Involving Ca Beams at 25 MeV/nucleon, *Physics of Atomic Nuclei* **74** (2011) 1562

I Lombardo†, C Agodi†, R Alba†, MB Chatterjee et al, Even-odd effects in Z and N distributions of fragments emitted at intermediate energies, *Physical Review* **C84** (2011) Art No: 024613

K Nikolopoulos†, P Bhattacharya, V Chernyatin, R Veenhoff†, Electron transparency of a Micromegas mesh, *Journal of Instrumentation* **6** (2011) Art No: P06011

I Lombardo†, C Agodi†, R Alba†,... MB Chatterjee, et al, Light clusters emission in nuclear reactions at 25 MeV/nucleon with different N/Z of entrance channels, *International Journal of Modern Physics* **E20** (Special Issue) (2011) 1066

PS Chowdhury†, P Mukherjee†, N Gayathri†, PMG Nambissan, Post irradiated microstructural characterization of Zr-1Nb alloy by X-ray diffraction technique and positron annihilation spectroscopy, *Bulletin of Materials Science* **34** (2011) 507

S Bhowal† S Bhattacharya, et al, Development of collective structures over noncollective excitations in Nd-139, *Physical Review* **C84** (2011) Art No: 024313

S Biswas, P Bhattacharya, S Bhattacharya, et al, Performances of silicone coated high resistive bakelite RPC, NIM **A661** (2012) S94

3.4.1.2 High Energy Nuclear & Particle Physics

ALICE Collaboration, Particle-Yield Modification in Jetlike Azimuthal Dihadron Correlations in Pb-Pb Collisions at $\sqrt{s_{NN}}=2.76$ TeV, Physical Review Letters **108** (2012) Art No: 092301

ALICE Collaboration, Harmonic decomposition of two particle angular correlations in Pb-Pb collisions at $\sqrt{s_{(NN)}}=2.76$ TeV, Physics Letters **B708** (2012) 249

ALICE Collaboration, Heavy flavour decay muon production at forward rapidity in proton-proton collisions at $\sqrt{s}=7$ TeV, Physics Letters **B708** (2012) 265

ALICE Collaboration, J/ψ Polarization in pp Collisions $\sqrt{s}=7$ TeV, Physical Review Letters **108** (2012) Art No: 082001

ALICE Collaboration, Measurement of charm production at central rapidity in proton-proton collisions at $\sqrt{s}=7$ TeV, Journal of High Energy Physics, **Issue: 1** (2012) Art No: 128

ALICE Collaboration, Femtoscopy of pp collisions at $\sqrt{s}=0.9$ and 7 TeV at the LHC with two-pion Bose-Einstein correlations, Physical Review **D84** (2011) Art No: 112004

ALICE Collaboration, Rapidity and transverse momentum dependence of inclusive J/ψ production in pp collisions at $\sqrt{s}=7$ TeV, Physics Letters **B704** (2011) 442

ALICE Collaboration, Event Reconstruction Performance of the ALICE High Level Trigger p plus p for Collisions, IEEE Transactions on Nuclear Science **58** (2011) 1706

ALICE Collaboration, ALICE HLT High Speed Tracking on GPU, IEEE Transactions on Nuclear Science **58** (2011) 1845

ALICE Collaboration, Production of pions, kaons and protons in pp collisions at $\sqrt{s}=900$ GeV with ALICE at the LHC, European Physical Journal **C71** (2011) Art No: 1655

ALICE Collaboration (Debasish Das), Performance and First Physics Results of the ALICE Muon Spectrometer, Nuclear Physics **A862** (2011) 223

ALICE Collaboration, Higher Harmonic Anisotropic Flow Measurements of Charged Particles in Pb-Pb Collisions at $\sqrt{s_{NN}}=2.76$ TeV, Physical Review Letters **107** (2011) Art No: 032301

CMS Collaboration, Measurement of the charge asymmetry in top-quark pair production in proton-proton collisions at $\sqrt{s}=7$ TeV, Physics Letters **B709** (2012) 28

CMS Collaboration, Search for the Standard Model Higgs Boson in the Decay Channel $H \rightarrow ZZ \rightarrow 4\ell$ in pp Collisions at $\sqrt{s}=7$ TeV, Physical Review Letters **108** (2012) Art No: 111804

CMS Collaboration, Search for Signatures of Extra Dimensions in the Diphoton Mass Spectrum at the Large Hadron Collider, *Physical Review Letters* **108** (2012) Art No: 111801

CMS Collaboration, Search for the standard model Higgs boson in the $H \rightarrow ZZ \rightarrow \ell^+ \ell^- \tau^+ \tau^-$ decay channel in pp collisions at $\sqrt{s}=7$ TeV, *Journal of High Energy Physics*, **Issue:3** (2012) Art No: 081

CMS Collaboration, Study of high- p_T charged particle suppression in PbPb compared to pp collisions at $\sqrt{s_{NN}}=2.76$ TeV, *European Physical Journal* **C72** (2012) Art No: 1945

CMS Collaboration, Measurement of the rapidity and transverse momentum distributions of Z bosons in pp collisions at $\sqrt{s}=7$ TeV, *Physical Review* **D85** (2012) Art No: 032002

CMS Collaboration, $J\psi$ and $\psi(2S)$ production in pp collisions at $\sqrt{s}=7$ TeV, *Journal of High Energy Physics*, **Issue: 2** (2012) Art No: 011

CMS Collaboration, Inclusive search for squarks and gluinos in pp collisions at $\sqrt{s}=7$ TeV, *Physical Review* **D85** (2012) Art No: 012004

CMS Collaboration, Exclusive gamma gamma $\rightarrow \mu^+ \mu^-$ production in proton-proton collisions $\sqrt{s}=7$ TeV, *Journal of High Energy Physics*, **Issue: 1** (2012) Art No: 052

CMS Collaboration, Jet production rates in association with W and Z bosons in pp collisions at $\sqrt{s}=7$ TeV, *Journal of High Energy Physics*, **Issue: 1** (2012) Article Number: 010

CMS Collaboration, Forward energy flow, central charged-particle multiplicities, and pseudorapidity gaps in W and Z boson events from pp collisions at $\sqrt{s}=7$ TeV, *European Physical Journal* **C72** (2012) Art No: 1839

CMS Collaboration, Search for a Vectorlike Quark with Charge 2/3 in $t + Z$ Events from pp Collisions at $\sqrt{s}=7$ TeV, *Physical Review Letters* **107** (2011) Art No: 271802

CMS Collaboration, Measurement of the weak mixing angle with the Drell-Yan process in proton-proton collisions at the LHC, *Physical Review* **D84** (2011) Art No: 112002

CMS Collaboration, Search for Supersymmetry at the LHC in Events with Jets and Missing Transverse Energy, *Physical Review Letters* **107** (2011) Art No: 221804

CMS Collaboration, Measurement of the $t\bar{t}$ production cross section in pp collisions at 7 TeV in lepton plus jets events using b-quark jet identification, *Physical Review* **D84** (2011) Art No: 092004

CMS Collaboration, Search for New Physics with a Monojet and Missing Transverse Energy in pp Collisions at $\sqrt{s}=7$ TeV, *Physical Review Letters* **107** (2011) Art No: 201804

CMS Collaboration, Search for $B_s(0) \rightarrow \mu^+ \mu^-$ and $B^0 \rightarrow \mu^+ \mu^-$ Decays in pp Collisions at $\sqrt{s}=7$ TeV, *Physical Review Letters* **107** (2011) Art No: 191802

CMS Collaboration, Search for physics beyond the standard model using multilepton signatures in pp collisions at $\sqrt{s}=7$ TeV, Physics Letters **B704** (2011) 411

CMS Collaboration, Search for resonances in the dijet mass spectrum from 7 TeV pp collisions at CMS, Physics Letters **B704** (2011) 123

CMS Collaboration, A search for excited leptons in pp collisions at $\sqrt{s}=7$ TeV, Physics Letters **B704** (2011) 143

CMS Collaboration, Measurement of the Drell-Yan cross section in pp collisions $\sqrt{s}=7$ TeV, Journal of High Energy Physics, **Issue: 10** (2011) Art No: 007

CMS Collaboration, Measurement of the inclusive W and Z production cross sections in pp collisions $\sqrt{s} = 7$ TeV with the CMS experiment, Journal of High Energy Physics, **Issue: 10** (2011) Art No: 132

CMS Collaboration, Measurement of the B-s(0) Production Cross Section with B-s(0) \rightarrow J/ ψ ϕ Decays in pp Collisions $\sqrt{s}=7$ TeV, Physical Review **D84** (2011) Art No: 052008

CMS Collaboration, Measurement of the underlying event activity at the LHC with $\sqrt{s}=7$ TeV and comparison with $\sqrt{s}=0.9$ TeV, Journal of High Energy Physics, **Issue: 9** (2011) Art No: 109

CMS Collaboration, Measurement of the t(t)over-bar production cross section in pp collisions $\sqrt{s}=7$ TeV using the kinematic properties of events with leptons and jets, European Physical Journal **C71** (2011) Art No: 1721

CMS Collaboration, Search for new physics with jets and missing transverse momentum in pp collisions $\sqrt{s}=7$ TeV, Journal of High Energy Physics, **Issue: 8** (2011) Art No: 155

CMS Collaboration, Search for supersymmetry in pp collisions $\sqrt{s}=7$ TeV in events with a single lepton, jets, and missing transverse momentum, Journal of High Energy Physics, **Issue: 8** (2011) Art No: 156

CMS Collaboration, Dependence on pseudorapidity and on centrality of charged hadron production in PbPb collisions $\sqrt{s(NN)}=2.76$ TeV, Journal of High Energy Physics, **Issue: 8** (2011) Art No: 141

CMS Collaboration, Search for same-sign top-quark pair production $\sqrt{s}=7$ TeV and limits on flavour changing neutral currents in the top sector, Journal of High Energy Physics, **Issue: 8** (2011) Art No: 005

CMS Collaboration, Indications of Suppression of Excited Upsilon States in Pb-Pb Collisions $\sqrt{(NN) - N - s}=2.76$ TeV, Physical Review Letters **107** (2011) Art No: 052302

CMS Collaboration, Search for supersymmetry in events with b jets and missing transverse momentum at the LHC, Journal of High Energy Physics, **Issue: 7** (2011) Art No: 113

CMS Collaboration, Measurement of the t(t)over-bar production cross section and the top quark

mass in the dilepton channel in pp collisions at $\sqrt{s}=7$ TeV, Journal of High Energy Physics, **Issue: 7** (2011) Art No: 049

CMS Collaboration, Search for light resonances decaying into pairs of muons as a signal of new physics, Journal of High Energy Physics, **Issue: 7** (2011) Art No: 098

CMS Collaboration, Search for supersymmetry in events with a lepton, a photon, and large missing transverse energy in pp collisions at $\sqrt{s}=7$ TeV, Journal of High Energy Physics, **Issue: 6** (2011) Art No: 093

CMS Collaboration, Search for first generation scalar leptoquarks in the $e \nu jj$ channel in pp collisions at $\sqrt{s}=7$ TeV, Physics Letters **B703** (2011) 246

CMS Collaboration, Search for Three-Jet Resonances in pp Collisions at $\sqrt{s}=7$ TeV, Physical Review Letters **107** (2011) Art No: 101801

CMS Collaboration, Measurement of the t-Channel Single Top Quark Production Cross Section in pp Collisions at $\sqrt{s}=7$ TeV, Physical Review Letters **107** (2011) Art No: 091802

CMS Collaboration, A GEM Detector System for an Upgrade of the CMS Muon Endcaps, CMS Internal Note, **CMS IN 2012/001**, FEB 10 2012

Sreemoyee Sarkar, Abhee K Dutt-Mazumder, Non-Fermi liquid behavior of the drag and diffusion coefficients in QED plasma, Physical Review **D84** (2011) Art No: 096009

S Biswas†, P Roy, AK Dutt-Mazumder, rho-omega mixing and density dependent CSV potential, Indian Journal of Physics **85** (2011) 1185

T Trivedi†, R Palit† J Sethi† S Roy, S Chattopadhyay, Small quadrupole deformation for the dipole bands in ^{112}In , Physical Review **C85** (2012) Art No: 014327

Mahatsab Mandal, Lusaka Bhattacharya, Pradip Roy, Nuclear modification factor in an anisotropic quark-gluon plasma, Physical Review **C84** (2011) Art No: 044910

Kausik Pal†, Abhee K Dutt-Mazumder, Non-Fermi liquid corrections to the neutrino mean free path in dense quark matter, Physical Review **D84** (2011) Art No: 034004

K Pal, AK Dutt-Mazumder, Fermi liquid description of relativistic high density matter, Indian Journal of Physics **85** (2011) 831

Pradip Roy, Abhee K Dutt-Mazumder, Radiative energy loss in an anisotropic quark-gluon plasma, Physical Review **C83** (2011) Art No: 044904

Lusaka Bhattacharya, Estimation of isotropization time ($\tau(\text{iso})$) of QGP from direct photons, Nuclear Physics **A855** (2011) 351

Lusaka Bhattacharya, Pradip Roy, Effect of running coupling on photons from jet-plasma interaction in relativistic heavy-ion collisions, Journal of Physics **G38** (2011) Art No: 045001

3.4.1.3 Nuclear Physics

C Basu, S Adhikari, AK Mitra, et al, Observation of heavy cluster structure of O-18 by inclusive measurement of intermediate mass fragment emitted in O-18+C-12 reaction at 80 MeV, International Journal of Modern Physics **E20** (Special Issue) (2011) 1058

D Gupta, JM Chatterjee, R Ghosh, AK Mitra, Subinit Roy and M Sarkar, Radioisotope induced EDXRF investigation of a elemental uptake in cauliflower grown at MSW-contaminated site, X-Ray Spectrometry **39** (2010) 364

Dhrubajyoti Gupta, Rita Ghosh, Ajoy K Mitra, Subinit Roy, Manoranjan Sarkar, et al, Nondestructive Characterization of Municipal-Solid-Waste-Contaminated Surface Soil by Energy-Dispersive X-ray Fluorescence and Low-Z (Atomic Number) Particle Electron Probe X-ray Microanalysis, Journal of The Air & Waste Management Association **61** (Special Issue) (2011) 1102

FRENA Grp, On the performance of the HVE high-current accelerator system light-ion 3 MV Tandetron (TM), Nuclear Instruments & Methods in Physics Research **B273** (2012) 231

H Pai†, G Mukherjee†, A Raghav† A Goswami, Structural change of the unique-parity $\pi h(11/2)$ circle times $\nu h(11/2)$ configuration in Cs-134, Physical Review **C84** (2011) Art No: 041301

K Wimmer†, M Saha Sarkar, et al, Identification of the slow $E3$ transition $^{136}\text{Cs}^m \rightarrow ^{136}\text{Cs}$ with conversion electrons, Physical Review **C84** (2011) Art No: 014329

MK Pradhan, A Mukherjee, P Basu, A Goswami, R Kshetri, Subinit Roy, P Roy Chowdhury, M Saha Sarkar, et al, Fusion of ^6Li with ^{159}Tb at near-barrier energies, Physical Review **C83** (2011) Art No: 064606

M Sinha, H Majumdar, P Basu, S Roy, R Bhattacharya, M Biswas, MK Pradhan, R Palit, I Mazumdar, S Kailas, Sub and above barrier fusion of loosely bound ^6Li with ^{28}Si , European Physical Journal **A44** (2010) 403

Madhubrata Bhattacharya†, G Gangopadhyay†, G, Subinit Roy, Helium nuclei around the neutron drip line, Physical Review **C85** (2012) Art No: 034312

S Ganguly†, Aparajita Dey, P Banerjee, S Bhattacharya, RP Singh, S Muralithar†, R Kumar†, RK Bhowmik, Study of Three-Quasiparticle Band in ^{83}Kr , Brazilian Journal of Physics **41** (2011) 135

S Ganguly†, P Banerjee, A Dey†, S Bhattacharya, Experimental study of the $\pi h(11/2)$ band in Sb-113, Pramana-Journal of Physics **77** (2011) 277

Sucheta Adhikari, Chinmay Basu, The ANC of O-16 subthreshold states from C-12(Li-6, d) reaction at energies near the barrier, Physics Letters **B704** (2011) 308

Sucheta Adhikari, Chinmay Basu, Alpha spectroscopic factor of O-16 from its breakup using continuum discretized coupled channel (CDCC) method, International Journal of Modern Physics **E20** (Special Issue) (2011) 958

Sunil Kalkal†...Santosh Chakraborty, et al, Measurements and coupled reaction channels analysis of one- and two-proton transfer reactions for the $^{28}\text{Si} + ^{90,94}\text{Zr}$ systems, *Physical Review* **C85** (2012) Art No: 034606

Sunil Kalkal†, UD Pramanik, et al, Multinucleon transfer reactions for the $^{28}\text{Si}+^{90,94}\text{Zr}$ systems in the region below and near the Coulomb barrier, *Physical Review* **C83** (2011) Art No: 054607

Maitrayee Saha Sarkar, S Sarkar, Study of neutron-rich nuclei near doubly magic ^{132}Sn , *AIP Conf Proc* **1444** (2012) 117

Maitrayee Saha Sarkar, Experimental study of upper sd shell nuclei and evolution of sd fp shell gap, *AIP Conf Proc* **1444** (2012) 190

3.5 Seminars/Lectures given in Conference/Symposium/Schools

Debasish Das

Quarkonium production at forward rapidities in ALICE experiment, Meeting on Quarks, Hadrons, and LHC, IIT Bombay, Aug 28-30, 2011

Maitrayee Saha Sarkar

Study of n-rich nuclei near doubly magic $A=132$ mass region, National Workshop on Nuclear Physics Using Ion Beams From Cyclotrons, VECC organized by UGC-DAE Consortium for Scientific Research, Kolkata Centre and Variable Energy Cyclotron Centre, Aug 24-26, 2011

Study of neutron rich nuclei near doubly magic ^{132}Sn , 8th International Conference on Progress in Theoretical Physics, organized by Universit Mentouri, Route de Ain-Bey, Constantine, Constantine, Algeria, Oct 23-25, 2011

Experimental study of upper sd shell nuclei and evolution of sd fp shell gap, 8th International Conference on Progress in Theoretical Physics, organized by Universit Mentouri, Route de Ain-Bey, Constantine, Constantine, Algeria, Oct 23-25, 2011

Nuclei in the upper sd shell and evolution of sd-fp shell gap, ANUP: Advances in Nuclear Physics(an ICTS, TIFR program), atwo day workshop International Centre, Goa, Nov 7-8, 2011

Understanding Nuclei in the upper sd shell, International workshop on 'Frontiers in Gamma Spectroscopy (FIG12) organized by Inter University Accelerator Centre (IUAC), New Delhi, Mar 5-7, 2012

The mass-energy balance sheet of nuclei and our well being for under-graduate students, Basantidevi College, Kolkata, Nov 16, 2011

Glimpses of new excitements in Nuclear Physics, Meeting on Recent trends in Physics organized

by Department of Physics, University of Calcutta, Kolkata, Feb 7-8, 2012

Nayana Majumdar

Effect of Surface Roughness on the Induced Charge of a RPC (Nayana Majumdar, Supratik Mukhopadhyay, Saikat Biswas, Purba Bhattacharya, Sudeb Bhattacharya, Subhasis Chattopadhyay, Satyajit Saha) (EVO Presentation), XI Workshop on Resistive Plate Chambers and Related Detectors (RPC2012), INFN Frascati, Italy, Feb 6-10, 2012

Topographic Effect of Bakelite Surface on Induced Charge in a RPC (Nayana Majumdar, Supratik Mukhopadhyay, Saikat Biswas, Purba Bhattacharya, Sudeb Bhattacharya, Subhasis Chattopadhyay, Satyajit Saha), INO Collaboration Meeting, BARC, Mumbai, Feb 13-15, 2012

Research and Applications of Gas Detector Simulation (Supratik Mukhopadhyay, Nayana Majumdar, Purba Bhattacharya, Sudeb Bhattacharya), National Symposium on Particles, Detectors and Instrumentation (NSPDI2012), TIFR, India, Mar 21-24, 2012

Studies on Detailed Dynamics of Gaseous Detectors (Nayana Majumdar, Supratik Mukhopadhyay, Purba Bhattacharya, Sudeb Bhattacharya), National Symposium on Particles, Detectors and Instrumentation (NSPDI2012), TIFR, India, Mar 21-24, 2012

PMG Nambissan

Evolving faces of science, Sir Syed College, Taliparamba, Kannur, Kerala, Jun 2, 2011

Positron annihilation studies of defects in Ti-6Al-4V subjected to heat treatments and rolling, International Workshop on Positron Studies of Defects 2011 (PSD-11), Technical University of Delft, Delft, The Netherlands, Aug 28-Sept 2, 2011

Precipitation behavior investigated through positron annihilation in Sc-doped Al-6Mg followed by the effects of Zr-addition, International Workshop on Positron Studies of Defects 2011 (PSD-11), Technical University of Delft, Delft, The Netherlands, Aug 28-Sept 2, 2011

Ni-substitution induced inversion in ZnFe₂O₄ seen by positron annihilation, Tenth International Workshop on Positron and Positronium Chemistry (PPC10), Bratislava, Slovakia. Sept 5-9, 2011

Positron and positronium annihilation as probes to identify cation substitution effects in CoCr_xFe_{2-x}O₄, Tenth International Workshop on Positron and Positronium Chemistry (PPC10), Bratislava, Slovakia, Sept 5-9, 2011

Positron annihilation as a unique probe for nanomaterial research, Tyndal National Institute, Lee Maltings, Cork, Ireland, Sept 13, 2011

Bulk structural changes in solids by particle irradiation and their studies using positrons, Seventeenth National Symposium on Solid State Nuclear Track Detectors and Their Applications (SSNTD-17), Department of Physics, The MS University of Baroda, Vadodara, Gujarat, Oct 17-19, 2011

Positron annihilation spectroscopy as a versatile tool for nanomaterial studies, Guru Gobind Singh Indraprastha University, New Delhi, Oct 21, 2011

Positron annihilation spectroscopic studies of wide band gap semiconductor nanomaterials and nanospinels, Second International Conference on Nanomaterials Synthesis, Characterization & Applications (ICN 2012), Mahatma Gandhi University, Kottayam, Kerala, Jan 10-12, 2012

New results from positron annihilation studies of certain nanomaterial systems, National Conference on Nanoscience and Nanotechnology, (ALIGARH NANO-II), Aligarh Muslim University, Aligarh, Mar 10-12, 2012

Positron annihilation studies of oxide semiconductor nanoparticles Some recent results, National Meeting on Positrons in materials, medicine and industry, Bhabha Atomic Research Centre, Mumbai, Mar 12-14, 2012

Recent positron annihilation studies on certain nanosemiconductors and nanospinels, Second National Seminar on Recent Trends in Condensed Matter Physics including Laser Applications (SNSCMPLA2012), Burdwan, Mar 22-23, 2012

Shaibal Saha

Development of GUI based Test and Measurement facilities for studying properties of MOS devices in cleanroom environment, International Joint Conferences on Computer, Information, and Systems Sciences, and Engineering (CISSE 11), University of Bridgeport, USA, Dec 3-12, 2011

3.6 Teaching elsewhere

Subinit Roy

Evolution of Stars, Astrophysics (Elective), 12 Lectures at M Sc(Physics), University of Calcutta, Kolkata, Jan-Mar, 2010 and 2011

3.7 Miscellany

Debasish Das

Driving the analysis effort on Upsilon into dimuons topic in ALICE as Coordinator of the dedicated PAG (Physics Analysis Group) from January 2012 and continuing.

Chapter 4

Plasma Physics & Computational Science

4.1 Summary of Research Activities of Divisions

4.1.1 Plasma Physics

Lagrangian fluid approach has been developed to study magnetized plasmas. Nonlinear solutions for compressional waves in a magnetized plasma of arbitrary resistivity show competition among hydrodynamic convection, magnetic field diffusion and dispersion. Dispersive effects arrest collapse of density but not of magnetic field. The results lead to possible applications to the early stages of magnetic star formation. In the context of large amplitude upper hybrid modes, magnetic field inhomogeneity causes various nonlinearly excited modes to couple, resulting in phase mixing and eventual wave breaking of the initially excited mode as seen by the appearance of spikes in the density profile.

The linear and nonlinear propagation characteristics of collective modes and their instabilities in a dusty plasma are influenced by strong correlation effects between the dust particles and studied using the generalized hydrodynamics model.

The propagation of transverse shear waves in inhomogeneous strongly coupled dusty plasmas are governed by equations similar to zero-energy Schrodinger's equation. The analogy enables study of multipolar vortex solutions for certain nontrivial density profiles. Viscoelastic properties of dusty plasmas have been characterized to be of non-Newtonian nature with both shear thinning and thickening properties invoking new interest in this direction.

Studies on shear flow driven Kelvin-Helmholtz instability and nonlinear shear wave propagation have carried out for such non-Newtonian strongly coupled dusty plasmas.

Stationary solutions of Vlasov-Maxwell equations are obtained by exploiting the invariants of single particle motion leading to various types of magnetic configurations including multiple current sheets and singular current layers. A third order nonlinear ordinary differential (JERK) equation has been obtained for chaotic plasma fluctuations in a magnetic field.

On the experimental front we have added a new data acquisition system to the tokamak and a new microwave source has been procured for the MaPLE device. Some interesting results have been

obtained on the plasma propulsion experiment.

4.2 Research Activities

4.2.0.1 Structure of hydrogenated diamond like carbon by Micro-Raman spectroscopy

The first-, second- and higher order Raman spectra of hydrogenated diamond like carbon (HDLC) are analyzed considering the effect of partial hydrogenation of hexagonal $sp(2)$ (C=C) carbons on the characteristic G and D bands of graphitic materials. That coherency of $sp(3)$ C-H and $sp(2)$ C=C carbons in HDLC can produce a continuous, non-porous thin film having atomically smooth surface is reported as a new result.

Jagannath Datta, Nihar R Ray, et al

4.2.0.2 Investigation of long-range temporal correlation in electron cyclotron resonance produced linear magnetized plasma of the MaPLE device

Long range temporal correlation of the low frequency fluctuations is investigated in a linear electron cyclotron resonance produced magnetized plasma at different radial positions and filling gas pressures. These fluctuations turn from chaotic to coherent and again chaotic as one moves radially outwards from the center towards the edge region. The power spectrum of these fluctuations shows three distinct frequency regions characterized by their power exponents. Long range temporal correlation of these fluctuations is investigated by estimating the self similarity parameter (Hurst exponents) using rescaled range (R/S) statistics as well as from power spectrum analysis. Dependence of this long range temporal correlation on filling gas pressure has also been investigated.

Subir Biswas, ANS Iyengar, Rabindranath Pal

4.2.0.3 Vlasov-Maxwell equilibria: Examples from higher-curl Beltrami magnetic fields

Stationary solutions of Vlasov-Maxwell equations are obtained by exploiting the invariants of single particle motion and lead to linear or nonlinear functional relations between current and vector potential. The nonlinear relations support various special types of magnetic configurations including multiple current sheets and magnetic field discontinuities leading to singular current layers. It is demonstrated through the examples that in one dimension, the description of the equilibrium magnetic fields obeys double or higher-curl Beltrami equation. For the linear case, such representation gives the advantage of obtaining exact analytic solutions that are expressed as a superposition of the single-curl Beltrami fields.

MS Janaki, Brahmananda Dasgupta†

4.2.0.4 Gottwald Melborune (0-1) test for chaos in a plasma

Plasma is a highly complex system exhibiting a rich variety of nonlinear dynamical phenomena. In the last two decades or so there has been a spurt of growth in exploring unconventional nonlinear dynamical methods of analysis, like chaos theory, multi fractal analysis, self organized criticality etc. of experimental data from different plasma systems. Investigation of fluctuating plasma parameters is very important since they are correlated with transport of particles, and energy. In time series analysis, it is considered of key importance to determine whether the data measured from the system is regular, deterministically chaotic, or random. The two important parameters that are in general estimated are the correlation dimension and the Lyapunov exponent. Though correlation dimension helps in determining the complexity of a system, Lyapunov exponent reveals if the system is chaotic or not and also helps in prediction to some extent. In spite of its extensive usage, estimation of Lyapunov exponent can be quite tedious and sometimes suffers from some disadvantages like reliability in the presence of noise, requirement of phase space reconstruction etc., and hence it is necessary to explore other possibilities of estimating the chaoticity of a data. In this paper we have analysed for chaoticity, the nonlinear floating potential fluctuations from a glow discharge plasma system by the 0-1 test and compared it with the results obtained from Lyapunov exponent.

DR Chowdhury†, ANS Iyengar, S Lahiri†

4.2.0.5 Nonlinear lower hybrid oscillations in a cold viscous plasma

An analytical description of nonlinear lower hybrid oscillations in a cold quasi-neutral plasma in the presence of viscosity is presented in one spatial dimension by using Lagrangian variables. By treating viscosity coefficients of the electron and ion fluids as inversely proportional to their respective densities, an exact solution is obtained. It is found that the damping rate of such oscillations is directly proportional to the effective viscosity coefficients of electron and ion fluids. A possible implication of such solutions is briefly outlined.

Chandan Maity, Nikhil Chakrabarti

4.2.0.6 Negative edge plasma currents in the SINP tokamak

A tokamak plasma discharge having an increase in duration accompanied with enhanced runaway electron flux has been experimentally studied in this paper. The discharges have been obtained by controlling the applied vertical magnetic field ($B_{v\text{appl}}/B_{v\text{appl}}$) to below a critical value. Such discharges have been observed to have negative edge plasma currents, detected using an internal Rogowski coil (IRC). We have tried to correlate the runaway behaviour with the negative edge plasma currents and have explained that these observations are a result of beam plasma instabilities.

Narayanan Ramesh, AN Sekar Iyengar

4.2.0.7 Nonlinear generation of sheared flows and zonal magnetic fields by electron whistlers in plasmas

The nonlinear generation of shear field and flow in whistler waves is considered. It is shown that a coherent parametric process leads to modulational instability of four waves whistler interaction. Growth rates for the flow/field are compared with published simulation results.

Chakrabarti Nikhil, Padma K Shukla†

4.2.0.8 Nonlinear wave propagation in a gravitating quantum fluid

The nonlinear wave propagation in a Bose-Einstein gravitationally condensate gas is investigated using a gravitating quantum fluid model. The small-amplitude dynamics is shown to be governed by a Korteweg-de Vries equation with a nonlocal term. The quantum effect provides the necessary dispersion, and the gravitational effect is responsible for the nonlocal term. This novel equation is solved analytically. The implications of such a soliton-like solution are outlined.

Samiran Ghosh†, Nikhil Chakrabarti

4.2.0.9 Nonlinear behavior of electron acoustic waves in an un-magnetized plasma

The nonlinear electron acoustic wave, which is found in the earth's magnetosphere by satellite observations, is studied analytically by Lagrangian fluid description. The basic linear mode is observed in a two temperature electron species plasma where ions form stationary charge neutral background. We have obtained nonlinear description of this mode, which depends on both time and space. A possible solution shows a soliton like structure, which is localized in space, and the amplitude increases with time in the absence of dispersion. Small dispersive correction, however, shows spread of the solution in space. This method can be generalized to study the nonlinear behavior of a general class of multispecies plasma.

Manjitha Dutta†, Nikhil Chakrabarti, et al

4.2.0.10 Shear waves in an inhomogeneous strongly coupled dusty plasma

The properties of electrostatic transverse shear waves propagating in a strongly coupled dusty plasma with an equilibrium density gradient are examined using the generalized hydrodynamic (GH) equation. In the usual kinetic limit, the resulting equation has similarity to zero energy Schrodinger's equation. This has helped in obtaining some exact eigenmode solutions in both Cartesian and cylindrical geometries for certain nontrivial density profiles. The corresponding velocity profiles and the discrete eigenfrequencies are obtained for several interesting situations and their physics discussed.

MS Janaki, D Banerjee, N Chakrabarti

4.2.0.11 Ceria associated manganese oxide nanoparticles: Synthesis, characterization and arsenic(V) sorption behavior

Four samples of ceria incorporated manganese oxide (NCMO) were prepared by co-precipitation-calcinations and sol-gel methods, and characterized by X-ray diffraction, scanning electron microscopy, transmission electron microscopy, atomic force microscopy. BET surface area etc. The synthetic samples were nanoparticle agglomerates with irregular surface morphology (Ce:Mn = 1:1). The NCMO-1b sample, prepared by the calcination of metal hydroxide at 573 K for 3.0 h, was a nano-crystalline (70-90 nm) and hydrated material having high BET surface area (116.96 m² g⁻¹). The arsenic(V)-sorption by the samples at pH 7.0 (± 0.2) and 30° C showed that the NCMO-1b is a most efficient material. Optimum pH range for the arsenic(V) sorption is 3.0-7.0 at 303 (± 1.0) K. Kinetics and equilibrium data obtained (pH = 7.0 \pm 0.2, T = 303 \pm 1.0 K and I = 0.01 M) had described the pseudo-second order kinetics and the Freundlich isotherm models well, respectively. Thermodynamics of the sorption reaction showed that the changes of enthalpy (ΔH°), entropy (ΔS°) and Gibbs free energy (ΔG°), respectively, were +23.901 kJ mol⁻¹, +0.175 kJ mol⁻¹ K⁻¹ and -25.737 to 32.753 kJ mol⁻¹ at T = 283-323 K. Estimation of the sorption energy (E = 17.15 kJ mol⁻¹) indicated that the arsenic(V) was chemisorbed on NCMO-1b. The phosphate only reduced the arsenic(V) removal efficiency of NCMO-1b.

Kaushik Gupta†...Harishankar Biswas†, Jagannath Dutta, Nihar Ranjan Ray

4.2.0.12 Nonlinear wave propagation in a strongly coupled collisional dusty plasma

The propagation of a nonlinear low-frequency mode in a strongly coupled dusty plasma is investigated using a generalized hydrodynamical model. For the well-known longitudinal dust acoustic mode a standard perturbative approach leads to a Korteweg-de Vries (KdV) soliton. The strong viscoelastic effect, however, introduced a nonlinear forcing and a linear damping in the KdV equation. This novel equation is solved analytically to show a competition between nonlinear forcing and dissipative damping. The physical consequence of such a solution is also sketched.

Samiran Ghosh†...Nikhil Chakrabarti, et al

4.2.0.13 Secondary instability of Jeans mode in a gravitating fluid with uniform rotation

An axisymmetric rotating gas in a gravitational field is examined for its stability to two dimensional disturbances with first azimuthal mode. It is shown that a quasi-equilibrium is established when pressure and Coriolis force act against primary Jeans instability. A linear perturbation on this inhomogeneous equilibrium gives rise to secondary instability, which grows differently from homogeneous case. A stationary phase integral method demonstrates that the instability grows algebraically due to the free energy associated with the axisymmetric equilibrium. This secondary Jeans instability may have some bearing with the structure formations in the universe.

Nikhil Chakrabarti

4.2.0.14 Exact Time-Dependent Nonlinear Dispersive Wave Solutions in Compressible Magnetized Plasmas Exhibiting Collapse

Compressional waves in a magnetized plasma of arbitrary resistivity are treated with the Lagrangian fluid approach. An exact nonlinear solution with a nontrivial space and time dependence is obtained with boundary conditions as in Harris' current sheet. The solution shows competition among hydrodynamic convection, magnetic field diffusion, and dispersion. This results in a collapse of density and the magnetic field in the absence of dispersion. The dispersion effects arrest the collapse of density but not of the magnetic field. A possible application is in the early stage of magnetic star formation.

Nikhil Chakrabarti, Chandan Maity, et al

4.2.0.15 Relativistic effects on nonlinear lower hybrid oscillations in cold plasma

Nonlinear lower hybrid mode in a quasineutral magnetized plasma is analyzed in one space dimension using Lagrangian coordinates. In a cold fluid, we treat electron fluid relativistically, whereas ion fluid nonrelativistically. The homotopy perturbation method is employed to obtain the nonlinear solution which also finds the frequency-amplitude relationship for the lower hybrid mode. The solution indicates that the amplitude of oscillation increases due to the weak relativistic effects. The appearance of density spikes is not ruled out in a magnetized plasma.

Chandan Maity, Nikhil Chakrabarti, Sudip Sengupta†

4.3 Developmental Work

4.3.1 Plasma Physics

4.3.1.1 The double layer experiment (DLX)

An experimental setup has been constructed for the study of plasma propulsion using the concept of electric double layer. An inductive RF discharge has been produced in a quartz tube by a loop antenna connected to a RF source (13.56 MHz, 1.25 kW) through a p-type matching network. The tube is kept in an axial magnetic field (500 G maximum) provided by a Helmholtz coil pair. The plasma ($n \approx 1 \times 10^{11} \text{ cm}^{-3}$, $T_e \approx 10 \text{ eV}$) diffuses into a larger chamber (50 cm diameter, 50 cm long) along a diverging magnetic field. Formation of an electric double layer has been observed under such situations, which can accelerate ions to high energies as a beam. A RF-compensated Langmuir probe, an emissive probe and a four-grid retarding field ion energy analyser have also been constructed and used to find the density, electron temperature, plasma potential and energy distribution function of the ions in two dimensions. These diagnostics are mounted on guided vacuum bellow arrangements and driven by stepper motors. Commands are issued from a computer to obtain precise movement of the probes. The complete setup has been designed and fabricated in-house from scratch. The system is fully operational and experiments are in progress. The axial profile of the plasma potential shows the presence of an electric double layer which is confirmed by the evidence of an accelerated ion beam in the ion energy distribution function in the downstream region. The potential drop of the DL is 40 V at $p=1.00-4$ torr and is higher at lower pressures. The peak energy of the ion beam is independent of the axial position and the beam intensity is

highest on the chamber axis, decreasing with radial and axial distances. A 2-D map of the plasma potential shows convex equipotential surfaces near the axis and a secondary lobe off-axis. Magnetic field-aligned electric field is also found to be present on a conical surface. Both these findings are new results, unreported so far. Such studies carried out in a laboratory device have important implications in astrophysical plasmas, for example, in the formation of aurora borealis, solar flares and shock-like variation of potential observed in the earth's magnetosphere.

SK Saha, S Chowdhury, S Raychaudhuri, AK Hui† and MS Janaki

4.3.1.2 Upgradation of the SINP Tokamak

The SINP Tokamak works in a different parameter region than other machines of the world. Many interesting phenomena have already manifested themselves here; examples being ease of obtaining low and ultra low q discharges, anomalous ion heating both in low q and runaway discharges, peculiarity of runaway phenomena, magneto hydrodynamic and turbulent phenomena and transport. The nature of the runaway phenomena is yet to be fully characterized. So with improved diagnostics like adding two neutral particle analyzers to look at tangential and radial ports simultaneously we plan to work on core magnetic turbulence using low energy (μ MeV) hard X-ray emissivity simultaneously with anomalous ion temperature to establish their correlation and if the work could be extended to normal (non-runaway) regime. To investigate the role of core magnetic turbulence on runaway transport a parametric study is desirable. Biasing an electrode inserted in the edge region evolved in some interesting new results. For the first time suppression of drift-Alfven mode fluctuations was observed in both low- q and normal- q discharges and improved confinement regime is achieved. Fast biasing leads to modification of the toroidal current density profile at the edge region, which seems to take the key role in the fluctuation suppression. It is highly desirable that some of these phenomena are examined in details. In order to enrich this exciting field of Tokamak research we proposed to revitalize SINP Tokamak and a fund was granted by our present director for this purpose. From this proposal various accessories are already ordered and many of them are procured and installed on the Tokamak. We wish to further study the above mentioned phenomena in a challenging device like SINP Tokamak. The newly purchased 24 channel data acquisition system from Kingsly Instruments has already started functioning. Two new neutral particle analyzers have been designed, constructed and added to two of the tangential and radial ports. The soft x-ray diagnostic system also have been redesigned and tested. A new pumping system has been ordered to replace and improve the pumping system for the soft x-ray diagnostics from the old diffusion pumps. Lead blocks and containers have been designed, ordered and to arrive soon to replace the old ones to improve the hard x-ray diagnostic system. The water cooling pumping system for the Tokamak main turbo vacuum pumps have been replaced with new ones. Most of the new parts, which have arrived and installed are working successfully. The CAMAC data acquisition parts also for the hard x-ray diagnostics are on the way of procurement. The small pumping system for the soft x-ray diagnostics has arrived and is on the process of installation. In the meantime we are testing the system with already available accessories.

Santwana Raychaudhuri, Shantanu Chowdhury, Amit Kumar Hui†, AN Sekar Iyengar, Rabinathan Pal, Nikhil Chakrabarty, Sujit Kumar Saha, M Sita Janaki

4.3.2 Computational Science

The year 2012 saw the formation of a new division named Computational Science Division at Saha Institute of Nuclear Physics. The division was created to take care of activities of the then existing Computer Section and to promote research in the areas of Computational Physics, Chemistry and Biology. The division in its inception has inherited the rich hardware and networking infrastructure that was created and managed by the now erstwhile Computer Section. The division has also adopted the project proposals of the earlier Computer Section for the XIIth Five Year Plan. In addition the newly formed division is also playing an important role in planning and implementation of e-governance and automation services and the website application development project.

Proposed Developmental Work:

Post April 2012, the newly formed Computational Science Division has proposed the following development and infrastructural enhancement works for the plan year 2012-2013 under the project head Centre for Computational Sciences(CCS).

1. Creation of a Tier 2 Data Center for installation of Grid Computation hardware, High Performance Computing facilities and other high end Computational Servers.
2. Installation of the existing grid hardware for LHC experiments.
3. Procurement and installation of HPC solutions for Scientific Computing.
5. Installation of appliance based perimeter security solutions.
6. Commissioning of new E-mail and other network services to the users of the Institute.
7. Commissioning of Modular Data Center for achieving DC-DR configuration for the Institute Data Center.
8. A solution for displaying multimedia content with text tickers displayed at different screens of the campus.
9. Up-gradation of Storage Cache of the existing Enterprise Storage.
10. Procurement and Installation of scientific software and libraries and other software licenses.

4.4 Publications

4.4.1 Papers in Journals

4.4.1.1 Plasma Physics

Chandan Maity, Nikhil Chakrabarti, Nonlinear lower hybrid oscillations in a cold viscous plasma, *Physics of Plasmas* **18** (2011) Art No: 124502

Chandan Maity, Nikhil Chakrabarti, Sudip Sengupta†, Relativistic effects on nonlinear lower hybrid oscillations in cold plasma, *Journal of Mathematical Physics* **52** (2011) Art No: 043101

DR Chowdhury†, ANS Iyengar, S Lahiri†, Gottwald Melborune (0-1) test for chaos in a plasma, *Nonlinear Processes in Geophysics* **19** (2012) 53

Jagannath Datta, Nihar R Ray, Pintu Sen†, Hari S Biswas†, Erwin A Vogler†, Structure of hydrogenated diamond like carbon by Micro-Raman spectroscopy, *Materials Letters* **71** (2012) 131

Kaushik Gupta†, *Sayan Bhattacharya*†, *Dhrubajyoti Chattopadhyay*†, *Aniruddha Mukhopadhyay*†, *Harishankar Biswas*†, *Jagannath Dutta*, *Nihar Ranjan Ray*, *Uday Chand Ghosh*, Ceria associated manganese oxide nanoparticles: Synthesis, characterization and arsenic(V) sorption behavior, *Chemical Engineering Journal* **172** (2011) 219

MS Janaki, *Brahmananda Dasgupta*†, Vlasov-Maxwell equilibria: Examples from higher-curl Beltrami magnetic fields, *Physics of Plasmas* **19** (2012) Art No: 032113

MS Janaki, *D Banerjee*, *N Chakrabarti*, Shear waves in an inhomogeneous strongly coupled dusty plasma, *Physics of Plasmas* **18** (2011) Art No: 092114

Manjistha Dutta†, *Nikhil Chakrabarti*, *et al*, Nonlinear behavior of electron acoustic waves in an un-magnetized plasma, *Physics of Plasmas* **18** (2011) Art No: 102301

Nikhil Chakrabarti, *Padma K Shukla*†, Nonlinear generation of sheared flows and zonal magnetic fields by electron whistlers in plasmas, *Physics Letters* **A375** (2011) 3880

Nikhil Chakrabarti, Secondary instability of Jeans mode in a gravitating fluid with uniform rotation, *Physics of Plasmas* **18** (2011) Art No: 062903

Nikhil Chakrabarti, *Chandan Maity*, *Schamel Hans*, Exact Time-Dependent Nonlinear Dispersive Wave Solutions in Compressible Magnetized Plasmas Exhibiting Collapse, *Physical Review Letters* **106** (2011) Art No: 145003

Ramesh Narayanan, *AN Sekar Iyengar*, Negative edge plasma currents in the SINP tokamak, *Pramana-Journal of Physics* **77** (2011) 1135

Samiran Ghosh†, *Mithil Ranjan Gupta*†, *Nikhil Chakrabarti*, *Manis Chaudhuri*†, Nonlinear wave propagation in a strongly coupled collisional dusty plasma, *Physical Review* **E83** (2011) Art No: 066406

Samiran Ghosh†, *Nikhil Chakrabarti*, Nonlinear wave propagation in a gravitating quantum fluid, *Physical Review* **E84** (2011) Art No: 046601

Subir Biswas, *ANS Iyengar*, *Rabindranath Pal*, Investigation of long-range temporal correlation in electron cyclotron resonance produced linear magnetized plasma of the MaPLE device, *Physics of Plasmas* **19** (2012) Art No: 032310

4.4.1.2 Computational Science

Gautam Garai, *Biswanath Chowdhury*, A novel Genetic Approach for optimized Biological Sequence Alignment, *Journal of Biophysical Chemistry* **3** (2012) 201

4.5 Seminars/Lectures given in Conference/Symposium/Schools

AN Sekar Iyengar

Low g_a experiments in the SINP tokamak, Indo-US Fusion collaboration meeting, IPR, Gandhinagar, Feb 7-8, 2012

Plasmas and its applications, DST-Inspire lecture for school students, Guru Gobin Singh University, Delhi, Jan 12, 2012

R Pal

Important Steps towards Fusion Reactor, National Workshop on Plasma Processing for Thermonuclear Fusion and Industrial Applications, KIIT University, Bhubaneswar, Nov 10-11, 2011

Sujit K Saha

Solving physical problems with MATLAB, National Institute for Technical Teachers Training and Research, Kolkata, June 13, 2011

4.6 Teaching elsewhere

AN Sekar Iyengar

Nonlinear dynamics Experiments in Plasmas (2 lectures), IPR, Feb 6 & 9, 2012

N Chakrabarti

Basic Quantum Mechanics, M Sc, Narendrapur Ramkrishana Mission College (University of Calcutta) (2011)

Basic Plasma physics, M Sc, Narendrapur Ramkrishana Mission College (University of Calcutta) (2011)

4.7 Miscellany

N Chakrabarti

Indian representative of International Union of Radio Science (URSI) [Commission-H] (2011 to 2014)

Chapter 5

Theoretical Physics

5.1 Summary of Research Activities of Divisions

5.1.1 Astroparticle Physics and Cosmology

Astroparticle Physics and Cosmology (APC) Division pursues research in the interface areas spanning Astrophysics, Cosmology, and high energy particle and nuclear physics. During the year under review, members of the Division have carried out research on a variety of topics in AstroParticle Physics. Some highlights are given below.

(i) Physics of Neutron Star interiors: The shear viscosities of different species in hot and neutrino-trapped dense matter relevant to protoneutron stars have been studied. It has been shown that the shear viscosity owing to neutrinos is higher by several orders of magnitude than that of other species in neutrino-trapped matter. The effect of shear viscosity, in particular, neutrino shear viscosity, on the thermal nucleation rate of droplets of antikaon condensed matter in protoneutron stars has also been studied. It has been shown that neutrino shear viscosity enhances the prefactor in the nucleation rate by several orders of magnitude compared with the T^4 approximation of earlier calculations, raising the possibility that thermal nucleation of an antikaon droplet might be possible in neutrino-trapped matter before neutrino diffusion takes place.

In another work, the ground-state properties of inner crusts of neutron stars in the presence of strong magnetic fields of $\sim 10^{17}$ Gauss have been studied within the framework of Thomas-Fermi model. It has been shown that the phase space modification of electrons due to Landau quantization in the presence of strong magnetic fields leads to a significant enhancement of electron as well as proton fractions at lower densities of $\sim 0.001\text{fm}^{-3}$. It is also found that, compared to the case of zero magnetic field, nuclei with relatively larger mass and atomic numbers are possible in the inner crust of neutron stars in the presence of strong magnetic fields.

(ii) Theoretical research on Dark Matter: Several theoretical as well as phenomenological issues pertaining to direct and indirect detection of WIMP dark matter have been investigated. In particular, one specific topic, namely the diurnal and annual variations of the expected directional detection rates of WIMP candidates of dark matter, has been studied in detail. Because of a particular orientation of Earth's axis of rotation with respect to the WIMP wind direction, the apparent direction of the WIMP wind as observed at a detector can alter widely in a day. The

directional detection rates with their daily and yearly modulations in Earth-bound dark matter experiments have been calculated considering detailed features of the geometry and dynamics of the Earth-Sun system along with the solar motion in the Galactic frame, and the sensitive ranges of mass and nuclear recoil energies for some types of direction sensitive detectors have been probed.

(iii) Experimental search for WIMP Dark Matter Candidates using Superheated Drop Detectors (SDD), as a part of the international PICASSO Collaboration. The experiment is currently underway at the SNOLab underground facility in Sudbury, Canada. The SINP group has made major contributions in obtaining new results pertaining to calibrations of SDDs using various different radiation sources (n, α, γ) . Also a model has been developed that describes how the observed intensities of particle-induced acoustic signals can be related to the dynamics of bubble growth in superheated liquids.

(iv) Observational High Energy Gamma Ray Astronomy with the High Altitude GAMMA Ray (HAGAR) Cherenkov telescope system located at Hanle, Ladakh, J&K, as a part of the HAGAR collaboration involving SINP, TIFR (Mumbai) and IIAp (Bangalore): The SINP group has taken the main role in determining the performance parameters of the HAGAR Cherenkov telescope system (including determination of the detector threshold energy) by doing extensive Monte Carlo simulations of the cosmic ray and gamma ray induced showers in the earth's atmosphere together with simulations of the detector system.

(v) Neutrino mass models: A particular structure of neutrino mass matrix, known as four zero Yukawa textures, has been studied in the context of $\mu - \tau$ symmetry and the so-called Type-I see-saw mechanism. It is shown that this allows two alternately viable 3X3 light neutrino Majorana mass matrices with inverted/normal mass ordering, which can be experimentally probed with $0\nu\beta\beta$ decay. The effects of departure from $\mu\tau$ symmetry due to RG evolution from a high scale and consequent CP violation have also been studied.

(vi) Field theory: The implications of the gauge-free electroweak theory for the classical interpretation of the Higgs scalar as the dilaton field in a background conformal gravity theory have been studied. The Higgs scalar is shown to radiatively acquire a one-loop vacuum expectation value which gives masses to the W and Z bosons but not to photons, without any notion of spontaneous gauge symmetry breaking. Further, the renormalization scale is fixed in this theory by requiring that W and Z boson masses coincide with their experimentally measured values, thereby precluding any naturalness problem usually associated with uncontrolled running of such a scale.

A fairly general class of field configurations (of spins 0, 1/2 and 1) which preserve Lorentz invariance in effective field theories of Lorentz violation characterized by a constant time-like vector, has been identified. These fields are found to concomitantly satisfy the equations of motion yielding cubic dispersion relations similar to those found earlier. Prospective applications of such fields in inflationary scenarios have been pointed out. Gauge invariant coupling of 2- or 3-form (Abelian or non-Abelian) gauge fields to torsion has been studied. As in heterotic string theory, such couplings lead to new interactions which may have interesting astrophysical implications. The Coleman-Weinberg potential for this theory has been explicitly calculated. The possibility of such terms in loop quantum gravity is also explored.

5.1.2 Theory

Research in the Theory Division branches out in several areas of theoretical physics. This has created various subgroups within the division, which are, theoretical nuclear physics, high energy phenomenology, mathematical physics, quantum field theories and strings & gravity. Summary of the important results obtained during this period is given below.

a) Theoretical Nuclear Physics:

The correlations between electric dipole polarizability and the neutron-skin in ^{208}Pb nucleus has been studied using several non-relativistic and relativistic mean-field models. Our analysis indicates that whereas individual models exhibit a linear dependence between polarizability and neutron-skin, this correlation is not universal when one combines predictions from a host of different models. It is concluded that precise measurements of r_{skin} in both ^{48}Ca and ^{208}Pb combined with the recent measurement of dipole polarizability should significantly constrain the isovector sector of the nuclear energy density functional.

The heavy-ion experiments can show us glimpse of the predicted plasma phase of QCD depends how well one understands the collective behaviour of a system composed of quarks and gluons at high temperature/baryon density around and above the QCD phase transition point. Thermodynamic properties of such matter based on field theory at finite temperature and baryon density, and also other phenomenological aspects of very hot and dense matter created in heavy-ion collisions are being pursued.

The strangeness -2 sector has been investigated by studies of the (K_-, K_+) reactions on proton and heavier nuclei.

b) Mathematical Physics:

Fiber guided optical signal propagating in a Erbium doped nonlinear resonant medium is known to produce cleaner solitonic pulse, described by the self induced transparency (SIT) coupled to non-linear Schrodinger equation. Two new possibilities hidden in its integrable structure, for amplification and control of the optical pulse are explored. Using the variable soliton width permitted by the integrability of this model, the broadening pulse can be regulated by adjusting the initial population inversion of the dopant atoms. The effect can be enhanced by another innovative application of its constrained integrable hierarchy, proposing a system of multiple SIT media. Using negative powers in the spectral flow to deform the time Lax operator, a class of perturbations are found that unlike the usual perturbations, which spoil the system integrability, exhibit a twofold integrable hierarchy, including those for the KdV, modified KdV, sine-Gordon, nonlinear Schrodinger (NLS), and derivative NLS equations.

The eigenvalue problem of the D_N type of Calogero model is solved by mapping it to a set of decoupled quantum harmonic oscillators through a singular similarity transformation. It is shown that the eigenfunctions of such Calogero model can be constructed from those of bosonic harmonic oscillators having either all even parity or all odd parity. The level density distributions for a class of 1-dimensional classical vertex models related to Haldane-Shastry like spin chains have been studied.

Work has been done on topological defects in graphene in the presence of an external charge. Both the sub and supercritical regimes of gapless and gapped graphene have been studied and their properties investigated. Phases of matter at the Planck scale, where quantum effects of gravity are important have been studied. The twisted statistics of quantum fields in the vicinity of a noncommutative black hole at the Planck scale have been investigated.

c) High Energy Phenomenology:

Angular analysis of diphoton final state at the LHC, to discriminate the KK excitations of warped extra dimensions, from a scalar model excitation, based on the center-edge asymmetry to NLO in

QCD has been done. Estimation of the impact of QCD corrections to NNLO and beyond (dominant soft gluon contributions at N3LO), for resonant production of sneutrinos and sleptons, possible in SUSY theories with R-parity violating interactions is also worked out. The full NLO QCD corrections to the associated production of the vector gauge boson and the graviton in theories with large extra dimensions at the LHC have been computed.

Different avenues of electroweak symmetry breaking keeping in mind following two key issues have been studied. First, how fine-tuned different models are that trigger this phenomenon? Second, is the Higgs boson necessarily elementary or it can be composite as well? Some phenomenological applications of R-parity violating supersymmetry in LHC physics and neutrino physics have also been studied. Testable signatures of CPT violation have been studied. Lepton number violating neutrino oscillations are also studied.

The observability of collective flavor oscillations in Diffuse Supernova Neutrino Background (DSNB) is studied in detail and the dependence of the number of expected events in present and future neutrino detectors on the neutrino and antineutrino flux distributions stressed. The windows in parameter space which may give rise to identification of neutrino mass hierarchy are discussed.

d) Quantum Field Theory:

In a first time study in India, the chiral regime of lattice QCD with investigations of the low lying spectrum and its consistency with chiral perturbation theory, and topological aspects of QCD have been studied. The topological susceptibility with naive Wilson fermions is found to be suppressed with decreasing quark mass, an observation consistent with chiral Ward Identity and chiral perturbation theory that has eluded the lattice community for a decade. On-going work includes the study of correlators of the topological charge density and the autocorrelations of a host of observables like gauge plaquette, Wilson loop, pion and nucleon propagator, and topological charge and susceptibility, with the Domain-Decomposed Hybrid Monte Carlo algorithm. Analytic studies were also done regarding the emergence of the chiral anomaly in lattice QCD with different lattice fermion formulations. It was shown that the averaging over the Wilson hopping parameter 'r' in the case of the naive Wilson fermions produces better result for the emergence of the chiral anomaly in the chiral limit than many of the improved Wilson fermions. Interplay between cut-off effects and finite volume effects were also studied.

In the Schwinger model at finite temperature, a closed form result for the chiral anomaly which arises from the long distance behavior of the electric field is derived. The general properties associated with this thermal anomaly as well as its relation with the index of the Dirac operator are discussed. It is further shown that the thermal anomaly, like the zero temperature anomaly which arises from the ultraviolet behavior of the theory, does not receive any contribution from higher loops. Finally, the complete effective action as well as the anomaly functional on both the thermal branches in the closed time path formalism are determined.

e) Strings and Gravity:

A particular decoupling limit of the nonextremal (D1, D3) brane bound state system of type IIB string theory is known to give the gravity dual of space-space noncommutative Yang-Mills theory at finite temperature. A string probe in this background is used to compute the jet quenching parameter in a strongly coupled plasma of hot noncommutative Yang-Mills theory in $(3 + 1)$ dimensions from gauge/gravity duality. In further studies, it is found that a necessary completion of phase structure of D-dimensional charged black p-brane in a cavity requires two additional thermodynamical phases, the so-called bubble of nothing and/or the extremal brane, in canonical ensemble.

This finding resolves the puzzle about the missing phases which are needed for the underlying phase diagram. Next, the expectation values of both the time-like and the light-like Wilson loops in a strongly coupled plasma of $(p + 1)$ -dimensional Yang-Mills theories have been computed by using gravity/gauge theory correspondence. From the time-like Wilson loop the velocity dependent quark-antiquark potential has been obtained, where the dipole is moving through the plasma with an arbitrary velocity $0 < v < 1$, and also the expressions for the screening lengths are obtained.

An uplift of 5-dimensional super-Yang-Mills theory to a 6-dimensional gauge theory with the help of a constant space-like vector has been studied. The norm of this constant vector also determines the 5D Yang-Mills coupling constant. After employing the Lagrange multiplier techniques, the 6D gauge theory is shown to be Lorentzian invariant as well as scale invariant. Importantly the 6D gauge theory admits extended solutions like 1/2-BPS ‘strings’ and the monopole solitons. Further, some applications of ‘vanishing’ horizon double-limits of ‘boosted’ black D3-branes having AdS geometries were studied. It is now well known that the resulting solutions obtained by taking these particular ‘double limits’ are found to describe non-relativistic ‘Lifshitz spacetimes’. In present works these limits were applied to TsT black-holes of type IIB string theory. Separately the non-relativistic AdS_4XCP_3 solutions having dynamical exponent as 3 in type IIA string theory were also obtained, both with and without Romans’ mass term. The compactifications of these to four dimensions are found to describe Proca fields in anti-de Sitter spacetime.

Black hole entropy has been studied in loop quantum gravity using both the standard U(1) and the SU(2) formulations. The possibility of an exact area law without logarithmic corrections is discovered for large eigenvalues of the area operator.

Entropy of Black holes has been computed in the framework of Loop Quantum Gravity and modifications have been suggested from all earlier calculations. The new framework may lead to some testable consequences of Loop Quantum Gravity at lower energies.

5.2 Research Activities

5.2.1 Astroparticle Physics and Cosmology

5.2.1.1 Diurnal and annual variations of directional detection rates of dark matter

Direction-sensitive direct detection of weakly interacting massive particles (WIMPs) as dark matter would provide an unambiguous non-gravitational signature of dark matter. The diurnal variation of dark matter signal due to Earth’s rotation around its own axis can be a significant signature for Galactic WIMPs. Because of a particular orientation of Earth’s axis of rotation with respect to the WIMP wind direction, the apparent direction of WIMP wind as observed at a detector can alter widely in a day. In this work, we calculate the directional detection rates with their daily and yearly modulations in Earth-bound dark matter experiments considering detailed features of the geometry and dynamics of the Earth-Sun system along with the solar motion in a Galactic frame. A separate halo model, namely the dark disk model other than the usual standard halo model for dark matter halo, is also considered and the results for two models are compared. We demonstrate the results for two types of gas detectors, namely DRIFT (target material CS_2) and NEWAGE (target material CF_4), which use Time Projection Chamber techniques for measuring directionality of the recoil nucleus. The WIMP mass and recoil energy dependence of the daily variation of event rates are computed for a specific detector, and the sensitive ranges of mass and recoil energies for the considered detector are probed.

Abhijit Bandyopadhyay†, Debasish Majumdar

5.2.1.2 Shear viscosity and the nucleation of antikaon condensed matter in protoneutron stars

We study shear viscosities of different species in hot and neutrino-trapped dense matter relevant to protoneutron stars. It is found that the shear viscosities of neutrons, protons and electrons in neutrino-trapped matter are of the same orders of magnitude as the corresponding shear viscosities in neutrino-free matter. Above all, the shear viscosity owing to neutrinos is higher by several orders of magnitude than that of other species in neutrino-trapped matter. Next we investigate the effect of shear viscosity, in particular, neutrino shear viscosity, on the thermal nucleation rate of droplets of antikaon condensed matter in protoneutron stars. The first-order phase transition from hadronic matter to antikaon condensed matter is driven by the thermal nucleation process. We compute the equation of state used for the calculation of shear viscosity and thermal nucleation time within the relativistic mean-field model. Neutrino shear viscosity enhances the prefactor in the nucleation rate by several orders of magnitude compared with the T^4 approximation of earlier calculations. Consequently the thermal nucleation time in the T^4 approximation overestimates our result. Furthermore, the thermal nucleation of an antikaon droplet might be possible in neutrino-trapped matter before neutrino diffusion takes place.

Sarmistha Banik, Rana Nandi, Debades Bandyopadhyay

5.2.1.3 Lorentz-preserving fields in Lorentz-violating theories

We identify a fairly general class of field configurations (of spins 0, 1/2 and 1) which preserve Lorentz invariance in effective field theories of Lorentz violation characterized by a constant time-like vector. These fields concomitantly satisfy the equations of motion yielding cubic dispersion relations similar to those found earlier. They appear to have prospective applications in inflationary scenarios.

O Ganguly†, D Gangopadhyay†, P Majumdar

5.2.1.4 Neutrino masses, cosmological bound and four zero yukawa textures

Four zero neutrino Yukawa textures in a specified weak basis, combined with $\mu\tau$ symmetry and type-I seesaw, yield a highly constrained and predictive scheme. Two alternately viable 3×3 light neutrino Majorana mass matrices $m_{\nu A}/m_{nuB}$ result with inverted/normal mass ordering. Neutrino masses, Majorana in character and predicted within definite ranges with laboratory and cosmological inputs, will have their sum probed cosmologically. The rate for $0\nu\beta\beta$ decay, though generally below the reach of planned experiments, could approach it in some parameter region. Departure from $\mu\tau$ symmetry due to RG evolution from a high scale and consequent CP violation, with a Jarlskog invariant whose magnitude could almost reach 6×10^{-3} , are explored.

Biswajit Adhikary, Ambar Ghosal, Probir Roy

5.2.1.5 Inner crusts of neutron stars in strongly quantizing magnetic fields

We study the ground-state properties of inner crusts of neutron stars in the presence of strong magnetic fields of $\sim 10^{17}$ G. Nuclei coexist with a neutron gas and reside in a uniform gas of electrons

in the inner crust. This problem is investigated within the Thomas-Fermi model. We extract the properties of nuclei based on the subtraction procedure of Bonche, Levit, and Vautherin. The phase space modification of electrons due to Landau quantization in the presence of strong magnetic fields leads to the enhancement of electron as well as proton fractions at lower densities of $\sim 0.001 \text{ fm}^{-3}$. We find the equilibrium nucleus at each average baryon density by minimizing the free energy and show that, in the presence of strong magnetic fields, it is lower than that in the field-free case. The size of the spherical cell that encloses a nucleus along with the neutron and electron gases becomes smaller in strong magnetic fields compared to the zero-field case. Nuclei with larger mass and atomic numbers are obtained in the presence of strong magnetic fields compared with cases of zero field.

Rana Nandi, Debades Bandyopadhyay...

5.2.1.6 Gauge invariant coupling of fields to torsion: A string inspired model

In a consistent heterotic string theory, the Kalb-Ramond field, which is the source of space-time torsion, is augmented by Yang-Mills and gravitational Chern-Simons terms. When compactified to 4 dimensions and in the field theory limit, such additional terms give rise to interactions with interesting astrophysical predictions like rotation of plane of polarization for electromagnetic and gravitational waves. On the other hand, if one is also interested in coupling 2- or 3-form (Abelian or non-Abelian) gauge fields to torsion, one needs another class of interaction. In this paper, we shall study this interaction and offer some astrophysical and cosmological predictions. We explicitly calculate the Coleman-Weinberg potential for this theory. We also comment on the possibility of such terms in loop quantum gravity where, if the Barbero-Immirzi parameter is promoted to a field, acts as a source for torsion.

Srijit Bhattacharjee, Ayan Chatterjee

5.2.1.7 Gauge-free electroweak theory: Radiative effects

A recent reformulation of the scalar-vector sector of standard electroweak theory (without a Higgs potential), in terms of manifestly $SU(2)_W$ gauge-invariant variables, is extended so that all field variables in the action are manifestly free of the residual $U(1)_{em}$ gauge transformations as well. Functional evaluation of the one-loop gauge-free effective Higgs potential is shown to precisely cancel effects due to the local functional measure of the Higgs field found earlier. The implications for the classical interpretation of the Higgs scalar as the dilaton field in a background conformal gravity theory are discussed. The Higgs scalar is shown to radiatively acquire a one-loop vacuum expectation value which gives masses to the W and Z bosons but not to photons, without any notion of "spontaneous gauge symmetry breaking" appearing anywhere. Further, the renormalization scale is fixed in this theory by requiring that W and Z boson masses coincide with their experimentally measured values, thereby precluding any "naturalness" problem usually associated with uncontrolled running of such a scale.

Srijit Bhattacharjee, Parthasarathi Majumdar

5.2.1.8 New insights into particle detection with superheated liquids

We report new results obtained from calibrations of superheated liquid droplet detectors used in dark matter searches with different radiation sources (n, α, γ). In particular, detectors were spiked with alpha-emitters located inside and outside the droplets. It is shown that the responses have different temperature thresholds, depending on whether alpha-particles or recoil nuclei create the signals. The measured temperature threshold for recoiling Pb^{210} nuclei from Po^{214} α -decays was found to be in agreement with test beam measurements using mono-energetic neutrons. A comparison of the threshold data with theoretical predictions shows deviations, especially at high temperatures. It is shown that signals produced simultaneously by recoil nuclei and α -particles have more acoustic energy than signals produced by one or the other separately. A model is presented that describes how the observed intensities of particle-induced acoustic signals can be related to the dynamics of bubble growth in superheated liquids. A growth scenario that is limited by the inertia of the surrounding liquid shows a trend that is supported by the data. An improved understanding of the bubble dynamics is an important first step in obtaining better discrimination between particle types interacting in detectors of this kind.

PICASSO Collaboration

5.2.2 Theory

5.2.2.1 Soft gluon emission off a heavy quark revisited

An improved generalized suppression factor for gluon emission off a heavy quark is derived within perturbative QCD, which is valid for the full range of rapidity of the radiated gluon and also has no restriction on the scaled mass of the quark with its energy. In the appropriate limit, it correctly reproduces the usual dead cone factor in the forward rapidity region. On the other hand, this improved suppression factor becomes close to unity in the backward direction. This indicates a small suppression of gluon emission in the backward region, which should have an impact on the phenomenology of heavy quark energy loss in the hot and dense matter produced in ultrarelativistic heavy ion collisions.

Raktim Abir...Munshi G Mustafa, et al

5.2.2.2 Screening masses in gluonic plasma

Both electric and magnetic screening masses in a nonperturbative gluonic background are investigated using operator product expansion. The magnetic screening mass is found to agree with lattice results whereas the electric screening mass is somewhat smaller than the one found on the lattice.

Purnendu Chakraborty†, Munshi G Mustafa, Markus H Thoma†

5.2.2.3 Lepton-number violating effects in neutrino oscillations

We develop a nonadiabatic perturbation theory for oscillations involving an arbitrary number of neutrino and antineutrino species, including the possibility of lepton-number violation which we

treat as a small effect. We interpret the physics of such an approach for the one generation case by introducing the notion of adiabaticity for neutrino and antineutrino oscillations in analogy to flavor oscillations. We find that in a CP-odd matter environment a small lepton-number violation in vacuo can be enhanced. Eventually, we apply the perturbation theory to the two generation case and work out an example for manifestations of lepton-number violation, which can be solved both perturbatively as well as analytically thereby further clarifying the nature of the perturbation expansion.

Sebastian Hollenberg†, Octavian Micu†, Palash B Pal

5.2.2.4 Quantum statistics and noncommutative black holes

We study the behavior of a scalar field coupled to a noncommutative black hole which is described by a kappa-cylinder Hopf algebra. We introduce a new class of realizations of this algebra which has a smooth limit as the deformation parameter vanishes. The twisted flip operator is independent of the choice of realization within this class. We demonstrate that the R-matrix is quasi-triangular up to the first order in the deformation parameter. Our results indicate how a scalar field might behave in the vicinity of a black hole at the Planck scale.

Kumar S Gupta, S Meljanac†, A Samsarov†

5.2.2.5 Temperature dependence of the symmetry energy of finite nuclei

The temperature dependence of the symmetry energy and the symmetry free energy coefficients of atomic nuclei is investigated in a finite temperature Thomas-Fermi framework employing the subtraction procedure. A substantial decrement in the symmetry energy coefficient is obtained for finite systems, contrary to those seen for infinite nuclear matter at normal and somewhat subnormal densities. The effect of the coupling of the surface phonons to the nucleonic motion is also considered; this is found to decrease the symmetry energies somewhat at low temperatures.

JN De, SK Samaddar

5.2.2.6 Calculating the jet quenching parameter in the plasma of noncommutative Yang-Mills theory from gauge/gravity duality

A particular decoupling limit of the nonextremal (D1, D3) brane bound state system of type IIB string theory is known to give the gravity dual of space-space noncommutative Yang-Mills theory at finite temperature. We use a string probe in this background to compute the jet quenching parameter in a strongly coupled plasma of hot noncommutative Yang-Mills theory in $(3 + 1)$ dimensions from gauge/gravity duality. We give expressions for the jet quenching parameter for both small and large noncommutativity. For small noncommutativity, we find that the value of the jet quenching parameter gets reduced from its commutative value. The reduction is enhanced with temperature as T^7 for fixed noncommutativity and fixed 't Hooft coupling. We also give an estimate of the correction due to noncommutativity at the present collider energies like in RHIC or in LHC and find it too small to be detected. We further generalize the results for noncommutative Yang-Mills

theories in diverse dimensions.

Somdeb Chakraborty, Shibaji Roy

5.2.2.7 The enriched phase structure of black branes in canonical ensemble

It is found that a necessary completion of phase structure of D-dimensional charged black p-brane () in a cavity requires two additional thermodynamical phases, the so-called bubble of nothing and/or the extremal brane, in canonical ensemble. This finding resolves the puzzle about the missing phases which are needed for the underlying phase diagram when and gives a new (bubble) phase which can become globally stable when . An analog of HawkingPage transition is also found among other new phase transitions, giving a complete phase structure in this setup.

JX Lu†, Shibaji Roy, Zhiguang Xiao†

5.2.2.8 Topological susceptibility in lattice QCD with unimproved Wilson fermions

We address a long standing problem regarding topology in lattice simulations of QCD with unimproved Wilson fermions. Earlier attempt with unimproved Wilson fermions at $\beta=5.6$ to verify the suppression of topological susceptibility with decreasing quark mass (m_q) was unable to unambiguously confirm the suppression. We carry out systematic calculations for two degenerate flavours at two different lattice spacings ($\beta=5.6$ and 5.8). The effects of quark mass, lattice volume and the lattice spacing on the spanning of different topological sectors are presented. We unambiguously demonstrate the suppression of the topological susceptibility with decreasing quark mass, expected from chiral Ward identity and chiral perturbation theory.

Abhishek Chowdhury, Asit K De, Sangita De Sarkar, A Harindranath, Santanu Mondal, Anwesa Sarkar, Jyotirmoy Maiti†

5.2.2.9 Phase structure of fuzzy black holes

Noncommutative deformations of the BTZ black holes are described by noncommutative cylinders. We study the scalar fields in this background. The spectrum is studied analytically and through numerical simulations we establish the existence of novel 'stripe phases'. These are different from stripes on Moyal spaces and stable due to topological obstruction.

S Digal†, TR Govindarajan†, KS Gupta, X Martin†

5.2.2.10 R-parity violating flavor symmetries, recent neutrino data, and absolute neutrino mass scale

We study the role of a very general type of flavor symmetry in controlling the strength of R-parity violation in supersymmetric models. We assume that only leptons are charged under a global symmetry whose breaking induces lepton number (and, hence, R-parity) violation. The charge assignments of leptons under this symmetry are such that the total number of independent lepton number violating couplings is reduced from 39 to 6. The most severe constraints on these flavor-correlated couplings arise from neutrino masses and mixing as well as from the nonobservation of

$K_L \longrightarrow \mu e$. We find that such a scenario predicts an almost vanishing smallest neutrino mass eigenvalue, allowing the upcoming generation of neutrinoless double beta decay experiments to shed light on the hierarchy.

Gautam Bhattacharyya, Heinrich Paes[†], Daniel Pidt[†]

5.2.2.11 Spin analysis of s-channel diphoton resonances at the LHC

The high mass neutral quantum states envisaged by theories of physics beyond the standard model can, at the hadron colliders, reveal themselves through their decay into a pair of photons. Once such a peak in the diphoton invariant mass distribution is discovered, the determination of its spin through the distinctive photon angular distributions is needed in order to identify the associated nonstandard dynamics. We discuss here the discrimination of the spin-2 Randall-Sundrum graviton excitation against the hypothesis of a spin-0 exchange giving the same number of events under the peak, by means of the angular analysis applied to resonant diphoton events expected to be observed at the LHC. The spin-0 hypothesis is modeled by an effective interaction of a high mass gauge singlet scalar particle interacting with the standard model fields. The basic observable of our analysis is the symmetrically integrated angular asymmetry A_{CE} , calculated for both graviton and scalar s-channel exchanges to next-to-leading order in QCD.

MC Kumar[†], Prakash Mathews, AA Pankov[†], et al

5.2.2.12 Black Hole Entropy and Isolated Horizons Thermodynamics

We present a statistical mechanical calculation of the thermodynamical properties of (nonrotating) isolated horizons. The introduction of the Planck scale allows for the definition of a universal horizon temperature (independent of the mass of the black hole) and a well-defined notion of energy (as measured by suitable local observers) proportional to the horizon area in Planck units. The micro-canonical and canonical ensembles associated with the system are introduced. Black hole entropy and other thermodynamical quantities can be consistently computed in both ensembles and results are in agreement with Hawking's semiclassical analysis for all values of the Immirzi parameter.

Amit Ghosh, Alejandro Perez[†]

5.2.2.13 A new approach to modified gravity models

We investigate f(R)-gravity models performing the ADM-slicing of standard General Relativity. We extract the static, spherically-symmetric vacuum solutions in the general case, which correspond to either Schwarzschild de-Sitter or Schwarzschild anti-de-Sitter ones. Additionally, we study the cosmological evolution of a homogeneous and isotropic universe, which is governed by an algebraic and not a differential equation. We show that the universe admits solutions corresponding to acceleration at late cosmological epochs, without the need of fine-tuning the model-parameters or the initial conditions.

Sayan K Chakrabarti, Emmanuel N Saridakis[†], Anjan A Sen[†]

5.2.2.14 Can flavor physics hint at distinctive signals for R-parity violation at the LHC?

Observation of some low-energy processes in the flavor physics regime may require the existence of supersymmetry with two relatively large R-parity-violating couplings of the λ' -type, together with reasonably light superparticles. At the LHC, such interactions would be expected to give rise to clear signals with convenient leptonic triggers, including some multileptons of the same sign. We undertake a detailed investigation of these signals taking care to correlate with low-energy requirements and taking proper account of the standard model backgrounds as well as the R-parity-conserving sector of the supersymmetric model. We find clear indications that R-parity violation as envisaged in this scenario can be detected at the LHC—even, perhaps, in the early runs.

Biplob Bhattacharjee†, Gautam Bhattacharyya, Sreerup Raychaudhuri†

5.2.2.15 The thermal chiral anomaly in the Schwinger model

In the Schwinger model at finite temperature, we derive a closed form result for the chiral anomaly which arises from the long distance behavior of the electric field Das and Frenkel (2011) [1]. We discuss the general properties associated with this thermal anomaly as well as its relation with the index of the Dirac operator. We further show that the thermal anomaly, like the zero temperature anomaly which arises from the ultraviolet behavior of the theory, does not receive any contribution from higher loops. Finally, we determine the complete effective action as well as the anomaly functional on both the thermal branches in the closed time path formalism.

Ashok Das, J Frenkel†

5.2.2.16 Production of a cascade hyperon in the K^- proton interaction

We investigate the production of a cascade hyperon (Ξ) through the $K + p \rightarrow K^+(K^0) + \Xi(\Xi^0)$ reactions, within an effective Lagrangian model where these reactions proceed via excitations of Λ and Σ resonance intermediate states in s and u channels. The coupling constants at the various vertices are taken from previous studies and SU(3) symmetry considerations. The calculated total cross sections of these reactions, which are in good agreement with the available data, are dominated by the contributions from the $\Lambda(1520)$ intermediate resonant state. However, the K^+ meson angular distributions show selectivity to other resonant states in different angular regions, and interference among these states leads to their strong backward peaking.

R Shyam, O Scholten†, AW Thomas†

5.2.2.17 Wilson loops in (p+1)-dimensional Yang-Mills theories using gravity/gauge theory correspondence

We compute the expectation values of both the time-like and the light-like Wilson loops in a strongly coupled plasma of $(p + 1)$ -dimensional Yang-Mills theories using gravity/gauge theory correspondence. From the time-like Wilson loop we obtain the velocity dependent quark-antiquark potential where the dipole is moving through the plasma with an arbitrary velocity $0 < \nu < 1$ and

also obtain expressions for the screening lengths. When the velocity $\nu \rightarrow 1$, the Wilson loop becomes light-like and we obtain the form of the jet quenching parameter in those strongly coupled plasma.

Somdeb Chakraborty, Shibaji Roy

5.2.2.18 Conserved density fluctuation and temporal correlation function in hard thermal loop perturbation theory

Considering recently developed hard thermal loop perturbation theory that takes into account the effect of the variation of the external field through the fluctuations of a conserved quantity we calculate the temporal component of the Euclidean correlation function in the vector channel. The results are found to be in good agreement with the very recent results obtained within the quenched approximation of QCD and small values of the quark mass ($\sim 0.1T$) on improved lattices of size $128^3 \times N_\tau$ at $(N_\tau = 40, T = 1.2T_C)$, $(N_\tau) = 48, T = 1.45T_C)$, and $(N_\tau = 16, T = 2.98T_C)$, where N_τ is the temporal extent of the lattice. This suggests that the results from lattice QCD and hard thermal loop perturbation theory are in close proximity for a quantity associated with the conserved density fluctuation.

Najmul Haque, Munshi G Mustafa, Thoma Markus H†

5.2.2.19 NNLO QCD corrections to the resonant sneutrino/slepton production at hadron colliders

We present a complete next to next to leading order QCD corrections to the resonant production of sneutrino and charged slepton at the Tevatron and the Large Hadron Collider within the context of R-parity violating supersymmetric model. We have demonstrated the role of NNLO QCD corrections in reducing uncertainties resulting from renormalisation and factorisation scales and thereby making our predictions reliable. We have incorporated soft gluon effects at N³LO level in order to study the stability of our results under perturbation. The results obtained in this article are also applicable to resonance production of any color-neutral scalar coupled to fermions through Yukawa interaction.

Swapan Majhi, Prakash Mathews, V Ravindran†

5.2.2.20 On the observability of collective flavor oscillations in diffuse supernova neutrino background

Collective flavor oscillations are known to bring multiple splits in the supernova (SN) neutrino and antineutrino spectra. These spectral splits depend not only on the mass hierarchy of the neutrinos but also on the initial relative flux composition. Observation of spectral splits in a future galactic supernova signal is expected to throw light on the mass hierarchy pattern of the neutrinos. However, since the Diffuse Supernova Neutrino Background (DSNB) comprises of a superposition of neutrino fluxes from all past supernovae, and since different supernovae are expected to have slightly different initial fluxes, it is pertinent to check if the hierarchy dependent signature of collective oscillations can survive this averaging of the flux spectra. Since the actual distribution

of SN with initial relative flux spectra of the neutrinos and antineutrinos is unknown, we assume a log-normal distribution for them. We study the dependence of the hierarchy sensitivity to the mean and variance of the log-normal distribution function. We find that the hierarchy sensitivity depends crucially on the mean value of the relative initial luminosity. The effect of the width is to reduce the hierarchy sensitivity for all values of the mean initial relative luminosity. We find that in the very small mixing angle (θ_{13}) limit considering only statistical errors even for very moderate values of variance, there is almost no detectable hierarchy sensitivity if the mean relative luminosities of ν_e and $\bar{\nu}_e$ are greater than 1.

Sovan Chakraborty, Sandhya Choubey†, Kamales Kar

5.2.2.21 Discrete R symmetries and F-term supersymmetry breaking

We have shown that in a large number of generic and renormalizable Wess-Zumino models, existence of a Z_n R-symmetry is sufficient to break supersymmetry spontaneously. This implies that the existence of a Z_n R-symmetry is a necessary condition for supersymmetry breaking in generic and renormalizable Wess-Zumino models.

Pritibhajan Byakti

5.2.2.22 Black Hole State Counting in Loop Quantum Gravity

The two ways of counting microscopic states of black holes in the U(1) formulation of loop quantum gravity: one counting all allowed spin network labels j, m and the other only m labels, are discussed in some detail. The constraints on m are clarified and the map between the flux quantum numbers and m discussed. Configurations with $|m| = j$, which are sometimes sought after, are shown to be important only when large areas are involved. The discussion is extended to the SU(2) formulation.

A Ghosh, P Mitra

5.2.2.23 Aharonov-Bohm effect in a class of noncommutative theories

The Aharonov-Bohm effect including spin-noncommutative effects is considered. At linear order in θ , the magnetic field is gauge invariant although spatially strongly anisotropic. Despite this anisotropy, the Schrodinger-Pauli equation is separable through successive unitary transformations and the exact solution is found. The scattering amplitude is calculated and compared with the usual case. In the noncommutative Aharonov-Bohm case the differential cross section is independent of θ .

Ashok Das, H Falomir†, M Nieto†, et al

5.2.2.24 Super-Yang-Mills and M5-branes

We uplift 5-dimensional super-Yang-Mills theory to a 6-dimensional gauge theory with the help of a space-like constant vector η^M , whose norm determines the YM coupling constant. After the

localization of η^M the 6D gauge theory acquires Lorentzian invariance as well as scale invariance. We discuss KK states, instantons and the flux quantization. The theory admits extended solutions like 1/2 BPS 'strings' and monopoles.

Harvendra Singh

5.2.2.25 Quark Number Susceptibility and Thermodynamics in HTL approximation

In HTL perturbation theory we obtain leading order quark number susceptibility as a response to an external disturbance, viz.. chemical potential (μ) that generates density fluctuation, which is related to the correlation function through the thermodynamic sum rule associated with the symmetry of the system. We also obtain various thermodynamic quantities in leading order.

Najmul Haque, Munshi G Mustafa

5.2.2.26 Effect of r averaging on chiral anomaly in lattice QCD with Wilson fermion: finite volume and cutoff effects

We demonstrate the effectiveness of averaging over the Wilson parameter r (which has been proposed earlier) in removing the cutoff effects of naive Wilson fermions in both the anomaly term and the pseudoscalar density term in the flavor singlet axial Ward Takahashi identity at $O(g^2)$ involving slowly varying background gauge fields. We show that it is the physical fermion contribution which is largely influenced by the r averaging. We have studied the possible interplay between finite size and cutoff effects by investigating in detail naive, $O(a)$ improved and OStm Wilson fermion cases for a range of volumes and lattice fermion mass (am). For naive Wilson fermions r averaging is shown to remove the effects of the interplay. We have shown that for the pseudoscalar density term to $O(g^2)$ the lattice result differs from the continuum result by exhibiting considerable a dependence which appears to be a manifestation of cutoff effects with naive Wilson fermion. The pseudoscalar density term to $O(g^2)$ is shown to be almost independent of a when r -averaging is performed.

Asit K De, A Harindranath, Mondal Santanu

5.2.2.27 Eigenvalue problem in two dimensions for an irregular boundary: Neumann condition

We formulate a systematic elegant perturbative scheme for determining the eigenvalues of the Helmholtz equation $(\Delta + k^2)\psi = 0$ in two dimensions when the normal derivative of ψ vanishes on an irregular closed curve. The unique feature of this method, unlike other perturbation schemes, is that it does not require a separate formalism to treat degeneracies. Degenerate states are handled equally elegantly as the non-degenerate ones. A real parameter, extracted from the parameters defining the irregular boundary, serves as a perturbation parameter in this scheme as opposed to earlier schemes where the perturbation parameter is an artificial one. The efficacy of the proposed scheme is gauged by calculating the eigenvalues for elliptical and supercircular boundaries and comparing with the results obtained numerically. We also present a simple and interesting semi-empirical formula, determining the eigenspectrum of the 2D Helmholtz equation

with the Dirichlet or the Neuman condition for a supercircular boundary. A comparison of the eigenspectrum for several low-lying modes obtained by employing the formula with the corresponding numerical estimates shows good agreement for a wide range of the supercircular exponent.

S Panda†, S Chakraborty, SP Khastgir†

5.2.2.28 CPT-violating effects in muon decay

We consider low-energy CPT-violating modifications in charged current weak interactions and analyze possible ramifications in muon and antimuon decays. We calculate the lifetime of muon and antimuon with these modifications, and from the result, put bounds on the CPT-violating parameters. Moreover, we elaborate on the muon and antimuon decay rate differentials in electron energy and spatial angle, which entail interesting phenomenological consequences presenting new ways to constrain CPT violation in charged lepton decays.

Sebastian Hollenberg†, Palash B Pal

5.2.2.29 Galilean type IIA backgrounds and a map

We study nonrelativistic $AdS_4 \times CP^3$ solutions with dynamical exponent 3 in type IIA string theory, both with and without Romans mass. The compactifications to four dimensions are found to describe Proca fields in anti-de Sitter spacetime. This leads us to conclude that the massive and massless IIA theories should be identified in four dimensions and the Romans' mass should be identified with the "flux" along CP^3 . From supergravity point of view, it suggests a four-dimensional symmetry that rotates Romans mass into the flux along CP^3 . We also identify M-theory Galilean (ABJM) background which gives rise to the nonrelativistic type IIA solution.

Harvendra Singh

5.2.2.30 A possible connection between neutrino mass generation and the lightness of a NMSSM pseudoscalar

One of the interesting properties of the NMSSM is that it can accommodate a light pseudoscalar of order 10 GeV. However, such scenarios are challenged by several experimental constraints, especially those related to the fermionic decays of the pseudoscalar. In this Letter, we extend the NMSSM field content by two gauge singlets, with lepton numbers +1 and -1. This serves the twin purpose of generating neutrino masses via the inverse seesaw mechanism and keeping the option of a very light pseudoscalar experimentally viable by opening dominant invisible decay channels of the pseudoscalar which help it evade the existing bounds.

Asmaa Abada†, Gautam Bhattacharyya, et al

5.2.2.31 Hidden possibilities in controlling optical soliton in fiber guided doped resonant medium

Fiber guided optical signal propagating in a Erbium doped nonlinear resonant medium is known to produce cleaner solitonic pulse, described by the self induced transparency (SIT) coupled to nonlinear Schrodinger equation. We discover two new possibilities hidden in its integrable structure, for amplification and control of the optical pulse. Using the variable soliton width permitted by the integrability of this model, the broadening pulse can be regulated by adjusting the initial population inversion of the dopant atoms. The effect can be enhanced by another innovative application of its constrained integrable hierarchy, proposing a system of multiple SIT media. These theoretical predictions are workable analytically in details, correcting a well known result.

Anjan Kundu

5.2.2.32 Integrable twofold hierarchy of perturbed equations and application to optical soliton dynamics

We construct well-known integrable equations with their Lax pairs from the corresponding linear equations using our nonlinearization scheme. Using negative powers in the spectral flow to deform the time Lax operator, we find a class of perturbations that unlike the usual perturbations, which spoil the system integrability, exhibit a twofold integrable hierarchy, including those for the KdV, modified KdV, sine-Gordon, nonlinear Schrodinger (NLS), and derivative NLS equations. We discover hidden possibilities of using the perturbed hierarchy of the NLS equations to amplify and control optical solitons propagating through a fiber in a doped nonlinear resonant medium.

A Kundu

5.2.2.33 Radiative and collisional jet energy loss in a quark-gluon plasma

We calculate radiative and collisional energy loss of hard partons traversing the quark-gluon plasma created at RHIC and compare the respective size of these contributions. We employ the AMY formalism for radiative energy loss and include additionally energy loss by elastic collisions. Our treatment of both processes is complete at leading order in the coupling, and accounts for the probabilistic nature of jet energy loss. We find that a solution of the Fokker-Planck equation for the probability density distributions of partons is necessary for a complete calculation of the nuclear modification factor $R(AA)$ for pion production in heavy ion collisions. It is found that the magnitude of $R(AA)$ is sensitive to the inclusion of both collisional and radiative energy loss, while the average energy is less affected by the addition of collisional contributions. We present a calculation of $R(AA)$ for $\pi(0)$ at RHIC, combining our energy loss formalism with a relativistic (3+1)-dimensional hydrodynamic description of the thermalized medium.

GY Qin†, J Ruppert†, J, MG Mustafa

5.2.2.34 Energy systematics of heavy nuclei-mean field models in comparison

We compare the systematics of binding energies computed within the standard and extended versions of the relativistic mean-field (RMF) model and the Skyrme-Hartree-Fock (SHF) model. The

general trends for the binding energies for super-heavy nuclei are significantly different for these models. The SHF models tend to underbind the super-heavy nuclei, while RMF models show just the opposite trend. The extended RMF model seems to provide remarkable improvements over the results obtained for the standard RMF model

PG Reinhard†, BK Agrawal

5.2.2.35 Graviton plus vector boson production to NLO in QCD at the LHC

We present the next-to-leading order QCD corrections to the associated production of the vector gauge boson (Z/W^\pm) and the graviton in the large extra dimension model at the LHC. We estimate the impact of the QCD corrections on the total cross sections as well as the differential distributions of the gauge bosons and find that they are significant. We also study the dependence of the cross sections on the arbitrary factorization scale and show the reduction in the scale uncertainties at NLO level. Further, we discuss the ultraviolet sensitivity of the theoretical predictions.

MC Kumar†, Prakash Mathews, V Ravindran†, Satyajit Seth

5.2.2.36 Phenomenological implications of S-duality symmetry

It is proposed that S-duality is a fundamental symmetry of nature which is spontaneously broken. Axion and dilaton are identified with the doublet of the S-duality symmetry group $SL(2, \mathbb{R})$. The symmetry is broken at a high scale corresponding to the experimentally estimated axion decay constant f_χ . The symmetry breaking mechanism is discussed in analogy with PCAC in pion physics. S-duality invariant interactions of fermions with axion and dilaton doublet are introduced. The symmetry breaking mechanism contributes negligibly small corrections to fermion masses in the QCD sector. Inspired by universality in string theory, the S-duality invariant interaction of the axion-dilaton doublet to QCD fermions is proposed to generalize to all fermions. Phenomenological consequences of this broken symmetry are explored.

Ashok Das, Jnanadeva Maharana†

5.2.2.37 Warm α -nucleon matter

The properties of warm dilute α -nucleon matter are studied in a variational approach in the Thomas-Fermi approximation starting from an effective two-body nucleon-nucleon interaction. The equation of state, symmetry energy, incompressibility of the said matter, and α fraction are in consonance with those evaluated from the virial approach, which sets the benchmark for such calculations at low densities.

SK Samaddar, JN De

5.2.2.38 Phase structure of black branes in grand canonical ensemble

This is a companion paper of our previous work [1] where we studied the thermodynamics and phase structure of asymptotically flat black p-branes in a cavity in arbitrary dimensions D in a

canonical ensemble. In this work we study the thermodynamics and phase structure of the same in a grand canonical ensemble. Since the boundary data in two cases are different (for the grand canonical ensemble boundary potential is fixed instead of the charge as in canonical ensemble) the stability analysis and the phase structure in the two cases are quite different. In particular, we find that there exists an analog of one-variable analysis as in canonical ensemble, which gives the same stability condition as the rather complicated known (but generalized from black holes to the present case) two-variable analysis. When certain condition for the fixed potential is satisfied, the phase structure of charged black p -branes is in some sense similar to that of the zero charge black p -branes in canonical ensemble up to a certain temperature. The new feature in the present case is that above this temperature, unlike the zero-charge case, the stable brane phase no longer exists and 'hot flat space' is the stable phase here. In the grand canonical ensemble there is an analog of Hawking-Page transition, even for the charged black p -brane, as opposed to the canonical ensemble. Our study applies to non-dilatonic as well as dilatonic black p -branes in D space-time dimensions.

JX Lu[†], Shibaji Roy, Zhiguang Xiao[†]

5.2.2.39 Exact solution of D_N -type quantum Calogero model through a mapping to free harmonic oscillators

We solve the eigenvalue problem of the D_N -type of Calogero model by mapping it to a set of decoupled quantum harmonic oscillators through a similarity transformation. In particular, we construct the eigenfunctions of this Calogero model from those of bosonic harmonic oscillators having either all even parity or all odd parity. It turns out that the eigenfunctions of this model are orthogonal with respect to a nontrivial inner product, which can be derived from the quasi-Hermiticity property of the corresponding conserved quantities.

Pratyay Banerjee, B Basu-Mallick

5.2.2.40 Dirac, Majorana, and Weyl fermions

We discuss the Dirac, Majorana, and Weyl fermion fields. The definitions and motivations for introducing each kind of field is discussed, along with the connections between them. It is pointed out that these definitions have to do with the proper Lorentz group and not with any discrete symmetry. The action of discrete symmetries, such as charge conjugation and CP on various types of fermion fields, which are particularly important for Majorana fermions, is also clarified.

Palash B Pal

5.2.2.41 Vector boson production in association with KK modes of the ADD model to NLO in QCD at the LHC

Next-to-leading order (NLO) QCD corrections to the associated production of the vector boson (Z/W^\pm) with the Kaluza-Klein (KK) modes of the graviton in large extra-dimensional model at the Large Hadron Collider (LHC) are presented. We have obtained various kinematic distributions using a Monte Carlo code which is based on the two-cutoff phase space slicing method that handles

soft and collinear singularities appearing at the NLO level. We estimate the impact of the QCD corrections on various observables and find that they are significant. We also show the reduction in factorization scale uncertainty when QCD corrections are included.

MC Kumar†, Prakash Mathews...Satyajit Seth

5.2.2.42 Generalization of the Cooper pairing mechanism for spin-triplet in superconductors

A generalization of the Cooper pairing mechanism is proposed which allows for a triplet state of lower energy. This is achieved by incorporating spin into the canonical commutation relations and by modifying the δ potential contact interaction. The gap equation contains as solutions both singlet and triplet states. It is shown that the triplet state is lower in energy than the singlet state which may explain the spin-triplet superconductivity observed.

Ashok Das, J Gamboa†, F Mendez†, F Torres†

5.2.2.43 Holographic flows to IR Lifshitz spacetimes

Recently we studied 'vanishing' horizon limits of 'boosted' black D3-brane geometry [1]. The type IIB solutions obtained by taking these special double limits were found to describe nonrelativistic Lifshitz spacetimes at zero temperature. In the present work we study these limits for TsT black-hole solutions which include B-field. The new Galilean solutions describe a holographic RG flow from Schrödinger ($a = 2$) spacetime in UV to a nonrelativistic universe in the IR.

Harvendra Singh

5.2.2.44 Area law for black hole entropy in the SU(2) quantum geometry approach

Black hole thermodynamics suggests that a black hole should have an entropy given by a quarter of the area of its horizon. Earlier calculations in U(1) loop quantum gravity have led to a dominant term proportional to the area, but there was a correction involving the logarithm of the area. We find however that SU(2) loop quantum gravity can provide an entropy that is strictly proportional to the area as expected from black hole thermodynamics.

P Mitra

5.3 Developmental Work

5.3.1 Astroparticle Physics and Cosmology



R & D work on neutron and alpha discrimination for Superheated Droplet Detector (SDD) has been done with self made detector at SINP using low background supporting matrix. R & D are also done for the new scheme of increasing the active mass of the detector for PICASSO experiment (shown above). The detector, nickname, Meghla akash (det # 155) for PICASSO dark matter search experiment was fabricated with improved techniques at the detector fabrication centre, Univ. de Montreal, Canada during May-June, 2011 and installed at SNOLab.

5.4 Publications

5.4.1 Publications in Books/Monographs & Volumes Edited

K Kar, S Chakraborty, S Choubey, Collective oscillations and diffuse supernova neutrino background, in Exploring Fundamental Issues in Nuclear Physics, Ed. Debades Bandyopadhyay (ed), (World Scientific, 2012, p108)

Debades Bandyopadhyay, Ed., Exploring Fundamental Issues in Nuclear Physics, (World Scientific, Singapore, 2012)

5.4.2 Papers in Journals

5.4.2.1 Astroparticle Physics & Cosmology

Abhijit Bandyopadhyay†, Debasish Majumdar, Diurnal and annual variations of directional detection rates of dark matter, *Astrophysical Journal* **746** (2012) Art No: 107

Biswajit Adhikary, Ambar Ghosal, Probir Roy, Neutrino masses, cosmological bound and four zero yukawa textures, *Modern Physics Letters* **A26** (2011) 2427

PICASSO Collaboration, New insights into particle detection with superheated liquids, *New Journal of Physics* **13** (2011) Art No: 043006

Rana Nandi, Debades Bandyopadhyay, Neutron star crust in strong magnetic fields, *Journal of Physics Conference Series* **312** (2011) 042016

Rana Nandi, Debades Bandyopadhyay, Igor N Mishustin†, Walter Greiner†, Inner crusts of neutron stars in strongly quantizing magnetic fields, *Astrophysical Journal* **736** (2011) Art No: 156

Sarmistha Banik, Rana Nandi, Nucleation of antikaon condensed matter in protoneutron stars, *AIP Conf Proc* **1441** (2012) 396

Sarmistha Banik, Rana Nandi, Debades Bandyopadhyay, Shear viscosity and the nucleation of antikaon condensed matter in protoneutron stars, *Physical Review* **C84** (2011) Art No: 065804

Srijit Bhattacharjee, Ayan Chatterjee, Gauge invariant coupling of fields to torsion: A string inspired model, *Physical Review* **D83** (2011) Art No: 106007

Srijit Bhattacharjee, Parthasarathi Majumdar, Gauge-free electroweak theory: Radiative effects, *Physical Review* **D83** (2011) Art No: 085019

5.4.2.2 Theory

Abhishek Chowdhury, Asit K De, Sangita De Sarkar, A Harindranath, Santanu Mondal, Anwesha Sarkar, Jyotirmoy Maiti†, Topological susceptibility in lattice QCD with unimproved Wilson fermions, *Physics Letters* **B707** (2012) 228

A Ghosh, P Mitra, Black Hole State Counting in Loop Quantum Gravity, *Modern Physics Letters* **A26** (2011) 1817

A Kundu, Integrable twofold hierarchy of perturbed equations and application to optical soliton dynamics, *Theoretical and Mathematical Physics* **167** (2011) 800

Amit Ghosh, Alejandro Perez†, Black Hole Entropy and Isolated Horizons Thermodynamics, *Physical Review Letters* **107** (2011) Art No: 241301

Anjan Kundu, Hidden possibilities in controlling optical soliton in fiber guided doped resonant medium, *AIP Advances* **1** (2011) Art No: 022137

Asmaa Abada†, Gautam Bhattacharyya, Debottam Das†, Cric Weiland†, A possible connection between neutrino mass generation and the lightness of a NMSSM pseudoscalar, *Physics Letters* **B700** (2011) 351

Ashok Das, H Falomir†, M Nieto†, et al, Aharonov-Bohm effect in a class of noncommutative theories, *Physical Review* **D84** (2011) Art No: 045002

Ashok Das, J Frenkel†, The thermal chiral anomaly in the Schwinger model, *Physics Letters* **B704** (2011) 85

Ashok Das, Jnanadeva Maharana†, Phenomenological implications of S-duality symmetry, *Physics Letters* **B699** (2011) 264

Ashok Das, J Gamboa†, F Medez†, F Torres†, Generalization of the Cooper pairing mechanism for spin-triplet in superconductors, *Physics Letters* **A375** (2011) 1756

Asit K De, A Harindranath, Santanu Mondal, Effect of r averaging on chiral anomaly in lattice QCD with Wilson fermion: finite volume and cutoff effects, *Journal of High Energy Physics*, **Issue: 7** (2011) Art No: 117

Biplob Bhattacharjee†, Gautam Bhattacharyya, Sreerup Raychaudhuri†, Can flavor physics hint at distinctive signals for R-parity violation at the LHC? *Physical Review* **D84** (2011) Art No: 075006

GY Qin†, J Ruppert†, MG Mustafa, Radiative and collisional jet energy loss in a quark-gluon plasma, *Indian Journal of Physics* **85** (2011) 873

Gautam Bhattacharyya, Heinrich Paes†, Daniel Pidt†, R-parity violating flavor symmetries, recent neutrino data, and absolute neutrino mass scale, *Physical Review* **D84** (2011) Art No: 113009

Harvendra Singh, Super-Yang-Mills and M5-branes, *Journal of High Energy Physics*, **Issue: 8** (2011) Art No: 136

Harvendra Singh, Galilean type iia backgrounds and a map, *Modern Physics Letters* **A26** (2011) 1443

Harvendra Singh, Holographic flows to IR Lifshitz spacetimes, *Journal of High Energy Physics* **Issue: 4** (2011) Art No: 118

JX Lu†, Shibaji Roy, Zhiguang Xiao†, Phase structure of black branes in grand canonical ensemble, *Journal of High Energy Physics* **Issue: 5** (2011) Art No: 091

JN De, SK Samaddar, Temperature dependence of the symmetry energy of finite nuclei, *Physical Review* **C85** (2012) Art No: 024310

JX Lu†, Shibaji Roy, Zhiguang Xiao†, The enriched phase structure of black branes in canonical ensemble, *Nuclear Physics* **B854** (2012) 913

Kumar S Gupta, S Meljanac†, A Samsarov†, Quantum statistics and noncommutative black holes, *Physical Review* **D85** (2012) Art No: 045029

MC Kumar†, Prakash Mathews, AA Pankov†, N Paver†, V Ravindran†, AV Tsytrinov†, Spin analysis of s-channel diphoton resonances at the LHC, *Physical Review* **D84** (2011) Art No: 115008

MC Kumar†, Prakash Mathews, V Ravindran†, Satyajit Seth, Graviton plus vector boson production to NLO in QCD at the LHC, *Nuclear Physics* **B847** (2011) 54

MC Kumar†, Prakash Mathews, V Ravindran†, Satyajit Seth, Vector boson production in association with KK modes of the ADD model to NLO in QCD at the LHC, *Journal of Physics* **G38** (2011) Art No: 055001

Najmul Haque, Munshi G Mustafa, Thoma Markus H†, Conserved density fluctuation and temporal correlation function in hard thermal loop perturbation theory, *Physical Review* **D84** (2011) Art No: 054009

Najmul Haque Munshi G Mustafa, Quark Number Susceptibility and Thermodynamics in HTL approximation, *Nuclear Physics* **A862** (2011) 271

O Ganguly†, D Gangopadhyay†, P Majumdar, Lorentz-preserving fields in Lorentz-violating theories, *EPL* **96** (2011) Art No: 61001

PG Reinhardt†, BK Agrawal, Energy systematics of heavy nuclei-mean field models in comparison, *International Journal of Modern Physics* **E20** (2011) 1379

Palash B Pal, Dirac, Majorana, and Weyl fermions, *American Journal of Physics* **79** (2011) 485

Pratyay Banerjee, B Basu-Mallick, Exact solution of D_N -type quantum Calogero model through a mapping to free harmonic oscillators, *Journal of Mathematical Physics* **52** (2011) Art No: 052106

Pritibhajan Byakti, Discrete R symmetries and F-term supersymmetry breaking, *Physical Review* **D84** (2011) Art No: 035019

Purnendu Chakraborty†, Munshi G Mustafa, Markus H Thoma†, Screening masses in gluonic plasma, *Physical Review* **D85** (2012) Art No: 056002

R Shyam, O Scholten†, AW Thomas†, Production of a cascade hyperon in the K^- proton interaction, *Physical Review* **C84** (2011) Art No: 042201

Raktim Abir, Carsten Greiner†, Mauricio Martinez†, Munshi G Mustafa, Jan Uphoff†, Soft gluon emission off a heavy quark revisited, *Physical Review* **D85** (2012) Art No: 054012

S Digal†, TR Govindarajan†, KS Gupta, X Martin†, Phase structure of fuzzy black holes, *Journal of High Energy Physics*, **Issue: 1** (2012) Art No: 027

SK Samaddar, JN De, Warm α -nucleon matter, *Physical Review* **C83** Art No: 055802

S Panda†, S Chakraborty, SP Khastgir†, Eigenvalue problem in two dimensions for an irregular boundary: Neumann condition, *European Physical Journal Plus* **126** (2011) Art No: 62

Sayan K Chakrabarti, Emmanuel N Saridakis†, Anjan A Sen†, A new approach to modified gravity models, *General Relativity and Gravitation* **43** (2011) 3065

Sebastian Hollenberg†, Octavian Micu†, Palash B Pal, Lepton-number violating effects in neutrino oscillations, *Physical Review* **D85** (2012) Art No: 053004

Sebastian Hollenberg†, Palash B Pal, CPT-violating effects in muon decay, Physics Letters **B701** (2011) 89

Somdeb Chakraborty, Shibaji Roy, Calculating the jet quenching parameter in the plasma of non-commutative Yang-Mills theory from gauge/gravity duality, Physical Review **D85** Art No: 046006

Somdeb Chakraborty; Shibaji Roy, Wilson loops in (p+1)-dimensional Yang-Mills theories using gravity/gauge theory correspondence, Nuclear Physics **B850** (2011) 463

Sovan Chakraborty, Sandhya Choubey†, Kamales Kar, On the observability of collective flavor oscillations in diffuse supernova neutrino background, Physics Letters **B702** (2011) 209

Swapan Majhi, Prakash Mathews, V Ravindran†, NNLO QCD corrections to the resonant sneutrino/slepton production at hadron colliders, Nuclear Physics **B850** (2011) 287

5.5 Seminars/Lectures given in Conference/Symposium/Schools

Asit Kumar De

Topological Susceptibility with unimproved Wilson fermions, XXIX International Symposium on Fields Theories on Lattice (LATTICE 2011), Lake Tahoe, California, USA, Jul 11, 2011

Bireswar Basu-Mallick

Periodic boundary condition for a quantum integrable system with non-cubical configuration space, Condensed matter and Statistical Physics Division, Abdus Salam ICTP, Italy, Jun 17, 2011

Gautam Bhattacharyya

Electroweak Symmetry Breaking Beyond the Standard Model, Plenary talk in XXV International Lepton Photon Symposium 2011, TIFR, Mumbai, Aug 2011

BSM LHC: Results with 7 TeV collision data, ICTP, Trieste, Sep 2011

Debades Bandyopadhyay

Supernova Explosions, Presidency University, Kolkata, Apr 29, 2011

Inner Crust of Neutron Stars in Strong Magnetic Fields, Frankfurt Institute for Advanced Studies, Germany, 22 July, 2011

Nuclei in Neutron Star Crust, Invited talk in the conference "Exciting Physics", Makutsi, South Africa, Nov 14-19, 2011

Supernova Explosions: Searching for Exotica, Colloquium at Frankfurt Institute for Advanced Studies, Germany, Dec 8, 2011

Harvendra Singh

z = 3 Lifshitz space-times in string theory, International conference on New Trends in Field Theories, Dept of Phys, BHU, Varanasi, Feb 7-12, 2011

On 5d Super-Yang-Mills and M5-branes, National Strings Meeting' (NSM-2011), Dept of Physics, Delhi Univ, New Delhi, India, Dec 7-12, 2011

5D Super-Yang-Mills and M5-branes, TIFR, Mumbai, India, Nov 03, 2011

Kamales Kar

Collective neutrino flavor oscillations in supernovae, International Symposium on 'Amazing particles and light- Horizons in accelerator and enabled sciences', IISc, Bengaluru, Dec 15-16, 2011

Neutrinos from supernovae and their diffuse background, Advances in Astroparticle Physics and Cosmology, Darjeeling, Mar 7-12, 2012

Death of Large Stars, University of Calicut, Jun 28, 2011

Nuclei, Chaos and Statistical Spectroscopy, University of Calicut, Jun 29, 2011

r-Process Nucleosynthesis and Collective Neutrino Oscillations, The Institute of Mathematical Sciences, Sep 8, 2011

Mala Das

Dark matter search with PICASSO, Workshop on Advances in Astroparticle Physics & Cosmology (AAPCOS), Darjeeling, Mar 8-11, 2012

Activities related to superheated droplet detector at SINP, PICASSO collaboration meeting, University of Montreal, Montreal, Canada, Jun 1-3, 2011

Superheated liquid and radiation detection, Laurentian University, Sudbury, Canada, May 25, 2011

Munshi Golam Mustafa

Analysis of Vector Correlation Function and its Spectral Representation: Properties of the Strongly interacting Deconfined Matter, STAR-CBM Collaboration Meeting, VECC, Kolkata, India, Apr 18-20, 2011

Vector Correlation Function and its Spectral Representation: Some quantities in QGP and LQCD, workshop on Hadrons, Quarks and LHC, IIT Mumbai, Mumbai, Aug 28-29, 2011

Equation of States of Hot and Dense Matter, 20th CBM Collaboration (International) Meeting, VECC, Kolkata, India, Sept 24-28, 2012

Palash Baran Pal

Non-standard GUTs "Grand unification and baryogenesis", organized by Physics Department, University of Calcutta, Nov 23-25, 2011

Different formulations of Quantum Mechanics, Saint Xavier's College, Kolkata, Feb 15, 2012

The birth of quantum mechanics Conference organized by Narasimha Dutt College, Howrah, Nov 24, 2011

Science, God and fads, Debiprasad Chattopadhyay Memorial Lecture organized by Anushtup, the Kolkata Book Fair, Feb 2, 2012

Small particles at high energies, the Heritage Institute of Technology, Kolkata, Mar 21, 2012

Kaler torjoni (The arrow of time) A series of five small talks (5 minutes each), Broadcast from the Akashbani Calcutta Radio Station, Mar 13-18, 2012

Kyalendarer rohosyo (The mystery of calendars), St Paul's College, Kolkata, Feb 29, 2012

Poetry and science Talk given at the Refresher Course organized by Department of Bengali, Jadavpur University, Dec 8, 2011

Prashanta Chandra Mahalanobish and Bengali orthography Conference on "Tagore, Bose and Mahalanobis : confluence of minds", organized by the J C Bose Trust, Kolkata, Nov 21, 2011

The elementary and the energetic Summer camp for high school students, Bengal Engineering and Science University, Howrah, May 24, 2011

Pijushpani Bhattacharjee

Status of the DINO (Dark matter @ INO) proposal, INO Collaboration Meeting, BARC, Mumbai, Feb 14, 2012

Sizing-up the WIMPs of Milky Way: Constraints on Dark Matter from Direct- and Indirect Detection Experiments, Indian Conference on Cosmology & Galaxy Formation (ICCGF-2011), IISER, Mohali, India, Nov 5-7 2011

A self-consistent model of Milky Ways Dark Matter Halo: Implications for direct and indirect detection of WIMP Dark Matter, PICASSO Dark Matter Search Collaboration Meeting, University of Montreal, Montreal, Jun 13, 2011

A self-consistent model of Milky Ways Dark Matter Halo: Implications for direct and indirect detection of WIMP Dark Matter, Workshop on Dark Matter: Interface of Cosmology and Particle Physics, PRL, Ahmedabad, Apr 6-8, 2011

Chasing the WIMPs of Milky Way: Direct and Indirect Detection of Dark Matter, Colloquium at Physical Research Laboratory (PRL), Ahmedabad, Feb 15, 2012

Pratik Majumdar

Perspectives in Very High Energy Gamma-ray Astronomy Using Imaging Techniques, AAPCOS (Advances in Astroparticle Physics and Cosmology) 2012, Darjeeling, Mar 7-12, 2012

Recent results and progress in Very High Energy Gamma-ray Astronomy, 2nd Theme meeting on VHE Gamma Ray Astronomy, Mt Abu, Mar 2012

Rana Nandi

Shear Mode Oscillations of Magnetars, Conference on Advances in Astroparticle Physics and Cosmology 2012, Darjeeling, Mar 7-12, 2012

Sarmistha Banik

Nucleation of Antikaon Condensed Matter in Protoneutron Stars, 19th International Conference on Particles and Nuclei (PANIC11), MIT, USA, Jul 24-29, 2011

Role of Exotic Matter on the Core Collapse Supernovae, Conference on Advances in Astroparticle Physics and Cosmology 2012, Darjeeling, Mar 7-12, 2012

5.6 Honours and Distinctions

P Mitra

Elected Fellow of INSA with effect from 1st January 2012

5.7 Teaching elsewhere

Prakash Mathews

Introduction to perturbative QCD, SERC School on Experimental High Energy Physics, VECC, Kolkata, Jun 20-Jul 10, 2011

Pijushpani Bhattacharjee

Introduction to Astroparticle Physics (5 lectures), the Vietnam School of Physics, Hue, Vietnam, Jul 18-24, 2011

5.8 Miscellany

Gautam Bhattacharyya

(i) Adjunct faculty of TIFR, Mumbai (2009-12)

(ii) Program Committee Member of International Centre for Theoretical Sciences (ICTS) TIFR, Mumbai (Aug 1, 2010 to July 31, 2012)

Prakash Mathews

Organiser of the Advanced School on Radiative Corrections for the LHC, SINP, Kolkata, India,
Apr 4-11, 2011

Chapter 6

Teaching

6.1 The Post-M Sc Associateship Course

6.1.1 Physics

6.1.1.1 58th Session (2010-11)

THIRD TERM: Review [Student, Review Title (Supervisor)]

1. Abhik Mukherjee, Fracture, friction and flow: Tsunami dynamics (Abhik Basu & Bikas Chakrabarti)
2. Amit Dey, Understanding quantum entanglement and decoherence (Y Sudhakar)
3. Amit Dutta Banik, Dark matter and their models (Debashis Majumdar)
4. Atanu Modak, Quantum fields on curved spacetimes (Amit Ghosh)
5. Atanu Rajak, Fracture, friction and flow: Earthquake dynamics (Abhik Basu & Bikas Chakrabarti)
6. Bijoy Kumar Daga, Community structure in complex networks (Pradeep Kumar Mohanty)
7. Biswarup Paul, Muon spectrometer of ALICE and Pb-Pb data analysis (Sukalyan Chattapadhyay)
8. Chandrachur Chakraborty, Gravitational collapse and horizons (Parthasarathi Majumdar)
9. Choudhury Aminul Islam, Photon rates from relativistic plasmas (Munshi Golam Mustafa)
10. Debarati Roy, Validation of GEANT4 Hadronic Physics model (Chanda Samanta & Sunanda Banerjee)
11. Debashis Saha, Study of Simplified Parametrization of EM Showers in the Fast Simulation Software of CMS (Sunanda Banerjee)
12. Debashree Chowdhury, Study of surface morphology by negative ion bombardment (Debebrata Ghosh)
13. Dipankar Das, Beyond the standard model phenomenology (Gautam Bhattacharya)
14. Hitesh Vijay Rahangdale, Atomic and molecular excitations by electrons (Satyajit Saha)
15. Jayati Ray, Gamma-ray spectroscopy (Ushasi Dutta Pramanik)
16. Kalyanmoy Chatterjee, Study of simplified parametrization of hadronic shower in fast simulation software of CMS (Sunanda Banerjee)

17. Kamalkshya Prasad Modak, Asymmetric dark matter (Debashis Majumdar)
18. Kaustabh Dan, Two dimensional liquid crystals and phase transitions (Alokmay Datta)
19. Kousik Bagani, Exchange bias in thin films (Sangam Banerjee)
20. Madhumita Choudhuri, Two dimensional liquids (Alokmay Datta)
21. Mala Mukhopadhyay, STM and STS studies (Satyajit Hazra)
22. Mayukh Kumar Ray, Tailoring Heusler Alloys (Sangam Banerjee)
23. Moumita Nandi, Griffiths phase in Co doped Manganite (Prabhat Mandal)
24. Md. Moin Shaikh, Reaction mechanism of weakly bound nuclei (Subinit Roy)
25. Niyaz Ahmed Rather, Anti-magnetic rotation of heavy nuclei (Sukalyan Chattapadhyaya)
26. Prithwish Dutta, Topological insulator (Prabhat Mandal)
27. Rajani Raman, Neuromorphic VLSI (Sandip Sarkar)
28. Rajeswari Roy Chowdhury, Single electron effect in Quantum structure (Indranil Das)
29. Sanchayita Mondal, Properties of Heusler Alloy (Chandan Majumdar)
30. Souvik Priyam Adhya, Fermionic Damping rate in ultradegenerate plasma (Abhee Dutta Maumdar)
31. Subhendu Rajbanshi, Deep inelastic reactions using Y-ray spectroscopy (Asimananda Goswami)
32. Sudip Garai, Cosmic ray, gamma ray and neutrino astrophysics (Pijushpani Bhattacharjee)
33. Susmita Dhara, Low field magneto-resistance (Indranil Das)
34. Sutapa Ghosh, Plasma discharges in SINP tokamak (AN Sekar Iyengar)
35. Swagata Mukherjee, CP violation (Palash Baran Pal)
36. Tanmay Ghosh, Probing low Dimensional objects using analytical Transmission Electron Microscopy (Biswarup Satpati)
37. Tapas Pramanik, Magneto-caloric effect (Indranil Das)
38. Uttam Kumar Basak, Wetting and de-wetting of complex liquids (Alokmay Dutta)

The following 37 Physics students successfully completed the course:

1. Abhik Mukherjee 2. Amit Dey 3. Amit Dutta Banik 4. Atanu Modak 5. Atanu Rajak 6. Bijoy Kumar Daga 7. Biswarup Paul 8. Chandrachur Chakraborty 9. Ch. Aminul Islam 10. Debarati Roy 11. Debashis Saha 12. Debashree Chowdhury 13. Dipankar Das 14. Hitesh Vijay Rahangdale 15. Jayati Ray 16. Kalyanmoy Chatterjee 17. Kamakshya Prasad Modak 18. Kaustabh Dan 19. Kousik Bagani 20. Madhumita Choudhuri 21. Mala Mukhopadhyay 22. Mayukh Kumar Ray 23. Moumita Nandi 24. Md. Moin Shaikh 25. Niyaz Ahmad Rather 26. Prithwish Dutta 27. Rajani Raman 28. Rajeswari Roy Chowdhury 29. Sanchayita Mondal 30. Souvik Priyam Adhya 31. Subhendu Rajbanshi 32. Sudip Garai 33. Susmita Dhara 34. Swagata Mukherjee 35. Tanmay Ghosh 36. Tapas Pramanik 37. Uttam Kumar Basak

6.1.1.2 59th Session (2011-12)

The following 23 Physics students were admitted in the session 2011-12:

1. Abhijit Ghosh 2. Alpha Michael Wharton 3. Apurba Kheto 4. Arijit Chatterjee 5. Arka Bikash Dey 6. Arnab Roy 7. Arup Singha Roy 8. Asish Kumar Kundu 9. Debaleen Biswas 10. Gourab Majumder 11. Goutam Das 12. Minakshi Roy 13. Prasanta Char 14. Rajendra Prasad Giri 15. Sabyasachi Nag 16. Sagnik Chakraborty 17. Santanu Pakhira 18. Santu Manna 19. Sk Abdul Kader Md Faruque 20. Sourav Dey 21. Sourav Kundu 22. Sourav Pramanik 23. Suraj Kumar Karmakar

First Term**Courses (Teachers)**

Quantum Mechanics (Sibaji Roy, Theory)

Statistical Mechanics (Bikas Chakraborty)

Quantum Fields (Asit De)

Experimental Methods (Palash Baran Pal)

Mathematical & Computational Methods (PK Mohanty)

Basic Experiments & Techniques (Bijay Bal, Sandip Sarkar)

Mr Goutam Das received the Professor AP Patro Memorial Award (2011-12 Session)

6.1.1.3 Second Term:**Advanced Courses (Teachers)**

Soft Condensed Matter Systems: Alokmay Datta

Optical & Infrared Spectroscopy: Alokmay Datta

Scanning Probe Microscopy: Alokmay Datta

Gravitation and Cosmology: Amit Ghosh

Integrable & Nonlinear Systems: Anjan Kundu

Nonlinear Dynamics: ANS Sekar Iyengar

Quantum Many Body Systems: Arti Garg

Quantum Field Theories: Asit De

Groups & Lie Algebras: Bireswar Basu-Mallick

Astrophysics and Astroparticle Physics: Debades Bandyppadhyay & Pijushpani Bhattacharjee

Dark Matter Experiments: Mala Das

Nonlinear Complex Plasmas: Nikhil Chakrabarti & MS Janaki

Positron Anihilation and Gamma ray spectroscopy: PMG Nambissan

Condensed Matter Physics: Y Sudhakar

Numerical and Statistical techniques: Subir Sarkar & Satyaki Bhattacharya

6.1.2 Biophysical Sciences

REVIEW: [Students, Review Title (Supervisor)]

Piyali Mitra, Photochemistry of Host-guest Interactions using Therapeutically Important Molecules (Prof Samita Basu)

Banabithi Koley, Spectroscopic Investigation on Binding Interactions between Biological Macromolecules and Metal Complexes with Antioxidant Study (Prof Samita Basu)

Angana Ray, Structural Analysis of G-quadruplex Blocks of Telomeric DNA (Prof Dhananjay Bhattacharyya)

Subhas Chandra Bera, Single Molecule Study of Macromolecular Folding (Prof Soumen Basak)

Debashree Das, Peroxidoxins: The Anti-Oxidant Proteins (Prof Abhijit Chakrabarti)

Anupa Majumdar, Drug Induced Membrane Fusion: Effect of Membrane Parameters and Additives (Prof Munna Sarkar)

Pritha Bhattacharjee, Self Association of Lamin A and its Implications in Health and Disease: A

Biophysical Approach (Prof Kaushik Sengupta and Prof Dipak Dasgupta)

Neha Rai, COX-2 Inhibitors: Effectual Target for Cancer Chemotherapy (Prof Sanghamitra Raha)

Mohar Biplab Sengupta, Spinal Cord Injury: Traumas and Tribulations (Prof Debashis Mukhopadhyay)

Srijan Haldar, MiRNA, Cell Signaling and Myeloproliferative Neoplasm and Analysing The Gene Expression in Myeloproliferative neoplasms (Prof Subrata Banerjee)

Sayantani Ghosh, Beats with Battered Spine-Animal Model of Spinal Cord Injury (Prof Debasis Mukhopadhyay)

Devika Srivastava, Role of miRNA in Regulation of Endoplasmic Reticulum Stress Response (Prof Oishee Chakrabarti)

Priyanka Majumder, Lysosomal Dysfunction in Late Onset Neurodegenerative Diseases (Prof Oishee Chakrabarti)

Arpita Saha, The role of Histone Acetylation in Initiation of Eukaryotic DNA Replication (Prof Partha Saha)

Avinanda Banerjee, Nuclear Lamin A and its Role in Dilated Cardiac Myopathy, (Prof Kaushik Sengupta)

Supratim Ghatak, Dietary Phytochemicals and Histone Modifications in Cancer (Prof Sanghamitra Raha)

Present Students:

Arijita Mukherjee, Chaitrali Sengupta, Manindra Bera, Nidhi Agnihotri, Pradip Das, Rukmini Mukherjee, Sanghati Roy Choudhuri, Sathi Goswami, Soumita Mukherjee, Sudha Bucha

Courses offered:

(a) Compulsory courses

3. Macromolecular Structure (D Bhattacharya, R Banerjee, M Sarkar)

4. Protein Crystallography and Structural Biology (U Sen, S Biswas)

5. Molecular Biology (P Saha and K Sengupta)

6. Experimental Techniques in Cellular & Molecular Biology (P Saha, K Sengupta and PK Ray)

7. Basics in Cell Biology (S Raha)

8. Immunology (S Banerjee)

9. Basic Neurobiology (NP Bhattacharya, D Mukhopadhyay and O Chakrabarti)

10. Chemical Biology (D Dasgupta)

11. Spectroscopy (S Basu, M Sarkar)

12. Applied biophysical spectroscopy and imaging: (PP Mishra)

13. Basic Radiochemistry (S Lahiri)

14. Basic Radiation Physics (M Nandy)

15. Computer Programming and Statistical Analysis (P Ray, D Bhattacharya)

(b) Advanced optional courses:

1. Applied Spectroscopy (Samita Basu and Munna Sarkar)

2. Polymer Chemistry (Amithabha De)

3. Green Chemistry (Sushanta Lahiri)

4. Chemical Biology I: Enzyme Kinetics (Padmaja Mishra)

5. Chemical Biology II: Chromatin Structure & Remodeling (Dipak Dasgupta)

6. Macromolecular Crystallography (Udayaditya Sen and Sampa Biswas)

7. Numerical Computational Methods (Pulak Ray)

8. Drug Discovery: Modern Day Approach (Munna Sarkar)

9. Structural Bioinformatics (Dhananjay Bhattacharyya)
10. Protein Folding (Soumen Basak)
11. Genomics and Proteomics (Debashis Mukhopadhyay)
12. Cell Biology I: Story of Lysozomes (Oishee Chakrabarti)
13. Cell Biology II: A Cytoskeletal/Nucleoskeletal aspect (Kaushik Sengupta)
14. Membrane Biology (Abhijit Chakrabarti)
15. Cell Signaling (Sanghamitra Raha)
16. Cell Cycle (Partha Saha)
18. Stem Cell Biology (Subrata Banerjee)

6.2 Undergraduate Associateship Course

6.2.0.1 List of Summer project students: 2011 [Name, Affiliation (Supervisor)]

1. Abhishek Dey Calcutta University (Sunanda Banerjee)
2. Anindita Chakraborty St Xaviers College, Kolkata (Partha Saha)
3. Arnab Bose Calcutta University (Nitai Pada Bhattacharyya)
4. Chhavi Jain Amity University (Sangam Banerjee)
5. Debasis Atta IIT Kanpur (Ushasi Dutta Pramanik)
6. Debosree Pal St Xaviers College, Kolkata (Udayaditya Sen)
7. Devnidhi Sharma Bits Pilani (Padmaja Prasad Mishra)
8. Deya Das IIT Madras (Kamal Kumar Bardhan)
9. K Kiran Kumar IIT Roorkee (Soumen Basak)
10. Merin Jose Madras Christian College (Maitreyee Saha Sarkar)
11. Moumita Dasgupta St Xaviers College, Kolkata (Sampa Biswas)
12. Pavan Sharma IISER Thiruvananthapuram (Susanta Lahiri)
13. Pritha Yadav Haldia Institute of Technology (Nitai Pada Bhattacharyya)
14. Priyanka De Haldia Institute of Technology (Kaushik Sengupta)
15. Sourav Biswas IIT Kanpur (Nihar Ranjan Ray)
16. Sujyoti Chandra St Xaviers College, Kolkata (Debashis Mukhopadhyay)

6.3 Summer Students' Programme

Physics 2011

- Supriti Sen (Mentor: Maitreyee Saha Sarkar)
Soumita Mondal (Mentor: Pradip Roy)
Srijita Tapader (Mentor: Maitreyee Saha Sarkar)
Sana Ahmed (Mentor: Mala Saha)
Sucharita Saha (Mentor: Mala Saha)
Deep Chatterjee (Mentor: Sankar De)
Habib Ahmad Mondal (Mentor: PMG Nambisan)
Shruti Menon (Mentor: Debasish Majumdar)

Biophysics 2011

Anirup Mondal (Mentor: Debasish Mukhopadhyay)

Sreyoshe Mallik (Mentor: Samita Basu)

Chapter 7

Research Fellows/Visiting Fellows/Research Associates

7.1 Research Fellows [as on March 31, 2012]

Theory Division

1. Smt. Bhramar Chatterjee: Senior Research Fellow
2. Shri Priti Bhajan Byakti: Senior Research Fellow
3. Shri Santanu Mondal: Senior Research Fellow
4. Shri Raktim Abir: Senior Research Fellow
5. Smt. Sangita De Sarkar: Senior Research Fellow
6. Md. Najmul Haque: Senior Research Fellow
7. Smt. Baishali Chakraborty: Senior Research Fellow
8. Shri Arindam Majumdar: Senior Research Fellow
9. Shri Somdeb Chakraborty: Senior Research Fellow
10. Shri Pratyay Banerjee: Senior Research Fellow
11. Shri Avirup Ghosh: Senior Research Fellow
12. Shri Abhishek Chowdhury: Senior Research Fellow
13. Shri Dipankar Das: Junior Research Fellow
14. Shri Abhik Mukherjee: Junior Research Fellow

Astro Particle Physics& Cosmology Division

1. Shri Srijit Bhattacharjee: Senior Research Fellow
2. Smt. Soumini Chaudhury: Senior Research Fellow
3. Shri Rana Nandi: Senior Research Fellow
4. Smt. Susmita Kundu: Senior Research Fellow
5. Smt. Susnata Seth: Senior Research Fellow
6. Shri Lab Saha: Senior Research Fellow
7. Shri Mainak Chakraborty: Senior Research Fellow
8. Shri Abhishek Majhi: Senior Research Fellow
9. Shri Anirban Biswas: Senior Research Fellow
10. Shri Debabrata Adak: Senior Research Fellow
11. Shri Chandrachur Chakraborty: Junior Research Fellow
12. Shri Kamakshya Prasad Modak: Junior Research Fellow
13. Shri Amit Dutta Banik: Junior Research Fellow

Plasma Physics Division

1. Shri Subir Biswas: Senior Research Fellow
2. Shri Debabrata Banerjee: Senior Research Fellow
3. Shri Chandan Maity: Senior Research Fellow
4. Shri Sudip Garai: Junior Research Fellow
5. Smt. Anwesha Sarkar: Senior Research Fellow

Surface Physics Division

1. Shri Sirshendu Gayen: Senior Research Fellow
2. Shri Suman Mandal: Senior Research Fellow
3. Shri Mojammel Haque Mandal: Senior Research Fellow
4. Shri A.K.M. Maidul Islam: Senior Research Fellow
5. Smt. Paramita Chatterjee: Senior Research Fellow
6. Md. Safiul Alam Mollick: Senior Research Fellow
7. Shri Abhisakh Sarma: Senior Research Fellow
8. Shri Sanjoy Kumar Mahatha: Senior Research Fellow
9. Shri Bishnudas Ghosh: Senior Research Fellow
10. Smt. Manjula Sharma: Senior Research Fellow
11. Smt. Tanusree Samanta: Senior Research Fellow
12. Shri Pabitra Das: Senior Research Fellow
13. Shri Amaresh Metya: Senior Research Fellow
14. Shri Santanu Maiti: Senior Research Fellow
15. Shri Jayanta Das: Senior Research Fellow
16. Shri Shyamal Mondal: Senior Research Fellow
17. Smt. Ishani Roy: Senior Research Fellow
18. Shri Suvankar Chakraborty: Senior Research Fellow
19. Shri Kousik Bagani: Junior Research Fellow
20. Shri Tanmay Ghosh: Junior Research Fellow
21. Smt. Mala Mukhopadhyay: Junior Research Fellow
22. Smt. Debashree Chowdhury: Junior Research Fellow

Applied Materials Science Division

1. Shri Kaustabh Dan: Junior Research Fellow
2. Ms. Nupur Biuswas: Junior Research Fellow

Nuclear Physics Division

1. Shri Mukesh Kr. Prodhan: Senior Research Fellow
2. Md. Anisur Rahaman: Senior Research Fellow
3. Shri Santosh Chakraborty: Senior Research Fellow
4. Smt. Debasmita Kanjilal: Senior Research Fellow
5. Shri Subhajit Karmakar: Senior Research Fellow
6. Smt. Purba Bhattacharya: Senior Research Fellow
7. Shri Hitesh Vijay Rahangdale: Junior Research Fellow
8. Smt. Rajani Raman: Junior Research Fellow

High Energy Nuclear & Particle Physics Division

1. Shri Indranil Das: Senior Research Fellow
2. Smt. Lusaka Bhattacharya: Senior Research Fellow
3. Smt. Sreemoyee Sarkar: Senior Research Fellow
4. Shri Mahatsab Mandal: Senior Research Fellow
5. Shri Debashis Saha: Junior Research Fellow
6. Smt. Debarati Roy: Junior Research Fellow
7. Shri Atanu Modak: Junior Research Fellow
8. Smt. Swagata Mukherjee: Junior Research Fellow
9. Shri Kalyanmoy Chatterjee: Junior Research Fellow
10. Ms. Sandhya Jain: Junior Research Fellow
11. Ms. Payal Mohanty: Senior Research Fellow (Extended)

Theoretical Condensed Matter Physics Division

1. Shri Debashis Samanta: Senior Research Fellow
2. Shri Rakesh Chatterjee: Senior Research Fellow
3. Smt. Mahashweta Basu: Senior Research Fellow
4. Shri Debarshee Bagchi: Senior Research Fellow
5. Shri Asim Ghosh : Senior Research Fellow
6. Smt. Paramita Dutta: Senior Research Fellow
7. Shri Niladri Sarkar: Senior Research Fellow
8. Smt. Moumita Dey: Senior Research Fellow
9. Smt. Srilekha Saha: Senior Research Fellow
10. Shri Soumyajyoti Biswas: Senior Research Fellow
11. Shri Sourish Bondyopadhyay: Senior Research Fellow
12. Mr. Muzafar Qadir Lone: Senior Research Fellow
13. Shri Amit Dey: Junior Research Fellow
14. Shri Atanu Rajak: Junior Research Fellow

Experimental Condensed Matter Physics Division 1.

1. Shri Deep Talukdar: Senior Research Fellow
2. Shri Dilip Kumar Bhoi: Senior Research Fellow
3. Md. Nazir Khan: Senior Research Fellow
4. Shri Mayukh Majumder: Senior Research Fellow
5. Shri Arindam Midya: Senior Research Fellow
6. Shri Sudipta Mandal: Senior Research Fellow
7. Smt. Susmita Dhara: Junior Research Fellow
8. Smt. Moumita Nandi: Junior Research Fellow
9. Smt. Rajeswari Roy Chowdhury: Junior Research Fellow
10. Shri Tapas Paramanik: Junior Research Fellow

Crystallography & Molecular Biology Division

1. Shri Anup Kumar Maity: Senior Research Fellow
2. Smt. Jayeeta Ghose: Senior Research Fellow
3. Shri Sudip Majumder: Senior Research Fellow
4. Smt. Kamalika Roy Choudhury: Senior Research Fellow

5. Shri Sankar Chandra Basu: Senior Research Fellow
6. Smt. Kasturi Sengupta nee Guha: Senior Research Fellow
7. Smt. Eashita Das: Senior Research Fellow
8. Shri Saurav Roy: Senior Research Fellow
9. Smt. Barnali Waugh: Senior Research Fellow
10. Smt. Seema Nath: Senior Research Fellow
11. Shri Mahan Ray: Senior Research Fellow
12. Smt. Rakhi Paul: Senior Research Fellow
13. Smt. Arpita Saha: Junior Research Fellow

Structural Genomics Division

1. Smt. Sutapa Saha: Senior Research Fellow
2. Shri Mithun Sinha: Senior Research Fellow
3. Smt. Nandini Pal Basak: Senior Research Fellow
4. Shri Samir Das: Senior Research Fellow
5. Shri Sudip Kundu: Senior Research Fellow
6. Smt. Kasturi Roy: Senior Research Fellow
7. Smt. Suchismita Halder: Senior Research Fellow
8. Shri Shounak Baksi: Senior Research Fellow
9. Smt. Shilpita Karmakar: Senior Research Fellow
10. Smt. Madhurima Mitra: Senior Research Fellow
11. Shri Srijan Haldar: Junior Research Fellow
12. Smt. Debashree Das: Junior Research Fellow
13. Smt. Devika Srivastava: Junior Research Fellow

Biophysics Division

1. Smt. Parijat Majumder: Senior Research Fellow
2. Shri Shibojoyoti Lahiri: Senior Research Fellow
3. Smt. Sukanya Halder: Senior Research Fellow
4. Smt. Swati Panigrahi: Senior Research Fellow
5. Shri Biswapathik Pahari: Senior Research Fellow
6. Smt. Sanchita Mukherjee: Senior Research Fellow
7. Smt. Saptarni Ghosh: Senior Research Fellow
8. Shri Manas Mondal: Senior Research Fellow
9. Smt. Amrita Banerjee: Senior Research Fellow
10. Smt. Angana Ray: Junior Research Fellow
11. Smt. Pritha Bhattacharjee: Junior Research Fellow

Chemical Sciences Division

1. Smt. Sutapa Mondal: Senior Research Fellow
2. Shri Manas Kumar Sarangi: Senior Research Fellow
3. Smt. Mousumi Banerjee: Senior Research Fellow
4. Smt. Binita Dutta: Senior Research Fellow
5. Smt. Moupiya Nag: Senior Research Fellow

7.2 CSIR/UGC/DST/DBT/CAMCS Fellows, etc**CSIR**

- Dr. J.K. Dattagupta: Emeritus Scientist: C&MB
 Shri Srijit Das: Junior Research Fellow(NET): C&MB
 Shri Ramanuj Banerjee: Junior Research Fellow(NET): C&MB
 Smt. Nupur Biswas: Senior Research Fellow(NET): AMS
 Shri Satya Ranjan Halder: Senior Research Fellow(NET): SPD
 Smt. Anuradha Bhattacharya: Junior Research Fellow(NET): SPD
 Shri Arpan Bhattacharyya: Junior Research Fellow(NET): SPD
 Shri Atanu Kumar: Junior Research Fellow(NET): Theory
 Sm. Parijat Dey: SPM Fellow: Theory
 Smt. Anita Roy: Senior Research Fellow(NET): SGS
 Shri Arunabha Chakrabarti: Senior Research Fellow(NET): SGS
 Shri Avik Basu: Junior Research Fellow(NET): SGS

Smt. Shreyasi Dutta: Junior Research Fellow(NET): Biophysics
 Smt. Sreeja Chakraborty: Junior Research Fellow(NET): CSD
 Shri Kaustab Ghosh: Junior Research Fellow(NET): CSD
 Shri Kallol Bera: Junior Research Fellow(NET): CSD
 Shri Ankan Datta Chowdhury: Junior Research Fellow(NET): CSD
 Shri Sujay Ghosh: Junior Research Fellow(NET): CSD
 Shri Samik Dutta Gupta: Junior Research Fellow(NET): ECMP
 Shri Kalipada Das: Junior Research Fellow(NET): ECMP
 Shri Ujjal Kumar Gayen: Junior Research Fellow(NET): TCMP
 Smt. Urna Basu: SPM Fellow: TCMP
 Shri Sohan Kr. Jha; Junior Research Fellow(NET): TCMP
 Shri Abhijit Bisoi: Junior Research Fellow(NET): NPD
 Smt. Anindita Deb: Junior Research Fellow(NET): SGD

UGC

Shri Swadesh Mandal: Junior Research Fellow(NET): CSD
 Shri Ajoy Mondal: Junior Research Fellow(NET): CSD
 Shri Satyajit Seth: Junior Research Fellow(NET): Theory
 Smt. Ajanta Kundu: Junior Research Fellow(NET): ANP
 Smt. Sumona Sinha: Junior Research Fellow(NET): SPD
 Shri Palash Khan: Junior Research Fellow(NET): HENPPD
 Shri Rabindra Pankaj: Junior Research Fellow(NET): TCMP

DST

Dr.(Smt.) Debi Chowdhury: "Principal Investigator (Women Scientist Scheme-A)"
 Dr.(Smt.) Papri Dasgupta: Women Scientist-A: ECMP
 Dr. Subarna Mitra: Post Doctoral Fellow: SPD
 Dr. Santosh Kumar Samaddar: Principal Investigator: DBT
 Dr.(Smt.) Lakshmeshri Lahiry: Research Associate-I: SGS

CAMCS

Md. Sahinur Reja: Cavendish-Saha Research Fellow: TCMP
 Dr. Sanjoy Gupta: Research Associate: TCMP

7.3 Research Associate & Post Doctoral Fellow

<i>Division</i>	<i>Name</i>	<i>Designation</i>
Theory	Dr. Tapan Naskar	Post Doctoral Fellow
Theory	Dr. Santosh Kr. Singh	Post Doctoral Fellow
APCD	Shri Prasanna Kumar Mondal	Post Doctoral Fellow
APCD	Dr. (Smt.) Sarmistha Banik	Post Doctoral Fellow
APCD	Dr. Richard J. Britto	Post Doctoral Fellow
APCD	Ms. Amna Ali	Post Doctoral Fellow
SPD	Dr. Amulya Krishna Mahapatra	Post Doctoral Fellow
SPD	Dr.(Smt.) Sananda Jana	Post Doctoral Fellow
NPD	Dr. (Smt.) Sucheta Adhikari	Research Associate-III
NPD	Dr. (Smt.) Sudatta Ray	Research Associate-II
NPD	Shri Dhruvajyoti Gupta	Post Doctoral Fellow
NPD	Smt. Mandira Sinha	Research Associate-I
NPD	Dr. Ritesh Kshetri	Post Doctoral Fellow
ANPD	Dr. Sreetama Dutta	Research Associate-I
HENPPD	Dr. Kushal Das	Post Doctoral Fellow
HENPPD	Shri Santosh Roy	Post Doctoral Fellow
TCMP	Dr.(Smt.) Anasuya Kundu	Post Doctoral Fellow
TCMP	Dr. Anabha Ray	Post Doctoral Fellow
ECMP	Dr. (Smt.) Rangana Bhattacharya	Research Associate-I
ECMP	Dr. Kausik Sengupta	Post Doctoral Fellow
CSD	Smt. Aurkie Ray	Post Doctoral Fellow
AMSD	Dr. Kuntal Chakrabarti	Research Associate-I
AMSD	Dr. Ratan Kr. Saha	Post Doctoral Fellow
C&MB	Dr. (Smt.) Paramita Bhattacharya	Post Doctoral Fellow
Biophysics	Dr.(Smt.) Sangeeta Kundu	Research Associate-II

Chapter 8

Facilities

8.1 Centre for Advanced Research & Education

The CARE has been making efforts in research-education linkages towards identifying and nurturing young talent in science. Post-M.Sc Training Program, Undergraduate Associate (UGA) Program and Summer Students Program have been running successfully. Science Day has been celebrated through seminars and open house for undergraduate students. Visits of High School and College Students to the Science Gallery, SINP Labs and Lectures at a semi popular level have been arranged. Seminars, Institute Colloquiums, Lectures and School Workshops on different disciplines of Physics, Biology and Issues on Social and Historical aspects of Science have been organized by the CARE. The CARE has been maintaining Meghnad Saha Archive which helps the students of History of Science in their research within India and abroad. The CARE published Annual Report 2010-11. Overwhelming response of about 500 high school students is received in several different CARE conducted outreach programs. CARE took major responsibility in the organization of the 19th West Bengal State Science and Technology Congress, held during March 1-2, 2012 with about 800 delegates taking part in the SINP campus in Salt Lake, Kolkata. Few other programs organized by the CARE in 2011-12 are listed below.

1. Discussion Meeting on Crop Culture, Biotechnology & Biodiversity. July 8, 2011, SINP, Kolkata.
2. Participation of the Institute in 15th National EXPO and Science & Cultural Exhibition organized by Central Calcutta Science & Culture Organization for Youth. Sept, 7-11, 2011, Bhairav Chandra Ganguly College, Belgharia, North 24 Parganas.
3. Participation of the Institute in a Science & Cultural Exhibition named 8th Jatiya Sanhati Utsav-O-Bharat Mela 2011. Dec.10-17, 2011, Gabindanagar, Taldi, South 24 Parganas.
4. CARE Seminar. 2 December, 2011. Speaker was Prof. Jayashree Ramdas (Teacher Education in West Bengal and Bihar: a proposal of the Homi Bhabha Centre for Science Education)
5. Organized International School on Storage Ring Design. Jan.16-20, 2012, SINP, Kolkata.
6. Meeting between Indian Laboratories and KEK. Feb. 8-9, 2012, SINP, Kolkata.
7. Two days Science Exhibition cum Workshop to observe 150th Birth Anniversary of Acharya Prafulla Chandra Roy for celebration of International Year of Chemistry. Feb.10-11, 2012, Pandua. Hoogly.
8. 6th School on Genomics and Proteomics for Clinicians, Feb. 20-24, 2012, SINP, Kolkata.

8.2 Electron Microscope Facility

The Electron Microscope Facility is working as a central facility and equipped with a 200keV Transmission Electron Microscope and a 300keV Field Emission Gun Transmission Electron Microscope. The facility caters to the researchers from Biological Sciences and Material Sciences both.

Biophysics Div., Chemical Sc. Div., C & MB Div. and Structural Genomic Div. use the facility to study biological samples like bacteria & their thin section, lipid vesicles, detergent micelles, lipid-protein complexes, peptide aggregation etc. ECMP, Surface Physics, Applied Material Sciences and Applied Nuclear Physics Div. use the facility to study material sciences samples like nanomaterials, metal oxides, nanocrystalline solids etc. More than 30 faculty members of the institute and 4 scientists from VECC use the facility on regular basis during this period.

Other research institutes and universities e.g. IISER, BESU, UGC-DAE, Jadavpur University, IACS, Presidency College, ISI, Kalyani University, Calcutta University, Bose Inst., WBUT etc. use the E.M. Facility extensively. Some of the institutes outside West Bengal, also use the facility e.g. Benaras Hindu University, NIT-Rourkela, NIT-Durgapur to name a few.

The instrument has been utilized more than 80 % of the available days. More than 16 publications have come out in reputed scientific journals, contributed by different scientists using the 200keV Transmission Electron Microscope during this period.

8.3 Library

The Library of SINP is one of the major information resource centres within Eastern India in the field of Physical and Biophysical sciences and is privileged to support the institutes march towards its vision- to be the pioneer research Institute of India. Through our well equipped and digitized library, the members of our institute and the other members associated with our research and development program are being benefited and this will aid towards scientific development of our Institute and country at large.

The Library not only acquires, organizes and disseminates knowledge; it has put its foot ahead towards policies and procedures, systems and services and created a suitable atmosphere which facilitates assimilation and generation of new knowledge through single window. The details of our library are given below.

Collection: The library of SINP is one of the leading science-library within Eastern Region. In addition to huge collection of books and e-books on science and technology it also subscribe more than 252 leading journals in the field of physical, chemical and biophysical sciences. Library has a huge collection of books, e-books and non-book materials. The details are given below:

- * Books: 31345 (technical) + 3908 (non-technical) [452 books are added in this year]
- * E- books: 1000
- * Bound volumes of journals: 50794
- * Current subscribed journals: 252 (Foreign 193 + Indian 59)[19 titles added in this year]
- * Online journals: 3000 titles
- * Reports: 26000+
- * Number of CD/DVD Rom: 967

Major items/equipments available:

- * Library has two IBM servers where Libsys 4 (Rel 6.1 upgraded version) database is running.
- * 32 Pcs are in the library out of 22 are for library user.
- * One hp Design jet plotter printer & one Canon plotter printer.
- * One hp colour printer & 3 hp black & white printers.
- * Six Xerox machines cum printers (black & white).
- * One colour Xerox cum network printer (Sharp).
- * Three lamination machines.
- * Three scanner & one spiral binding machine.

Membership:

In addition to our more than 700 institute members (faculties, fellows and staff), library has the privilege to serve about six hundred (666) users coming from different scientific and educational institutes of Eastern India. The list of external users includes Calcutta University, Jadavpur University, Viswa Bharati, IACS, IICB, ISI, Bengal Engineering and Science University, CMERI, Guwahati University, North East Hilly University, Patna University etc. apart from numerous Under-Graduate/Post-Graduate colleges and project students

* Number of members & types of facilities are available for each category of members.

* (A) SINP members (No. 700)

* (1) Borrowing facility

* (2) Xerox facility

* (3) Inter-library-loan

* (4) Online searching & downloading.

* (B) VECC members (No. 104)

* (1) Borrowing facility

* (2) Online searching & downloading

* (C) External members (No. 562)

* (1) Reading room facility for reference use

* (2) Xerox facility against payment

* (3) Online searching & downloading

* (D) Institutional Members

* (1) Reading room facility for reference use

* (2) Borrowing facility

(3) Online searching & downloading

Online facilities:

Successfully the library has implemented the online and archival facilities of various journals, e-books of the following publishers from XI plan project grant (LDRM). More than 3000 online journals as well as online archives and 1000 e-books are available (full-text pdf) from our site:

1. Institute of Physics, London
2. American Institute of Physics
3. American Physical Society
4. American Chemical Society
5. John Wiley online library
6. World Scientific
7. Springer
8. Taylor & Francis
9. Science Classic
10. Nature Publishing Group
11. Cambridge University Press
12. Royal Society of Chemistry
13. Oxford

Library has the online e-books collection of Annual Reviews, Lecture Notes in Physics and 500 e-books of T&F, CUP, Wiley and World Scientific. Currently the library is subscribing Web of Knowledge & Science Citation Index from 1945 to current, JSTOR (Mathematics & Statistics) and Springer protocols database.

8.4 Radiological Safety

As per the rules of Atomic Energy Regulatory Board, Government of India, centralised documentation of personal dose records of radiation workers of the Institute are maintained. Renewal and issuance of TLD and CR39 personnel monitoring badges, radiation protection survey of radioactive hot laboratory, maintenance of inventory and supervision of safe storage and handling of radioactive isotopes, disposal of solid and liquid radioactive wastes, maintenance of the Environmental TLD monitor as supplied by the Environmental Assessment Division, BARC, Mumbai, through HPU, VECC, Calcutta are carried out.

8.5 Central Workshop

The Computerized Numerical Control (CNC) machine tools, installed in the workshop, are being used in fabrication of precision experimental devices for different departments of the Institute. The welding section in the workshop is equipped with a pulse TIG welding machine, a plasma cutting machine, an arc welding machine and gas welding facility. This section has successfully developed its skill in welding of thin walled stainless steel and aluminium components. The Glass blowing section is one of the best performing sections of the workshop. Most of the components, fabricated in the workshop were designed and drafted by the design & drafting section.

8.6 Medical Unit

The Institute runs a Contributory Medical Benefit Scheme (CMBS) for all its employees and their dependents with credit facilities in 13 leading hospitals of Kolkata.

8.7 Building Maintenance (Civil)

Building Maintenance (Civil) section was involved in activities of different nature related to the day-to-day maintenance work, up-keeping of the whole institute campus and its surroundings and implementation of various Infrastructural development projects of this institute. The section was involved in maintenance of all R.C.C. & steel building structures, (ii) water supply, plumbing and sanitary systems, (iii) carpentry trade, (iv) gardening and landscaping, (v) housekeeping etc. in the office premises as well as in two housing complexes. The Section also renders their services in renovation, modification and extension works of various laboratories according to their requirements.

8.8 Building Maintenance (Electrical)

The divisional activity is multifaceted and spread over, developmental electrical projects, extension of existing electrical system to suit requirements, induce flexibility in existing electrical system by introducing improvised mechanism, imposing higher protection to system depending on their vulnerability and maintenance of the total electrical system on annual and daily basis.

8.9 Telephone Section

The Telephone Section was set up in 1984 with 3+9 EPBX. Since then the Section has been grown up steadily. Presently a large EPABX system (ARIA-1000, AGC Networks Ltd.) with 500 extension lines is being operated. The reception counter of the Section usually attends the visitors. The Section maintains telephone lines, extensions and cables with the help of Building Maintenance Electrical Division and processes the monthly Telephone Bills of Institute through proper channel. The Section always keeps contact with BSNL, local exchange for rectification of any type of external fault. Updating of Telephone Directory at Website is carried out routinely. Telephone section prepared a new Internal Telephone Directory which has been inaugurated by our Director on 11th January, 2012, the Foundation Day of the Institute.

8.10 Auditorium Complex

The SINP Auditorium Complex is mainly used for holding various programmes, seminars, symposium, Conferences of national and international stature, etc. 159 Programmes Held during 2011-12.

8.11 Guest House

Guest House provides accommodation in 4 rooms with double occupancy throughout the year. Student hostel provides accommodation of 13 Girl student and 36 Boy students. There is separate canteen facility for the students only. These facilities for the students are provided throughout the year.

8.12 Departmental Canteen

The SINP Departmental Canteen remains active from 8 AM to 8 PM for preparation and serving food to members and guests of the Institute. The performance begins by receiving raw materials

early morning, followed by preparation of cooking lunch and breakfast items. The Canteen serves breakfast, lunch, afternoon tea and snacks and evening meal. Occasionally canteen also serves special food for guest of the Institute coming for meeting and small conferences.

Chapter 9

Administration

9.1 Governing Council

Chairman:

Dr. R. K. Sinha
Chairman, Atomic Energy Commission &
Secretary to the Government of India
Department of Atomic Energy
Mumbai-400 001

Members:

Professor Dhruvajyoti Chattopadhyay
Pro Vice-Chancellor (Academic)
University of Calcutta
Kolkata-700 073

Professor P. K. Kaw
Director, Institute for Plasma Research
Near Indira Bridge Ghat
Gandhinagar 382 428

Shri Satish Chandra Tewary, IAS,
Principal Secretary
Higher Education Department,
Government of West Bengal
Bikash Bhavan
Salt Lake city
Kolkata-700 064

Professor Mustansir Barma
Director, Tata Institute of Fundamental Research
Mumbai - 400 005

Dr. C B Venkataramana
Joint Secretary (I&M) and (R&D) to the Government of India
Department of Atomic Energy
Mumbai

Shri. V. R. Sadasivam
Joint Secretary (Finance)
Govt. of India
Department of Atomic Energy
Mumbai- 400 001

Prof. Susanta Sen
Professor, Institute of Radiophysics & Electronics,
Deputy Director, Centre for Research in Nanoscience &
Nanotechnology, University of Calcutta
Kolkata- 700 009

Professor Amitava Raychaudhuri
Palit Professor of Physics,
University of Calcutta
Kolkata

Professor Milan K. Sanyal
Director
Saha Institute of Nuclear Physics
Kolkata-700 064

Mr. V V Mallikarjuna Rao (Ex-Officio Secretary)
Registrar
Saha Institute of Nuclear Physics
Kolkata-700 064

9.2 Members of the Institute [as on March 31, 2012]

Prof Milan Kr Sanyal: Director

Director's Office

- 1.Sri Amalesh Ch. Saha: A.O.(D.O.)
- 2.Sri Jeevan Kr. Shaw; A.A.O.(D.O.)
- 3.Sri Subhasish Ghoshal: Superintendent
- 4.Sri Goutam Mandal: Superintendent
- 5.Sri Ratanlal Ram: Technician 'C'
- 6.Sri Babu Rajak: Helper 'C'

Registrar's Office

- 1.Sri V.V. Mallikarjuna Rao: Registrar
- 2.Shri Biplab Kumar Ray: A.A.O.(E-I)
- 3.Sri Bimlesh Kr. Tripathi: Senior Hindi Translator
- 4.Shri Bibekbijay Bandyopadhyay: Superintendent
- 5.Shri Aditya Dhara: Lower Division Clerk
- 6.Sri Rudal Prasad Ram: Technician 'D'
- 7.Sri Mahadev Das: Helper 'E'

Academic Departments and Divisions

AstroParticle Physics & Cosmology (APC)

- 1.Prof. Pijushpani Bhattacharjee: Sr. Professor 'H' & HOD
- 2.Prof. Parthasarathi Majumdar: Sr. Professor 'H+'
- 3.Prof. Debades Bandyopadhyay: Professor 'G'
- 4.Prof. Debasish Majumdar: Professor 'F'
- 5.Prof. Ambar Ghosal: Professor 'F'
- 6.Dr. Mala Das: Associate Professor 'E'
- 7.Dr. Pratik Majumder: Associate Professor 'E'
- 8.Shri Nilanjan Biswas: Scientific Assistant 'B'

Theory Division

- 1.Prof. Kamales Kar: Sr. Professor 'H+'
- 2.Prof. Radhey Shyam: Sr. Professor 'H+'
- 3.Prof. Anjan Kundu: Sr. Professor 'H+'
- 4.Prof.Parthasarathi Mitra: Sr. Professor 'H+'
- 5.Prof. Avaroth Harindranath: Sr. Professor 'H+'
- 6.Prof. Polish B. Pal: Sr. Professor 'H+'
- 7.Prof. Tarun Kanti Roy: Professor 'G'
- 8.Prof. Asit Kr. De: Professor 'G' & HOD
- 9.Prof. Kumar Sankar Gupta: Professor 'G'
- 10.Prof. Sibaji Roy: Professor 'G'
- 11.Prof. Gautam Bhattacharyya: Professor 'G'
- 12.Prof. Munshi Golam Mustafa: Professor 'G'
- 13.Prof. Bireswar Basu Mallick: Professor 'G'
- 14.Prof. Amit Ghosh: Professor 'G'
- 15.Prof. Debabrata Mukhopadhyay: Professor 'F'
- 16.Prof. Prakash Mathews: Professor 'F'
- 17.Prof. Harvendra Singh: Professor 'F'
- 18.Prof. Bijay Kr. Agrawal: Professor 'F'
- 19.Smt. Sangita Pande: Scientific Assistant 'B'
- 20.Sri Prodyut Kr. Mitra: Technician 'E'
- 21.Sri Sudarshan Hazra; Technician 'A'
- 22.Sm. Dola Mallick: Superintendent
- 23.Sri Arun Kr. Bose: Helper 'E'

Plasma Physics Division

1. Prof. ANS Iyengar: Sr. Professor 'H' & HOD, Chairman, Housing Allotment Committee
2. Prof. Rabindra Nath Pal: Sr. Professor 'H'
3. Prof.Santwana Roychowdhury: Professor 'G'
4. Prof. Nihar Ranjan Ray: Professor 'G'
5. Prof. Sujit Kr. Saha: Professor 'G'
6. Prof. Mylavarapu Sita Janaki: Professor 'G'

7. Prof. Nikhil Chakraborty: Professor 'F'
8. Sri Shantanu Chowdhury: Engineer 'F'
9. Sri Parthasarathi Bhattacharya: Scientific Officer 'C'
- 10.Sri Subhasis Basu: Scientific Officer 'C'
- 11.Sri Monobir Chattopadhyay: Scientific Officer 'C'
- 12.Sri Amalendu Bal: Scientific Assistant-E
- 13.Sri Abhijit Betal: Scientific Assistant-D
- 14.Sri Dulal Chatterjee: Superintendent
- 15.Sri Sib Sankar Sil: Technician 'E'
- 16.Sri Dipankar Das: Technician 'D'
- 17.Sri Ashok Kr. Ram: Helper 'C'

Surface Physics Division

1. Prof. Purushottam Chakraborty: Sr.Professor 'H' & HOD
2. Prof. Debabrata Ghosh: Sr. Professor 'H'
3. Prof. S. R. Bhattacharyya: Professor 'G'
4. Prof. Tapas Kr. Chini: Professor 'G'
5. Prof. Sangam Banerjee: Professor 'G'
6. Prof. Manabendra Mukherjee: Professor 'G'
7. Prof. Srinanda Kundu: Professor 'F'
8. Prof. Satyajit Hazra: Professor 'F'
9. Prof. Satyaban Bhunia: Professor 'F'
- 10.Prof. Krishnakumar SR Menon: Professor 'F'
- 11.Dr. Biswarup Satpati: Scientist 'E'
- 12.Sri Avijit Das: Scientific Officer 'C'
- 13.Sri Subir Roy: Scientific Officer 'C'
- 14.Sri Susanta Bandyopadhyay: Scientific Officer 'C'
- 15.Sri Souvik Banerjee: Scientific Assistant 'C'
- 16.Shri Debraj Dey: Scientific Assistant 'B'
- 17.Sri Goutam Sarkar: Scientific Assistant 'C'
- 18.Sri Mukul Ch Das: A.A.O.
- 19.Sri Harendra Nath Jana: Caretaker
- 20.Sri Gobardhan Jana: Helper 'C'

Applied Nuclear Physics Division

1. Prof. Satyajit Saha: Professor 'G' & HOD
2. Prof. (Smt.) Bichitra Ganguly: Professor 'G'
3. Prof. P. M. G. Nambissan: Professor 'G'
4. Prof. Supratik Mukhopadhyay: Professor 'G'
5. Prof. Chandi Charan Dey: Professor 'F'
6. Prof. (Sm.) Nayana Majumdar: Professor 'F'
7. Prof. Sandip Sarkar: Professor 'F'
8. Dr. Sankar De: Associate Professor 'E'
9. Sri Amal Ghosal: Scientific Officer 'C'

- 10.Sri Pradipta Kumar Das: Scientific Officer 'C'
- 11.Sri Saibal Saha: Scientific Officer 'C'
- 12.Sri Haradhan Dhar: Scientific Assistant 'E'
- 13.Sri Chandra Nath Marik: Scientific Assistant 'C'
- 14.Smt. Soma Roy: Scientific Assistant 'C'
- 15.Sri Asim Kumar Sarkar: Sr. Superintendent
- 16.Sri Dilip Kr. Sardar: Technician 'C'
- 17.Sri Kuntal Sarkhel: Helper 'C'
- 18.Sri Prabir Das: Helper 'C'

Nuclear Physics Division

1. Prof. Polash Banerjee: Professor 'G' & HOD
2. Prof. Padmanava Basu: Professor 'G'
3. Prof. Maitreyee Saha Sarkar: Professor 'G'
4. Prof. Subinit Roy: Professor 'G'
5. Prof. Ashimananda Goswami: Professor 'G'
6. Prof. Ushasi Datta Pramanik: Professor 'F'
7. Prof. Chinmay Basu: Professor 'F'
8. Prof. (Smt.) Anjali Mukherjee: Professor 'F'
9. Sri Sujib Ch. Chattopadhyay: Scientific Officer 'C'
10. Sri Kaushik Chatterjee: Scientific Officer 'C'
11. Smt. Jonaki Panja: Scientific Officer 'C'
12. Sri Ajoy Kr. Mitra: Scientific Officer 'C'
13. Smt. Rita Ghosh: Scientific Assistant 'E'
14. Sri Dilip Sil: Scientific Assistant 'D'
15. Sri Pradip Barua: Technician 'C'
16. Sri Sankar Prasad Singh: Technician 'C'
17. Smt. Tultul Dutta: Superintendent
18. Sri Siladitya Chakraborty: Helper 'A'

High Energy Nuclear & Particle Physics Division

1. Prof. Sunanda Banerjee: Professor & Head
2. Prof. Pratap Bhattacharya: Professor 'G'
3. Prof. Sukalyan Chattopadhyay: Professor 'G'
4. Prof. Pradip Kr. Roy: Professor 'F'
5. Prof. Abhee Kanti Dutt-Mazumdar: Professor 'F'
6. Prof. Manoj K. Sharan: Professor 'F'
7. Dr. (Smt.) Tinku Sinha: Scientist 'E'
8. Dr. Satyaki Bhattacharya: Associate Professor 'F'
9. Dr. Subir Sarkar: Associate Professor 'F'
- 10.Dr. Suchandra Dutta: Associate Professor 'F'
- 11.Dr. Debasish Das: Associate Professor 'E'
- 12.Sri Debasish Bandyopadhyay: Scientific Assistant 'E'
- 13.Sri Dwijendra Das: Scientific Assistant 'C'
- 14.Sri Dipankar Das: Scientific Assistant 'C'
- 15.Smt. Lipy Das Bose: Scientific Assistant 'C'
- 16.Sri Sanjib Kr. Mondal: Superintendent
- 17.Sri Rakesh Kr. Ram: Helper 'C'
- 18.Sri Sudam Bagdi: Helper 'C'
- 19.Sri Singh Bahadur Thapa: Helper 'C'

Applied Material Science Division

1. Prof. Alokmay Datta: Professor 'G' & HOD
2. Dr. Madhusudan Roy: Associate Professor 'F'
3. Dr. Supratic Chakraborty: Associate Professor 'E'
4. Dr. Mrinmay Kr. Mukhopadhyay: Associate Professor 'E'
5. Sri Abhijit Sanyal: Engineer 'G'
6. Sri Shyama Prasad Mallick: Technician 'F'
7. Sri Ramkrishna Deb Das: Scientific Assistant 'B'
8. Sri Subhasish Sanyal: Superintendent
- 9.Sri Provash Halder: Helper 'D'

Theoretical Condensed Matter Physics Division

- Prof. Bikas Kanta Chakrabarti: Sr. Professor 'I' & HOD

- Prof. Atindra Nath Das: Sr. Professor 'H'
- Prof. S. N. Karmakar: Professor 'G'
- Prof. Sudhakar Yarlagadda: Professor 'G'
- Prof. Pradeep Kr. Mohanty: Professor 'F'
- Prof. Abhik Basu: Professor 'F'
- Prof. Arti Garg: Associate Professor 'E'
- Sri Kausik Das: Scientific Assistant 'C'
- Smt. Suparna Das: Superintendent
- Sri Jhantu Mallick: Helper 'C'
- Sri Asish Ram: Helper 'C'

Experimental Condensed Matter Physics Division

1. Prof. Amitabha Ghosh Ray: Sr. Professor 'H'
2. Prof. R. Ranganathan: Sr. Professor 'H' & HOD
3. Prof. Abu Ismail Jaman: Sr. Professor 'H'
4. Prof. (Smt.) Kajal Ghosh Ray: Sr. Professor 'H'
5. Prof. Chandidas Mukherjee: Professor 'G'
6. Prof. Indranil Das: Professor 'G'
7. Prof. Prabhat Kr. Mandal: Professor 'G'
8. Prof. Barnana Pal: Professor 'F'
9. Prof. Asok Podder: Professor 'F'
- 10.Prof. Bilwadal Bandyopadhyay: Professor 'F'
- 11.Prof. Chandan Mazumdar: Professor 'G'
- 12.Sri Ajoy Kr. Bhattacharya: Scientific Officer 'D'
- 13.Sri Tapan Kr. Pyne: Scientific Officer 'C'
- 14.Sri Arun Kumar Pal: Technician 'H'
- 15.Smt. Sankari Chakrabarti: Scientific Assistant 'D'
- 16.Sri Arindam Chakraborti: Scientific Assistant 'C'
- 17.Sri Dhruvajyoti Seth: Scientific Assistant 'C'
- 18.Smt. Papia Bhowmik (Mondal): Scientific Assistant 'C'
- 19.Sri Anish Karmahapatra: Technician 'E'
- 20.Sri Tapan Kr. Sarkar: Superintendent
- 21.Sri Sambu Hembrom: Technician 'C'
- 22.Sri Prabir Das: Technician 'B'
- 23.Sri Patit Paban Ranjit: Helper 'E'
- 24.Shri Rajeshwar Dubey: Helper 'A'

Crystallography & Molecular Biology Division

1. Prof. Nitai Pada Bhattacharyya: Sr.Professor 'H' & HOD
2. Prof. Sanghamitra Raha: Professor 'G'
3. Prof. Rahul Banerjee: Professor 'F'
4. Prof. Sampa Biswas: Professor 'F'
5. Prof. Partha Saha: Professor 'F'
6. Prof. Udayaditya Sen: Professor 'F'
7. Sri Utpal Basu: Scientific Officer 'C'
8. Sri Abhijit Bhattacharya: Scientific Assistant 'D'
9. Sri Bikram Nath: Scientific Assistant 'C'
- 10.Sri Sushanta Debnath: Scientific Assistant 'C'
- 11.Sri Saikat Mukhopadhyay: Scientific Assistant 'C'
- 12.Sri Ashis Kumar Dutta: Scientific Assistant 'C'
- 13.Smt. Durga Hazra: Superintendent
- 14.Sri Samir Kr. Majumdar: Technician 'C'
- 15.Sri Chinmoy Chatterjee: Helper 'D'
- 16.Sri Sakal Dev Ram: Helper 'C'
- 17.Sri Bipin Bose: Helper 'C'

Structural Genomics Division

1. Prof. Subrata Banerjee: Professor 'G' & HOD
2. Prof. Abhijit Chakrabarti: Professor 'G'
3. Prof. Debashis Mukhopadhyay: Professor 'F'
4. Dr. (Smt.) Oishee Chakrabarti: Associate Professor 'E'
5. Shri Madhu Sudan Samal: Asstt. Halwai-cum-Cook
6. Smt. Mahuya Dutta: Lower Division Clerk
7. Sri Raju Dutta: Technician 'B'
8. Sri Sanjay Shaw: Helper 'C'

Biophysics Division

1. Prof. Dipak Dasgupta: Sr. Professor 'H+' & HOD
2. Prof. Dhananjay Bhattacharyya: Professor 'G'
3. Sri Pulak Krmar Roy: Engineer 'G'
4. Prof. Arun Kr. Pal: Professor 'F'
5. Dr. Kaushik Sengupta: Associate Professor 'E'
6. Sri Shekhar Bhattacharya: Scientific Officer 'C'
7. Sri Arijit Pal: Scientific Assistant 'D'
8. Sri Bijay Kr. Das: Superintendent
9. Sri Nirmal Ch. Das: Technician 'B'
10. Sri Shyamal Ch. Digar: Helper 'C'

Chemical Science Division

1. Prof. Soumen Basak: Sr. Professor 'H'
2. Prof. Amitabha De: Professor 'G'
3. Prof. Susanta Lahiri: Professor 'G'
4. Prof. Samita Basu: Professor 'G' & HOD
5. Prof. Maitreyee Nandy: Professor 'F'
6. Prof. Munna Sarkar: Professor 'F'
7. Dr. Padmaja Prasad Mishra: Associate Professor 'E'
8. Sri Ajay Das: Scientific Assistant 'E'

9. Smt. Chitra Raha: Scientific Assistant 'D'
10. Sri Avijit Shome: Scientific Assistant 'C'
11. Sri Subir Bandyopadhyay: Superintendent
12. Sri Bablu Ram: Technician 'C'
13. Sri Deepak Kr. Ram: Technician 'A'
14. Sri Jitendra Nath Roy: Technician 'A'

Computational Science Division

- Prof. Dhananjay Bhattacharyya: Professor 'G' & HOD
 Dr. Gautam Garai: Scientist 'G'
 Sri Deeptish Dey: Engineer 'F'
 Sri Gautam Datta: Scientific Assistant 'E'
 Sri Sumit Basu: Scientific Assistant 'C'
 Sri Nanda Lal Sanpui: Technician 'C'
 Sri Soumya Majumdar: Technician 'C'

Teaching

1. Prof. Alokmay Datta: Professor 'G' & HOD
2. Sri Jayant Kr. Mukherjee: Scientific Assistant 'C'
3. Sri Sudarshan Mondal: Superintendent
4. Sri Nirmal Ch. Biswas: Technician 'B'

Central Facilities

Centre for Advanced Research & Education (CARE)

Prof. Abhijit Chakraborti Professor 'G' & Head

1. Smt. Dipa Dasgupta: Scientific Officer 'C'
2. Sri Amit Kumar Saha: Scientific Officer 'C'
3. Sri Pradip Das: Scientific Assistant-A
4. Sri Sanjib Kr. Roy: Helper 'C'

Electron Microscope Facility

1. Sri Pulak Krmar Roy: Engineer 'G' & Head
2. Dr. Biswarup Satpati: Scientist 'E'
3. Sri Ajay Chakraborty: Scientific Assistant 'D'

Library

Prof. R. Ranganathan: Chairman

1. Sri Swapan Kr. Banerjee: Librarian (F)
2. Smt. Ratna Raychaudhuri: Scientific Officer 'C'
3. Sri Abhijit Kumar Malakar: Scientific Assistant 'E'
4. Sri Samit De: Scientific Assistant 'E'
5. Shri Mahesh Hembram: Scientific Assistant 'B'
6. Smt. Manlunching: Scientific Assistant 'B'
7. Sri Subrata Chowdhury: Technician 'E'
8. Smt. Anupama Saha: Technician 'C'
9. Sri Manoj Karmakar: Technician 'C'
10. Sri Kishori Lal Ram: Technician 'C'
11. Sri Kartick Ch. Panigrahi: Helper 'C'

Building Maintenance (Civil)

Prof. Ashimananda Goswami: Chairman, BM(Civil) Committee

1. Sri Rajkumar Sengupta: Engineer 'E'
2. Sri Nil Kanta Sinha: Scientific Assistant 'D'
3. Sri Gobinda Pal: Scientific Assistant 'C'
4. Shri Sujoy Halder: Scientific Assistant 'B'

5. Sri Subha Sankar Kundu: Technician 'G'
6. Sri Arup Polley: Technician 'G'
7. Sri Asok Kumar Das: Technician 'G'
8. Sri Sisir Kumar Mondal: Technician 'E' (Structural Draftsman)
9. Sri Sunil Murmu: Technician 'C'
10. Sri Subir Modak: Superintendent
11. Sri Samir Kr. Chakraborty: Caretaker (Mali)
12. Sri Dulal Dey: Helper 'E' (Mali)
13. Sri Shyamal Kr. Bose: Helper 'E'

Building Maintenance (Electrical)

Prof. P. M. G. Nambissan: Chairman, BM(Electrical) Com.

1. Sri Debi Prasad Ghosh: Engineer 'G'
2. Sri Paresh Ch. Majumdar: Scientific Assistant 'E'
3. Sri Swapan Kr. Mandal: Scientific Assistant 'D'
4. Sri Somenath Ghosh: Scientific Assistant 'D'
5. Sri Saral Guha: Technician 'G'
6. Sri Kali Kanto Dey: Technician 'G'
7. Sri Madhusudan Kaity: Technician 'G'
8. Sri Asok Kr. Majumdar: Technician 'E'
9. Sri Kalyan Paul Roy: Technician 'D'
10. Sri Gautam Kr. Sabui: Technician 'C'
11. Sri Pratap Dhanuk: Technician 'C'
12. Sri Dilip Kr. Chakraborty: Technician 'C'
13. Sri Jai Prakash Tiwari: Technician 'C'
14. Sri Jagannath Mondal: Technician 'C'
15. Sri Mahendra M. Khapekar: Technician 'C'
16. Sri Dilip Ram: Helper 'E'
17. Sri Bijay Ram: Helper 'C'
18. Sri Sankar Adhikari: Helper 'C'

Workshop

Prof. Manabendra Mukherjee: Professor 'F' & Chairman
 1. Dr. Jisnu Basu: Engineer 'F' & Officer-In-Charge

2. Sri Asit Kr. Mondal: Technician 'H'
3. Sri Sadananda Dutta: Technician 'G'
4. Sri Ramen Jana: Technician 'G'
5. Sri Sudipta Barman: Scientific Assistant 'C' (Fitter)
6. Sri Narayan Chandra Dey: Scientific Assistant 'C'(CNC Operator)
7. Sri Debasish Sen: Technician 'G'
8. Sri Supriya Mondal: Technician 'G'
9. Sri Biplab Kr. Dey: Technician 'E'
10. Sri Partha Sarathi Karmakar: Technician 'F' (Turner)
11. Sri Tarun Tapan Biswas: Technician 'E' (Fitter)
12. Sri Gopal Kr. Chatterjee: Technician 'E'(Eng.Stores)
13. Sri Ramkrishna Roy: Technician 'E' (Machinist)
14. Sri Bhairab Ch. Nath: Technician 'D' (Mil. Fitter)
15. Sri Sunil Das: Technician 'D' (Mil. Fitter)
16. Sri Durlav Tudu: Technician 'D' (Turner)
17. Sri Subrata Baidya: Technician 'D' (Machinist)
18. Sri Sadip Patra: Technician 'D' (Welder)
19. Sri Himadri Chakraborty: Technician 'D' (Machinist)
20. Sri Subal Ch. Bindi: Technician 'C'
21. Sri C. Palanivel: Technician 'C' (Glass Blower)
22. Sri Adhir Sarkar: Technician 'B'
23. Sri Santosh Kr. Barman: Caretaker
24. Sri Deb Prasad Sardar: Helper 'E'
25. Sri Gopal Das: Helper 'C'

Administrative Departments

Establishment

1. Sri Suchintya Kumar Gupta: Establishment Officer
2. Sri Alok Mitra: A.A.O.(Establishment)
3. Sri Prasanta Kr. Das: A.A.O.
4. Smt. Chandana Basu: A.A.O.
5. Sri Biswajit Dutta: Accountant
6. Shri Subhendu Naskar: Lower Division Clerk
7. Sri Subhash Ch. Gayen: Technician 'B'

Despatch

1. Smt. Chandana Mitra: Sr. Superintendent
2. Sri Tapan Chakraborty: A.A.O.
3. Sri Swadesh Ch. Deb: Upper Division Clerk
4. Sri Tarak Nath Bhattacharya: Technician 'B'
5. Sri Gouri Sankar Singh: Driver - V
6. Shri Pintu Ram: Helper 'C'

Accounts

1. Sri Niladri Sanyal: Dy. Controller of Accounts
2. Shri Ved Prakash Mishra: Accounts Officer
3. Sri Asit Ranjan Deb: A.A.O.(Bills)
4. Sri Tapan Kr. Bhattacharyya: Sr.Superintendent
5. Sri Goutam Ghosh: Superintendent
6. Shri Nand Kishor Gond: Lower Division Clerk
7. Shri Pourjok Majumder: Lower Division Clerk
8. Shri Manoj Lakra: Lower Division Clerk
9. Sri Biswanath Paul: Helper 'E'
10. Shri Pradip Ram: Asst. Halwai-cum-cook

Accounts (Budget & Audit)

1. Sri Mrityunjoy Dey: A.O.(Accounts)
2. Sri Somnath Sarkar: A.A.O.(Cash)
3. Sri Pradip Dutta Sharma: Lower Division Clerk

Accounts (Cash)

1. Sri Swarup Kr. Bose: A.A.O.
2. Shri Raghunath Naskar: Superintendent
3. Sri Avijit Saha: Upper Division Clerk
4. Smt. Seethalakshmi Rath: Superintendent
5. Sri Sanat Kumar Kotal: Technician 'B'
6. Sri Kartick Hari: Helper 'E'

Accounts (Salary)

1. Sri Rammohan Moitra: A.A.O.(Salary)
2. Sri Ashoke Maity: Sr. Superintendent
3. Sm. Nirupama Halder: Superintendent
4. Smt. Monika Bhattacharya: Lower Division Clerk
5. Sri Madhu Bose: Helper 'E'

Accounts (PF & Pension)

1. Sri Niranjan Sarkar: A.A.O.(PF & Pension)
2. Sri Ranjit Dutta: A.A.O.
3. Sri Pradip Kr. Das: Driver - V

Purchase

1. Smt. Seema Bhattacharyya: A.O.-III & Off.-In-Charge of Purchase Cell

Purchase (Domestic Cell)

1. Sri Sanjoy Chakraborty: A.P.O.(Purchase-Domestic)
2. Sri Gautam Das: Superintendent
3. Sri Ajoy Kumar Biswas: Superintendent
4. Ms. Rekha Ram: Upper Division Clerk
5. Sri Asim Halder: Superintendent
6. Sri Ashoke Kr. Roy: Technician 'A'

Purchase (Foreign Cell)

1. Sri J.S. Raychaudhuri: A.P.O.(Purchase-Foreign)
2. Sri Debasish Das: A.A.O.
3. Sri Sankar Nath Dewan: Sr. Superintendent
4. Sri Ranjit Roy: Superintendent
5. Mr. James Wilson Keretta: Lower Division Clerk
6. Sri Gour Hari Das: Helper 'E'

Stores

1. Sri Shyamal Ch. Biswas: Superintendent
2. Sri Ramesh Hari: Helper 'C'

Medical Unit

- Prof. Abhijit Chakrabarti: Chairman, MAC
1. Dr. Sumalay Kar: Part-time Attending Physician
 2. Dr. Arup Kumar Sahu: Part-time Attending Physician

3. Smt. Dipali Saha: Sr. Superintendent
4. Sri Gautam Dutta: Technician 'E'
5. Sri Gobinda Chakraborty: A.A.O.
6. Sri Dipak Kr. Das: Superintendent
7. Smt. Chandana Nayak: Lower Division Clerk
8. Shri Abhishek Pal: Lower Division Clerk
9. Sri Nabin Kumar Halder: Technician 'B'

Telephone

- Prof. (Smt.) Samita Basu: Prof. & In-Charge
1. Smt. Sunanda Chakraborty: Technician 'G'
 2. Smt. Bithi Biswas: Technician 'E'
 3. Smt. Pampa Bhattacharjee: Technician 'D'

Auditorium Management Section

- Smt. Seema Bhattacharyya: Officer-In-Charge
1. Sri Sushanta Chakraborty: Scientific Assistant-E

Security

1. Sri Supriya Gangopadhyay: Sr.Security Officer
2. Sri Ratan Kr. Bose: Security Officer
3. Sri Tapas Kr. Dalal: Security Officer
4. Sri Swaraj Nath Sarkar: Security Officer
5. Sri Ashok Kr. Singh: Security Supervisor 'B'
6. Sri Ganesh Prasad Sharma: Security Supervisor 'B'
7. Sri Tarak Chandra Nath: Security Supervisor-A
8. Sri Gobinda Ch. Roy: Lower Division Clerk
9. Sri Balli Rana: Technician 'A'
10. Sri Dukha Krishna Reddy: Technician 'A'
11. Sri Subrata Kr. Chowdhury: Technician 'A'
12. Sri P.B. Thapa: Helper 'E' (Watchman)
13. Sri Joyram Murmu: Helper 'E' (Watchman)
14. Sri Madhusudan Bhakta: Helper 'E' (Watchman)
15. Sri Sudhangsu Sekhar: Mondal Helper 'D' (Watchman)
16. Sri Swapan Mukherjee: Helper 'D'
17. Sri Mongol Oraon: Helper 'D' (Watchman)
18. Sri Sibub Oraon: Helper 'C' (Watchman)
19. Sri Tapan Kr. Sinha: Helper 'C' (Watchman)
20. Sri Sudhir Kr. Debnath: Helper 'C' (Watchman)
21. Md. Manayar Hasan Mondal: Technician 'A'
22. Sri Ranjit Kr. Roy: Helper 'C' (Watchman)
23. Sri Arun Kumar Dutta: Helper 'B' (Watchman)
24. Sri Pran Gopal Das: Helper 'C' (Watchman)
25. Sri Gopal Chandra Saren: Helper 'C' (Watchman)

Security (Cosmetic)

1. Sri Badal Hari: Helper 'E' (Sweeper)
2. Sri Sakhi Chand Hari: Helper 'E' (Sweeper)
3. Sri Banarshi Mallick: Helper 'E' (Sweeper)
4. Sri Siblal Hari: Helper 'D' (Sweeper)
5. Smt. Anjali Hari: Helper 'C' (Sweeper)
6. Sri Gobinda Ch. Das: Helper 'C' (Sweeper)
7. Sri Santosh Hari: Helper 'C' (Sweeper)
8. Sri Ashok Mallick: Helper 'C'
9. Sri Kala Chand Hela: Helper 'C' (Sweeper)
10. Sri Amit Hari: Helper 'A'

11. Sri Gangadhar Maity: Tech 'E' (Supervisor Mali)
12. Sri Sushil Kr. De: Helper 'E' (Mali)
13. Sri Santosh Kr. Sarkar: Helper 'E' (Mali)
14. Sri Kamala Kanta Sarkar: Helper 'E' (Mali)
15. Sri Santosh Kr. Bachar: Helper 'E' (Mali)
16. Sri Swapan Kr. Mondal: Helper 'E' (Mali)
17. Sk. Mostakin: Helper 'C'

Transport

- Prof. Subrata Banerjee: Chairman, Transport Committee
- Sri Kaushik Chatterjee: Officer-in-Charge, Transport Sec.
1. Sri Dharmendra Prasad: Scientific Assistant-C
 2. Sri Aloke Kr. Sarkar: Transport Supervisor & Driver - V
 3. Sri Swapan Kumar Mondal: Technician 'G'
 4. Sri Trinath Maharana: Technician 'F' (Vehi.Mech.)
 5. Sri Surai Mandi: Technician 'C' (Vehi.Mech.)
 6. Sri Kanai Lal Malakar: Technician 'C'
 7. Sri Tarak Nath Ghosh: Driver - IV
 8. Sri Dilip Baidya: Driver - IV
 9. Sri Madhusudan Mondal: Driver - IV
 10. Sri Gopal Ch. Ghosh: Driver - III
 11. Sri Uttam Kr. Roy: Driver - III
 12. Sri Kartick Ch. Pal: Driver - III
 13. Sri Prabir Kr. Mistri: Driver - III
 14. Sri Prabir Biswas: Driver - II
 15. Sri Asit Kr. Mahapatra: Technician 'B'
 16. Sri Mongol Ch. Mondal: Helper 'E'
 17. Sri Sankar Ram: Helper 'C'

Guest House & Hostel

- Prof. Sukalyan Chattopadhyay: Prof.-in-Charge, Guest House & Hostel, SINP Housing Com.(MSA-II)"
- Prof. Nihar Ranjan Ray: Prof.-In-Charge, Guest House & Hostel, Salt Lake Campus (MSA-I)"
1. Shri Ramesh Singh: Helper 'C'
 2. Sri Somenath Das: Helper 'C'
 3. Smt. Suro Mahato: Helper 'C' (Sweeper)
 4. Sri Suresh Ch. Das: Asst. Halwai-cum-cook
 5. Sri Sakti Pada Bisui: Asst. Halwai-cum-cook

Canteen (Salt Lake Campus)

- Prof. Dhananjay Bhattacharyya: Chairman, Canteen Committee
1. Sri Ashok Roy: Asstt. Manager-cum-Storekeeper
 2. Sri Prabhat Maity: Halwai-cum-cook
 3. Sri Kartick Ch. Maity: Asst. Halwai-cum-cook
 4. Sri Sujan Ch. Mistri: Asst. Halwai-cum-cook
 5. Sri Shankar Andia: Asst. Halwai-cum-cook
 6. Sri Sailen Halder: Bearer-II
 7. Sri Nema Ch. Das: Bearer-II
 8. Sri Amar Das: Bearer-II
 9. Sri Barun Kr. Barua: Bearer-II
 10. Sri Subodh Kr. Pradhan: Bearer-I
 11. Sri Sunil Ram: Bearer

9.3 List of Retirement: 2011-2012

<i>Sl No</i>	<i>Name</i>	<i>Division/Section</i>	<i>Date of Retirement</i>
1	Sri D. N. Debnath	Wks	30.04.2011
2	Sri Sukumar Kundu	Wks	30.04.2011
3	Dr. P. K. Sengupta	Biophysics	30.06.2011
4	Sri Dulal Ch. Das	EWf	31.07.2011
5	Dr. (Smt.) Radha Bhattacharya	Biophysics	31.07.2011
6	Sri K. P. Panja	BM(E)	31.08.2011
7	Sri Rajeswar Seal (Roy)	T.U.	31.08.2011
8	Dr. S. N. Das	ECMP	30.11.2011
9	Prof. Asok Sen	TCMP	30.11.2011
10	Dr. B. B. Bal	Teaching	30.11.2011
11	Sri B. K. Mallick	P&D	31.12.2011
12	Sri M. B. Das	N&AP	31.12.2011
13	Dr.(Mrs.) C. Samanta	N&AP	31.12.2011
14	Prof. Sudeb Bhattacharyya	N&AP	31.12.2011
15	Sri Shankar Panda	Canteen	31.01.2012
16	Dr. Suwendu Bose	EWf	31.01.2012
17	Dr. K. K. Bardhan	ECMP	31.01.2012
18	Prof. Gautam Ghosh	Theory	29.02.2012
19	Sri N. C. Sarkar	N&AP	29.02.2012
20.	Sri Sujit Kr. De	BM(E)	31.03.2012

9.4 Voluntary Retirement: 2011-2012

<i>Sl No</i>	<i>Name</i>	<i>Division/Section</i>	<i>Date of Retirement</i>
1.	Sri H. B. Dhar	Wks	02.05.2011
2.	Sri P. S. Bhattacharya	TCMP	01.01.2012

9.5 List of Demise: 2011-2012

<i>Sl No</i>	<i>Name</i>	<i>Division/Section</i>	<i>Died on</i>
1.	Late A. K. Nayak	TCMP	15.06.2011
2.	Late Avedananda Bhattacharya	MED	30.06.2011
3.	Late K. N. Prasad	T.U.	24.09.2011

9.6 Audited Accounts

SAHA INSTITUTE OF NUCLEAR PHYSICS

Balance Sheet as at 31st March, 2012

	Schedule	2011-12	2010-11
CAPITAL FUND & LIABILITIES			
CAPITAL FUND	1	447050420.38	471,596,119.37
CAPITAL RESERVE	2	7116996.30	7,116,996.30
EARMARKED FUNDS	3	28407395.00	24,285,445.00
CURRENT LIABILITIES AND PROVISIONS	4	2880426010.92	2,652,865,831.69
TOTAL		3363000822.60	3155864392.36
ASSETS			
FIXED ASSETS			
Gross Block	5	3371943886.26	2,781,459,183.90
Less : Accumulated Depreciation	5	1339150305.66	1060751456.38
		2032793580.60	1720707727.52
INVESTMENT	6	20824200.00	370908556.00
CURRENT ASSETS, LOANS & ADVANCES	7	1309383042.00	1064248108.84
TOTAL		3363000822.60	3155864392.36
SIGNIFICANT ACCOUNTING POLICES	15		
CONTINGENT LIABILITIES AND NOTES ON ACCOUNTS	16		

The Schedules referred to above form part of these Accounts

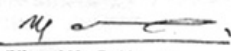

(V. P. Mishra)
Accounts Officer


(N. Sanyal)
Dy. Controller of Accounts


(V.V. Mallikarjuna Rao)
Registrar

In terms of our attached Report of even date
For Nemani Garg Agarwal & Co
CHARTERED ACCOUNTANTS


(Milan K. Sanyal)
Director


(Nirmal Kr. Pal)
Partner
Membership No. 11277
135, B R Basu Road,
2nd Floor, Kolkata - 700001
Dated :- 17th September, 2012




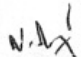
SAHA INSTITUTE OF NUCLEAR PHYSICS

Income & Expenditure Account for the year ended 31st March, 2012

	<u>Schedule</u>	<u>2011-12</u>	<u>2010-11</u>
INCOME :-			
Income from Sales/Services	8	735190.00	595260.00
Grants	9	465910761.25	694193494.78
Interest Earned	10	57279374.00	16410804.00
Other Income	11	3984941.00	4513072.00
Excess of Expenditure over Income transferred to Capital Fund		620870831.35	516591414.30
		<u>1148781097.60</u>	<u>1232304045.08</u>
EXPENDITURE :-			
Establishment Expenses	12	641413051.00	807647602.00
Administrative Expenses	13	228938319.32	210688498.78
Interest/Bank charges	14	30878.00	52893.00
Depreciation	5	278398849.28	213915051.30
		<u>1148781097.60</u>	<u>1232304045.08</u>


The Schedules referred to above form part of these Accounts


(V. P. Mishra)
Accounts Officer


(N. Sanyal)
Dy. Controller of Accounts


(V.V. Mallikarjuna Rao)
Registrar

In terms of our attached Report of even date
For Nemani Garg Agarwal & Co
CHARTERED ACCOUNTANTS


(Nirmal Kr. Pal)
Partner
Membership No. 11277
135, B R Basu Road,
2nd Floor, Kolkata - 700001
Dated :- 17th September, 2012




(Milan K. Sanyal)
Director

SAHA INSTITUTE OF NUCLEAR PHYSICS

Receipts & Payments Account for the year ended 31st March, 2012

Receipts	2010-11	2011-12	Payments	2010-11	2011-12
Opening Balance b/f :-					
Cash in hand	409,422.00	198,788.00	Establishment Expenses	424,330,602.00	499,997,051.00
Current Account Balances	268,304,075.73	418,018,075.30	Administrative Expenses	208,667,335.78	226,093,003.32
Grant-in-aid received from DAE :-			Bank Charges	52,893.00	30,878.00
Recurring	469,000,000.00	587,700,000.00	Assets	435,020,801.65	590,484,702.36
Non-Recurring	700,000,000.00	514,200,000.00	Expenses paid for ongoing projects of other agencies	93,762,932.21	100,300,489.80
Grant received from other agencies			HBA & Other Advances paid	1,083,630.00	1,267,166.00
for on going projects	332,800,445.00	119,296,672.14	Investment	158,450,108.00	4,915,644.00
HBA & Other Advance recovery	3,764,574.00	3,614,089.00	Margin Money deposit	292,069,396.00	506,103,600.00
Realisation of Margin Money Deposit	234,767,306.21	551,613,770.00	Other Deposit	348,500.00	211,500.00
Realisation from other Deposit		355,000,000.00	Advances paid		57,347,015.93
Realisation of other advances	6,284,804.00		Last Year's provision paid	6,574,842.00	2,009,267.00
Interest Received	16,410,804.00	57,279,374.00	Last Year's current liabilities paid	1,737,513.00	
Income Receipts	5,108,332.00	4,720,131.00	Closing Balance c/f :-		
Current Liabilities		23,916,337.00	Cash in hand	198,788.00	68,284.00
Pension Fund Receipts	3,465,654.00	5,462,176.00	Current Account Balances	418,018,075.30	652,190,811.03
	<u>2,040,315,416.94</u>	<u>2,641,019,412.44</u>		<u>2,040,315,416.94</u>	<u>2,641,019,412.44</u>

(Signature)
(V. P. Mishra)

Accounts Officer

(Signature)
(N. Sanyal)

Dy. Controller of Accounts

(Signature)
(V.V. Mallikarjuna Rao)

Registrar

(Signature)
(Milan K. Sanyal)

Director

In terms of our attached Report of even date
For Nemani Garg Agarwal & Co
CHARTERED ACCOUNTANTS

(Signature)

(Nirmal Kr. Pal)

Partner

Membership No. 11277

135, B R Basu Road, 2nd Floor, Kolkata 700001

Dated :- 17th September, 2012



9.7 Purchase Section

Order Placed by Purchase Section

Year	Domestic Order
2011-12	1163
Year	Foreign Order
2011-12	209

Chapter 10

External Collaborators

- A Priyant*, Indian School of Mines, Dhanbad, India
Abada, Asmaa, Laboratoire de Physique Thrique, Universitde Paris-sud 11, Biment 210, 91405 Orsay Cedex, France
Adak, Laksmikanta, IACS, Dept Organ Chem, Calcutta-700032
Alzamora, M, Centro Brasileiro de Pesquisas Ficas, Rua Xavier Sigaud, Rio de Janeiro, RJ, Brazil
Amenitsch, H, Austrian Acad Sci, Inst Biophys & Nanosyst Res, A-8042 Graz, Austria
Arumugam, S, Center for High Pressure Research, School of Physics, Bharathidasan University, Tiruchirappalli 620 024
Ayyer, A, CEA Saclay, Inst Phys Theor, IPhT, F-91191 Gif Sur Yvette, France
B Chatterjee, Kalpana Chawla Centre for Space and Nano Sciences, Kolkata
Balasubramanian, T, Lund Univ, MAXLAB, S-22100 Lund, Sweden
Ballofa, J, Institut fr Kernchemie, Johannes Gutenberg-Universitt Mainz, 55099 Mainz, Germany
Bandyopadhyay, Abhijit, Department of Physics, RKM Vivekananda University, Belur Math, Howrah 711202
Bandyopadhyay, Debashree, ASTAR, Bioinformat Inst, Singapore 138671, Singapore
Bangal, Prakriti Ranjan, Indian Inst Chem Technol, Inorgan & Phys Chem Div, Hyderabad 500607
Barma, Mustansir, Department of Theoretical Physics, TIFR, Homi Bhabha Road, Mumbai
Basu, Tanmoy, Inst Phys, Bhubaneswar 751005, Orissa
Bedi, SC, Rayat-Bahra Group, 126-127, Sector 34, Chandigarh 160022
Behera, Bivash, Department of Physics, Panjab University, Chandigarh
Bhattacharjee, A, Department of Physics, Visva-Bharati University, Santiniketan, India
Bhattacharjee, Ashis, Visva Bharati Univ, Dept Phys, Santini Ketan 731235, India
Bhattacharya, Dipten, CSIR, Cent Glass & Ceram Res Inst, Nanostruct Mat Div, Kolkata-700032
Bhattacharya, Madhubrata, Department of Physics, Univ of Calcutta, Kolkata-700009
Bhattacharya, Sayan, Univ Calcutta, Dept Environm Sci, Calcutta-700019
Bhattacharyya, Manjit K, Cotton Coll, Dept Chem, Gauhati 781001
Bhattacharjee, Biplob, Department of Theoretical Physics, TIFR, Mumbai-400005
Bhowmik, Asit, W Bengal Pollut Control Board, Kolkata
Bhowmik, RN, Department of Physics, Pondicherry University, Pondicherry-605014
Biswas, Maitree, Department of Biotechnology, St Xavier's College, Kolkata-700 016
Bora, Sanchay J, Gauhati Univ, Dept Chem, Gauhati 781014
Borderie, B, Institut de Physique Nuclire, CNRS/IN2P3, UniversitParis-Sud 11, Orsay, France
Botha, AJ, Laboratory for Microscopy and Microanalysis, University of Pretoria, South Africa
Brüchleb, W, GSI Helmholtzzentrum fr Schwerionenforschung GmbH, 64291 Darmstadt, Germany
Carlen, EA, Rutgers State Univ, Dept Math, Piscataway, NJ 08854 USA
Chakrabarti, Arunava, Univ Kalyani, Dept Phys, Kalyani 741235, India
Chakrabarti, Omprakash, Non-Oxide Ceramics and Composite Division, CGCRI, Kolkata-700032
Chakraborty, Purnendu, Phys Res Lab, Ahmadabad 380009, India
Chatterjee, Arnab, Abdus Salam Int Ctr Theoret Phys, CMSP Sect, I-34014 Trieste, Italy
Chattopadhyay, Dhruvajyoti, BC Guha Ctr Genet Engr & Biotechnol, Calcutta-700019
Chernyatin, V, Brookhaven Natl Lab, Dept Phys, Upton, NY 11973 USA
Choudhury, Ananyo, Dept of Biophys, Mol Biol & Bioinformatics, Univ of Calcutta, Kolkata-700009
Choudhury, P, Central Glass and Ceramic Research Institute, Kolkata-700032
Chowdhury, PS, Ctr Variable Energy Cyclotron, Kolkata-700064
Chowdhury, Subhajit, W Bengal Pollut Control Board, Kolkata
Conder, Kazimierz, Laboratory for Developments and Methods, Paul Scherrer Institute, CH-5232 Villigen, Switzerland
D Pramanik, Bengal Engineering and Science University, Shibpur, W Bengal, India
Das, Birinchi K, Gauhati Univ, Dept Chem, Gauhati 781014
Das, Debottam, Laboratoire de Physique Thrique, Universitde Paris-sud 11, Biment 210, 91405 Orsay Cedex, France
Dasgupta, Brahmananda, Univ Alabama, Ctr Space Plasma & Aeron Res, Huntsville, AL 35805 USA
Dasgupta, Jhimli, Dept of Biotech, St Xavier's College, Kolkata-700016
Das, NC, Applied Spectroscopy Division, BARC, Mumbai-400085
De Martino, Daniele, Int Sch Adv Studies SISSA, I-34136 Trieste, Italy
Deng, Guochu, Laboratory for Developments and Methods, Paul Scherrer Institute, CH-5232 Villigen, Switzerland
Devarajan, U, Center for High Pressure Research, School of

- Phys, Bharathidasan University, Tiruchirappalli 620 024
Dey, A, Ctr Variable Energy Cyclotron, Calcutta-700064
Dey, Sanjay, SRM Univ, Dept Bioinformat, Madras 600089
Dey, S, Centre for Astroparticle Physics and Space Science, Bose Institute, Kolkata-700091
Dhar, Deepak, Department of Theoretical Physics, TIFR, Mumbai-400005
Digal, S, Inst Math Sci, Madras 600113, Tamil Nadu, India
Doert, Th, Institut fr Anorganische Chemie, Technische Universit Dresden, Helmholtzstrasse 10, D-01062 Dresden, Germany
Dutta, Manjistha, Jadavpur Univ, Dept Instrumentat Sc, Calcutta 700032
Emmanuel, N Saridakis, Univ Athens, Dept Phys, GR-15771 Athens, Greece
Evena, J, Institut fr Kernchemie, Johannes Gutenberg-Universitt Mainz, 55099 Mainz, Germany
Falomir, H, Univ Nacl La Plata, Fac Ciencias Exactas, Dept Fis, IFLP, CONICET, RA-1900 La Plata, Argentina
Fontes, MB, Centro Brasileiro de Pesquisas Ficas, Rua Xavier Sigaud, Rio de Janeiro, RJ, Brazil
Forsberg, U, Lund Univ, S-22100 Lund, Sweden
Gambo, J, Univ Nacl La Plata, Fac Ciencias Exactas, Dept Fis, IFLP, CONICET, RA-1900 La Plata, Argentina
Ganesan, V, UGC-DAE Consortium for Scientific Research, University Campus, Khandwa Road, Indore 452017
Gangopadhyay, D, SN Bose Natl Ctr Basic Sci, Calcutta 700098
Gangopadhyay, G, Department of Physics, University of Calcutta, Kolkata-700009
Ganguly, O, SN Bose Natl Ctr Basic Sci, Calcutta-700098
Ganguly, S, Chandernagore Coll, Dept Phys, Chandernagore 712136, Hooghly, India
Garg, Ritika, Department of Physics & Astrophysics, University of Delhi, Delhi
Garg, Sandeep Kumar, Inst Phys, Bhubaneswar 751005, Orissa
Gayathri, N, Ctr Variable Energy Cyclotron, Calcutta 700064
Gehlot, J, Inter University Accelerator Center, New Delhi
Geraci, E, INFN, Sezione di Catania, Italy
Ghosh, Uday Chand, Presidency Univ, Dept Chem, Calcutta 700073
Giglia, Angelo, TASC INFN Natl Lab, Trieste, Italy
Giri, SK, Indian Inst Technol, Dept Phys & Meteorol, Kharagpur-721302, India
Golda, KS, Inter University Accelerator Center, New Delhi
Golubev, P, Lund Univ, S-22100 Lund, Sweden
Govindarajan, TR, Inst Math Sci, Madras 600113, Tamil Nadu, India
Goyal, Savi, Department of Physics & Astrophysics, University of Delhi, Delhi
Grabowski, Slawomir J, Basque Fdn Sci, Bilbao 48011, Spain
Greiner, Carsten, Goethe Univ Frankfurt, Inst Theoret Phys, D-60438 Frankfurt, Germany
Greiner, Walter, Frankfurt Institute for Advanced Studies (FIAS), JW Goethe Universit, Ruth Moufang Strasse, Germany
Grote, Wiebke, X-ray Diffraction Laboratory, Department of Geology, University of Pretoria, South Africa
Gupta, Ajay, UGC-DAE Consortium for Scientific Research, University Campus, Khandawa Road, Indore, India
Gupta, Kaushik, Presidency Univ, Dept Chem, Calcutta 700073, India
Gupta, Shamik, Department of Theoretical Physics, TIFR, Homi Bhabha Road, Mumbai
Gupta, Tribikram, Flat-2A, Sharad Apartment, 142A NSC Bose Road, Kolkata-700040
Hegde, Ramanujan S, Eunice Kennedy Shriver Natl Inst Child Hlth & Hum, Cell Biol & Metab Program, NIH, Bethesda, MD 20892 USA
Hering, EN, Centro Brasileiro de Pesquisas Ficas, Rua Xavier Sigaud, Rio de Janeiro, RJ, Brazil
Hinrichsen, Haye, Univ Wurzburg, Fak Phys & Astron, D-97074 Wurzburg, Germany
Hlatshwayo, TT, Physics Department, University of Pretoria, South Africa
Hofmeister, W, Institut fr Geowissenschaften der Universit, Mainz, Germany
Hollenberg, Sebastian, Tech Univ Dortmund, Fak Phys, D-44221 Dortmund, Germany
Jemetio, JPF, Institut fr Anorganische Chemie, Technische Universit Dresden, Helmholtzstrasse 10, D-01062 Dresden, Germany
Jhingan, A, Inter University Accelerator Center, New Delhi, India
Maiti, Jyotirmoy, Department of Physics, Barasat Government College, Barasat, Kolkata 700124
Kalkal, Sunil, Department of Physics & Astrophysics, University of Delhi, Delhi
Kanjilal, D, Interuniv Accelerator Ctr, Delhi 110067
Karmakar, B, Univ Burdwan, Dept Phys, Burdwan 713104, W Bengal, India
Khan, Manoranjan, Jadavpur Univ, Dept Instrum Sci, Calcutta 700032
Khastgir, SP, Indian Inst Technol, Dept Phys & Meteorol, Kharagpur 721302, W Bengal, India
Kumar, MC, Regional Centre for Accelerator-based Particle Physics, Harish-Chandra Research Institute, Allahabad-211019
Kumar, P Hemant, Indian Inst Chem Technol, Inorgan & Phys Chem Div, Hyderabad-500607
Kundu, Sarathi, Physical Sciences Division, Institute of Advanced Study in Sc & Tech, Vigyan Path, Paschim Boragaon, Garchuk, Guwahati, Assam 781035
Kundu, Souvik, Indian Inst Technol, Ctr Mat Sci, Kharagpur 721302, India
Roy, Sandipta, Indian Inst Technol, Ctr Mat Sci, Kharagpur-721302, India
Banerji, P, Indian Inst Technol, Ctr Mat Sci, Kharagpur 721302, India
Shripathi, T, UGC DAE Consortium Sci Res, Indore 452001, India
Kusz, J, Institute of Physics, University of Silesia, Katowice, Poland
Lahiri, Ansuman, Dept of Biophys, Mol Biol & Bioinformatics, Univ of Calcutta, Kolkata-700009
Lanke, Srinivasa Rao, Indian Inst Chem Technol, Inorgan & Phys Chem Div, Hyderabad 500607, India
Lebowitz, JL, Rutgers State Univ, Dept Math, Piscataway, NJ 08854 USA
Lu, JX, Interdisciplinary Center for Theoretical Study, University of Sc and Tech of China, Hefei, Anhui 230026, China
Maccherozzi, Francesco, Diamond Light Source, Harwell Science and Innovation Campus, Didcot, Oxfordshire OX11
Madhavan, N, Inter University Accelerator Center, New Delhi, India
Mahne, Nicola, TASC INFN Natl Lab, Trieste, Italy
Maiti, Prabal K, Indian Inst Sci, Ctr Condensed Matter Theory, Bangalore-560012, India
Maiti, Santanu K, Tel Aviv Univ, Sch Chem, IL-69978 Tel Aviv, Israel
Maiti, Anvesha, Non-Oxide Ceramics and Composite Division, CGCRI, Kolkata-700032
Malherbe, Johan B, Physics Department, University of Pretoria, South Africa
Mandal, Haradhan, Department of Physics, Visva-Bharati University, Santiniketan, India
Mandal, S, Department of Physics & Astrophysics, University

- of Delhi, Delhi, India
Marsili, Matteo, Abdus Salam Int Ctr Theoret Phys, CMSP Sect, I-34014 Trieste, Italy
Martinez, Mauricio, Univ Santiago de Compostela, Dept Fis Particulas, E-15782 Santiago De Compostela, Galicia, Spain
Martin, X, Univ Tours, UFR Sci & Tech, LMPT, F-37200 Tours, France
Maskey, Shila, Inha Univ, Dept Chem, Inchon 402751, South Korea
Meljanac, S, Rudjer Boskovic Inst, HR-10002 Zagreb, Croatia
Mendez, F, Departamento de Fica, Universidad de Santiago de Chile, Casilla 307, Santiago, Chile
Micu, Octavian, Inst Space Sci, RO-077125 Bucharest, Romania
Mishustin, Igor N, FIAS, JW Goethe Universit, Ruth Mofang Strasse 1, 60438 Frankfurt am Main, Germany
Mohanto, Gayatri, Inter University Accelerator Center, New Delhi, India
Mondal, Parthasarathi, Nanostructured Materials Division, CGCRI, Kolkata 700032
Mukhawana, Mxolisi B, Physics Department, University of Pretoria, South Africa
Mukherjee, P, Ctr Variable Energy Cyclotron, Calcutta 700064, India
Mukherjee, Rajarshi, Department of Physics, The University of Burdwan, Burdwan 713104, India
Mukherjee, Sanjoy, Univ Burdwan, Dept Phys, Burdwan 713104, India
Mukhopadhyay, Aniruddha, Univ Calcutta, Dept Environm Sci, Kolkata-700019, India
Mukhopadhyay, Ujjal, W Bengal Pollut Control Board, Kolkata, India
Murugeswari, A, Center for High Pressure Research, School of Physics, Bharathidasan University, Tiruchirappalli 620 024, India
Nannarone, Stefano, TASC INFM Natl Lab, Trieste, Italy
Nares, N, Department of Physics, Pondicherry University, Pondicherry-605014, India
Nath, TK, Indian Inst Technol, Dept Phys & Meteorol, Kharagpur 721302, India
Nikolopoulos, K, Univ Athens, Dept Phys, GR-15771 Athens, Greece
Pal, D, Maulana Azad Coll Retd, Calcutta 700013, India
Pal, Kausik, Serampore Coll, Dept Phys, Serampore 712201, India
Pal, M, Cent Mech Engn Res Inst, Council Sci & Ind Res, Durgapur 713209, India
Palit, R, Department of Nuclear and Atomic Physics, TIFR, Mumbai 400005
Panda, S, Indian Inst Technol, Ctr Theoret Studies, Kharagpur 721302, India
Pandey, Abhishek, SN Bose National Centre for Basic Sciences, Block-JD, Sector-III, Salt Lake, Kolkata
Pandya, S, UGC-DAE Consortium for Scientific Research, University Campus, Khandwa Road, Indore 452 017
Pankov, AA, The Abdus Salam ICTP Affiliated Centre, Technical University of Gomel, 246746 Gomel, Belarus
Paulose, PL, Tata Institute of Fundamental Research, Homi Bhabha Road, Colaba, Mumbai 400005, India
Paver, N, University of Trieste and INFN-Trieste Section, 34100 Trieste, Italy
Perez, Alejandro, Centre de Physique Thrique, Aix-Marseille Univ, CNRS UMR 6207, Univ Sud Toulon Var, 13288 Marseille, France
Pomjakushina, Ekaterina, Laboratory for Developments and Methods, Paul Scherrer Institute, CH-5232 Villigen, Switzerland
Prashanthi, Suthari, Indian Inst Chem Technol, Inorgan & Phys Chem Div, Hyderabad 500607, Andhra Pradesh
Qin, GY, McGill Univ, Dept Phys, Montreal, PQ H3A 2T8, Canada
Radheep, D Mohan, Center for High Pressure Research, School of Physics, Bharathidasan University, Tiruchirappalli-620024, India
Raduta, Ad R, Institut de Physique Nuclire, CNRS/IN2P3, UniversitParis-Sud 11, Orsay, France
Raja, SO, Department of Biochemistry, University of Calcutta, 35 BC Road, Kolkata-700019, India
Sardar, M, Material Science Division, Indira Gandhi Center for Atomic Research, Kalpakkam 603 102, India
Ramos, SM, Centro Brasileiro de Pesquisas Ficas, Rua Xavier Sigaud, Rio de Janeiro, RJ, Brazil
Rane, Neena S, Eunice Kennedy Shriver Natl Inst Child Hlth & Hum, Cell Biol & Metab Program, NIH, Bethesda, MD 20892 USA
Ranu, Brindaban C, Indian Assoc Cultivat Sci, Dept Organ Chem, Calcutta 700032
Rao, V Jayathirtha, Indian Inst Chem Technol, Organ Chem Div 2, Hyderabad 500607
Ravindran, V, Regional Centre for Accelerator based Particle Physics, Harish-Chandra Research Institute, Allahabad 211 019, India
Raychaudhuri, Sreerup, Department of Theoretical Physics, TIFR, 1 Homi Bhabha Road, Mumbai 400 005
Ray, Samriddhi Sankar, Univ Nice Sophia Antipolis, Lab Casiopee, Observ Cote dAzur, Ctr Natl Rech Sci, F-06304 Nice 4, France
Reddy, V Raghavendra, UGC-DAE Consortium for Scientific Research, University Campus, Khandawa Road, Indore
Reinhard, PG, Univ Erlangen Nurnberg, Inst Theoret Phys 2, D-91058 Erlangen, Germany
Ro, Chul-Un, Inha Univ, Dept Chem, Inchon 402751, South Korea
Roy, B, Univ Burdwan, Dept Phys, Burdwan 713104, W Bengal, India
Roychoudhury, Rajkumar, Indian Stat Inst, Calcutta 700108
Roy, Trina, St Xaviers Coll, PG Dept Biotechnol, Calcutta 700016
Ruppert, J, Goethe Univ Frankfurt, Inst Theoret Phys, D-60438 Frankfurt, Germany
Saha, Debasree, Indian Assoc Cultivat Sci, Dept Organ Chem, Calcutta 700032
Saitovitch, EMB, Centro Brasileiro de Pesquisas Ficas, Rua Xavier Sigaud, Rio de Janeiro, RJ, Brazil
Samsarov, A, Rudjer Boskovic Inst, HR-10002 Zagreb, Croatia
Sampathkumaran, EV, Tata Institute of Fundamental Research, Homi Bhabha Road, Colaba, Mumbai 400005, India
Sandal, Rohit, Department of Physics, Panjab University, Chandigarh, India
Santosh, Mogurampelly, Indian Inst Sci, Ctr Condensed Matter Theory, Bangalore 560012, Karnataka, India
Sarmiento, LG, Univ Nacl Colombia, Bogota 111321, Colombia
Sasidevan, V, Department of Theoretical Physics, TIFR, Homi Bhabha Road, Mumbai-400005
Scholten O, Kernfysisch Versneller Instituut, University of Groningen, NL-9747 AA Groningen, The Netherlands
Sehanobish, Esha, Univ Calcutta, Ballygunge Sci Coll, Dept Biochem, Kolkata
Sen, Arjan A, Jamia Millia Islamia, Ctr Theoret Phys, New Delhi 110025
Sen, Kamalika, Univ Calcutta, Dept Chem, Calcutta 700009, India
Sen, Pintu, Ctr Variable Energy Cyclotron, Dept Phys, Calcutta 700064

- Sengupta, K*, Centro Brasileiro de Pesquisas Ficas, Rua Xavier Sigaud, Rio de Janeiro, RJ, Brazil
- Sethi, J*, Department of Nuclear and Atomic Physics, TIFR, Mumbai 400005
- Shukla, Padma K*, Institute for Theoretical Physics, International Centre for Advanced Studies in Physical Sciences, Ruhr University Bochum, D-44780 Bochum, Germany
- Sil, Shreekantha*, Visva Bharati, Dept Phys, Santini Ketan 731235, India
- Singh, R*, AINST, Amity University, Noida, India
- Sinha, Om Prakash*, Amity Univ, Amity Inst Nanotechnol, Noida 201303, India
- Siva, D*, Indian Inst Chem Technol, Inorgan & Phys Chem Div, Hyderabad-500607, India
- Som, T*, Inst Phys, Bhubaneswar 751005, Orissa, India
- Sood, AK*, Indian Inst Sci, Dept Phys, Bangalore 560012, India
- Srivastava, Dinesh K*, Bhabha Atom Res Ctr, VECC, Calcutta 700064, India
- Sugathan, P*, Inter University Accelerator Center, New Delhi, India
- Theron, Christiaan C*, Physics Department, University of Pretoria, South Africa
- Thiyagarajan, R*, Center for High Pressure Research, School of Physics, Bharathidasan University, Tiruchirappalli 620 024, India
- Thoma, Markus H*, Max Planck Inst Extraterr Phys, D-85748 Garching, Germany
- Thomas, AW*, Centre for the Subatomic Structure of Matter (CSSM), School of Chemistry and Physics, University of Tomar, BS, BARC, Div Radiochem, Bombay-400085, India
- Torres, F*, Departamento de Fica, Universidad de Santiago de Chile, Casilla 307, Santiago, Chile
- Trivedi, T*, Department of Nuclear and Atomic Physics, Tata Institute of Fundamental Research, Mumbai 400005, India
- Tsytrinov, AV*, The Abdus Salam ICTP Affiliated Centre, Technical University of Gomel, 246746 Gomel, Belarus
- Kumar, Uday*, Department of Physical Sciences, IISER Kolkata, Mohonpur 741252, India
- Uphoff, Jan*, Goethe Univ Frankfurt, Inst Theoret Phys, D-60438 Frankfurt, Germany
- van der Berg, NG*, Physics Department, University of Pretoria, South Africa
- Veenhof, R*, Univ Wisconsin, Dept Phys, Madison, WI 53706 USA
- Venugopal, V*, VIT Univ, Div Phys, Sch Adv Sci, Madras 600048, India
- Verma, Shashi*, Department of Physics & Astrophysics, University of Delhi, Delhi, India
- Vogler, Erwin A*, Penn State Univ, Dept Mat Sci & Engr, University Pk, PA 16802 USA
- Wang, CH*, Natl Synchrotron Radiat Res Ctr, Hsinchu 30077, Taiwan
- Weiland, Cric*, Laboratoire de Physique Thrique, Universitde Paris-sud 11, Biment 210, 91405 Orsay Cedex, France
- Wendler, Elke*, Institut fr Festkerphysik, Friedrich-Schiller-Universit Jena, Jena, Germany
- Wesch, Werner*, Institut fr Festkerphysik, Friedrich-Schiller-Universit Jena, Jena, Germany
- Wimmer, K*, Fakult fr Physik, Ludwig-Maximilians-Universit Mnchen, D-85748 Garching, Germany
- Wollersheim, HJ*, GSI, D-64291 Darmstadt, Germany
- Xiao, Zhiguang*, Interdisciplinary Center for Theoretical Study, Univ of Sc & Tech of China, Hefei, Anhui 230026, China
- Yang, YW*, Natl Tsing Hua Univ, Dept Chem, Hsinchu 30013, Taiwan
- Yunus, Mohammed*, Bhabha Atom Res Ctr, Ctr Variable Energy Cyclotron, Calcutta-700064

Chapter 11

Index

Index

- Abada, Asmaa, 140, 146
Abir, Raktim, 132, 148
Adak, Laksmikanta, 58, 79
Adhikari, S, 102, 104, 110
Adhikary, Biswajit, 130, 145
Agodi, C, 90, 92, 105
Agrawal, BK, 142, 148
Alba, R, 90, 92, 105
ALICE Collaboration, 96, 97, 106
Amenitsch, H, 61, 79
Ayyer, A, 81
- Bagchi, Debarshee, 76, 81
Bal, JK, 62, 65, 79, 80
Balasubramanian, T, 64, 80
Ballofa, J, 26, 33
Bandyopadhyay, Abhijit, 129, 145
Bandyopadhyay, Debades, 130, 131, 145, 146, 149
Bandyopadhyay, Debashree, 33
Banerjee, D, 118, 123
Banerjee, Debasis, 31, 36
Banerjee, Mousumi, 21, 24, 29, 34, 36
Banerjee, P, 102, 103, 110
Banerjee, Pratyay, 143, 148
Banerjee, R, 68, 80
Banerjee, Rahul, 14, 19, 32, 36
Banerjee, S, 52, 61, 67, 68, 78–80
Banerjee, Sangam, 11, 14, 32, 33, 57, 61, 77, 81
Banerjee, Sunanda, 105
Banerji, P, 77
Bangal, Prakriti Ranjan, 35
Banik, Sarmistha, 130, 146, 152
Bardhan, KK, 55, 78
Barma, Mustansir, 64, 83, 171
Basak, Soumen, 25, 35
Basu, A, 75, 82
Basu, Abhik, 70–72, 74, 81, 82
Basu, Avik, 31, 36
Basu, C, 102, 104, 110
Basu, Mahashweta, 74, 83
Basu, P, 103, 110
Basu, Samita, 21, 22, 24, 27–29, 32–34, 36, 39, 41
Basu, Sankar, 19, 36
Basu, Sumanta, 30, 36
Basu, Tanmoy, 81
Basu, Urna, 64, 73, 74, 81, 83
Basu-Mallick, B, 143, 148, 149
Bedi, SC, 92, 105
Belkhou, Rachid, 80
- Bera, MK, 63, 68, 79, 80
Bhattacharjee, A, 49, 76
Bhattacharjee, Ashis, 51, 77
Bhattacharjee, Jayanta K, 70, 81
Bhattacharjee, Pijushpani, 151, 152
Bhattacharjee, Srijit, 131, 146
Bhattacharya, Anuradha, 11, 14, 32, 33
Bhattacharya, Dipankar, 29, 36
Bhattacharya, Dipten, 56, 80
Bhattacharya, Lusaka, 98, 99, 109
Bhattacharya, Madhubrata, 100, 110
Bhattacharya, P, 91, 105, 106
Bhattacharya, Purba, 104, 105
Bhattacharya, Rangana, 78
Bhattacharya, S, 90, 91, 102, 103, 105, 106, 110
Bhattacharya, Sayan, 123
Bhattacharya, Sudeb, 104, 105
Bhattacharyya, Dhananjay, 11, 12, 14, 19, 21, 32, 33, 36, 38, 41
Bhattacharyya, Gautam, 135, 136, 140, 146, 147, 149, 152
Bhattacharyya, Manjit K, 32
Bhattacharyya, Nitai P, 15–18, 35, 36
Bhattacharyya, R, 110
Bhattacharyya, SR, 59, 79, 81
Bhattacharyya, SS, 78
Bhattacharjee, Biplob, 136, 147
Bhoi, D, 53, 57, 77
Bhowal, S, 91, 105
Bhowmik, RK, 102, 110
Bhowmik, RN, 79
Bisoi, A, 31
Biswas, Harishankar, 119, 122, 123
Biswas, M, 110
Biswas, Maitree, 15, 35
Biswas, S, 98, 106, 109
Biswas, Saikat, 104
Biswas, Sampa, 18, 19, 36
Biswas, Soumyajyoti, 63, 69, 83
Biswas, Subir, 116, 123
Bora, Sanchay J, 32
Borderie, B, 90, 105
Bose, Adity, 32
Botha, AJ, 79, 81
Brüchle, W, 33
Brüchle, W, 26
Byakti, Pritibhajan, 138, 148
- Carlen, EA, 81
Chakrabarti, Abhijit, 21, 24, 29–31, 34, 36, 37

- Chakrabarti, Arunabha, 32
 Chakrabarti, Arunava, 82
 Chakrabarti, BK, 69, 70, 72, 73, 81, 83
 Chakrabarti, Chandana, 19, 36
 Chakrabarti, Madhumita, 37
 Chakrabarti, N, 117–120, 122–124
 Chakrabarti, Oishee, 31, 36, 39
 Chakrabarti, Sayan K, 135, 148
 Chakrabarty, Nikhil, 121
 Chakraborti, Anirban, 81
 Chakraborty, Brahmananda, 79
 Chakraborty, Brotati, 22, 27, 32, 33
 Chakraborty, P, 59, 63, 79, 81
 Chakraborty, Purnendu, 132, 148
 Chakraborty, Purushottam, 60, 67, 76, 78–80, 83, 85, 86
 Chakraborty, S, 140, 145, 148
 Chakraborty, Sandipan, 12, 32
 Chakraborty, Santosh, 100, 111
 Chakraborty, Somdeb, 134, 137, 149
 Chakraborty, Sovan, 138, 149
 Chakraborty, Sreeja, 20, 35
 Chakraborty, Supratic, 51, 76, 77
 Chandra, AK, 71, 81, 82
 Chandra, Anjan Kumar, 70
 Chatterjee, Arnab, 81, 83
 Chatterjee, Ayan, 131, 146
 Chatterjee, B, 31
 Chatterjee, J, 110
 Chatterjee, MB, 90, 92, 105
 Chatterjee, P, 61, 79
 Chatterjee, Rakesh, 74, 82
 Chatterjee, Souvik, 78
 Chattopadhyay, Dhrubajyoti, 123, 171
 Chattopadhyay, S, 97, 109
 Chattopadhyay, Subhasis, 104
 Chaudhuri, Manis, 123
 Chernyatin, V, 105
 Chini, Tapas Kumar, 51, 62, 77, 80, 86
 Chinni, TK, 79
 Chopra, Shradha, 36
 Choubey, S, 138, 145, 149
 Choudhury, Ananyo, 17, 35
 Choudhury, Debi, 18, 19, 36
 Choudhury, P, 53, 57
 Chowdhury, Abhishek, 134, 146
 Chowdhury, Biswanath, 123
 Chowdhury, DR, 117, 122
 Chowdhury, PS, 91, 105
 Chowdhury, S, 121
 Chowdhury, Shantanu, 121
 CMS Collaboration, 93–95, 106–109

 Das, Ashok, 136, 138, 142, 144, 146, 147
 Das, Birinchi K, 32
 Das, Debashree, 36
 Das, Debasish, 97, 106, 111
 Das, Debottam, 146
 Das, Eashita, 18, 35
 Das, Jayanta, 64, 79

 Das, Mala, 150
 Das, Mili, 32
 Das, NC, 65, 79
 Das, Niladri Sekhar, 13, 33
 Das, P, 62, 79, 80
 Das, Piyal, 34
 Das, S, 56, 77
 Das, Samir, 15, 30, 35, 36
 Das, Saurabh, 22, 34
 Das, SK, 35
 Das, SN, 53, 77
 Dasgupta, Brahmananda, 116, 123
 Dasgupta, Dipak, 13, 14, 32
 Dasgupta, Jhimli, 35
 Datta, Alokmay, 50–52, 76, 77, 83
 Datta, D, 59, 79
 Datta, Jagannath, 116, 122
 Datta, Moumita, 16, 17, 35
 Dattagupta, JK, 18, 19, 36
 De Martino, Daniele, 81
 De Sarkar, Sangita, 134, 146
 De, A, 55, 78
 De, Amitabha, 57, 77
 De, Antara, 16, 35
 De, Asit K, 134, 139, 146, 147, 149
 De, JN, 133, 142, 147, 148
 Derry, Trevor, 78
 Devi, P Grihanjali, 32
 Dey, A, 110
 Dey, Aparajita, 102, 110
 Dey, CC, 92, 105
 Dey, Debarati, 28, 33
 Dey, Moumita, 69, 72, 74, 82
 Dey, S, 92, 105
 Dey, Sanjay, 35
 Dhar, Deepak, 72, 81
 Digal, S, 134, 148
 Dutt-Mazumder, AK, 98, 99, 109
 Dutta, Binita, 25, 33, 41
 Dutta, Jagannath, 119, 123
 Dutta, Manjistha, 118, 123
 Dutta, Sruti, 18, 36

 Evena, J, 26, 33

 Falomir, H, 138, 146
 Forsberg, U, 21, 35
 Franklyn, Paul, 78
 FRENA Grp, 100, 110
 Frenkel, J, 136, 146

 Gamboa, J, 144, 147
 Gangopadhyay, D, 130, 148
 Gangopadhyay, G, 100, 110
 Ganguly, O, 130, 148
 Ganguly, S, 102, 103, 110
 Garai, Gautam, 123
 Garg, Arti, 83
 Garg, Sandeep Kumar, 81

- Gates, JM, 26, 33
 Gayathri, N, 105
 Geraci, E, 90, 105
 Ghosal, Ambar, 130, 145
 Ghose, D, 58, 80
 Ghose, Jayeeta, 15, 18, 35
 Ghosh, A, 138, 146
 Ghosh, Amit, 135, 146
 Ghosh, Asim, 69, 70, 73, 81, 83
 Ghosh, B, 68, 79
 Ghosh, Binita, 60, 67, 76, 78, 79, 83
 Ghosh, Mita, 32
 Ghosh, R, 110
 Ghosh, Rita, 102, 110
 Ghosh, Samiran, 118, 119, 123
 Ghosh, Saptaparni, 39
 Ghosh, Sayantani, 32
 Ghosh, Tanmay, 69, 81
 Ghosh, Uday Chand, 123
 Giglia, Angelo, 77
 Giri, SK, 55, 78
 Golubev, P, 35
 Goswami, A, 90, 102, 103, 105, 110
 Goswami, Alakananda, 17, 35
 Govindarajan, TR, 134, 148
 Grabowski, Slawomir J, 33
 Greiner, Carsten, 148
 Greiner, Walter, 146
 Grote, Wiebke, 79
 Guin, Partha Sarathi, 22, 34
 Gupta, D, 110
 Gupta, Dhruvajyoti, 102, 110
 Gupta, Kaushik, 119, 123
 Gupta, Kumar S, 133, 134, 147, 148
 Gupta, Mithil Ranjan, 123
 Gupta, Sanjay, 71, 82
 Gupta, Shamik, 64, 83
 Gupta, Tribikram, 71, 82
- Hajra, KB, 71, 82
 Hans, Schamel, 123
 Haque, Najmul, 137, 139, 148
 Harindranath, A, 134, 139, 146, 147
 Hasan, Rashid, 104
 Hazra, S, 61, 65, 79
 Hegde, Ramanujan S, 31, 36
 Hinrichsen, Haye, 83
 Hlatshwayo, TT, 59, 81
 Hofmeister, W, 76
 Hollenberg, Sebastian, 133, 140, 148, 149
 Hui, AK, 121
- Islam, AKM Maidul, 63, 65, 78–80
 Iyengar, ANS, 116, 117, 121–124
- Jamil, Umme, 101
 Jana, Nihar R, 18, 35
 Janaki, MS, 116, 118, 121, 123
- Kailas, S, 110
- Kalkal, Sunil, 100, 104, 111
 Kanjilal, D, 81, 90, 105
 Kar, K, 145, 149
 Kar, Kamales, 138, 150
 Karmakar, B, 92
 Karmakar, S, 58, 80
 Karmakar, SN, 69, 72, 74, 82
 Kaw, PK, 171
 Khamrui, Susmita, 15, 35
 Khan, N, 54, 78
 Khastgir, SP, 148
 Khastgir, SP, 140
 Kore, Rajkumar, 80
 Kozakiewicz, Anna, 60, 78
 Kshetri, R, 90, 103, 105, 110
 Kumar, DM Raj, 58, 78
 Kumar, MC, 135, 142, 144, 147, 148
 Kumar, P Hemant, 35
 Kumar, R, 102, 110
 Kumar, Uday, 52
 Kundu, A, 141, 146
 Kundu, Anasuya, 74, 75, 81, 83
 Kundu, Anjan, 141, 146
 Kundu, Sarathi, 62, 80
 Kundu, Souvik, 51, 77
 Kusz, J, 76
- Lahiri, Ansuman, 17, 35
 Lahiri, S, 21–26, 28, 33–35, 40, 117, 122
 Lahiry, Mohini, 29, 36
 Lanke, Srinivasa Rao, 35
 Lebowitz, JL, 81
 Littlewood, Peter B, 73, 82
 Loidl, A, 54
 Lombardo, I, 90, 92, 105
 Lu, JX, 134, 143, 147
- Maccherozzi, Francesco, 66, 80
 Maharana, Jnanadeva, 142, 147
 Mahatha, SK, 61, 64, 80
 Mahne, Nicola, 77
 Maiti M, 33
 Maiti Moumita, 34
 Maiti, Jyotirmoy, 134, 146
 Maiti, M, 21, 23, 26, 34, 35
 Maiti, Moumita, 19, 22, 24, 25, 28, 33, 34, 38, 42
 Maiti, Prabal K, 32
 Maiti, Santanu K, 69, 72–76, 82
 Maity, Anup Kumar, 17, 35
 Maity, Anwasha, 80
 Maity, Chandan, 117, 120, 122, 123
 Majhi, Swapan, 137, 149
 Majumdar, Debasish, 129, 145
 Majumdar, H, 110
 Majumdar, Nayana, 104, 105, 112
 Majumdar, P, 130, 131, 146, 148
 Majumdar, Pratik, 152
 Majumder, Parijat, 13, 32, 39
 Malherbe, JB, 81

- Malherbe, Johan B, 79
 Mandal, Ajoy, 26, 33
 Mandal, Arup Ratan, 61, 81
 Mandal, H, 49, 76
 Mandal, Haradhan, 77
 Mandal, Mahatsab, 98, 109
 Mandal, P, 53, 54, 56, 57, 77, 78
 Mandal, PC, 22, 34
 Mandal, Prabhat, 85
 Mandal, S, 100
 Mandal, Suman, 60, 61, 64, 66, 79, 80
 Mandal, Swapan K, 61, 81
 Mandal, Tapas Kumar, 13, 33
 Marsili, Matteo, 81
 Martin, X, 134, 148
 Martinez, Mauricio, 148
 Mathews, Prakash, 135, 137, 142, 144, 147–149, 152, 153
 Mazumdar, Chandan, 54, 56, 77
 Mazumdar, I, 110
 Meljanac, S, 133, 147
 Mendez, F, 144, 147
 Menon, Krishnakumar SR, 60, 61, 64, 66, 79, 80
 Metya, A, 58, 80
 Micu, Octavian, 133, 148
 Midya, A, 53, 54, 77, 78
 Mishustin, Igor N, 146
 Mitra, AK, 102, 104, 110
 Mitra, P, 138, 144, 146, 152
 Modak, P, 79
 Mohanty, PK, 64, 74–76, 81–83
 Mollick, SA, 58, 80
 Mondal, Parthasarathi, 56, 78, 80
 Mondal, Santanu, 134, 139, 146, 147
 Mondal, Shyamal, 59, 79
 Mondal, Sutapa, 23, 35
 Mukhawana, Mxolisi B, 60, 79
 Mukherjee S, 79
 Mukherjee, A, 103, 110
 Mukherjee, B, 105
 Mukherjee, CD, 55, 78
 Mukherjee, G, 105, 110
 Mukherjee, M, 58, 63, 65, 67, 78–81
 Mukherjee, P, 105
 Mukherjee, Rajarshi, 52
 Mukherjee, S, 52, 65, 78
 Mukherjee, Smita, 50–52, 77
 Mukhopadhyay, Aniruddha, 123
 Mukhopadhyay, Debashis, 30, 32, 36, 37, 40
 Mukhopadhyay, MK, 63, 79
 Mukhopadhyay, Supratik, 104, 105
 Muralithar, S, 102, 105, 110
 Mustafa, Munshi G, 132, 137, 139, 141, 147, 148, 150
 Mydeen, K, 54, 78

 Naidoo, SR, 78
 Nambissan, PMG, 91–93, 105, 112
 Nandi, Rana, 130, 131, 146, 152
 Nandi, UN, 55
 Nandy, Maitreyee, 31, 38

 Nannarone, Stefano, 77
 Narayanan, Ramesh, 117, 123
 Naresh, N, 68, 79
 Naskar, Tapan, 69, 83
 Nath, TK, 55
 Nayak, D, 26, 33
 Nieto, M, 138, 146
 Nikolopoulos, K, 91, 105

 Paes, Heinrich, 135, 147
 Pahari, Biswapathik, 12, 32
 Pai, H, 102, 110
 Pal, AK, 32
 Pal, Barnana, 77
 Pal, D, 32
 Pal, K, 99, 109
 Pal, Kausik, 98, 109
 Pal, M, 92
 Pal, Palash B, 133, 140, 143, 148, 149, 151
 Pal, R, 124
 Pal, Rabindranath, 116, 121, 123
 Pal, Rahul, 12, 33
 Pal, Sudipta, 14, 32
 Pal, Uttam, 21, 34
 Palchoudhuri, Shreoshi, 36
 Palit, R, 109, 110
 Panda, S, 140, 148
 Pandey, Abhishek, 54, 77
 Panigrahi, Swati, 11, 12, 14, 32, 33
 Pankov, AA, 135, 147
 Paver, N, 147
 Perez, Alejandro, 135, 146
 PICASSO Collaboration, 132, 146
 Pidt, Daniel, 135, 147
 Poddar, A, 55, 78
 Poddar, Asok, 56–58, 77, 78
 Prabhakaran, D, 54
 Pradhan, MK, 103, 110
 Pramanik, D, 31
 Pramanik, Malini, 29, 36
 Pramanik, UD, 104, 111
 Prashanthi, Suthari, 25, 35
 Priyant, A, 31
 Pyne, Santanu, 27, 34

 Qin, GY, 141, 147

 Raduta, Ad R, 90, 105
 Raghav, A, 110
 Raja, SO, 67, 80
 Ramanathan, Rajeswari, 31, 36
 Rane, Neena S, 31, 36
 Ranganathan, R, 52, 54, 58, 77, 78
 Ranu, Brindaban C, 79
 Rao, V Jayathirtha, 35
 Rao, V V Mallikarjuna, 171
 Raut, R, 105
 Ravindran, V, 137, 142, 147–149
 Ray, Nihar R, 116, 119, 122, 123

- Ray, S, 31
 Ray, Samriddhi Sankar, 72, 82
 Raychaudhuri, Amitava, 171
 Raychaudhuri, Mithu, 30, 36
 Raychaudhuri, S, 121
 Raychaudhuri, Sreerup, 136, 147
 Raychaudhuri, Swasti, 36
 Reinhard, PG, 142, 148
 Reja, Sahinur, 73, 82
 Roy Choudhury, Kamalika, 36
 Roy Chowdhury, P, 103, 110
 Roy, B, 56, 77, 92, 105
 Roy, M, 49, 76
 Roy, Madhusudan, 51, 76, 77
 Roy, P, 98, 109
 Roy, Pradip, 98, 99, 109
 Roy, Probir, 130, 145
 Roy, S, 97, 109, 110
 Roy, Sandipta, 77
 Roy, Shibaji, 134, 137, 143, 147, 149
 Roy, Subinit, 100, 102, 103, 110, 113
 Roy, Sumana, 19, 36
 Roy, Trina, 35
 Ruppert, J, 147
- Sadasivam, VR, 171
 Saha Sarkar, M, 31, 103, 110, 111
 Saha, B, 63, 79
 Saha, Debasree, 58, 79
 Saha, Partha, 17, 35, 39, 41
 Saha, S, 90, 104, 105
 Saha, Shaibal, 113
 Saha, SK, 121, 124
 Saha, Sutapa, 31, 36
 Sahoo, RK, 55
 Salim, Md, 104
 Samaddar, SK, 133, 142, 147, 148
 Samanta, Tanusree, 67, 81
 Samsarov, A, 133, 147
 Santosh, Mogurampelly, 11, 32
 Sanyal, MK, 63, 68, 79, 80, 84, 171
 Sarangi, Manas Kumar, 21, 27, 29, 33, 34
 Sardar, M, 67, 80
 Saridakis, Emmanuel N, 135, 148
 Sarkar, Anwesa, 134, 146
 Sarkar, M, 102, 110
 Sarkar, Munna, 20, 23, 35
 Sarkar, N, 75, 82
 Sarkar, Niladri, 71, 82
 Sarkar, Priyanka, 27, 34
 Sarkar, S, 111
 Sarkar, Sreemoyee, 98, 109
 Sarmiento, LG, 35
 Sasidevan, V, 72, 81
 Satpati, B, 69, 79–81, 83
 Satyanarayana, B, 104
 Scholten, O, 136, 148
 Sehanobish, Esha, 20, 35
 Sen, Anjan A, 135, 148
 Sen, Kamalika, 36
 Sen, Pintu, 122
 Sen, Susanta, 171
 Sen, Udayaditya, 15, 30, 35, 36
 Sengupta, Joydip, 55, 78
 Sengupta, K, 52, 78
 Sengupta, Pradeep K, 12, 32
 Sengupta, Sudip, 120, 122
 Seth, Satyajit, 142, 144, 147, 148
 Sethi, J, 109
 Sharma, M, 63, 79
 Shripathi, T, 77
 Shukla, Padma K, 118, 123
 Shyam, R, 136, 148
 Sil, Shreekantha, 82
 Singh, Harvendra, 139, 140, 144, 147, 150
 Singh, RP, 102, 105, 110
 Sinha, M, 110
 Sinha, Mithun, 15, 18, 35
 Sinha, Om Prakash, 81
 Sinha, RK, 171
 Sinha, Suman, 50, 83
 Siva, D, 35
 Som, T, 81
 Sood, AK, 32
 Srivastava, Dinesh K, 101
 Srivastava, Rajendra, 80
 Subudhhi, Arijita, 21, 34
- Talukdar, D, 55, 78
 Tewary, Satish Chandra, 171
 Theron, Christiaan C, 79
 Thiyagarajan, R, 53, 78
 Thoma, Markus H, 132, 137, 148
 Thomas, AW, 136, 148
 Tomar, BS, 22, 28, 34
 Torres, F, 144, 147
 Trivedi, T, 97, 109
 Tsytrinov, AV, 147
- Uphoff, Jan, 148
- van der Berg, NG, 79, 81
 Veenhof, R, 105
 Venkataramana, CB, 171
 Venugopal, V, 59, 81
 Vogler, Erwin A, 122
- Wang, C -H, 65, 79
 Weiland, Cric, 146
 Wendler, Elke, 79
 Wesch, Werner, 79
 Wimmer, K, 103, 110
- Xiao, Zhiguang, 134, 143, 147
- Yang, Y W, 79
 Yarlagadda, Sudhakar, 73, 82, 85
 Younus, Mohammed, 101